The role of desmoplakin and plakoglobin in desmosome associated disease

Rita Meira e Cruz de Vasconcelos Cabral

Supervisors: Prof. David Kelsell
Dr. Andrew South

This thesis is submitted for the degree of Doctor of Philosophy

Centre for Cutaneous Research, Blizard Institute of Cell and Molecular Science,
Barts and The London School of Medicine and Dentistry, Queen Mary,
University of London

February 2010

The work presented in this thesis is my own unless otherwise stated, and is in accordance with the University of London's regulations for the degree of Doctor of Philosophy.

Rita M C V Cabral

Abstract

Desmosomes are intercellular junctions that connect intermediate filaments (IFs) of adjacent cells within tissues, generating a large and mechanically resilient network. Desmosomes are prominent in epithelia and the myocardium. Their importance for maintenance of the strength and flexibility of these tissues is underlined by mutations in desmosomal genes which compromise skin or heart and in some instances both. This thesis is focused on two obligate plaque proteins of the desmosome, desmoplakin (DP) and plakoglobin (PG), and their role in disease of skin and heart.

A novel homozygous nonsense mutation, p.S24X, in the gene encoding PG, *JUP*, was identified in three non-consanguineous Argentinean patients, resulting in skin fragility, palmoplantar keratoderma (PPK) and woolly hair with no symptoms of cardiomyopathy. p.S24X mRNA was readily detected and an alternative AUG codon translates an N-terminally truncated PG, which is expressed in patient and parental skin samples at barely detectable levels. At the same time another novel homozygous mutation, c.468G>A, was identified in *JUP* causing a very similar phenotype in two Kuwaiti siblings and resulting also in very low levels of PG in the skin. These results suggest that PG is essential for maintenance of skin integrity, but not for normal heart development in children.

The gene encoding DP, *DSP*, produces two alternative splice variants, DPI and DPII. A novel DP alternative splice isoform, DPIb, is described. As shown by RT-PCR, *DSPIb* is expressed in several epithelial and cardiovascular tissues and is the only *DSP* isoform detected in the aorta. Western blotting proteins from HaCaT and K1 cells identified this novel isoform, which has been previously missed due to its similarity in size to DPII. DPIb may help compensate defects in patients with *DSPI*-specific mutations.

The molecular mechanisms of three different *DSP* mutations leading to skin disease or skin disease associated with cardiomyopathy were investigated. Mutations causing DPI/DPII haploinsufficiency and DPI knock-out lead to decreased expression levels of the desmosomal proteins DSC2, DSC3 and PKP1 in an experimental system using HaCaT keratinocytes. Expression of a mutant *DSPI* construct harbouring a dominant 30 bp insertion results in the formation of large DPI aggregates at the cell membrane of HaCaT cells. The spectrum of *DSP* and *JUP* mutations which cause different clinical phenotypes is discussed.

Table of contents

List of figures and tables

Figures:

Chapter 4 – Identification of DPIb – a novel desmoplakin splice variant

Chapter 5 – Functional studies of desmoplakin mutants

Appendix A: Genetic analysis in patients with recessive skin disease and woolly hair

Appendix B: Optimisations of siRNA knock-down experiment for transient down-regulation of DP isoforms

Appendix C: Functional studies of *DSPI*-nonsense and DP haploinsufficiency mutants

Appendix D: Flexcell adhesion assay

Tables:

Chapter 1 – Introduction

Chapter 2 – Materials and Methods

Chapter 5 – Functional studies of desmoplakin mutants

Chapter 6 – Final Discussion and Future Work

Appendix B: Optimisations of siRNA knock-down experiment for transient down-regulation of DP isoforms

Abbreviations

5'P	5 prime Phosphate
APC	Adenomatous Polyposis Coli
ARVC/D	Arrhythmogenic Right Ventricular Cardiomyopathy/Dysplasia
ARVCF	Armadillo Repeat gene deleted in Velocardiofacial syndrome
ASSP	Alternative Splice Site Predictor
AT	Annealing Temperature
ATP	Adenosine Triphosphate
B2M	β_2 microglobulin gene
BMZ	Basement Membrane Zone
BP (BPA)	Bullous Pemphigoid Antigen
bp	base pair
BSA	Bovine Serum Albumin
c.	coding
$CaCl_2$	Calcium Chloride
CAM	Cell Adhesion Molecule
cDNA	complementary DNA
CO_2	Carbon dioxide
Ct	Cycle threshold
DAPI	4'-6-Diamidino-2-Phenylindole
ddH_2O	double-distilled water
DEJ	Dermal-Epidermal Junction
DMEM	Dulbecco's Modified Eagle's Medium
DMSO	Dimethyl Sulfoxide
DNA	Deoxyribonucleic Acid
dNTP	Deoxynucleotide Triphosphate
DP	Desmoplakin
DSC	Desmocollin
DSG	Desmoglein
DSP	Desmoplakin gene
DTD	DSG Terminal Domain
DTT	Dithiothreitol
E	Embryonic day
E. coli	*Escherischia coli*
EB	Epidermolysis Bullosa
EC	Extracellular

E-cadherin	Epithelial cadherin
ECD	Extracellular Core Domain
ECM	Extracellular Matrix
EDTA	Ethylenediaminetetraacetic Acid
EJC	Exon Junction Complex
EPPK	Epidermolytic Palmoplantar Keratoderma
ERK	Extracellular signal-Regulated Kinase
ESE	Exon Splicing Enhancer
ESS	Exon Splicing Silencer
EST	Expressed Sequence Tag
FBS	Foetal Bovine Serum
g	Standard gravity
G3PDH	Glyceraldehyde-3-Phosphate Dehydrogenase
GFP	Green Fluorescent Protein
GSK	Glycogen Synthase Kinase
GTP	Guanosine Triphosphate
h	hour
HCl	Hydrochloric acid
HD1	Hemidesmosome associated protein 1
HEK	Human Embryonic Kidney
hnRNP	heterogenous nuclear Ribonucleoprotein
HPRT	Hypoxanthine Phosphoribosyl-Transferase gene
HpV	Human papilloma Virus
IA	Intracellular Anchor
ICS	Intracellular Cadherin-typical Sequence
IDP	Inner Dense Plaque
IF	Intermediate Filaments
IFAP	Intermediate Filament Associated Protein
IgG	Immunoglobulin G
IPL	Intracellular Proline-rich Linker
ISE	Intron Splicing Enhancer
ISS	Intron Splicing Silencer
Kb	Kilobase
KDa	Kilodalton
LB broth	Luria Bertani broth
LSM	Laser Scanning confocal Microscope
LTRs	Long Terminal Repeats

LVDC	Left Ventricular Dilated Cardiomyopathy
M	Methionine
MACF	Microtubule-Actin Crosslinking Factor
Mb	Megabase
MCS	Multiple Cloning Site
MDCK	Madin-Darby Canine Kidney
$MgCl_2$	Magnesium Chloride
min	minute
miRNA	micro RNA
M-MLV RT	Moloney Murine Leukemia Virus Reverse Transcriptase
n	Number of repetitions of a single experiment
NaCl	Sodium Chloride
N-cadherin	Neuronal cadherin
NCBI	National Center for Biotechnology Information
NEPPK	Non-Epidermolytic Palmoplantar Keratoderma
NHK	Normal Human Keratinocytes
NMD	Nonsense Mediated Decay
nt	Nucleotide
OD	Optical Density
ODP	Outer Dense Plaque
O-GlcNAc	O-N-acetylglucosamine
p.	protein
PAGE	Polyacrylamide Gel Electrophoresis
PBS	Phosphate Buffered Saline
PBST	PBS-Triton X-100
PCR	Polymerase Chain Reaction
PEG	Polyethylene Glycol
PFA	Paraformaldeyde
PG	Plakoglobin
PKC	Protein Kinase C
PKP	Plakophilin
PPK	Palmoplantar Keratoderma
PRD	Plakin Repeat Domain
PTC	Premature Termination Codon
qRT-PCR	Quantitative RT-PCR
RISC	RNA-Induced Silencing Complex
RNA	Ribonucleic Acid

RNAi	RNA interference
RNase	Ribonuclease
rpm	revolutions per minute
RT	Room Temperature
RT-PCR	Reverse Transcription PCR
RUD	Repeated-Unit Domain
RyR	Ryanodine Receptor
SCF	Skp1-Cullin-F box protein
SDS	Sodium Dodecyl Sulfate
SEM	Standard Error of the Mean
siRNA	short interfering RNA
SNP	Single Nucleotide Polymorphism
SPPK	Striate Palmoplantar Keratoderma
SR	Serine/arginine-Rich
STE	Sodium-chloride Tris EDTA
TBE	Tris-Borate EDTA
TBS	Tris-Buffered Saline
TCF/LEF	T-Cell Factor/Lymphoid-Enhancer Factor
TFIIIB	Transcription Factor IIIB
TGF	Transforming Growth Factor
TM	Transmembrane
TTBS	Tween-20 TBS
U	Unit
ULF	Unit Length Filaments
UTR	Untranslated Region
UV	Ultraviolet
VE-cadherin	Vascular Endothelial cadherin
ZO	Zona Occludens
β-TrCP	β-Transducin repeat Containing Protein

Publications, oral presentations and awards arising from this thesis

Publications

Peer reviewed publications:

RM Cabral, L Liu, C Hogan, PJC Dopping-Hepenstal, BC Winik, RA Asial, R Dobson, C Mein, P Baselaga, JE Mellerio, A Nanda, M del C Boente, DP Kelsell, JA McGrath, AP South (2010). *Homozygous mutations in the 5' region of the JUP gene result in cutaneous disease but normal heart development in children.* Journal of Investigative Dermatology (see Appendix F).

Invited publications:

Cabral RM and South AP. (2008). Inherited disease of the desmosome. *In* "Pathophysiology of the Desmosome" (Cirillo, N., Lanza, A., and Gombos, F., Eds), pp121-156, Research Signpost. Kerala.

Abstracts:

RM Cabral, L Liu, C Hogan, PJC Dopping-Hepenstal, BC Winik, RA Asial, R Dobson, C Mein, P Baselaga, JE Mellerio, A Nanda, M del C Boente, DP Kelsell, JA McGrath, AP South. *Homozygous mutations in the 5' region of the JUP gene result in cutaneous disease but normal heart development.* (abstract/program #453W). Presented at the 59th Annual Meeting of The American Society of Human Genetics, October 21, 2009, Honolulu, Hawaii. Available at http://www.ashg.org/2009meeting/abstracts/fulltext/.

RM Cabral, BC Winik, RA Asial, C Mein, P Baselga, PJ Dopping-Hepenstal, MC Boente, DP Kelsell, JA McGrath and AP South. *A novel plakoglobin mutation reveals distinct roles for plakoglobin in heart and skin.* Journal of Investigative Dermatology 128, Supplement 1 (April 2008). Presented at the International Investigative Dermatology (IID) meeting, May 17, 2008, Kyoto, Japan.

RM Cabral, BC Winik, RA Asial, C Mein, P Baselga, M del C Boente, DP Kelsell, JA McGrath, AP South. *A novel plakoglobin mutation reveals distinct functional properties for plakoglobin in heart and skin.* Presented at the Annual William Harvey Research Day, October 16, 2007, St Bartholomews Hospital, West Smithfield, London, UK.

Oral presentations

Talk at the Institute of Cell and Molecular Science (ICMS) Graduate School Day*, "Desmosomal defects in skin disease and ARVC", April 24, 2009, QMUL, London, UK.*

Talk at the University of Dundee, *"Characterising the roles of desmoplakin isoforms in keratinocyte biology", March 19, 2009, Dundee, UK.*

Talk at the Annual Meeting of the British Society for Investigative Dermatology (BSID), *"Analysing isoform- and tissue-specific functions of desmoplakin" April 8, 2008, Oxford, UK.*

Awards

1st prize for Best Oral Presentation at the Institute of Cell and Molecular Science (ICMS) Graduate School Day*, "Desmosomal defects in skin disease and ARVC"*, April 24, 2009, QMUL, London, UK.

International Investigative Dermatology (IID) 2008 Travel Award supported by the European Society for Investigative Dermatology (ESDR), to attend the IID meeting in May 2008, Kyoto, Japan.

Travel award, Annual Meeting of the British Society for Investigative Dermatology (BSID), 2008, Oxford, UK.

Acknowledgements

There are many people I would like to thank for the last three years, which on the whole have been immensely rewarding and enjoyable.

Firstly, a special thank you to both my supervisors Andy South and David Kelsell for their endless support, guidance and enthusiasm throughout the last three years. I was lucky to have two supervisors with such an active interest in my work at all times. Andy's experienced advice and training at the bench were particularly crucial during my first year in the lab.

Lab members during this time, particularly Maxine Holder and Celine Pourreyron, were invaluable in my training and integration in the lab. A special thanks to Dan Tattersall, who had an enourmous input in my work thereafter, for his infinite encouragement, friendship and invaluable theoretical and technical advice as well as for thorough and critical reading of this thesis.

I would like to thank Graham Neill for his extensive help with retroviral transductions, Charles Mein and Richard Dobson for SNP array data analysis, Dominique Abrams for providing atrium tissue samples and Clare Cole for assistance with qPCR experiments. I would also like to thank other lab members, past and present, and everyone in the Centre for Cutaneous Research, in particular Georgie Cox, Trond Aasen, Claire Scott, Diana Blaydon, Tiago Matos, Anna Thomas, Claire Sinclair, Shefali Rajpopat, Kathrin Smuda, Manos Papadakis, Rudolf van Koningsveld, Manu Singh and Monika Cichon for their friendly advice, help and support in one way or another, and for making the lab a fun place to be.

Finally a very special thank you to the following people who have contributed to the successful completion of this work: Joana Martins, Vera Martins, Neil Cummins, Ana Marta Diniz and Lynne Archibald for their exceptional friendship; my granny Matilde M Cruz for her day to day support and caring; and my dad Luis Cabral who has always been my inspiration.

– Chapter 1 –

Introduction

1.1. The skin

The skin and its appendages, which in humans consist of hair, nails, sebaceous glands and sweat glands, form a physical barrier that covers the whole surface of the organism and protects it from the external environment. The specialised functions of the skin include protection and defence of the body from external microorganisms, water loss and UV radiation; exchange of gases and solutes, excretion of wastes, temperature regulation as well as synthesis and storage of nutrients. The skin is also a sensory organ capable of detecting pain, sensation, pressure, temperature, and assaults by external microorganisms or other chemical and physical stresses (Proksch & Jensen, 2007).

The skin is the largest organ of the human body and is comprised of two major regions, the epidermis and the dermis, which are described below (sections 1.1.1 and 1.1.2). Underneath the dermis there is another layer called the hypodermis or subcutaneous adipose layer, which is formed of connective tissue, elastin, large blood vessels, sweat glands and nerves. This layer contains about 50% of fat tissue and its main functions are to connect the skin to the underlying muscle and bone, to conserve the body's heat and to serve as insulation or shock absorber for the body (Haake *et al.*, 2001).

1.1.1. The epidermis

The epidermis is the outermost region of the skin and originates primarily from the embryonic ectoderm (Blanpain & Fuchs, 2009). The thickness of the epidermis ranges from 0.05 mm (on the eyelids) to 1.5 mm (on palms and soles), which is usually only a small fraction of the full thickness-skin which varies between 1.5 mm and 4 mm. The skin epidermis and its appendages play the major role in providing the protective barrier to the body. Because they are constantly assaulted by physical, chemical and mechanical traumas, these tissues continuously regenerate and are capable of responding to injury by repairing wounds and damaged areas (Fuchs, 2007).

The epidermis is a multilayered or stratified squamous epithelium composed of different types of cells, namely melanocytes, Largerhans cells, Merkel cells and keratinocytes (Chu, 2008). Melanocytes are dendritic cells found in the basal layer of the epidermis and are responsible for the production of the photoprotective pigment

melanine. This pigment is accumulated in specialised organelles called melanosomes, which are then transferred into other epidermal cells. In recipient cells, melanosomes localise over the nucleus to protect the DNA from the harmful effects of ionising UV-radiation (Boulais & Misery, 2008). Largerhans cells are another type of dendritic cells found in the spinous layer of the epidermis. They are antigen-presenting cells which respond to a skin infection by internalising and processing the antigen, which is then recognised by immune cells in local lymph nodes (Boulais & Misery, 2008). Merkel cells are present in the basal layer of the epidermis and are usually closely associated, in a synapse-like like fashion, with the ends of nerve fibres. These complexes are designated as Merkel nerve endings and constitute one of the skin mechanoreceptors. They are sensitive to touch, pressure, texture and low frequency vibrations. In response to these stimuli, Merkel cells release neurotransmitters or neuromodulators which are sensed by the nerve terminals and transmitted to the brain (Halata *et al.*, 2003).

Keratinocytes constitute 95% of the epidermis and populate, from the bottom to the top, basal, spinous, granular and cornified layers, according to their differentiation stage (Figure 1.1). The innermost basal layer is a single cell layer of keratinocytes which have the unique property of being able to undergo mitosis. These cells continually exit the cell cycle and commit to the program of terminal differentiation. During this process, keratinocytes move upwards until they reach the uppermost layer, or cornified layer, at the skin surface. At this stage, these cells are dead, enucleated and flattened squames ready to be shed from the skin surface (Figure 1.1). The whole process of terminal differentiation (also called keratinisation or cornification), since the keratinocyte leaves the basal layer until it is slough from the surface, takes approximately four weeks (Fuchs, 2009). The correct balance between proliferation and differentiation must occur in order to maintain a constant number of cells within the epidermis, a process called homeostasis (Fuchs, 2007).

The keratinocyte transcriptional profile, morphology and biochemistry change as it moves from the bottom to the top of the epidermis. Basal keratinocytes express keratin 5 and keratin 14 which form the cytoskeletal network of keratin IFs (IF proteins are described in section 1.4). As they move to the spinous layer, keratin 5 and keratin 14 expression switches to keratin 1 and keratin 10, and this switch marks the beginning of the differentiation process. Keratinocytes in spinous and granular layers are post-mitotic but still metabolically active. When in the granular layer, these cells express the

cornified envelope glutamine- and lysine-rich proteins, such as involucrin, which accumulate beneath the plasma membrane. These cells also synthesize keratohyaline granules which are mainly formed by pro-filaggrin. Pro-filaggrin is the precursor of filaggrin, a histidine-rich protein that participates in the formation of large keratin-IF aggregates when cells transit to the cornified layer. Loricrin is another protein produced in the granular layer and is the main constituent of the cornified envelope, together with involucrin. Finally, an increase of intracellular calcium activates transglutaminase 1 which biochemically cross-links the envelope proteins (such as involucrin, envoplakin, and periplakin) forming a macromolecular complex that lies underneath the plasma membrane and is reinforced by lipids. This macromolecular protein- and lipid-complex surrounds the keratin macrofibrillar aggregates of the dead corneocytes, which are now impermeable and insoluble protective structures, devoid of organelles and plasma membrane, at the skin surface (Fuchs, 1990; Fuchs, 2007; Houben *et al.*, 2007; Proksch *et al.*, 2008).

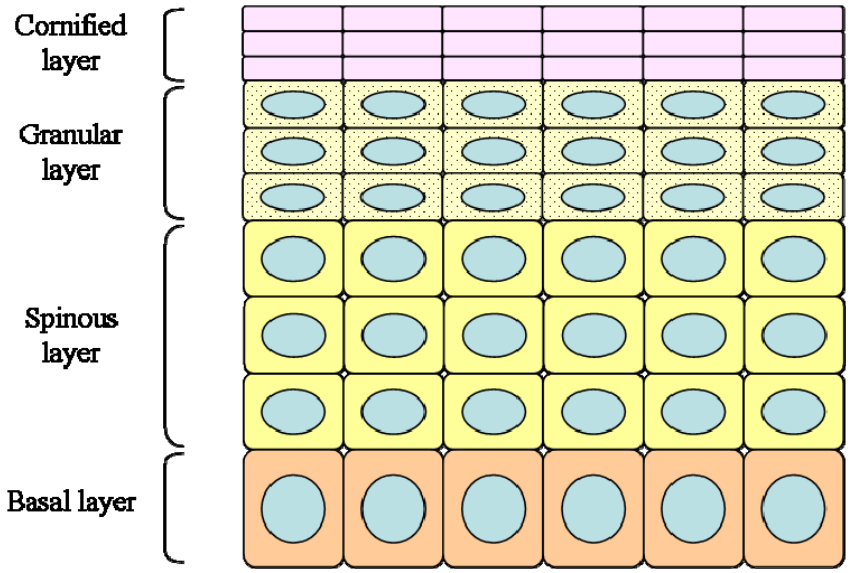

Figure 1.1. Schematic structure of the human epidermis. The different epidermal layers indicative of distinct keratinocyte differentiation stages are shown, including the basal, spinous, granular and cornified layers.

1.1.2. The dermis

The dermis is the region of the skin below the epidermis and its primary functions are to provide a physical support (including flexibility and tensile strength)

and also a supply of nutrients to the epidermis. The dermis is also involved in thermal regulation and contains receptors of sensory stimuli. It is mainly composed of connective tissue and in contrast with the epidermis, it is primarily derived from the embryonic mesoderm (Haake *et al.*, 2001).

The dermis is divided into two regions, the more superficial papillary dermis and the deeper reticular dermis. The papillary dermis contains blood vessels, which are essential to deliver nutrients to and receive wastes from the avascular epidermis. These exchanges are made via the dermal-epidermal junction (section 1.1.3), which is the region between the epidermis and the dermis. The papillary dermis also contains elastic and fibrous tissue and sensory nerve endings. Fibroblasts, which represent the major cell type in the dermis, are predominant in the papillary dermis, essentially in the dermal papillae which is the region just adjacent to the epidermis. Fibroblasts have mesenchymal origin and are responsible for the synthesis and maintenance of precursors of the extracellular matrix (ECM) components, including collagen and elastin fibres. Collagens are the most abundant components of the dermis (approximately 75% of its weight) and provide strength and resistance to the skin. Elastic fibres (such as elastin) constitute a very small fraction of the dermis (approximately 4% of the dermal matrix-protein dry weight) and are responsible for the flexibility and resilience of the skin. The deeper reticular dermis is the thickest region of the dermis and is composed of larger blood and lymph vessels, thicker elastic and collagen bundles as well as nerve endings and epidermal appendages (Chu, 2008; Haake *et al.*, 2001).

The ECM, which is mainly produced by fibroblasts in the dermis, is a complex and heterogeneous interconnected network of macromolecules, including proteins and polysaccharides. These macromolecules form a gel-like structure that surrounds cells and can also be present in basement membranes. This molecular arrangement provides a scaffold through which cells can move (Lodish *et al.*, 2003). Besides collagens and elastic fibres, this matrix also contains non-collagenous glycoproteins such as fibronectin (which cross-links cell surface proteins and other ECM components), laminins (which are adhesion molecules) and proteoglycans (which support cells) as well as hyaluronic acid (which resists compressive forces). The dermal ECM serves not only as a static structural support for the epidermis, but is also highly dynamic due to the constant turnover and remodelling of its components which influences cell behaviour. Growth factors and signalling molecules (such as cytokines) can be

produced either by keratinocytes in the epidermis or fibroblasts in the dermis under regulated conditions, which signal through membrane-bound receptors (Werner & Grose, 2003) (see sections 1.2 and 1.2.1.3) to control processes such as cell growth and differentiation.

1.1.3. The dermal-epidermal junction

The dermal-epidermal junction (DEJ) is the region that separates the epidermis from the dermis. The cutaneous basement membrane zone (BMZ) is included in this region and represents the interface between cells (in the epidermis) and their surrounding connective tissue (in the dermis) (Figure 1.2). The DEJ is composed of four distinct regions that can be distinguished by electron microscopy: (1) the plasma membrane of the basal keratinocyte; (2) the lamina lucida; (3) the lamina densa; (4) the sub-basal lamina densa (Burgeson & Christiano, 1997). The lamina lucida and lamina/sub-basal lamina densa compose the BMZ (Woodley & Chen, 2001). The plasma membrane of basal keratinocytes contains hemidesmosomes (see section 1.2.1.3) which are anchoring points for keratin IFs (Figure 1.2). The lamina lucida is transversed by anchoring filaments which are thin threadlike structures consisting of laminin 5 that connect hemidesmosomes to the lamina densa. The lamina densa is connected to the underlying dermis through anchoring fibrils which are fibrillar structures composed mainly of collagen VII. Therefore, basal keratinocytes are connected to the dermis through a very complex series of protein-protein interactions which provide the DEJ with a high level of mechanical stability. These protein-protein interactions occur within the anchoring complex which is formed by hemidesmosomes together with anchoring filaments and anchoring fibrils. The DEJ serves as a support for the epidermis while it is selectively permeable to certain molecules and cells between the epidermis and the dermis. It also influences keratinocyte behaviour in terms of cell polarity, proliferation, differentiation and migration as well as playing roles in wound healing and remodelling of the skin (Burgeson & Christiano, 1997; Woodley & Chen, 2001).

1.2. Keratinocyte adhesion and communication within the skin

In the development of multicellular organisms, differentiated cells of a certain type are organised into tissues, which in turn are organised into organs that perform specific functions. For a group of cells to become part of a specific tissue, molecular interactions have to occur at the cellular level, which allow cells to communicate with each other. Another very important characteristic of cells is their ability to adhere to one another and perform given functions in a spatial and temporal manner. Adhesion and communication among cells and between cells and their extracellular environment are therefore crucial for morphogenesis and to maintain tissue integrity (Green & Gaudry, 2000). These molecular interactions depend on the expression of a wide range of specific adhesion molecules, which is tightly regulated in space and time (Lodish *et al.*, 2003).

There are two basic types of cell junctions, namely cell-cell and cell-matrix junctions. Cell-cell (or intercellular) junctions connect one cell to another. Cell-matrix junctions occur where one cell adheres to components of the surrounding ECM (Figure 1.2). Cell junctions can also be organised into three functional groups, namely occluding junctions, anchoring junctions and communicating junctions (Figure 1.3). In vertebrates, occluding junctions are represented by tight junctions, which are specialised to seal cells together and to create a diffusion barrier (see below). Anchoring junctions are important to strongly hold cells (and their cytoskeletons) together or cells to the ECM. Communicating junctions, represented by gap junctions in vertebrates, are responsible for the interchange of small molecules and solutes between the cytoplasm of adjacent cells (Alberts *et al.*, 2002; Lodish *et al.*, 2003). Figure 1.3 shows a basic schematic of these three types of cell junctions and their representatives in animal (vertebrate) tissues and Figure 1.2 shows their localisation in basal epidermal cells.

A common feature of tight junctions and anchoring junctions is their structural composition and organisation. Firstly, the adhesive interface between adjacent cells is mediated by a complex of transmembrane proteins designated as cell adhesion molecules (CAMs). In a similar way, the adhesive interface between cells and the ECM is accomplished by transmembrane adhesion receptors. These adhesion molecules interact extracellularly to seal two cells together or one cell to the ECM. Secondly, CAMs or adhesion receptors are connected to the cytoskeleton or to signalling

molecules through adaptor proteins (Alberts *et al.*, 2002, Figure 1.2; Lodish *et al.*, 2003) (Figure 1.2).

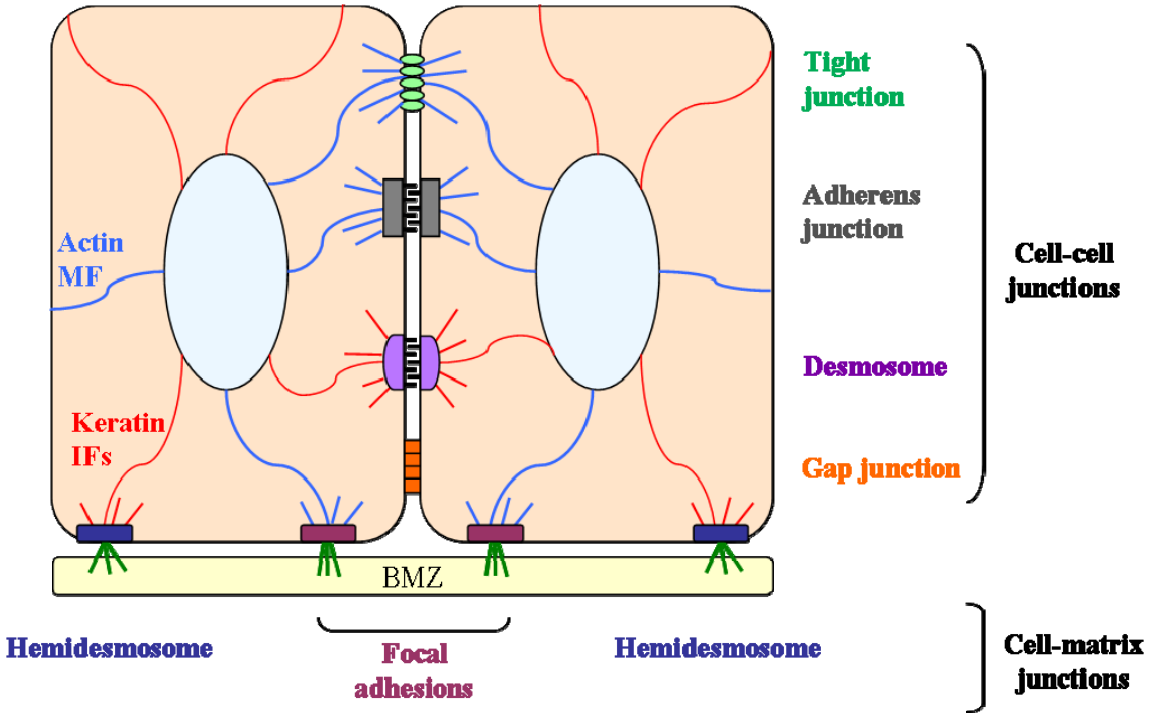

Figure 1.2. Schematic diagram of epithelial cell-cell and cell-matrix junctions. Cell-cell junctions include tight junctions (in green), adherens junctions (in grey), desmosomes (in purple) and gap junctions (in orange), connecting two basal keratinocytes. Cell-matrix junctions include hemidesmosomes (in blue) and focal adhesions (in pink), connecting the basal keratinocytes to the basement membrane zone (BMZ). Adherens junctions and focal adhesions are shown to be connected to actin microfilaments (in light blue). Desmosomes and hemidesmosomes are connected to keratin IFs (in red). Adhesion in hemidesmosomes and focal adhesions is mediated by integrins (in green), which are involved in connecting the plasma membrane of basal keratinocytes to the BMZ. Adhesion in desmosomes and adherens junctions is mediated by cadherins (in black), which are involved in bonds between two keratinocytes. Adapted from Green and Gaudry (2000).

There are four kinds of anchoring junctions, namely adherens junctions, desmosomes, hemidesmosomes and focal adhesions (see Figures 1.2 and 1.3). Adherens junctions and desmosomes (in blue, Figure 1.3) participate in cell-cell adhesion and their transmembrane adhesion proteins belong to the cadherin family. In contrast, hemidesmosomes and focal adhesions (in green, Figure 1.3) participate in cell-matrix adhesion and their transmembrane adhesion proteins belong to the integrin family (see below and Figure 1.2) (Alberts *et al.*, 2002). Both desmosomes and hemidesmosomes are connected to the resilient IF cytoskeleton. In contrast, adherens junctions and focal

adhesions are linked to the actin microfilament cytoskeleton at cell-cell or cell-matrix interfaces (Fuchs & Raghavan, 2002; Getsios *et al.*, 2004b). Tight junctions are also linked to actin microfilaments (dashed line, Figure 1.3 and Figure 1.2) (Getsios *et al.*, 2004b). Although governed by similar architectural principles, each of these junctions has a distinct set of protein components (see following sections).

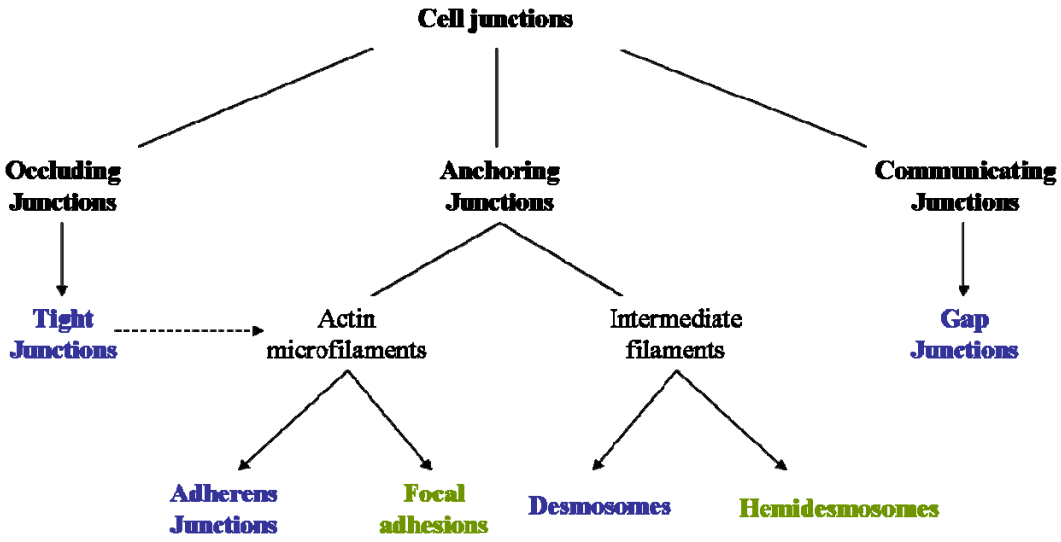

Figure 1.3. Functional classification of the vertebrate cell junctions. Schematic diagram of the three major types of cell junctions - occluding, anchoring and communication junctions - and their representatives in vertebrate animals. Occluding junctions are represented by tight junctions and communicating junctions are represented by gap junctions in vertebrates. Anchoring junctions are represented by adherens junctions and focal adhesions, which are connected to the actin microfilament cytoskeleton and by desmosomes and hemidesmosomes, which are connected to the IF cytoskeleton. Tight junctions, adherens junctions, desmosomes and gap junctions (in blue) are cell-cell junctions, while focal adhesions and hemidesmosomes (in green) are cell-matrix junctions.

Cell junctions are abundant in epithelial tissues, which all share the common functions of selective barrier and protection. Tight junctions contribute to this permeability barrier function by creating the diffusion barrier between the apical and basolateral membrane domains of these polarised epithelial cells (Green & Gaudry, 2000). Besides being physically attached to one another and to the underlying basement membrane by anchoring junctions, epithelial cells are also chemically linked by intercellular channels or communicating junctions known as gap junctions (Getsios *et al.*, 2004b). All together, these junctions are crucial to maintain the strength and flexibility of epithelial tissues which contribute to their protective function. The two basic types of interactions, named cell-cell and cell-matrix adhesion, therefore permit

the integration of cells into tissues and the transfer of information among cells and with their environment (Lodish *et al.*, 2003).

1.2.1. An overview of cell-cell and cell-matrix adhesion junctions

1.2.1.1. Tight junctions

Tight junctions contribute to the selective barrier function of epithelial tissues by separating the extracellular fluids that surround the apical and basolateral membranes of each polarised cell. This is accomplished by the formation of thin sealing bands of transmembrane proteins that totally surround each cell, and that interact with a similar array of transmembrane proteins in the neighbouring cell. Tight junctions can also control the paracellular transport of ions and solutes in between cells. The efficiency with which tight junctions restrict the transfer of ions between the membranes of two adjacent cells depends on the number of sealing bands composing the tight junction. The higher the number of sealing bands between two cells, the less permeable the tight junction is. Each sealing strand is formed by a long row of the transmembrane adhesion proteins, claudins and occludins, which interact in the intercellular space via their extracellular domains. The claudin gene family encodes multiple isoforms which have tissue-specific expression profiles. Claudins and occludins interact inside each of two apposing cells with intracellular peripheral membrane proteins named ZO-1, ZO-2 and ZO-3, which are cytoplasmic adaptor proteins. ZO proteins are in turn connected to the actin microfilament cytoskeleton. Many other proteins can be found associated with tight junctions, which are involved in the recruitment of binding partners and in the regulation of epithelial cell polarity (Alberts *et al.*, 2002; Hartsock & Nelson, 2008; Lodish *et al.*, 2003).

1.2.1.2. Anchoring junctions involved in cell-cell adhesion

The transmembrane glycoprotein components of both adherens junctions and desmosomes belong to the large cadherin family of calcium-dependent adhesion molecules. Desmosomes are the major cell-cell anchoring junction in the epidermis and will be described in detail in the following sections.

Adherens junctions are formed by homophilic associations of members of the classical cadherin sub-family. Approximately 20 members of this sub-family have been described, which were originally named according to the tissue where they are predominantly expressed, i.e., E- (epithelial), VE- (vascular endothelial) and N- (neuronal) cadherins (Rudini & Dejana, 2008). It is currently known that each cadherin can be expressed in a variety of different tissues. The extracellular domains of classical cadherins associate via *cis*- (between molecules of the same cell) and *trans*- (between molecules of apposing cells) interactions in the intercellular space, and the cytoplasmic tails bind to the adaptor proteins of the catenin family. Members of the catenin family perform various functions, such as stabilisation of cadherins, organisation of the actin cytoskeleton and involvement in intracellular signalling pathways that control gene transcription. Four major catenins are involved in adherens junction formation, namely PG, β-catenin, p120-catenin and α-catenin. PG, β-catenin and p120-catenin belong to the armadillo family of junctional and signalling proteins, whereas α-catenin has 20-30% sequence homology with vinculin (Herrenknecht *et al.*, 1991), which is another actin-binding protein present in adherens junctions as well as focal adhesions (see section 1.2.1.3). Both p120-catenin and β-catenin interact with the cytoplasmic tail of E-cadherin. Binding of p120-catenin is thought to be required to stabilise E-cadherin at the plasma membrane. β-catenin links E-cadherin to α-catenin which in turn interacts with actin microfilaments (Green & Gaudry, 2000). Although α-catenin interacts directly with both β-catenin and F-actin, this interaction might be mutually exclusive (Hartsock & Nelson, 2008; Yamada *et al.*, 2005). P120-catenin, PG and β-catenin can translocate to the nucleus and interact with transcription factors (Rudini & Dejana, 2008). The amount of β-catenin that is not junction-bound is either degraded by the ubiquitin-proteasome pathway or translocates to the nucleus, where it interacts with transcription factors of the T-cell factor/lymphoid-enhancer factor (TCF/LEF) family. Wnt signals lead to protection of β-catenin from degradation, which is then free to translocate to the nucleus. In the absence of Wnt signalling, the fraction of free β-catenin in the cytoplasm is very low. P120-catenin can interact with kaiso, a zinc finger transcription factor that represses target gene expression, and relieve its repression effect. P120-catenin is also regulated by the Wnt signalling pathway (Hartsock & Nelson, 2008; Jamora & Fuchs, 2002; Rudini & Dejana, 2008).

1.2.1.3. Anchoring junctions involved in cell-matrix adhesion

Hemidesmosomes are multiprotein complexes involved in linking epithelial cells to the underlying basement membrane. In the skin, they anchor basal epidermal keratinocytes and their keratin IF cytoskeleton to the lamina lucida and are connected to the lamina densa by anchoring filaments (see section 1.1.3). Hemidesmosomes are composed of: (1) cytoplasmic plaque proteins which link the IF cytoskeleton to the cytoplasmic surface of the cell membrane; (2) transmembrane proteins, which connect the cytoplasmic side of the cell to the ECM; and (3) basement membrane-associated proteins of ECM (Green & Jones, 1996). The cytoplasmic components include bullous pemphingoid antigen 230 (BP230 or BPAG1) and plectin, HD1, IFAP 300 and P200. BP230 and plectin belong to the plakin family of proteins which are cytoskeleton binding proteins. These molecules interact with keratin IFs. The transmembrane components include bullous pemphingoid antigen 2 (BPAG2, BP180 or collagen XVII) and α6β4 integrin (Borradori & Sonnenberg, 1996). These molecules are essential for hemidesmosome formation and for adhesion of keratinocytes to the ECM. BPAG2 interacts with the other transmembrane protein, α6β4 integrin. BPAG2 also binds BP230 and plectin which are involved in IF attachment. Finally, α6β4 integrin interacts with laminin 5, which is the ECM ligand. Laminin 5 in turn associates with the collagen VII-containing anchoring fibrils (Borradori & Sonnenberg, 1996; Green & Jones, 1996).

Focal adhesions and related structures (focal contacts, fibrillar adhesions and podosomes) are large and very dynamic multiprotein assemblies that (like hemidesmosomes) mediate adhesion of the cell cytoskeleton to the ECM. Cells use this type of contact, which comprises over 100 different proteins that are constantly being remodelled in response to signals and mechanical forces, for processes including motility, migration and morphogenesis. Focal adhesions are also signalling centres that convey information across the cell membrane and therefore play roles in the regulation of cell proliferation, differentiation and survival. Cell anchorage to the ECM by focal adhesions is also mediated by integrins, which are connected to actin microfilaments through the plaque proteins vinculin, talin, paxillin and tyrosine-phosphorylated proteins and to the ECM by fibronectin, laminin and collagen among other proteins. The Rho-family of GTPases, which are important molecular switches involved in the control of cytoskeletal assembly and contraction, stimulate the formation of focal adhesions. Enzymes including kinases, phosphatases, proteases, and lipases also contribute to the

formation and regulation of these adhesion complexes (Geiger *et al.*, 2001; Wozniak *et al.*, 2004).

1.3. The desmosome: a specialised cell-cell anchoring junction

Desmosomes were observed for the first time by the Italian pathologist Giulio Bizzozero in 1864, during his examination of the spinous layer of the epidermis under a light microscope. Notably, he described them as small dense nodules, subsequently named "nodes of Bizzozero", at sites of adhesion between adjacent cells (Bizzozero, 1864; Bizzozero, 1870). In 1920, Josef Shaffer named these nodules desmosomes, a name that originates from the Greek words "desmo", which means bond and "some", which means body (Schaffer, 1920). With the introduction of electron microscopy around 1944, a series of morphological studies emerged which revealed a high level of organisation within the desmosome (Calkins & Setzer, 2007). These studies led to a general view of the desmosome as structural "spot welds", based on their ultrastructural appearance, while their biological importance in intercellular communication and signalling was not yet considered. In 1974, Skerrow and Matoltsy isolated desmosomes from bovine epidermis and separated the desmosomal components by sodium dodecyl sulphate-polyacrylamide gel electrophoresis (SDS-PAGE). They identified eight large protein bands and characterized the chemical nature of these proteins. They correctly deduced that interactions between the glycoproteins (cadherins) were responsible for intercellular adhesion (Skerrow CJ. & Matoltsy AG., 1974a; Skerrow CJ. & Matoltsy AG., 1974b). This work marked a shift from the morphological era to the biochemical characterization and functional analysis of desmosomal components (Bass-Zubek & Green, 2007).

Desmosomes are classically known for their importance in intercellular adhesion and maintenance of tissue integrity. These junctions are specialised to form strong bonds between cells. Moreover, since each desmosome is connected to the IF cytoskeleton of two different cells, this resilient desmosome-IF network functions to distribute the physical impacts throughout tissues. Desmosomes therefore confer mechanical stability to a wide range of tissues, particularly epithelia (including epithelial cells of the skin, intestine, stomach, bladder, uterus, oviduct, liver, pancreas, salivary glands, thyroid gland and nephron) and the myocardium (Garrod & Chidgey,

2008; Holthofer *et al.*, 2007). Desmosomes are also present in meningeal cells and the follicular dendritic cells of lymph nodes (Green & Gaudry, 2000).

1.3.1. Ultrastructural organisation

When observed under a transmission electron microscope, the desmosome can be divided into three highly organised regions: (1) an extracellular light space bisected by an electron-dense midline (Odland, 1958), designated as the extracellular core domain (ECD); (2) two symmetrical cytoplasmic electron-dense plaques lying parallel to the plasma membranes of two apposing cells, called the outer dense plaques (ODP); and (3) two slightly less dense plaques located next to the ODP, named inner dense plaques (IDP). The cytoskeletal IF network is attached to the plasma membrane at the desmosomal IDP (North *et al.*, 1999). Figure 1.4 shows an electron micrograph of the desmosome where these three regions are highlighted. The ECD (or 'desmoglea') is approximately 34 nm wide (Al-Amoudi *et al.*, 2004) and only shows the electron dense midline in mature desmosomes. This midline is lost from desmosomes in wounded epidermis or cultured keratinocytes in a "wounded" monolayer (Garrod *et al.*, 2005 and see section 1.5; Wallis *et al.*, 2000). The thickness of both the ODP and the IDP is approximately 15-20 nm and the electron-lucent space separating both plaques is about 8 nm wide (North *et al.*, 1999). The diameter of the desmosome is less then 1 μm (Garrod & Chidgey, 2008).

The size and morphology of the desmosome differ between tissues (Cowin *et al.*, 1985) and in different regions of the same tissue. For instance, desmosomes are larger in palm epidermis compared to breast epidermis (Wan *et al.*, 2003) and are also larger and more electron dense in the suprabasal layers of the differentiating epidermis compared to smaller and less organised desmosomes in the basal proliferating layer (Green & Simpson, 2007).

1.3.2. Molecular composition

The major components of desmosomes consist of two desmosomal-specific cadherin family members, desmogleins (DSGs 1-4) and desmocollins (DSCs 1-3), and several cytoplasmic plaque proteins. The plaque proteins comprise members of the armadillo family of nuclear and junctional proteins, such as PG and plakophilins 1-3

(PKPs 1-3), and members of the plakin family, such as DP (Figure 1.4). Although a minimal group of these core proteins is sufficient to form a desmosome, additional proteins adapt the desmosome to cell type-specific functions. These additional proteins include the plakin members of the cornified envelope envoplakin and periplakin and the corneodesmosome protein corneodesmosin, among others (Desai *et al.*, 2009; Yin & Green, 2004).

The N-terminal domains of the desmosomal cadherins interact in the intercellular space to couple the two halves of the desmosome and constitute the adhesive ECD. Interactions between these proteins in the extracellular space form the electron dense midline observed by electron microscopy (Figure 1.4 and section 1.3.1). The C-terminal tails of these proteins span the plasma membrane into the ODP region and interact directly with PG and PKPs (Cowin, 1994; Garrod & Chidgey, 2008; Getsios *et al.*, 2004b; Hatzfeld, 1999; Kowalczyk *et al.*, 1994; Schmidt & Jager, 2005). DP, which extends into the IDP, is responsible for the incorporation of IFs into the desmosomal plaque (Green & Hobbs, 2006; Hatsell & Cowin, 2001). The N-terminus of DP is important to organise the desmosomal complex, by recruiting the desmosomal cadherins to the plasma membrane through interactions with PG (Kowalczyk *et al.*, 1997) and PKPs (Kowalczyk *et al.*, 1999). The C-terminal tail binds to IFs (Stappenbeck *et al.*, 1993) (see section 1.3.2.2.2). The stability of the desmosome is increased through lateral interactions among these and other proteins within the desmosomal plaques (Green & Hobbs, 2006). Figure 1.4 shows a basic schematic of the desmosome composition and relative positions of its main proteins.

Both desmosomes and adherens junctions are composed of different proteins, most of which belong to the same gene families (North *et al.*, 1999; Yin & Green, 2004). In both cases the protein chain starts with a cadherin family member, which binds an armadillo protein (β-catenin or PG in adherens junctions and PG in desmosomes). These armadillo proteins in turn bind to adaptor proteins (α-catenin in adherens junctions and DP in desmosomes) which belong to different gene families. This final link diverges to hold the different types of cytoskeletal fibres (actin microfilaments in adherens junctions and IFs in desmosomes) (Yin & Green, 2004). In the desmosome, PKPs interact with the desmosomal cadherins and DP, but also with PG (PKP2) and IF proteins (PKP2 and PKP3) (Bonne *et al.*, 2003; Chen *et al.*, 2002). Moreover, certain desmosomal cadherins can interact directly with DP in the absence of

PG (Bornslaeger *et al.*, 2001; Smith & Fuchs, 1998; Troyanovsky *et al.*, 1994). The existence of additional protein-protein interactions in these junctions suggests a higher level of specialisation, with each protein in the desmosomal plaque participating in multiple interactions with other partners. This observation, coupled to the fact that desmosomes arose later in metazoan evolution then their relatives, adherens junctions suggests that this more complex protein arrangement could provide greater tensile strength to desmosomes (Yin & Green, 2004).

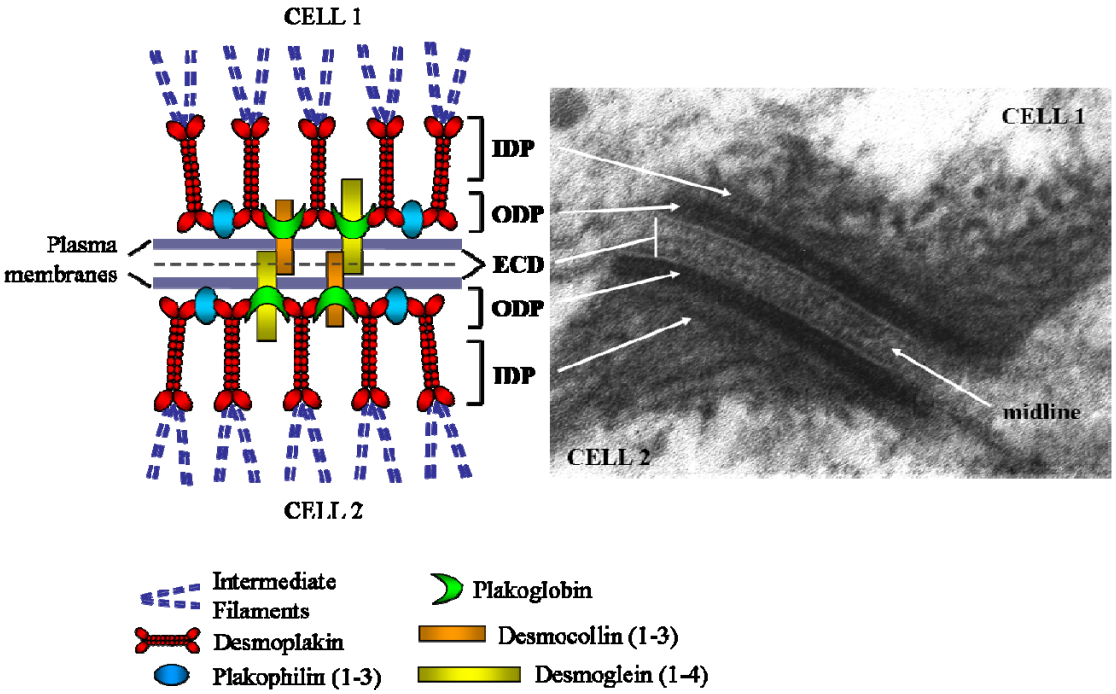

Figure 1.4. Structural organisation of the Desmosome. Schematic diagram of the desmosome (left hand side) showing the relative localisation of the desmosomal cadherins (desmocollins and desmogleins), plaque proteins (plakoglobin, plakophilins and desmoplakin) and keratin intermediate filaments, and electron micrograph of a human epidermal desmosome (right hand side) showing ultrastructural domains: IDP, inner dense plaque; ODP, outer dense plaque; ECD, extracellular core domain. Adapted from South (2004). Electron micrograph courtesy of Dr. Beatrice Winik (Servicio de Microscopía Electrónica, INSIBIO, Universidad Nacional de Tucumán—CONICET, Tucumán, Argentina).

1.3.2.1. The desmosomal cadherins form the adhesive core

The desmosomal cadherins are single-pass transmembrane glycoproteins encoded by seven individual genes (*DSC1-3* and *DSG1-4*) localised in chromosome 18. Each of the three *DSC* genes generates two splice variants through alternative splicing, a

longer ‘a’ isoform and a shorter ‘b’ isoform that differ in the length of the C-terminal tails (Green & Simpson, 2007) (see Figure 1.5A).

All cadherins have three functional domains. The first is an extracellular N-terminal domain which is calcium-dependent and important for intercellular associations. This region includes four highly conserved repeat subdomains (EC1 to EC4) and the more variable extracellular anchor subdomain (EA). The EC domains are separated by flexible linkers, which can accommodate up to three calcium ions each (Garrod *et al.*, 2005). The second is a single transmembrane domain (TM). The third is a cytoplasmic domain which interacts with plaque proteins. This domain includes the intracellular anchor (IA) and the intracellular cadherin-typical sequence (ICS). Both DSC ‘a’ and ‘b’ splice variants have an IA domain, but only the ‘a’ proteins have the complete ICS domain, whereas ‘b’ isoforms have a truncated version of this domain. The ICS domain is responsible for PG binding and therefore the ‘b’ splice variants are not able to interact with PG (Troyanovsky *et al.*, 1993), but can instead associate with the plaque protein PKP3 (Bonne *et al.*, 2003). The DSGs contain an extra cytoplasmic region downstream of the ICS which is absent from DSCs. This region is formed by an intracellular proline-rich linker (IPL) domain, a variable number of repeated-unit domains (RUD) and a glycine-rich DSG terminal domain (DTD) (Delva *et al.*, 2009; Garrod & Chidgey, 2008; Getsios *et al.*, 2004b; Holthofer *et al.*, 2007) (see Figure 1.5A).

A. Desmosomal Cadherins

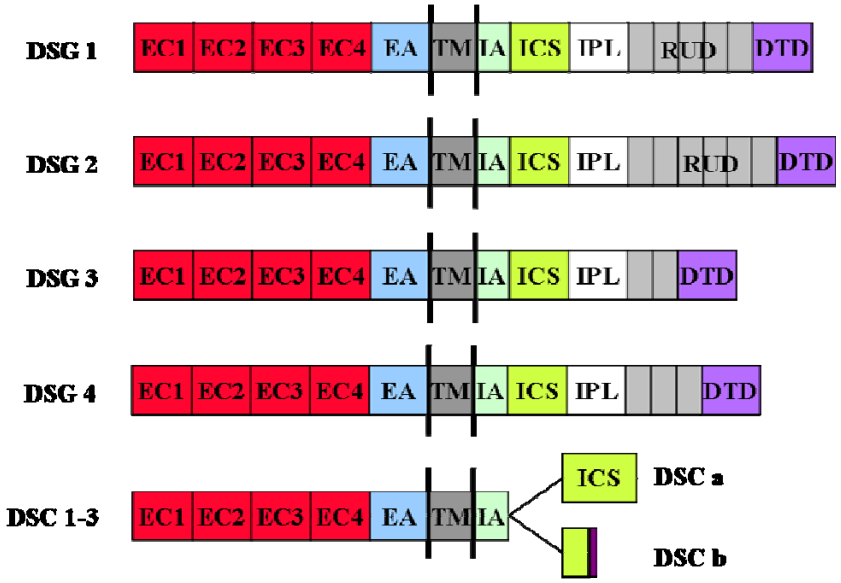

B. Armadillo proteins

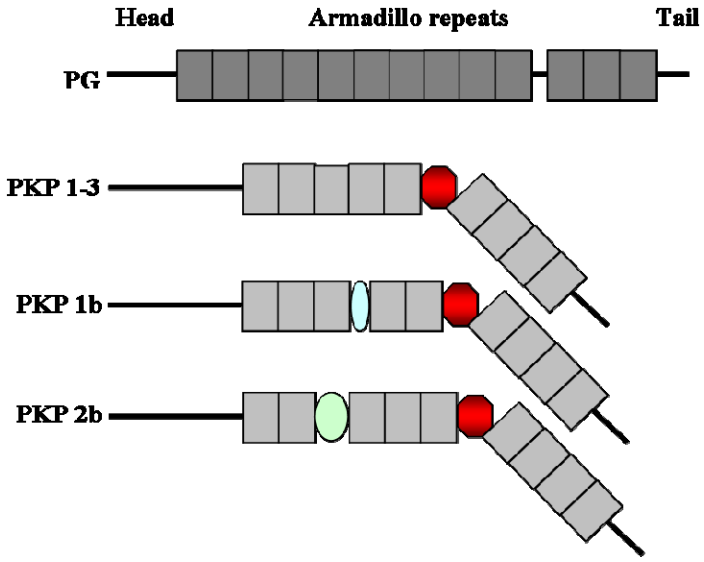

Figure 1.5. Structure of desmosomal proteins (continues).

C. Plakin proteins

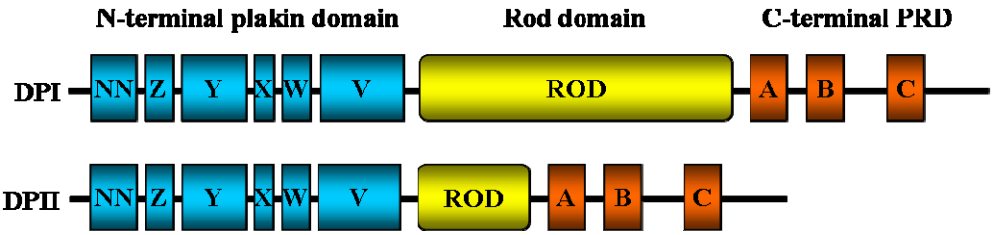

Figure 1.5. Structure of desmosomal proteins. (A) Domain structure of the desmosomal cadherins, DSG1-4 and DSC1-3. All desmosomal cadherins contain an extracellular domain formed by four conserved repeat subdomains (EC1 to EC4) and a variable extracellular anchor subdomain (EA), which is followed by a transmembrane subdomain (TM). Intracellularly, they possess an intracellular anchor domain (IA) followed by an intracellular cadherin-typical sequence (ICS). Additionally, DSGs 1-4 have an intracellular proline-rich linker (IPL) domain, a variable number of repeated-unit domains (RUD) and a glycine-rich DSG terminal domain (DTD). Alternatively, the intracellular domain of the 'a' splice variants of DSCs 1-3 have only the IA and ICS domains and the intracellular domain of the 'b' splice variants have a truncated version of the ICS domain followed by a number of unique amino acids (purple segment). **(B)** Armadillo proteins PG and PKPs 1-3. PG has 13 arm-repeat domains (armadillo repeats) and PKPs have nine arm-repeat domains with an insert between repeats five and six (red insert) which creates a bend in these proteins. PKP1 and PKP2 exist as two splice variants, 'a' and 'b'. PKP1b has 21 extra amino acids between arm-repeats three and four compared to PKP1a and PKP2a and 2b differ by the insertion of 44 amino acids between arm-repeats two and three. **(C)** DPI and DPII splice variants. The N-terminal plakin domain is formed by six α-helical fragments (NN, Z, Y, X, W and V) which form an antiparallel α-helical bundle. This domain is followed by a central coiled-coil rod domain and a C-terminal tail containing subdomains A, B and C which are the plakin repeat domains (PRD). Adapted from Desai *et al.* (2009).

Both homophilic and heterophilic interactions have been shown to occur *in vitro* between DSCs and DSGs. These interactions are thought to occur both in *cis* (between molecules in the same cell) and *trans* (between molecules of adjacent cells) conformations (Garrod & Chidgey, 2008; Getsios *et al.*, 2004b). Heterophilic, calcium-dependent interactions contributing to intercellular adhesion were observed between endogenous DSG2 and recombinant DSC1a in the human fibrosarcoma cell line HT1080 (Chitaev & Troyanovsky, 1997). Recombinant proteins containing the first two EC domains of DSC2 and DSG2 were also demonstrated to interact in solution, involving both homophilic and heterophilic associations. Homophilic interactions between DSG proteins were weaker and possibly calcium-independent whereas heterophilic associations were demonstrated to be calcium-dependent (Syed *et al.*, 2002). Other studies suggested that both DSCs and DSGs are necessary for strong cell-cell adhesion (Chitaev & Troyanovsky, 1997; Marcozzi *et al.*, 1998; Tselepis *et al.*, 1998). Moreover, the DSG1:DSC1 ratio was demostrated to be important for

desmosomal adhesion in fibroblasts (Getsios *et al.*, 2004a). Further studies will be necessary to define the mechanisms of *cis* and *trans* interactions between desmosomal cadherins, and whether homophilic, heterophilic or both types of interactions occur *in vivo* (Delva *et al.*, 2009; Holthofer *et al.*, 2007).

1.3.2.2. The desmosomal plaques contain armadillo and plakin proteins

Desmosomal plaque proteins refer to those found in the ODP and IDP (Figures 1.4 and 1.5) and facilitate binding of the IF network to the transmembrane desmosomal cadherins. Two families of proteins are found here, the armadillo and the plakin families.

1.3.2.2.1. Armadillo proteins

Armadillo proteins are characterized by their highly conserved central arm-repeat domains (Figure 1.5B). Each repeated motif has 42 amino acids and the number of repetitions varies among different members (Garrod & Chidgey, 2008). Armadillo members include β-catenin, PG, p120-catenin, p0071, ARVC, δ-catenin and PKPs (Delva *et al.*, 2009). The structure of the central arm-repeat domain has been resolved for β-catenin (Huber *et al.*, 1997) and PKP1 (Choi & Weis, 2005) by X-ray crystallography. Each repeat was found to consist of three α-helices. The repeats are organised together forming the arm-repeat domain which has the shape of a right-handed superhelix. In the case of these two proteins, the superhelix has a positively charged groove which interacts with binding partners.

PG is encoded by the *JUP* gene in chromosome 17 (Aberle *et al.*, 1995) and was the first member of this family to be discovered (Cowin *et al.*, 1986). PG is closely related in structure to β-catenin, which is the best characterised armadillo protein and is present in adherens junctions (Huber, 2003). Both of these proteins are composed of N- and C-terminal domains separated by a series of 12 arm-repeat domains in the case of β-catenin (Huber *et al.*, 1997) and 13 arm-repeat domains in the case of PG (Sacco *et al.*, 1995) (Figure 1.5B). PG can be found in desmosomes, adherens junctions and in the nucleus. In adherens junctions, PG interchanges with β-catenin. However, it appears to be localised predominantly in desmosomes, probably because its affinity for the desmosomal cadherins is higher than for E-cadherin (Chitaev *et al.*, 1996). In contrast,

β-catenin is usually only found in adherens junctions, possibly because its N- and C-terminal domains inhibit its interaction with DSG1 (Troyanovsky *et al.*, 1996a; Wahl *et al.*, 2000). Interactions between PG and its binding partners occur mainly through its central arm-repeat and C-terminal domains. Arm-repeats 1-3 are required for interactions with the ICS domain of DSG1 and DSC2a (Chitaev *et al.*, 1998). Also within this region of PG is the binding site for α-catenin. Binding of DSG to PG was shown to disrupt the interaction between PG and α-catenin, possibly explaining the absence of α-catenin in the desmosome (Aberle *et al.*, 1996; Chitaev *et al.*, 1998; Miravet *et al.*, 2003; Sacco *et al.*, 1995). The E-cadherin binding site in both PG and β-catenin is localised in the centre of the arm-repeat domain and lies in a different region from the desmosomal cadherin binding site (Chitaev *et al.*, 1998). PG also interacts with DP (Kowalczyk *et al.*, 1997), PKP2 and PKP3 (Bonne *et al.*, 2003; Chen *et al.*, 2002), p0071 (Hatzfeld *et al.*, 2003) and keratins (Smith & Fuchs, 1998), but the precise PG binding sites for these proteins have not been determined (Holthofer *et al.*, 2007). Deletion of the PG C-terminus led to the formation of large desmosomes by lateral association in cultured cells (Palka & Green, 1997a). It was therefore suggested that PG may participate in the control of desmosomal size by regulating lateral interactions between other desmosomal components (Palka & Green, 1997a).

Additionally to having a structural role in cell-cell junctions, PG also participates in intracellular signal transduction. PG is functionally related to β-catenin which is a modulator of the canonical Wnt/β-catenin signalling pathway (Moon *et al.*, 2002). Both PG and β-catenin interact with and compete for proteins involved in this signalling pathway. These common binding partners include adenomatosis polyposis coli (APC) (Rubinfeld *et al.*, 1993; Shibata *et al.*, 1994) and LEF-1/TCF (Huber *et al.*, 1996; Zhurinsky *et al.*, 2000). Similarly to β-catenin, PG interacts with axin leading to phosphorylation in the N-terminus (serine 28) by glycogen synthase kinase-3β (GSK-3β) (Kodama *et al.*, 1999) and interacts with the F-destruction box protein β-TrCP of the Skp-, Cullin-, F-box- (SCF) containing E3 ubiquitin ligase complex (Sadot *et al.*, 2000), which are all mediators of the Wnt/β-catenin signalling pathway. Although it is now accepted that PG has a role in the Wnt/β-catenin pathway, it is not clear whether it activates or represses Wnt/β-catenin target genes or whether it acts on a different set of genes (Garrod & Chidgey, 2008). Some studies indicate that PG's function in the Wnt/β-catenin pathway is independent from that of β-catenin (Maeda *et al.*, 2004;

Teuliere *et al.*, 2004; Williamson *et al.*, 2006) and that PG cannot compensate for the lack of β-catenin in β-catenin knock-out mice (Bierkamp *et al.*, 1996; Haegel *et al.*, 1995; Ruiz *et al.*, 1996). Other authors suggest PG interferes with β-catenin's turnover and/or transcriptional activity (Miravet *et al.*, 2002; Teuliere *et al.*, 2004). The idea that changes in desmosome composition or function could also alter Wnt/β-catenin signalling is supported by a study where suppression of DP expression in cardiac myocytes (using short interfering RNA [siRNA]) led to PG translocation to the nucleus and suppression of this signalling pathway (Garcia-Gras *et al.*, 2006).

PKPs are members of the p120-catenin subfamily of armadillo domain proteins and have a large N-terminal head domain followed by nine arm-repeat domains and a short C-terminal tail (Choi & Weis, 2005). PKPs contain a large and flexible insert between arm-repeats five and six which introduces a major bend in the overall structure (Choi & Weis, 2005) (see Figure 1.5B). PKP1 and PKP2 exist in two alternatively spliced variants, a shorter 'a' variant and a longer 'b' isoform (Figure 1.5B). PKP1b has an extra 21 amino acids between arm-repeats three and four compared to PKP1a (Schmidt *et al.*, 1997) and PKP2b has an extra 44 amino acids between arm-repeats two and three compared to PKP2a (Mertens *et al.*, 1996). The gene encoding PKP3 is only known to originate one transcript (Garrod & Chidgey, 2008; Schmidt *et al.*, 1999) (see Figure 1.5B).

All three PKPs localise to desmosomes and the nucleus, but the non-junctional function of PKPs is not yet clear. PKP1b splice variant was only found in the nucleus (Schmidt *et al.*, 1997). PKP2 has been reported to associate with β-catenin (Chen *et al.*, 2002), with RNA polymerase III and with the transcription factor TFIIIB (Mertens *et al.*, 2001). PKP3 was also found constitutively associated with RNA binding proteins (Hofmann *et al.*, 2006), however the significance of these observations is not clear. PKPs interact with several partners including cadherins, other armadillo proteins (including β-catenin and PG), the N-terminus of DP, and IFs directly, thus likely participating in lateral stabilising interactions in the plaque (Hatzfeld, 2007). All the interactions identified so far occur through the PKP head domain (Choi & Weis, 2005; Hatzfeld, 2007).

The p120-catenin subfamily member p0071 is also known as PKP4. In contrast with PG and the PKPs, which are essential for desmosomal adhesion, p0071 is considered to be an accessory protein (Garrod & Chidgey, 2008). However, it localises

to desmosomes and adherens junctions of epithelial cells and interacts with many junctional proteins including DSC3a, PG, DP, PKP2 and E-cadherin (Hatzfeld *et al.*, 2003). p0071 is also found in endothelial cell junctions, where it interacts with VE-cadherin and DP (Calkins *et al.*, 2003). Several splice variants of p0071 have been detected (Hatzfeld & Nachtsheim, 1996) and a cytoplasmic pool has been described which may be involved in cell signalling (Wolf *et al.*, 2006).

1.3.2.2.2. Desmoplakin is the most abundant plakin of the desmosome

Plakins are large molecules with multiple binding domains which provide linkage between cytoskeletal proteins and junctional complexes. Seven members of this family have been identified so far, namely DP, plectin, BPA-1, microtubule-actin crosslinking factor (MACF), envoplakin, periplakin and epiplakin. Four of the known mammalian plakins (DP, envoplakin, periplakin and plectin) have been reported to localise to the desmosome, of which DP is the most abundant and well characterised (Leung *et al.*, 2002).

Members of the plakin family are characterised by their N-terminal plakin domain and C-terminal plakin repeat domain (PRD). The plakin domain is formed by six α-helical fragments (NN, Z, Y, X, W and V) which form an antiparallel α-helical bundle (Virata *et al.*, 1992). This domain targets plakins to cell junctions and is possessed by all members of this family, except for epiplakin. The PRD is a repeated region that comprises three globular motifs designated as A, B and C. Each of these motifs contains 4.5 repetitions of a 38-amino acid strand. This domain interacts with IFs (Leung *et al.*, 2002) (see Figure 1.5C).

DP is an obligate component of the desmosomal plaque. It is a cytoplasmic protein composed of a typical N-terminal plakin domain, a central α-helical coiled-coil rod domain, and a C-terminal IF-binding PRD (Figure 1.5C). The globular head or plakin domain directs DP to the desmosome through interactions with the armadillo proteins PG and the PKPs (Bornslaeger *et al.*, 2001; Green & Hobbs, 2006; Hatzfeld, 1999; Hatzfeld, 2007; Kowalczyk *et al.*, 1997; Schmidt & Jager, 2005; Smith & Fuchs, 1998) and recent evidence suggests that it consists of two pairs of spectrin repeats separated by a Src-homology-3 domain (Jefferson *et al.*, 2007). The rod domain of plakins is mostly formed of heptad repeats that mediate homodimerisation and, in some

plakins, possibly heterodimerisation (Leung *et al.*, 2002). The subdomains A, B and C of the PRD of DP (Figure 1.5C) are separated by flexible linking regions and followed by a terminal 68-residue regulatory tail, which is glycine-serine-arginine rich. This C-terminal tail is a versatile domain that can interact with different types of IFs (see below).

DP is encoded by the *DSP* gene, located on chromosome 6p24, which contains 24 exons and produces two isoforms through alternative splicing: DPI (~332KDa) and DPII (~260KDa). An alternative donor splice site in exon 23 of the *DSP* gene generates the latter isoform. DPII retains both the N- and C-terminal domains, but lacks approximately two thirds (599 residues) of the rod domain (Green & Hobbs, 2006). Both DPI and DPII are abundantly expressed in the skin. DPI is also present in specialised vascular and lymphatic endothelial cell junctions named complexus adhaerentes, together with VE-cadherin and PG (Borrmann *et al.*, 2006; Franke *et al.*, 2006; Hammerling *et al.*, 2006). In the intercalated disc of the heart muscle, DP and other desmosomal molecules were shown by immunoelectron microscopy to interact with classical cadherin components in both desmosomes and adherens junctions. This observation led Franke *et al.* (2006) to re-name this region of the cardiomyocyte plasma membrane as the "area composita" of adhering junctions (Green & Hobbs, 2006). DPII expression is abundant in the skin and in most epithelial tissues but barely detectable in the heart (Uzumcu *et al.*, 2006).

Although the crucial role of the DPI splice variant in the anchorage of IFs to the desmosome is widely known, the function of the DPII isoform has not been determined. During the construction of a molecular map of the desmosomal plaque, antibodies against the N- and C-terminal domains of DP were used to map its functional regions within the desmosome (North *et al.*, 1999). This study demonstrated that the N-terminus is orientated toward the membrane and the C-terminus toward the nucleus, which is in agreement with experiments demonstrating that the N-terminus targets the molecule to the cell membrane and the C-terminus interacts with the IF network. In this study, the calculated length for both DPI and DPII was approximately 42 nm, measured perpendicular to the plasma membrane. However, this value corresponds to the predicted size of DPII based on sequencing analysis (Green *et al.*, 1990) and on rotary shadowing (O'Keefe *et al.*, 1989), whereas DPI was predicted to be about 130 nm in length. These results led North *et al.* (1999) to suggest that DPI is folded or coiled or

orientated at an angle to the membrane, and that DPII may determine the extent of the desmosomal IDP (Figure 1.4).

DP is the protein primarily responsible for mediating the various IF-desmosomal-protein interactions and is critical for normal desmosomal adhesion. The C-terminal domain of DP interacts with keratin IFs in epithelia, desmin IFs in the myocardial and Purkinje fibre cells of the heart and vimentin IFs in the meningeal cells and the follicular dendritic cells of lymph nodes (Fontao *et al.*, 2003; Franke & Moll, 1987; Kouklis *et al.*, 1994; Meng *et al.*, 1997; Stappenbeck *et al.*, 1993; Stappenbeck & Green, 1992). The relative contributions of the A, B and C subunits of PRD, of the flexible linker regions and of the terminal regulatory tail for interactions with IFs are not yet clear. However, several studies suggest that these contributions may differ according to the type of IF that is attached to the desmosome (Green & Hobbs, 2006). Phosphorylation of the serine residue at position 2849 within the terminal regulatory tail weakens the interaction between DP and keratin IFs (Stappenbeck *et al.*, 1994), which was supported by the observation that a point mutation at this site (S2849G) disrupts DP assembly into desmosomes (Godsel *et al.*, 2005) (1.7.2.4.3). Additional serine sites located in the key linking regions surrounding the PRD and tail were recently identified which could also influence the IF-binding properties of this domain (Beausoleil *et al.*, 2004; Green & Hobbs, 2006; Green & Simpson, 2007).

Besides DP's vital importance for the maintenance of tissue integrity, its involvement in the regulation of the ERK-Akt signalling pathway (Wan *et al.*, 2007) and in the organisation of microtubules during epidermal differentiation have been reported (Desai *et al.*, 2009).

1.4. The intermediate filament cytoskeleton

IFs are a type of protein fibres which, together with actin microfilaments and microtubules compose the cytoskeleton. IFs are pliant rod-shaped fibres with a diameter which is intermediate between those of microfilaments (7-8 nm) and microtubules (25 nm), and hence their designation as IFs. The IF super-family comprises five types (or families) of IF fibres, and each type contains a range of different proteins that are altogether encoded by approximately 70 different human genes. IFs are grouped into these five different types according to cell-, tissue-, differentiation- and development-

specific expression patterns. Most types of IFs are cytoplasmic (types I-IV) and extend from the nucleus to the cell membrane where they are anchored to cell-cell and cell-matrix junctions (Figure 1.6). Only type V-IFs (including lamins) are present within the nucleus. Type I IFs comprise the acidic keratins (keratins 9-20) and type II the basic keratins (keratins 1-8). Type III IFs include desmin, which is the IF fibre present in the heart muscle, and vimentin which is present in mesenchymal cells. Type IV IFs include neurofilaments. (Godsel *et al.*, 2008; Uitto *et al.*, 2007).

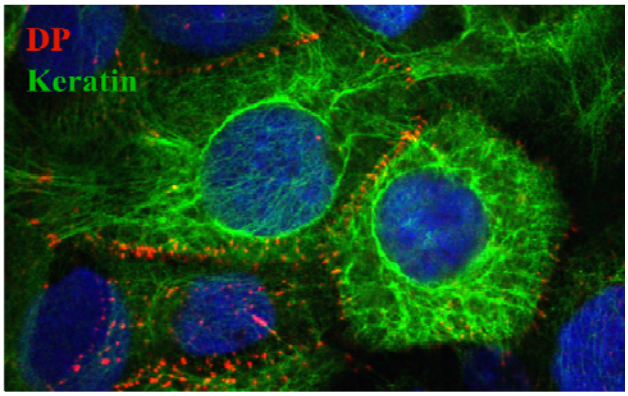

Figure 1.6. Double immunocytochemistry of HaCaT cells showing the keratin IF network and IF-desmosome attachments. Cytokeratin filaments extending from the nucleus to the cell periphery are shown (in green) connecting the cell sheet via desmosomes which are represented here by DP (in red).

All IF proteins are composed of a α-helical coiled-coil central rod domain, which is highly conserved, and more variable globular N- and C- terminal domains. The formation of IFs involves five sequential steps. First, similarly to DP, the rod domain is involved in dimerisation of IF proteins forming parallel coiled-coil apolar heterodimers (in the case of type I and type II keratins) or homodimers (in the case of type III IFs, such as desmin and vimentin). Second, these dimers associate laterally, in an anti-parallel fashion, to form tetramers with a staggered conformation. Third, these tetramers associate into higher order oligomers to form unit length filaments (ULF). Fourth, longitudinal annealing of ULF occurs to form filaments that are thicker than the mature IFs. Fifth, radial compression of these immature filaments results in the formation of the approximately 10 nm-wide mature filaments (reviewed in Godsel *et al.*, (2008).

Keratin IFs are major components of epithelial cells and are interconnected among cells or with the substratum via desmosomes and hemidesmosomes,

respectively. Together with these cell junctions, keratin IFs provide epithelial tissues with mechanical strength and resilience. Keratins always form heterodimers composed of one acidic and one basic keratin, which are tissue- and differentiation-specific (see section 1.6) (Kimyai-Asadi *et al.*, 2002).

1.5. Modulation of desmosomal adhesion

Desmosomes are not just static structures that glue cells together; instead, they are very dynamic and adaptable complexes as shown by their ability to adopt different conformations with different adhesive affinities (Garrod *et al.*, 2005; Kimura *et al.*, 2007; Wallis *et al.*, 2000). The "hyper-adhesive" state is the calcium-independent conformation, and therefore "hyper-adhesive" desmosomes do not disassemble in response to chelating agents (Garrod & Chidgey, 2008). Mature desmosomes in normal epidermis have this "hyper-adhesive" conformation which allows them to resist the forces of physical stress. However, this strongly adhesive state seems incompatible with cell motility which is necessary, for instance, during wound healing. For keratinocytes to migrate under the clot and close the wound, desmosomal adhesion needs to be down-regulated, and this coincides with a reversion to a calcium-dependent state. These more weakly adhesive desmosomes can separate into half desmosomes and be internalised following depletion of extracellular calcium. These different adhesive states correlate with ultrastructural changes within the desmosome. "Hyper-adhesive" desmosomes present with an electron-dense midline with cross-bridges extending to the plasma membrane, which is believed to represent a highly ordered and resistant structure. This midline is lost from desmosomes of wounded epidermis which have become calcium-dependent and less adhesive. Adherens junctions do not show this electron dense midline and are not able to become "hyper-adhesive", which is therefore a property thought to be unique to desmosomes (Garrod & Chidgey, 2008).

Protein kinase Cα (PKCα) activation was shown to occur at wound edges and to cause the switch to a calcium-dependent state (Wallis *et al.*, 2000). Additionally, in wound edge epidermis, PKCα becomes associated with the desmosomal plaque, where it co-localises with DP (Garrod *et al.*, 2005). These results indicate that the change in the adhesive state is produced by an "inside-out" signal by PKC which has been proposed to facilitate epithelial remodelling (Wallis *et al.*, 2000). Therefore, altered

phosphorylation of desmosome and/or associated cytoskeletal components, DP and PG being likely candidates, may shift the desmosome to a less adhesive state (Garrod & Chidgey, 2008).

Low calcium concentrations in culture inhibit the formation of cell-cell junctions and cause these junctions to be disassembled. Immature desmosomes, which refers to desmosomes that have not yet reached a calcium-independent conformation, are also disassembled by calcium chelating agents. However, mature or calcium-independent desmosomes in a confluent cell sheet will remain unaffected. Interestingly, South *et al.* (2003) demonstrated that PKP1-null immortalised keratinocytes were unable to become mature or calcium-independent in culture, suggesting a role for PKP1 in desmosome maturation. Further studies will be necessary to understand the detailed mechanisms leading to desmosome stability and the contributions of each desmosomal protein other than their adhesive functions.

1.6. The desmosome and intermediate filament network composition changes in a tissue- and differentiation-specific manner

As mentioned in section 1.3.1, desmosomes vary in appearance, size and composition in different cell types and during epidermal differentiation. IFs associated with desmosomes also exhibit tissue- and differentiation-specificity. DP and PG are expressed in all tissues that contain desmosomes and in all layers of the stratifying epidermis (Figure 1.7) despite these variations.

In the skin, desmosomes and adherens junctions appear to be distinct structures, the only component in common between the two junctions being PG. In contrast, the intercalated disc of the myocardium has mix-typed junctions (the “area composita”, see section 1.3.2.2.2) that resemble both desmosomes and adherens junctions. These mixed junctions contain the desmosomal proteins DP, PKP2, DSG2 and DSC2, together with the adherens junction proteins N-cadherin, cadherin-11, β-catenin, α-catenin, ARVCF, afadin and p120-catenin, the tight junction protein ZO-1, as well as proteins that can be present in more than one type of junction such as PG, p0071 and vinculin (Borrmann *et al.*, 2006). In these junctions PKP2 was also shown to associate with αT-catenin forming another link between the cadherin-catenin complex and the IF-network via a desmosomal protein (Goossens *et al.*, 2007).

DSG1, DSG3 and DSG4 as well as DSC1 and DSC3 are restricted to stratified epithelial tissues. In contrast, DSG2 and DSC2 are expressed in all desmosome-possessing tissues, including the myocardium and simple epithelia (Garrod *et al.*, 2002; Ishii & Green, 2001). Hence, desmosomes of tissues such as the colon and cardiac muscle only contain DSG2 and DSC2. In the epidermis, DSG2 is restricted to the basal layer. DSC2, DSC3 and DSG3 are expressed in a gradient with the highest levels in the basal layer and minimal levels in the spinous or granular layers (Figure 1.7). In contrast, the expression pattern of DSG1 and DSC1 follows a gradient pointing in the opposite direction, with the highest expression levels in the upper layers, particularly in the granular layer. DSG4 is highly represented in the hair follicle and is also expressed in the granular layer, predominantly in the upper cell layer (Figure 1.7). The same cell expresses several different desmosomal cadherin isoforms and single desmosomes contain more than one DSG and more than one DSC isoform (North *et al.*, 1996; Nuber *et al.*, 1996; Shimizu *et al.*, 1995).

PKPs 1-3 also show complex tissue-specific patterns of expression. PKP1 is a major component of desmosomes in stratifying and complex epithelia but is also widely expressed in the nuclei of cells that lack desmosomes (Schmidt *et al.*, 1997). PKP2 is expressed in all tissues that have desmosomes and also in some cell types lacking desmosomes, and is the only PKP isoform expressed in the myocardium (Chen *et al.*, 2002; Mertens *et al.*, 1996). PKP3 is present in desmosomes of most simple and almost all stratified epithelia, with the exception of hepatocytes, and is also absent from cardiomyocytes. All three isoforms are expressed in the epidermis. While PKP3 is expressed at similar levels throughout all layers of the epidermis, PKP2 is prominent in the basal and spinous layers and PKP1 is most abundant in the upper spinous and granular layers (South, 2004) (see Figure 1.7).

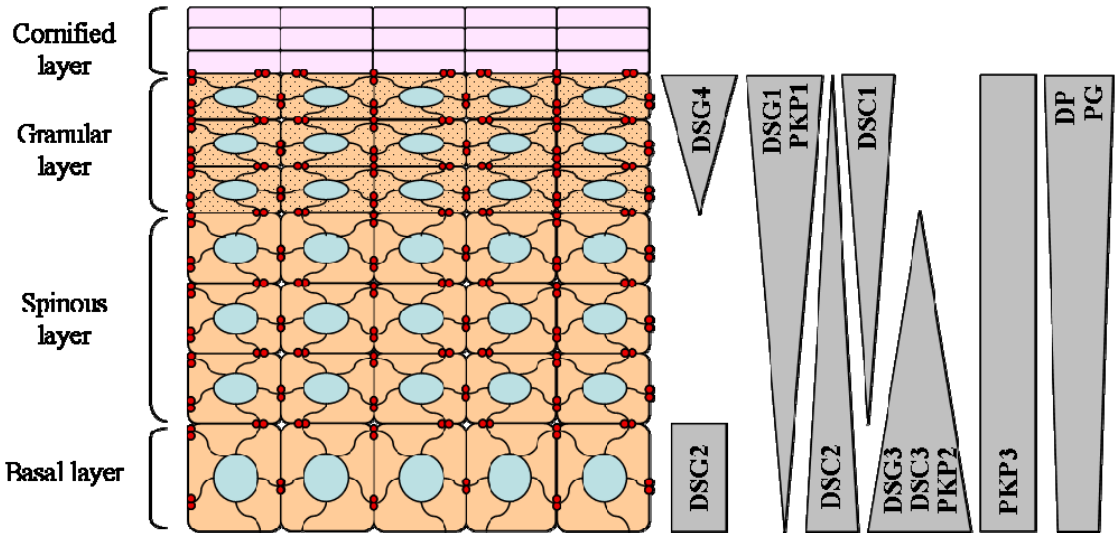

Figure 1.7. The desmosomal composition varies in a differentiation-specific manner. Schematic of the epidermis showing differential expression of desmosomal proteins according to differentiation stage. The basal epidermal layer is rich in DSG2/3, DSC2/3 and PKP2. Expression of these proteins ceases (in the case of DSG2) or decreases with increased differentiation, and is minimal in the granular layer. In contrast, expression of DSG4, DSG1, PKP1 and DSC1 is patterned in a gradient that points in the opposite direction. Expression of PKP3, PG and DP is approximately constant throughout all layers of the epidermis. Adapted from Desai *et al.* (2009).

The expression patterns of the desmosome-associated keratin IFs also vary according to the type of tissue and during epidermal differentiation. Keratins 8/18 are typical of simple epithelial cells. In interfollicular epidermis, keratins 5/14 are predominant in the basal keratinocytes, while keratins 1/10 are only expressed in suprabasal keratinocytes. The pair of keratins 2e/10 is also expressed in the upper spinous and granular layers. Keratins 6a/16 and 6b/17 are expressed in suprabasal keratinocytes of interfollicular epidermis during processes such as wound healing or hyperproliferation. In palmoplantar epidermis, keratins 1/9 are the major representatives of suprabasal cells, but keratins 6a/16 are also expressed. Palmoplantar epidermis (acral epidermis) is much thicker and expresses higher levels of keratin IFs than non-acral epidermis. These keratin IFs also form denser aggregates in the upper spinous and granular layers, which provide extra resistance and structural support to the mechanical stress-bearing palmoplantar epidermis (Kimyai-Asadi *et al.*, 2002).

1.7. Desmosome hereditary disease and mouse models

Skin and heart are tissues that experience mechanical stress on a daily basis. In order to resist these physical forces, the epidermis and the intercalated disc of the myocardium have evolved strong and resilient desmosomes that are tailored to serve these different tissues. When desmosomal components are disrupted, either by naturally occurring or engineered genetic mutations or in autoimmune disease, adhesion between keratinocytes and cardiomyocytes fails leading to diseases of skin, hair and heart (Cheng *et al.*, 2005; McGrath, 2005). These diseases are designated as cardio-cutaneous syndromes (Bolling & Jonkman, 2009).

1.7.1. Palmoplantar keratoderma and arrhythmogenic right ventricular cardiomyopathy

Hereditary PPKs are a large and highly heterogeneous group of skin disorders that can be inherited as both autosomal dominant and recessive traits. These disorders are generally characterised by thickening and hyperkeratosis of the epidermis from palms and soles. The PPKs can be divided into three groups – simple, complex and syndromic – according to the observed phenotypes. Simple (or non-syndromic) keratodermas affect only the palmoplantar epidermis whereas complex keratodermas also manifest as lesions of non-volar skin, hair, teeth, nails or sweat glands. Syndromic keratodermas involve abnormalities in other organs such as cardiomyopathy, cancer, or deafness (Braun-Falco, 2009; Hatsell & Kelsell, 2000). PPKs can also be divided into three sub-groups based on clinical appearance, namely focal, diffuse and punctate PPK. In focal PPK, the lesions are restricted to pressure points and sites of recurrent friction, whereas in diffuse PPK the thickening of the epidermis is uniformly observed across the palmoplantar surface. Striate PPK (SPPK) is a sub-type of focal PPKs characterised by linear hyperkeratosis on the digits. Punctate PPKs are characterised by the development of numerous and small hyperkeratotic nodules (Hatsell & Kelsell, 2000).

PPKs can additionally be classified as epidermolytic (EPPK) or non-epidermolytic (NEPPK) based on histological as well as clinical observations. Histologically, EPPK shows clear spaces of different sizes around keratinocyte nuclei (perinuclear vacuolisation) in the upper spinous and granular layers. Cytolysis, blistering, clumping of keratin IFs and keratohyalin granules of various shapes in

suprabasal layers are also observed in EPPK (Ross *et al.*, 2008). These characteristics are not observed in NEPPK.

Arrhythmogenic right ventricular cardiomyopathy/dysplasia (ARVC/D) is a genetic heart disorder that results in fibro-fatty replacement of right ventricular myocytes and consequent ventricular arrhythmias (Fontaine *et al.*, 1999). Involvement of the left ventricle may also occur. Although ARVC is an infrequent cardiomyopathy, it is one of the most common causes of unexpected sudden death in the young, particularly athletes (Basso *et al.*, 1996; Thiene *et al.*, 1988). The prevalence of ARVC/D is estimated to range between 1/2000 and 1/5000 in the general population and a genetic cause has been demonstrated in at least 50% of the cases (Corrado & Thiene, 2006). To date, seven genes have been implicated in the pathogenesis of ARVC, of which five encode proteins of the cardiac desmosome (Table 1.1). Two non-desmosomal genes have been associated with specific types of ARVC, namely the gene encoding the cardiac ryanodine receptor 2 (RyR2) reported in ARVC type 2 (ARVC2) (Danieli & Rampazzo, 2002; Tiso *et al.*, 2001) and the gene encoding transforming growth factor-β3 (TGFβ3) in ARVC type 1 (ARVC1) (Beffagna *et al.*, 2005).

ARVC can be inherited as an autosomal dominant trait with variable penetrance or as a recessive trait, usually associated with skin disease. The latter phenotype is called syndromic form of ARVC, of which Naxos disease and Carvajal syndrome are examples. Naxos disease manifests as diffuse PPK, woolly hair and right ventricular cardiomyopathy, whereas Carvajal syndrome consists of SPPK, woolly hair and dilated left ventricular cardiomyopathy (Braun-Falco, 2009). The Carvajal syndrome is clinically similar but more severe than Naxos disease in which ARVC usually appears later. Additionally, the cardiomyopathy in Carvajal syndrome affects usually the left ventricle which shows no adipose depositions, in contrast with Naxos cardiomyopathy which affects the right ventricle and which hallmark is the fibrofatty replacement (Bolling & Jonkman, 2009). McKenna *et al.* (1994) first described a number of clinical criteria, known as the "Task Force criteria" to diagnose patients with ARVC/D. These criteria include electrical and histopathological features of the myocardium as well as clinical characteristics (Vatta *et al.*, 2007).

1.7.2. Genetic mutations affecting desmosome components and associated proteins lead to cardio-cutaneous disease

Human inherited disease of the desmosome can be caused by mutations in genes encoding desmosomal cadherins, armadillo or plakin proteins, which are the three major desmosomal protein families. The target genes include *DSP*, *JUP*, *PKP1* and *PKP2*, *DSG1*, *DSG2* and *DSG4*, *DSC*2 and *DSC3*. Table 1.1 summarises the range of human phenotypes resulting from dominant or recessive mutations in desmosomal genes. Defects in different desmosomal components, such as DP and DSG1 or DP and PG, can lead to similar clinical phenotypes, such as SPPK and Carvajal/Naxos syndrome, respectively. Additionally, similar phenotypes can arise from mutations affecting different regions of the same protein, for instance ARVC caused by *DSP* mutations (Figure1.8). In contrast, mutations affecting the same functional domain of one protein can cause distinct clinical features in much the same way as mutations in different desmosomal components. This lack of correlation between the genotypes and phenotypic characteristics may suggest that apart from having a common adhesive function, some desmosomal proteins may participate in other overlapping processes, such as cytoskeletal organization, cell signalling, and tissue patterning (Kottke *et al.*, 2006).

Desmosomal proteins involved in disease restricted to the skin and/or its appendages are DSG1, DSG4, DSC3, PKP1 and DP. Heterozygous mutations in the genes encoding DSG1 (Rickman *et al.*, 1999), DP (Armstrong *et al.*, 1999; Whittock *et al.*, 1999) and additionally the gene encoding the IF protein keratin 1 (Whittock *et al.*, 2002a) can cause non-syndromic SPPK. Mutations in the gene encoding PKP1 cause a distinct phenotype involving skin and hair abnormalities called ectodermal dysplasia-skin fragility syndrome which was first described by McGrath *et al.* (1997). Mutations in the genes encoding DSG4 and recently DSC3, have been reported to lead to hypotrichosis, which is a hair disorder characterised by thin and sparse scalp hair as well as sparse or absent eyebrows and eyelashes and atrophic hair follicles (Ayub *et al.*, 2009; Kljuic *et al.*, 2003). The DSC3 mutation also resulted in recurrent skin vesicles filled with fluid (Ayub *et al.*, 2009).

Desmosomal proteins involved in non-syndromic cardiomyopathy are DSG2, DSC2, PKP2, DP and PG. Proteins that can cause both heart and skin disease are DP,

PG and DSC2 (Bolling & Jonkman, 2009). Dominant mutations are usually associated with the non-syndromic forms of either skin or heart disease whereas recessive mutations usually cause the syndromic forms (see Table 1.1).

Mutations in genes encoding the basal (epidermal) keratin pair 5/14 (Kang *et al.*, 2010) as well as plectin (Bolling *et al.*, 2009) (which is considered an accessory protein in the desmosome) can result in epidermolysis bullosa (EB) simplex. EB is a skin disease mainly characterized by severe skin fragility, including erosions and blistering in response to minor trauma. These plectin mutations were associated with early onset dilated cardiomyopathy additionally to EB simplex (Bolling *et al.*, 2009). Mutations in keratin 14 can also lead to keratoderma disorders in the same way as mutations in the suprabasal keratins 1, 2, 9, 10 and 16 (Uitto *et al.*, 2007). In particular, mutations in the genes encoding keratin 1 and keratin 9 cause EPPK (Godsel *et al.*, 2008; Uitto *et al.*, 2007), which is a phenotype that can also be caused by mutations in *DSP*. As expected, while mutations in basal keratins affect predominantly the basal layer of the epidermis, mutations in suprabasal keratins lead to problems in the upper epidermal layers. Mutations in desmin (which forms the heart muscle IF network, see section 1.4), in contrast, result in cardiomyopathies. Coupled with other mutations in desmosomal components, these observations suggest that an adhesion impairment, which is aggravated by mechanical stress, results from defects in any region of the desmosome-IF complex, leading to fragility of the skin and heart. This implies that the desmosome-IF complex provides mechanical integrity to these tissues.

This thesis will be focused on the desmosomal components DP and PG; therefore an overview of the consequences of natural or engineered mutations in the genes encoding these proteins is given in the following sections.

Table 1.1. Distinct phenotypes resulting from dominant and recessive mutations in desmosomal genes

<table>
<tr><th rowspan="2">Gene</th><th rowspan="2">Mode of inheritance</th><th colspan="3">Phenotypes</th></tr>
<tr><th>Skin</th><th>Hair</th><th>Heart</th></tr>
<tr><td>PKP1</td><td>Recessive</td><td colspan="2">Ectodermal-dysplasia skin fragility syndrome</td><td></td></tr>
<tr><td rowspan="2">PKP2</td><td>Dominant</td><td></td><td></td><td>ARVC</td></tr>
<tr><td>Recessive</td><td></td><td></td><td>ARVC</td></tr>
<tr><td rowspan="2">JUP</td><td>Dominant</td><td></td><td></td><td>ARVC</td></tr>
<tr><td>Recessive</td><td colspan="3">Naxos disease</td></tr>
<tr><td rowspan="7">DSP</td><td rowspan="2">Dominant</td><td>SPPK</td><td></td><td>ARVC</td></tr>
<tr><td colspan="3">SPPK, woolly hair and ARVC</td></tr>
<tr><td rowspan="5">Recessive</td><td colspan="3">Bullous dermatosis, PPK, total alopecia and ARVC</td></tr>
<tr><td colspan="3">Carvajal syndrome</td></tr>
<tr><td colspan="3">Lethal acantholytic epidermolysis bullosa</td></tr>
<tr><td colspan="3">Ectodermal-dysplasia skin fragility syndrome and ARVC</td></tr>
<tr><td colspan="2">Focal and diffuse PPK and woolly hair</td><td></td></tr>
<tr><td>DSG1</td><td>Dominant</td><td>SPPK</td><td></td><td></td></tr>
<tr><td rowspan="2">DSG2</td><td>Dominant</td><td></td><td></td><td>ARVC</td></tr>
<tr><td>Recessive</td><td></td><td></td><td>ARVC</td></tr>
<tr><td>DSG4</td><td>Recessive</td><td></td><td>Hypotrichosis</td><td></td></tr>
<tr><td rowspan="2">DSC2</td><td>Dominant</td><td></td><td></td><td>ARVC</td></tr>
<tr><td>Recessive</td><td colspan="3">PPK, woolly hair and ARVC</td></tr>
<tr><td>DSC3</td><td>Recessive</td><td colspan="2">Hypothrichosis and recurrent skin vesicles</td><td></td></tr>
</table>

1.7.2.1. Plakoglobin mouse models

Mouse knock-out studies have highlighted the importance of PG in both the epidermis and the heart during development. PG-null mutant mouse embryos generated through gene targeting die between embryonic days E10.5-E16 due to severe heart problems (Bierkamp *et al.*, 1996; Ruiz *et al.*, 1996). Although some mutant embryos developed further (12 out of 121 embryos), they died around birth with additional severe skin fragility, reminiscent of the human blistering disease, epidermolytic hyperkeratosis (EPPK) (Bierkamp *et al.*, 1996). Ultrastructural analysis revealed that desmosomes had altered structure and were reduced in number in both the skin and heart of PG-null mice (Bierkamp *et al.*, 1996). Additionally, PG's closest homologue, β-catenin, was shown to become localized to desmosomes in the heart of *JUP*$^{-/-}$ embryos (Ruiz *et al.*, 1996) and to associate with DSGs in *JUP*$^{-/-}$ embryonic skin (Bierkamp *et al.*, 1996).

1.7.2.2. Plakoglobin and Naxos disease or ARVC

Following these studies with PG knock-out mouse models, it was found that the autosomal recessive Naxos disease mapped to 17q21.2, a locus that was known to include the *JUP* gene (Coonar *et al.*, 1998). Sequence analysis of Naxos patient DNA revealed a homozygous deletion of 2 bp (*JUP*2157delTG) close to the 3' end of *JUP* (McKoy *et al.*, 2000). This deletion caused a frameshift and resulted in the truncation the C-terminal domain of PG (McKoy *et al.*, 2000). Although PG-null mice exhibited a more severe phenotype with skin blistering from acantholysis, Naxos patients present with diffuse PPK which does not show blistering. Heterozygous carriers of this mutation show minor abnormalities on electrocardiography but no skin phenotype (Protonotarios *et al.*, 2001). Genetic linkage has demonstrated that loci other than *JUP* can cause Naxos disease, but to date no other candidate genes have been described (Stuhrmann *et al.*, 2004).

Recently, a second human *JUP* mutation has been identified. This is an autosomal dominant 3 bp-insertion mutation, S39K40insS, found in a family with ARVC but no cutaneous abnormalities (Asimaki *et al.*, 2007).

1.7.2.3. Desmoplakin mouse models

Ablation of DP in the germline of mice through the use of gene targeting results in embryonic lethality at E6.5 (Gallicano *et al.*, 1998), which is earlier than in PG-null mice (Bierkamp *et al.*, 1996; Ruiz *et al.*, 1996) (see section 1.7.2.1). These developing embryos had a reduced number of desmosomes (approximately 10 times) and the few remaining desmosomes showed a disrupted IF network and lack of keratin IF attachment. These results suggested a role for DP in the formation and stabilisation of the desmosome, besides its previously known role in desmosome-IF attachment (Gallicano *et al.*, 1998). To study the function of DP specifically in later embryonic development, a tetraploid aggregation approach was carried out by the same researchers to rescue the lethal phenotype and the functions of extraembryonic tissues in $DSP^{-/-}$ embryos. The resulting mice were partially rescued up to E10 of embryonic development but still exhibited heart, skin and neuroepithelium abnormalities, which were more severe than the ones observed in PG-null embryos. Defects in

microvasculature, which have complexus adherens instead of desmosomes, were also observed (Gallicano *et al.*, 1998).

Recently, another report described the conditional ablation of DP in the heart of mice generated by crossing α–myosin heavy chain–Cre recombinase transgenic mice and floxed *DSP* mice. The resulting animals also died from E11 onwards due to severe cardiac abnormalities (Garcia-Gras *et al.*, 2006). A conditional DP mouse knock-out was also generated to investigate the role of DP in the skin (Vasioukhin *et al.*, 2001). The *DSP* gene was inactivated specifically in the epidermis by breading *DSP* floxed mice with mice transgenic for the Cre recombinase under the control of the keratin 14 promoter, which is active in basal cells of the epidermis. Newborn mice lacking DP in the epidermis showed severe skin defects including stress-induced intercellular separations, terminal differentiation problems and loss of barrier function. Although the number of desmosomes in DP-null epidermis was comparable to wild type epidermis, they lacked an IDP and IF attachment was impaired. DP-null cultured keratinocytes derived from these mice showed reduced number of desmosomes as well as lack of actin reorganisation and reduced adherens junctions. This result highlighted the interdependence between desmosomes and the microfilament-associated adherens junctions, as adherens junctions failed to properly mature in DP-null cells *in vivo* and *in vitro* (Vasioukhin *et al.*, 2001). DP has also recently been implicated in the rearrangement of the microtubule cytoskeleton during epidermal differentiation (Lechler & Fuchs, 2007).

Taken together, these studies revealed the importance of DP for morphogenesis, integrity and function of epithelial and cardio-vascular tissues both during early development and later for the correct architecture and function of tissues such as the epidermis and the heart (Green & Hobbs, 2006).

1.7.2.4. Human mutations in desmoplakin lead to defects of skin, hair and heart

Human *DSP* mutations can be inherited with both autosomal dominant and recessive modes of transmission. In contrast with only two *JUP* mutations identified so far, 36 mutations have been described in the *DSP* gene. These mutations can result in different cardio-cutaneous disorders that range from relatively mild skin conditions caused by DP haploinsufficiency, to severe skin fragility and morphogenetic defects or

death due to ARVC (Green & Hobbs, 2006). Figure 1.8 and the following sections summarise the *DSP* mutations identified so far and their associated phenotypes.

1.7.2.4.1. Desmoplakin and skin disease

The first reported *DSP* mutations were autosomal dominant nonsense (p.Q331X) and splice site (939+1G>A) mutations leading to haploinsufficiency (Armstrong *et al.*, 1999; Whittock *et al.*, 1999). Affected individuals presented with SPPK, aggravated by mechanical trauma. Histological and ultrastructural analysis of lesional skin revealed widening of intercellular spaces between suprabasal keratinocytes, fewer desmosomes and clumping of keratin IFs. Heterozygous DP-null newborn mice, in contrast, did not show any histological defects (Gallicano *et al.*, 1998).

Whittock *et al.* (2002b) described two unrelated individuals with autosomal recessive mutations in *DSP*. These patients had focal or diffuse PPK and woolly hair with varying degrees of alopecia. Both of these cases were compound heterozygotes for nonsense/missense combinations of mutations (p.C809X/p.N287K and p.Q664X/p.R2366C). While heterozygous carriers of any of these mutations displayed no phenotypic abnormalities, the combination of DP haploinsufficiency with a missense mutation led to a disease phenotype (Figure 1.8).

1.7.2.4.2. Desmoplakin and cardio-cutaneous disease

The first human autosomal recessive mutation in *DSP* leading to a cardio-cutaneous phenotype was described by Norgett *et al.* (2000). Following an earlier clinical description of the same family (Carvajal-Huerta, 1998), this phenotype is now referred to as Carvajal syndrome (see section 1.7.1). Affected family members were homozygous for 7901delG (p.S2542fsX2560), a deletion that results in the truncation of DP just downstream of the B plakin repeat domain (PRD), and presented with heart failure early in life due to cardiomyopathy. Histological analysis of these patients' skin revealed widened intercellular spaces and collapsed IFs. Cells derived from these patients exhibited weakened adhesion when subject to stress *in vitro* (Huen *et al.*, 2002). Another C-terminal homozygous missense mutation (p.G2375R) was shown to cause defects in skin, hair and heart in a Naxos-like fashion (Alcalai *et al.*, 2003). As mentioned above, a mutation in the same domain of DP (p.R2366C, motif B of the

PRD, Figure 1.8) led to skin abnormalities only, when in a haploinsufficiency background (Whittock *et al.*, 2002b). Compound heterozygous mutations (p.R1934X/ p.L2031fsX2058) within the last exon of *DSP* leading to truncations of the IF-binding domain of DP were shown to cause a lethal condition named "lethal acantholytic epidermolysis bullosa" (Jonkman *et al.*, 2005). This patient presented with extremely severe fragility of the skin and mucous membranes, complete alopecia, neonatal teeth and nail loss and died 10 days after birth from heart failure, probably in combination with massive trans-cutaneous fluid loss. This is the most severe human phenotype caused by *DSP* mutations and resembles the phenotype of conditional epidermal DP-null mice which die early after birth. Histological analysis revealed acantholysis throughout the spinous layer of the epidermis, with an intracellular split between the desmosomal IDP and the IF network. Electron microscopy revealed relatively normal desmosomes, but which were often torn out of adjacent cells due to the lack of cytoskeletal attachment to the plaque. These observations underscored the importance of DP and IF attachment for epidermal integrity (Bolling & Jonkman, 2009).

Norgett *et al.* (2006) went on to describe a dominant case of left sided ARVC, SPPK and woolly hair in a patient harbouring a 30 bp insertion in exon 14 of *DSP* (c.1823_1824 ins30 bp, p.I608ins10), predicted to result in the insertion of 10 extra amino acids to the N-terminus of DP (Norgett *et al.*, 2006) (see Chapter 5).

The rod domain of DP is thought to be involved in the dimerisation of this protein (see section 1.3.2.2.2). A homozygous nonsense mutation within the DPI-specific region (p.R1267X) was found to result in complete loss of DPI, without affecting DPII (Uzumcu *et al.*, 2006). This patient had a severe form of a Naxos-like syndrome with skin, heart and hair involvement and died at the age of four of heart failure (see Chapter 5). Other mutations affecting the DPI-specific region of the rod domain were found recently, also associated with cardiomyopathy with or without skin disease. These cases are introduced here and in the following section (1.7.2.4.3). Compound heterozygous deletions affecting the N-terminus (p.H839fsX23) and the DPI-specific rod domain (p.N1324fsX23) were found in a patient with a phenotype involving PPK, skin fragility, woolly hair and severe biventricular dilated cardiomyopathy (Tanaka *et al.*, 2009). Compound heterozygous nonsense mutations affecting the N-terminus (p.Q673X) and the DPI-specific region of the rod domain (p.Q1446X) were associated with complete alopecia, PPK, skin fragility and left sided

dilated cardiomyopathy leading to death at the age of nine. The phenotype of this child was designated as epidermolytic bullous dermatosis with associated lethal cardiomyopathy (Asimaki *et al.*, 2009a) (Figure 1.8).

1.7.2.4.3. Desmoplakin and arrhythmogenic right/left ventricular cardiomyopathy

The majority of *DSP* mutations leading to arrhythmogenic right/left ventricular cardiomyopathy (AR/LVC) without skin or hair involvement are inherited in a dominant fashion. Three heterozygous missense mutations (p.R1255K, p.R1755I and p.K1583R) affecting the DPI-specific part of the rod domain were found to cause ARVC (Basso *et al.*, 2006; Bauce *et al.*, 2005). One of these mutations (p.R1755I) was predicted by structural analysis to cause impairment on dimerisation (Bauce *et al.*, 2005). A heterozygous nonsense mutation (p.R1113X) affecting the region of the rod domain that is common to both DPI and DPII caused AR/LVC resulting in sudden cardiac death at the age of 36 (Asimaki *et al.*, 2009a). Immunohistochemistry of this patient's heart revealed markedly reduced expression of DP and PG at the intercalated disc but normal PKP2 and N-cadherin staining.

A heterozygous missense mutation (p.R2834H) in the region encoding the C-terminus was also found to be the cause of ARVC (Yang *et al.*, 2006). Transgenic mice conditionally over-expressing this mutant in the heart showed enlargement of both ventricles and cardiac dysfunction accompanied by an increased cardiomyocyte apoptosis, cardiac fibrosis and lipid accumulation, which are symptoms that recapitulate the human disease. In these mice, desmin IFs failed to co-localise with DP in the intercalated disc indicating disruption of DP-desmin interactions. Interestingly, this mutation occurs close to serine 2849, which is a phosphorylation site known to be important for regulation of DP-IF interactions (Godsel *et al.*, 2005). Two additional heterozygous C-terminal missense mutations caused ARVC leading to sudden death in one of the cases (p.R2541K) (Beffagna *et al.*, 2008). This patient also carried another missense mutation (p.V30M). In the other case (p.R2639Q), a rare SNP could not be excluded (Yu *et al.*, 2008).

Missense mutations in the N-terminus of DP were also found to cause AR/LVC. One of these mutations (p.S299R) modifies a potential phosphorylation site in this region (Rampazzo *et al.*, 2002). Two other DP mutants (p.V30M and p.Q90R) were

unable to localise to the plasma membrane and to interact with PG *in vitro* (Yang *et al.*, 2006). Two additional missense mutations (p.S507F and p.S442F) were found to cause cardiomyopathy with biventricular involvement and led to sudden death at the ages of 32 and 44 (Sen-Chowdhry *et al.*, 2008). Another two dominant missense mutations in the N-terminus of DP (p.K470E, p.A566T), as well as compound heterozygosity for these two mutations, were also found to lead to ARVC (Basso *et al.*, 2006).

Three heterozygous splice site mutations, possibly leading to haploinsufficiency, also in the N-terminus of DP caused AR/LVC, in one case leading to sudden death at the age of 25 (423-1G>A) (Asimaki *et al.*, 2009a; Basso *et al.*, 2006; Bauce *et al.*, 2005). A dominant nonsense mutant led to ARVC due to haploinsufficiency (p.W233X) (Yang *et al.*, 2006). A single bp insertion (c.2034insA) caused a frameshift which led to the production of a truncated protein, which contained the first 586 amino acids of the N-terminal domain and eight additional non-DP residues (p.T586fsX594) (Norman *et al.*, 2005). This mutation was associated with ALVC. A deletion of one bp also leading to a frameshift (p.S1015fsX1017) was associated with AR/LVC (with involvement of both ventricles) and sudden death at the age of 26 (Sen-Chowdhry *et al.*, 2008).

All together, these observations highlight the importance of DP for maintenance of heart integrity and normal function. Additionally, they indicate that cardiomyopathies involving the right or left ventricles as well as both can be caused by dominant or recessive mutations, including missense, splice site, insertion, deletion and nonsense mutations, which can lead to DP haploinsufficiency, absence of DP isoforms or C-terminal truncations as well as amino acid substitutions (Figure 1.8).

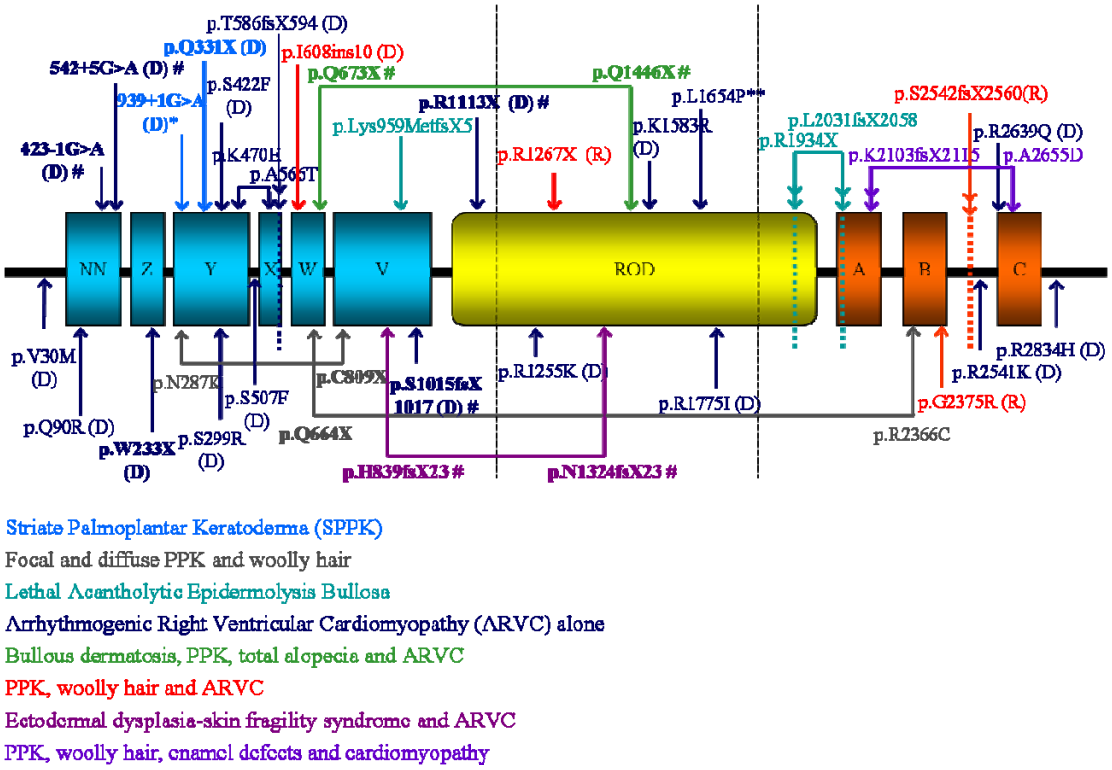

Figure 1.8. Schematic of DP showing the locations of reported mutations causing cardio-cutaneous disease. DP consists of three functionally distinct domains (N-terminus, Rod and C-terminus depicted in blue, yellow and orange, respectively). Mutations are colour coded according to the different resulting phenotypes. Mutations causing haploinsufficiency are depicted in bold print; # refers to mutations that are predicted to result in haploinsufficiency although confirmation is lacking; mutations resulting in a truncated protein are marked by vertical discontinuous bars; mutations connected by a horizontal line are compound heterozygous mutations; mutations located within the two discontinuous vertical black lines are DPI-isoform-specific. D = dominant; R = recessive; * 939+1G>A splice site mutation has also been reported to cause non-syndromic ARVC; ** L1654P mutation was present in conjunction with a heterozygous PKP2 nonsense mutation in a patient with ARVC. Adapted from Bolling and Jonkman (2009).

1.8. RNA interference as an experimental tool to study the effect of mutations causing protein loss

The RNA interference (RNAi) pathway is a conserved biological mechanism of post-transcriptional regulation of gene expression and of protection of the genome from internal and external threats in animals and plants (Hannon, 2002). It is triggered by either long, usually exogenous, double-stranded RNAs which are cleaved into double-stranded short interference RNAs (siRNAs) or by endogenous precursor transcripts named primary microRNAs (pri-miRNAs) which are subsequently processed into miRNAs. The RNase III enzyme Dicer is responsible for the excision of siRNAs and

miRNAs from their precursor RNA duplexes in the cytoplasm, producing 20-24 nucleotide duplexes paired in a way that leaves two-nucleotide 3' overhangs (Carthew & Sontheimer, 2009). One of the strands, the antisense or guide strand, is uploaded into the RNA-induced silencing complex (RISC), which is then guided to the complementary sequence of the target mRNA to be silenced. The other strand, the sense or passenger strand, is ultimately degraded (Ghildiyal & Zamore, 2009). Perfect complementarity between the guide strand and the target mRNA induces the catalytic component of RISC, named argonaute, to cleave the target mRNA at a very precise site (Tomari & Zamore, 2005) leading to its subsequent degradation by cellular exonucleases (Orban & Izaurralde, 2005).

As an experimental tool, chemically synthesized siRNAs which mimic Dicer products can be introduced into the cytoplasm of cultured cells. These synthetic siRNAs will transiently trigger the biological response of the RNAi pathway and lead to target mRNA degradation (Elbashir *et al.*, 2001).

One of the differences between siRNAs and miRNAs is that while siRNAs are perfectly complementary to sequences within the target mRNAs, most miRNAs bind with mismatches and bulges to the 3'UTRs of target mRNAs. Only nucleotides 2-8 within the 5' end of miRNAs, representing the seed region, need to be perfectly complementary to their targets in order to cause silencing. Given the small size of the seed region, a single miRNA can regulate many different genes. siRNAs can also bind imperfectly to unintended mRNA targets in a miRNA-like fashion. This is of considerable practical importance when performing siRNA mediated gene silencing, as it appears to account for most off-target effects of siRNAs (Carthew & Sontheimer, 2009).

1.9. Hypothesis of this study

Two major hypotheses, which are described below, prompted the work described in this thesis. The first hypothesis emerged from the finding that three non-consanguineous patients originating from Argentina presented with a cutaneous phenotype consisting of skin fragility, PPK and woolly hair, but no symptoms of cardiomyopathy. These patients were suspected of having a recessive desmosomal disease caused by a genetic mutation in one of the desmosomal genes.

The second hypothesis of this thesis is based on three different types of mutations in the *DSP* gene that were previously identified and affect different domains of DP. One of the mutations is a *DSPI* isoform-specific nonsense mutation leading to absence of DPI, two other mutations cause DPI/DPII haploinsufficiency and the third type is a dominant *DSPI/DSPII* 30 bp-insertion in the 5' end of the gene. All three mutations are associated with PPK, which is syndromic (affecting also the heart) both in the case of the *DSPI*-specific mutation and the *DSPI/DSPII* insertion mutation and non-syndromic for the DPI/DPII haploinsufficiency mutations. The clinical features of the affected patients vary in terms of the severity of skin and heart disease (see Chapter 5). The *DSPI*-specific nonsense mutation was shown to cause complete absence of DPI in patient skin by immunohistochemistry, but no further studies were carried out to investigate the effect and molecular mechanisms of this mutation (Uzumcu *et al.*, 2006). The DP haploinsufficiency mutations were shown by immunohistochemistry and electron microscopy to cause thickening of the epidermis and impaired cell-cell adhesion with widening of intercellular spaces and DP-IF detachment (Armstrong *et al.*, 1999; Wan *et al.*, 2004; Whittock *et al.*, 1999). The 30 bp-insertion mutation was shown to result in discontinuous distribution of DP and PG around the cell membrane with some cytoplasmic localisation, particularly in the lower layers of the epidermis (Norgett *et al.*, 2006). These results suggest that these different *DSP* mutations have different effects on intercellular adhesion and on the distribution and cellular localisation of DP and DP-associated proteins. Additionally, the different mutations seem to disrupt different differentiation-specific binding partners, as the 30 bp-insertion mutation appears to affect predominantly the lower regions of the epidermis while the haploinsufficiency mutations cause abnormalities mainly in the upper layers. Equally, different DP isoforms may have different functions within the desmosome, as shown by the fact that DPII alone cannot fully compensate for the absence of DPI in a patient harbouring the *DSPI*-specific nonsense mutation (see Chapter 5).

The hypothesis of this thesis are: (1) the three Argentinean unrelated patients, who present with similar clinical features, harbour a common disease-causing mutation in a desmosomal gene, inherited as a recessive trait; (2) different mutations in the same desmosomal gene, *DSP*, will affect different aspects of keratinocyte and cardiomyocyte adhesion, differentiation and/or signalling; and (3) the different DP isoforms and

different binding sites within this protein have separate roles in desmosome biology as determined by pathogenic variation in the human *DSP* gene.

1.9.1. Aims of this study

In order to test the first hypothesis, genetic and molecular analysis were undertaken in the three Argentinean patients, including the following approaches:

1) Identification of candidate gene by whole genome homozygosity SNP array;
2) Candidate gene approach: mutation screening in candidate gene using PCR and sequencing analysis;
3) Investigation of mutant mRNA and protein expression levels by RT-PCR and western blot, respectively.

In order to test the second and third hypotheses the following approaches were carried out:

4) RNAi technology was used to mimic the haploinsufficiency and *DSPI*-nonsense mutations
5) *DSPI* cDNA constructs were generated, including wild type *DSPI* and a mutant construct containing the 30 bp insertion mutation;
6) The effects of DP haploinsufficiency and *DSPI*-nonsense mutations on the expression levels of junctional proteins were examined in an experimental system using HaCaT cells by western blot.
7) The effects of the three different types of *DSP* mutations on the adhesive properties of the desmosome were examined by subjecting genetically engineered HaCaT cells to an adhesion assay followed by immunocytochemistry.

– Chapter 2 –

Materials and Methods

2.1. Chemicals and tissue culture consumables

All chemicals were purchased form Sigma-Aldrich (St. Louis, MO) and all laboratory consumables were purchased from Fisher (Leicestershire, UK), unless otherwise stated.

2.2. Molecular Biology I – DNA and RNA methods

2.2.1. RNA isolation from cells

Total RNA was isolated from cultured cells at 70-90% confluency, using the RNA-Bee reagent (AMS Biotechnology, Madrid, Spain) according to the manufacturer's specifications. Briefly, cells were washed in phosphate buffered saline (PBS), and subsequently lysed directly by the addition of approximately 20 µl/cm^2 of RNA-Bee reagent. The lysates was separated into aqueous and organic phases by the addition of 4 µl/cm^2 of chloroform followed by centrifugation, which removes DNA and proteins from the RNA-containing aqueous phase. The RNA was isolated from the aqueous phase by isopropanol precipitation, followed by ethanol wash and solubilisation in RNase free double-distilled water (ddH_2O). RNA was stored at -80ºC.

2.2.2. RNA isolation from tissue

Five µm-thick cryosections from patient skin biopsies samples were obtained from the National Diagnostic Epidermolysis Bullosa Laboratory, St Thomas' Hospital. Total RNA was isolated from 10 frozen skin sections using the RNAeasy mini kit (Qiagen, Duesseldorf, Germany), according to the manufacturer's specifications. Briefly, samples were lysed and ethanol was added to the lysates to provide ideal column binding conditions. The lysates were then loaded onto the RNeasy membrane which retains RNA, and the contaminants were washed away. Pure, concentrated RNA was eluted in RNase free ddH_2O. RNA was stored at -80ºC.

2.2.3. Reverse Transcription (RT)

cDNA was generated from total RNA using M-MLV reverse transcriptase (Promega, Madison, WI). Briefly, 7 µl of 5x M-MLV RT-PCR buffer (Promega), 1 µl of RNasin (Promega), 4 µl of 10 mM dNTPs (Invitrogen, Paisley, UK) and 1 µl of first-strand random primers (OD 90, Invitrogen) were added to 20 µl of RNase free ddH_2O containing: 150-300 ng of total RNA, when isolated from frozen tissue sections (see section 2.1.2); 10-60 µg of total RNA, when isolated from cells (section 2.1.1). RNA was denatured at 65^{o}C for 10 min. Samples were then placed directly onto ice, and 2 µl of M-MLV reverse transcriptase (400 U) were added; when performing a negative control, 2 µl of RNase free water were added to a duplicate sample. Samples were incubated in a thermal cycler at 42^{o}C for 90 min. cDNA was stored at -20ºC.

2.2.4. Nucleic acid quantification

Nucleic acid concentration was measured using a NanoDrop ND-1000 Spectrophotometer (Thermo Fisher Scientific, Waltham, MA), according to the manufacturer's specifications. An assessment of nucleic acid purity was achieved by determining the ratios of spectrophotometric absorbance of the sample at 260/230nm and 260/280nm. Pure preparations of DNA and RNA have an A260/A280 ratio of approximately 1.8 and 2.0, respectively, and an A260/A230 ratio of approximately 2.2.

2.2.5. Polymerase Chain Reaction (PCR)

2.2.5.1. Primer design

All primers were purchased from Sigma-Aldrich. Specific primer pairs were designed either to PCR amplify or sequence the regions of interest. The oligonucleotide length varied from 18 to 24 bp depending on the GC content, which ranged from 45-65%. The GC content of each primer in a pair was designed to be as close a match as possible. Primers were designed to contain a G or C nucleotide at the beginning and end of each primer sequence. Calculation of each primer annealing temperature (AT) was determined using the following equation:

$$AT = 69.3 + (0.41\times GC\%) - (650/\text{oligo length})$$

For each primer pair, the lowest AT was initially used in the PCR cycle and where necessary this parameter was optimised.

2.2.5.2. Genomic PCR for mutation screening

PCR for mutation screening was performed using the Fast Start High Fidelity PCR system (Roche, Basel, Switzerland). A typical 50 µl PCR reaction comprised: 5 µl of 10x reaction buffer containing 1.8 mM $MgCl_2$; 0.05 U/µl of Fast Start High Fidelity PCR enzyme blend; 200 µM of each nucleotide (Promega); 0.4 µM of each primer and 25-100 ng of template DNA. Cycling conditions consisted of 95ºC for 2 min, followed by 35-40 cycles of 95ºC for 10 sec, primer annealing for 10 sec and 72ºC for 30-40 sec, with a final extension step at 72ºC for 5 min.

Coding exons 2-7 of the *JUP* gene from three patients and three family members were screened for mutations. These exons were amplified using primers described previously (Whittock *et al.*, 2000) with some modifications, which are included in Table 2.1. The resulting DNA fragments were sequenced as described in section 2.2.18. In addition to patients and family members, control DNA from 54 unrelated individuals was used to amplify exon 2 of the *JUP* gene and the resulting DNA fragments were either digested with *Hinf*I restriction enzyme (see section 2.2.13) and resolved by agarose gel electrophoresis (section 2.2.7), or sequenced directly.

Table 2.1. Primers and cycling conditions used for PCR amplification of *JUP* exons.

Exon	Forward primer sequence (5'-3')	Reverse primer sequence (5'-3')	AT (ºC)	Product size (bp)
2	gtgcccccagtagccacg[†]	ctacaatctgcctcctttcac	58[†]	312
3	gagaggtagaatggccagtc	gtcagactcatcacacacgg	55	540
4	ccgtgtgtgatgagtctgac	ggcacatagtaggtgctcac	55	446
5	ccatgccaggctcacatgt	cagtcgcatgatgaagcatg	55	410
6	gctgaagctcagtaatgacag	gagcatggctgactgagcct	55	316
7	tgagtatgatggccttgagg	ccacagtacctcaggtcagat	55	295

[†]modifications to Whittock *et al.* (2000); AT = annealing temperature.

2.2.5.3. Reverse Transcription Polymerase Chain Reaction (RT-PCR)

PCR amplification of cDNA was performed as described in section 2.2.5.2, except that 3-5 µl of cDNA (generated as described in section 2.2.3) were used as template. When the region to be amplified was over 800 bp, denaturing and annealing times were raised to 30 sec. Extension times were calculated according to the size of the fragment to be amplified, based on the assumption that 1 min is required to amplify 1 Kb of sequence.

2.2.5.3.1. RT-PCR for expression profiling of desmoplakin isoforms in multiple tissues

Expression profiling of *DSP* isoforms in various tissues was carried out by RT-PCR on Clontech Human Multiple Tissue cDNA Panel 1 and Human Cardiovascular Multiple Tissue cDNA Panel (BD Biosciences, Franklin Lakes, NJ). Primers and cycling conditions indicated in Table 2.2 were designed to amplify and distinguish between *DSPI*, *DSPIb* and *DSPII* isoforms. *DSPIb* is a novel *DSP* splice variant described in Chapter 4. The primer pair *DSPIb*F/*DSP*R was used with an extension time of 23 sec, which allowed for the amplification of *DSPIb* but not the 1712 bp-isoform *DSPI*. In the same way, the primer pair *DSPII*F/*DSP*R was used with an extension time of 45 sec for selective amplification of the shorter *DSPII* isoform (Table 2.2).

Table 2.2. Primers and cycling conditions used for isoform-specific amplification of *DSP*

***DSP* isoform**	**Primer name**	**Primer sequence (5'-3')***	**AT (ºC)**	**Product size (bp)**	**Ext. time (sec)**
DSPI	*DSPI*F	cttggaactaaggagccag (5526-5544)	57	179	11
	*DSP*R	ccacctgagtacactgattc (5685-5704)			
DSPIb	*DSPIb*F	gcttgatagactttcaaggg (3993-4012)	55	383 (*DSPIb*)	23
	*DSP*R	ccacctgagtacactgattc (5685-5704)		1712 (*DSPI*)	
DSPII	*DSPII*F	gatcgaagttttggaagagg (3378-3397)	53	530 (*DSPII*)	45
	*DSP*R	ccacctgagtacactgattc (5685-5704)		998 (*DSPIb*)	
				2327 (*DSPI*)	

*Position of primers according to the NCBI reference sequence NM_004415.2 (*DSPI*) is given in parenthesis. *DSPIb* is a novel *DSP* isoform described in Chapter 4. AT = annealing temperature; Ext. time = extension time in seconds.

2.2.5.3.2. RT-PCR sequencing

The primers and cycling conditions used to amplify cDNA corresponding to exons 1-3 of *JUP* are indicated in Table 2.3. Primers which amplified the *hypoxanthine phosphoribosyl-transferase* (*HPRT*) housekeeping gene were used as a control of cDNA abundance (Table 2.3). Forty cycles were used for each reaction.

Table 2.3. Primers and cycling conditions used to PCR amplify *JUP* cDNA

Gene	Primer name	Primer sequence (5'-3')*	Product size (bp)	AT (ºC)	Ext. time (sec)
JUP	F1	gagctcagttcgctgtcc (37-54) [1]	465	59	28
	R1	caatggccgacttgagcag (483-501) [1]			
JUP	F2	ctatcaaggtgactgagtgg (148-167) [1]	375	58	23
	R2	cctggtagttgatgagatg (504-522) [1]			
HPRT	*HPRT*F	tgacactggcaaaacaatgca (578-598) [2]	94	58	10
	*HPRT*R	ggtccttttcaccagcaagct (651-671) [2]			

*Position of primers according to the NCBI reference sequence [1]NM_002230 (*JUP*) and [2]NP_386759 (*HPRT*) are given in parenthesis. AT = annealing temperature; Ext. time = extension time in seconds.

2.2.5.3.3. RT-PCR for mapping of the potential DSPIa splice variant

Primers and cycling conditions used to map the putative *DSPIa* splice variant are depicted in Table 2.4.

Table 2.4. Primers and cycling conditions used to map the potential *DSPIa* isoform

DSP isoform	Primer name	Primer sequence (5'-3')*	AT (ºC)	Ext. time (sec)
Potential *DSPIa*	*DSPIa*F	cagtttgagaccgagatcaac (4372-4392)	53-56	0-60
	*DSP*R	ccacctgagtacactgattc (5685-5704)		

*Position of primers according to the NCBI reference sequence NM_004415.2 (*DSPI*) is given in parenthesis. AT = annealing temperature; Ext. time = extension time in seconds.

2.2.5.3.4. RT-PCR cloning

The primer pairs and PCR conditions indicated in Table 2.5 were used to amplify overlapping fragments of *DSP* cDNA from primary normal human keratinocytes (NHK) in order to generate *DSP* constructs (see section 2.3).

Following TA cloning (section 2.2.8) and transformation of *E. coli* cells (section 2.2.9), one individual colony was picked with a tip and cells were released in a tube containing 25 µl of sterile ddH_2O. These cells were lysed at 95ºC for 5 min and then placed onto ice. The same tip was then placed in a tube containing 3 ml of LB broth (Invitrogen) with 50 µg/ml of the appropriate antibiotic (ampicilin or kanamycin), and cells were grown at 37ºC whilst shaking at 220 rpm overnight. The DNA contained in the boiled lysates was used as template for a diagnostic PCR to confirm the presence of the desired construct. PCR was performed as described, using 2 µl of the boiled lysates and the conditions summarised in Table 2.5. This procedure was used to screen a minimum of 8 colonies for each cloned fragment. After the screening PCR, the overnight cultures of the clones that contained the desired constructs were used to isolate plasmid DNA as described in section 2.2.11.

Table 2.5. Primers and cycling conditions used to generate *DSP* cDNA constructs

Fragment	Primer name	Primer sequence (5'-3')*	AT (ºC)	Size of PCR product (bp)	Ext. time (min)	No. of cycles
1	1F	gtccgcctatccttggcccc (188-207)	57	4111	4.12	40
	1R	cgcttggcctcctcctgaaac (4278-4298)				
2a	2F	ggctcaatgacagcatcttg (4043-4062)	57	1253	1.3	40
	4R	ctgttcctggagtaactgcc (5276-5295)				
2b	4F	cctgcaagaggaagaagctg (5042-5061)	57	1197	1.2	40
	2R	cgatcagctgacactcatag (6219-6238)				
2	2F	ggctcaatgacagcatcttg (4043-4062)	57	867	2.3	35
	2R	cgatcagctgacactcatag (6219-6238)				
3	3F	gagatcgaaagactccaagc (5971-5990)	55	3028	3.03	40
	3R	ctatcactctactgcaagcacc (8977-8998)				
4	1F	gtccgcctatccttggcccc (188-207)	57	3101	3.2	35
	5R	gtaccgagcatgaacatctg (3269-3288)				
5	5F	gagcagaagaacttgcacag (3064-3083)	62	1378	1.4	35
	2R	cgatcagctgacactcatag (6219-6238)				

*Position of primers according to the NCBI reference sequence NM_004415.2 (*DSPI*) is given in parenthesis. See relative position of each fragment in Figure 2.1. AT, annealing temperature; Ext. time, extension time in minutes.

2.2.5.3.5. Quantitative RT-PCR (qRT-PCR)

Quantitative RT-PCR amplification of 400 ng of cDNA was performed using the MiniOpticon detection system (BioRad, Berkeley, CA) and the DyNAmo SYBR Green qPCR kit (Finnzymes, Espoo, Finland). Primers which amplified *DSPI*, *DSPIb* and

DSPII are indicated in Table 2.2. The cDNA was added to a mixture containing qPCR Mastermix Plus for SYBR Green 2x reaction buffer, forward and reverse primers (0.4μM each), and ddH_2O to a final volume of 20 μl. A fragment from the housekeeping gene *β_2 microglobulin* (*B2M*) cDNA was also amplified as an internal control (reference gene). Cycling conditions consisted of 95ºC for 10 mins followed by 40 cycles of 94ºC for 10 sec, 60ºC for 20 sec and 72ºC for 20 sec, with a final extension step at 72ºC for 5 min. Relative quantification was established by defining the difference between the reference and target cycle threshold (Ct) values for each sample.

2.2.6. Illumina Beadchip mapping arrays and analysis

DNA from each patient was column purified (section 2.2.15) and sent to the Genome Centre, Charterhouse Square, London, to be hybridised to Illumina HumanHap550v3_A Genotyping Beadchips according to the manufacturer's specifications (Illumina Inc, San Diego, CA). These arrays allow for the interrogation of 550,000 tag single nucleotide polymorphisms (SNP) per sample. SNPs were called using BeadStudio v3 with Illumina-defined SNP cluster positions (Illumina). SNP-called data were analyzed by Dr. Charles Mein and Dr. Richard Dobson to identify blocks of 20 consecutive homozygous SNPs. The number of SNPs residing in consecutive blocks per chromosome was recorded.

2.2.7. Agarose gel electrophoresis

Agarose gels were used to identify and separate PCR products and restriction digest fragments. For separation of fragments shorter than 800 bp, 2% (w/v) agarose (Bioline, London, UK) gels were prepared. Briefly, the agarose was melted in the appropriate volume of TBE buffer (see Appendix E) and ethidium bromide was added at final concentration of 10 mg/ml. The clear solution was poured into a gel tray with a suitable comb to form the sample wells, and left to solidify. The gel was flooded with TBE in an electrophoresis tank. For detection of fragments longer than 800 bp, 1% (w/v) agarose gels were prepared in a similar way. DNA samples were mixed with DNA loading buffer (see Appendix E) in a 5:1 ratio and loaded on the gel alongside 1Kb Plus DNA ladder (10% (v/v) 1 Kb Plus DNA ladder (Invitrogen), 16% (v/v)

loading buffer). Samples were electrophoresed at a constant voltage of 80-100 V. DNA was visualised under UV transillumination.

2.2.8. TA Cloning

PCR products were cloned into pCRII-TOPO cloning vector using the TOPO TA Cloning Kit (Invitrogen) according to the manufacturer's specifications, with the following modifications. A reaction containing 2 μl of PCR product and 0.5 μl of pCRII-TOPO vector was gently mixed and incubated for 5 min at RT. The reaction was placed on ice and then used to transform competent cells (section 2.2.9).

2.2.9. Transformation of chemically competent bacterial cells

The generated constructs were used to transform chemically competent *E. coli* cells. The chemical transformation protocol was performed using One Shot TOP10 Chemically Competent *E. coli* cells (Invitrogen), according to the manufacturer's instructions. Briefly, 2 μl of each construct generated by TA cloning (section 2.2.8) or following ligation (section 2.2.17) were mixed with TOP10 Chemically Competent *E. coli* cells. Following an incubation of 15 min on ice, cells were heat-shocked for 30 sec at 42ºC and then immediately transferred to ice. After addition of 250 μl of RT SOC medium (Invitrogen), cells were incubated at 37ºC for 1h to allow expression of the antibiotic resistance genes. Cells were plated on a pre-warmed LB agar plate (LB broth with 1.5% (w/v) bacteriological agar) containing 50μg/ml ampicillin or kanamycin. When appropriate, 40 μl of 40 mg/ml X-gal (Qiagen) were spread on each LB plate. Inoculated agar plates were incubated at 37°C overnight.

2.2.10. Glycerol stocks of transformed bacterial cells

Glycerol stocks of transformed *E. coli* cells were prepared by the addition of 200 μl of 80% glycerol to 800 μl of freshly grown overnight bacterial cultures. Glycerol stocks were stored at -80°C.

2.2.11. Small scale plasmid preparation

Small scale plasmid DNA preparations were obtained using the Wizard Plus Minipreps DNA Purification Systems (Promega), according to the manufacturer's specifications, with some modifications. Briefly, a single colony was picked from a freshly streaked selective plate and grown in 3 ml LB broth (Invitrogen) containing 50 μg/ml of ampicilin or kanamycin for 16-18h at 37ºC. Cells were pelleted by centrifugation for 2 min at 7,063×*g* and the pellet was re-suspended in cell re-suspension solution. Cells were lysed and then neutralised. The lysate was centrifuged at 13,226×*g* for 5 min and the DNA in the supernatant was mixed with 1 ml of resin and bound to a minicolumn. The column was washed twice with 1 ml of Column Wash Solution each time and then centrifuged for 2 min at 13,226×*g* to dry the resin. The plasmid DNA was eluted with 30 μl of nuclease-free ddH_2O by centrifugation at 13,226×*g* and stored at 4ºC.

2.2.12. Large scale plasmid preparation

Large scale plasmid DNA preparations were obtained using the HiSpeed Plasmid Maxi kit (Qiagen) according to the manufacturer's specifications regarding low-copy number plasmids, with the following modifications. A single colony was picked from a freshly streaked selective plate and a starter culture of 5 ml LB medium containing 50 μg/ml of ampicilin or kanamycin was inoculated. The culture was incubated at 37ºC for 8h whilst shaking at 300 rpm. The starter culture was added into 250 ml of selective LB medium (~1/50 dilution) and incubated at 37ºC for 12-16h.

2.2.13. Restriction enzyme digests

Restriction enzyme digests were used to specifically linearise plasmid vectors and excise DNA inserts in subcloning experiments, as well as to confirm the presence of the required DNA constructs in the desired orientation after cloning experiments. This method was also used to confirm the presence of mutations in patient and control genomic DNA samples (see section 2.2.5.2). Restriction enzyme digests were performed according to the manufacturer's specifications. Generally, the required quantity of DNA (between 1-10 μg of plasmid DNA or 4-10 μl of PCR amplified DNA)

was incubated with 2 μl of the suitable restriction endonuclease (New England Biolabs, Ipswich, MA) and 2 μl of the appropriate 10x reaction buffer in a final volume of 20 μl. Where necessary, the reaction was scaled up to a larger final volume and when more than one enzyme was used in the same reaction the total volume of enzyme did not exceed 1/10 of the final reaction volume.

2.2.14. DNA purification from agarose gel

After restriction enzyme digest, or after PCR if non-specific DNA fragments were present, agarose gel purification was used to recover the desired band. In order to eliminate the risk of introducing mutations caused by exposure to the UV light, care was taken not to expose the band to be recovered. A duplicate sample, resolved alongside, was used to indicate the position of the required fragment by exposing only this duplicate sample to the UV light. After excision of the required band, a QIAquick Gel Extraction Kit (Qiagen) was used to purify the DNA, according to the manufacturer's specifications.

2.2.15. Purification of PCR products

The QIAquick PCR Purification Kit (Qiagen) was used for DNA purification prior to sequencing reactions as well as in sequential restriction digests for removal of the first enzyme's optimal buffer. Where necessary, it was also used to purify patient genomic DNA prior to exon PCR-amplification and mutation screening (section 2.2.5.2). This kit was used according to the manufacturer's specifications.

PCR products were cleaned up enzymatically using the ExoSAP-IT reagent (United States Biochemical, Cleveland, OH) according to the manufacturer's instructions, prior to sequencing reactions. ExoSAP-IT utilizes two hydrolytic enzymes, exonuclease I and shrimp alkaline phosphatase, to remove unconsumed dNTPs and primers from PCR products.

2.2.16. Ethanol/sodium acetate DNA precipitation

DNA was purified and/or concentrated when necessary by ethanol/sodium acetate precipitation. To this end, 2 volumes of 100% ethanol and 1/10 of a volume of

3M sodium acetate, pH 5.5 were added to the DNA and mixed. This mixture was incubated on ice for 90 min (or -80°C overnight) and then centrifuged at 14,000xg at 4°C for 30 min. The pelleted DNA was washed with ice cold 70% ethanol, air dried and re-suspended in the appropriate volume of ddH_2O.

2.2.17. Ligations

Ligations of linear DNA into a cloning vector were performed using the DNA ligation kit (Sigma-Aldrich) according to the manufacturer's specifications, with the following modifications. The molar ratio of insert DNA to plasmid DNA was 10:1. A 20 µl reaction mix was prepared by combining 5 ng of plasmid DNA, 50 ng of insert DNA, 1 µl of 10x ligation buffer, 1 µl of 10 mM ATP solution, 1 µl of 24% (w/v) PEG solution and 1 µl of T4 DNA Ligase with ddH_2O to bring the volume up to 20 µl. As negative controls, three additional reactions were prepared which are summarised in Table 2.6. These controls were used to check the efficiency of the restriction enzyme digests (section 2.2.13). All reactions were incubated at 16 ºC for 24-48h.

Table 2.6. Negative control ligation reactions

Control 1	Control 2	Control 3
5 ng plasmid DNA	5 ng plasmid DNA	50 ng insert DNA
1 µl 10x ligation buffer	1 µl 10x ligation buffer	1µl 10x ligation buffer
1 µl 10 mM ATP	1 µl 10 mM ATP	1µl 10 mM ATP
1 µl PEG	1 µl PEG	1µl PEG
-	1 µl T4 DNA Ligase	1µl T4 DNA Ligase

2.2.18. Sequencing

Sequencing was performed using the BigDye Terminator version 3.1 Cycle Sequencing Kit (Applied Biosystems, Foster City, CA). Between 5-15 ng purified PCR product (3.2.15) or 300 ng of plasmid DNA were added to a reaction containing 1 µl of Big Dye Terminator Master mix v3.1, 3 µl of better buffer (Microzone, Ottawa, Canada) 0.5 µl of 20 pmol/µl specific primer and ddH_2O up to a final volume of 10 µl. Cycling conditions consisted of 25 cycles of 96 ºC for 30 sec, 55ºC for 15 sec and 60ºC for 4 min, followed by a final incubation at 4 ºC for 10 min.

The reaction products were precipitated with ethanol/EDTA/sodium acetate. Briefly, 2 µl of 125 mM EDTA, 2 µl of 3M sodium acetate and 50 µl of ice cold 100% ethanol were added to the sequencing reaction and incubated on ice for 30 min. The mixture was centrifuged at 4100x*g* at 4ºC for 30 min; the pellet was washed with 70 % ethanol and air dried. Precipitated products were sent to the Genome Centre, Charterhouse Square, London, where sequences were read in an ABI sequencer.

2.3. Molecular Biology II – *DSP* cloning strategies

2.3.1. Generation of wild type *DSPI* and *DSPIb* constructs

To generate *DSPI* and *DSPIb* constructs, cDNA was first generated by reverse transcription of primary NHK mRNA (see section 2.2.3). *DSPIb* is a novel, previously unknown *DSP* splice variant described in Chapter 4. Five cDNA fragments were PCR amplified (Table 2.5) with primers shown in Figure 2.1. Fragments 1 and 3 (amplified with primers 1F/1R and 3F/3R, respectively) are common to both *DSPI* and *DSPIb* isoforms whereas fragments 2a and 2b (amplified with primers 2F/4R and 4F/2R, respectively) are *DSPI*-specific and fragment 2 (amplified with primers 2F/2R) is *DSPIb*-specific (see Table 2.5 and Figure 2.1). Each fragment was gel purified (section 2.2.14) where necessary and cloned into pCRII-TOPO cloning vector (Invitrogen) in the 3' to 5' direction (see section 2.2.8 and Figure 2.2).

To clone *DSPI*, and because of repetition of useful restriction enzyme sites (see Figure 2.1) fragments 2a and 2b were first joined. Fragment 2b in pCRII-TOPO was linearised with the vector MCS's *Not*I and insert's internal *Bmg*BI, and fragment 2a, cut out of the cloning vector with the same enzymes, was inserted. Next, fragment 1, similarly cut out of the cloning vector with *Afe*I and *Not*I was inserted into the new 2a/2b construct which had been linearised with the same enzymes. Finally, fragments 1/2a/2b were inserted into the vector containing fragment 3 in a similar way, using *Not*I and *Nde*I. This strategy is summarized in Figure 2.2.

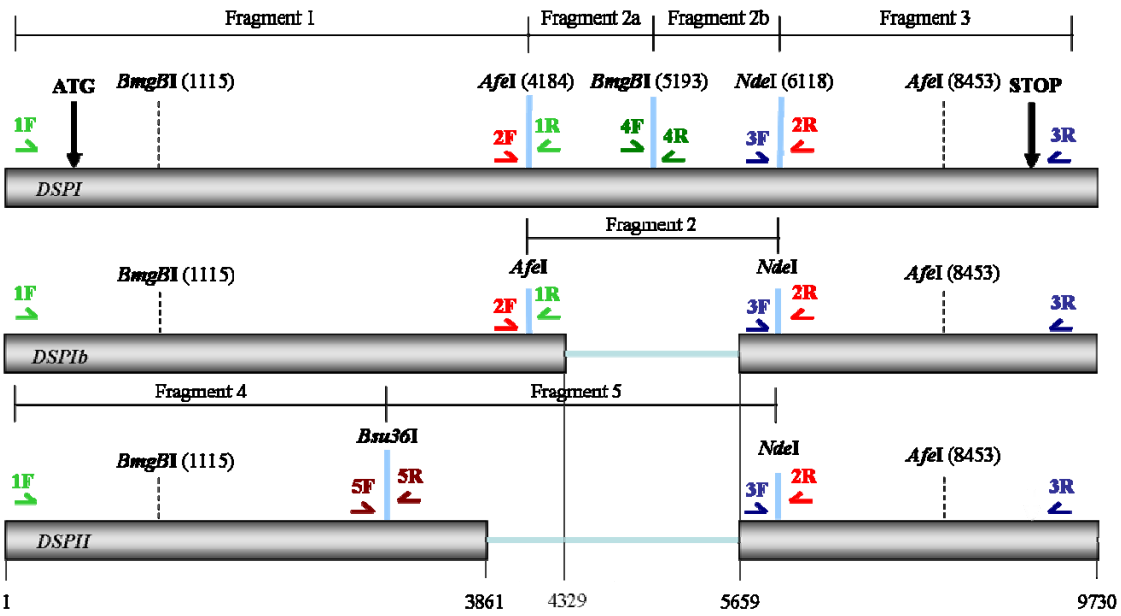

Figure 2.1. *DSPI* and *DSPIb* cloning strategies. Schematic diagram of the three *DSP* splice variants showing locations of primer pairs and restriction enzymes used to clone *DSPI* and *DSPIb*. To clone *DSPI*, four overlapping cDNA fragments were PCR amplified with primers 1F/1R (fragment 1), 2F/4R (fragment 2a), 4F/2R (fragment 2b) and 3F/3R (fragment 3). Fragments 2a and 2b were first ligated using *Bmg*BI (position 5193). This larger fragment was then ligated with fragment 1 using *Afe*I (position 4184) and then fragment 3 was joined using *Nde*I (position 6118) (see also Figure 2.2). To clone *DSPIb*, fragment 2 was PCR amplified with primers 2F/2R and joined to fragment 1 using *Afe*I. The generated fragment was subsequently ligated to fragment 3 using *Nde*I.

DSPIb and *DSPII* were cloned in a similar way. *DSPII* was constructed by first inserting fragment 4 into the cloning vector containing fragment 5 using the enzymes *Bsu*36I and *Not*I, followed by addition of fragment 4/5 to the fragment 3 construct using the enzymes *Nde*I and *Not*I. To generate *DSPIb*, fragments 1 and 2 were first ligated following digest of the respective pCRII-TOPO vectors with *Afe*I and *Not*I. Subsequently, these fragments were joined with fragment 3 using *Nde*I and *Not*I (Figure 2.1).

During the above cloning, where the restriction digest produced two fragments of similar size, an additional restriction enzyme (*Nco*I, shown in red, Figure 2.2) was used to aid separation by gel purification. When necessary (when two or more enzymes were not compatible in the same reaction buffer) sequential digests were performed (section 2.2.13). DNA purification columns (section 2.2.15) were used between the two enzymes to remove traces of the first buffer.

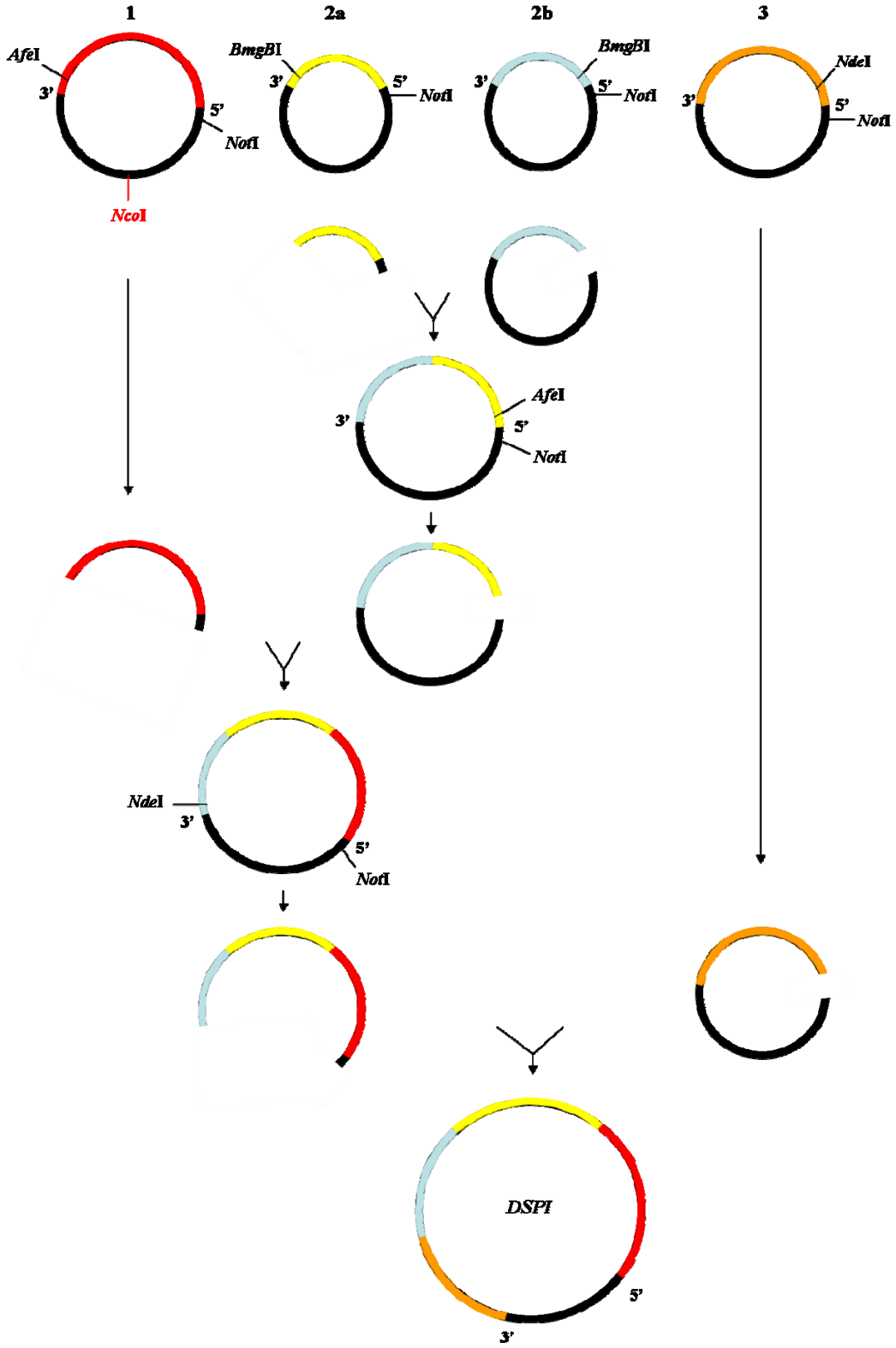

Figure 2.2. Graphical representation of *DSPI* cloning strategy. Fragments 1 (red), 2a (yellow), 2b (blue) and 3 (orange) were PCR amplified from NHK RNA and TA cloned into the pCRII-TOPO cloning vector. Vectors containing fragments 2a and 2b were digested with *Bmg*BI and *Not*I and fragment 2a was ligated with the vector containing fragment 2b. Fragment 1 was ligated to the vector containing fragment 2a/2b in the same way, following digests with *Afe*I and *Nde*I. Fragment 1/2a/2b was inserted in the vector containing fragment 3 using *Nde*I and *Not*I.

In order to subclone *DSPIb* into the pBabe puro retroviral vector (Morgenstern & Land, 1990), the pBabe vector was first digested with *Eco*RI (section 2.2.13) and then the 3' recessed ends were filled-in using Klenow DNA polymerase I (Invitrogen), according to the manufacturer's specifications. The linearised vector with blunt ends was de-phosphorylated using shrimp alkaline phosphatase (Roche), according to the manufacturer's specifications, and then gel purified (section 2.2.14). In the same way, *DSPIb* was excised from the pCRII-TOPO cloning vector using the unique MCS' enzymes *Kpn*I and *Not*I and its ends were made blunt using Klenow DNA polymerase I, prior to gel purification. To check the efficiency of the restriction enzyme digests and pBabe vector de-phosphorylation, the following ligation reactions were prepared as negative controls: vector alone, vector+ligase and vector+ligase+T4 polynucleotide kinase (Invitrogen). The *DSPIb* insert were then ligated to the linearised pBabe vector as described in section 2.2.17.

2.3.2. Generation of wild type- and I608ins10-*DSPI*-flag expression constructs

The 30 bp insertion mutation (I608ins10) was generated within the first fragment of *DSPI* (fragment 1; Figure 2.1) and a cDNA sequence encoding the flag tag was inserted into the third fragment (fragment 3; Figure 2.1) immediately upstream of the natural stop codon (TAG). These fragments were then ligated to fragment 2a/2b in the order described above (section 2.3.1), to generate the full length I608ins10-*DSPI*-flag construct which was then sub-cloned into one pBabe puro vector as described (section 2.3.1).

The strategy used to generate the 30 bp insertion mutation consisted of inserting a 155 bp oligonucleotide duplex containing the mutation into fragment 1. To generate the 155 bp duplex, the four compatible oligonucleotides with 5' phosphate (5'P) groups shown in Figure 2.3A were re-suspended in ddH_2O at a concentration of 1 µg/µl and diluted to 500 ng/µl in STE buffer (see Appendix E). Equal volumes (30 µl) of oligonucleotides I30 Sense A and I30 AsenseB were duplexed by incubation at 95°C for 5 min followed by 5°C decrements of 1 min each from 95°C to 25°C. Oligonucleotides I30 Sense B and I30 Asense A were duplexed in the same way. The resulting duplexes are shown in Figure 2.3B.

A

I30 Sense A
5'P ATGGCCAGGGTCTGGTAATGCTTCTGGGGCATCGGTGAACTGAGACTGTatttccgggcatcggtgaactgagactgtATTTTCCGCT 3'

I30 Sense B
5'P TGTCATCATCTCCAAACATCTCTGAGCCTTGGCTATTTCTGATGAACTCTTGGTAATGTAACTCAAGGTCG 3'

I30 Asense A
5'P TAGCCGACCTTGAGTTACATTACCAAGAGTTCATCAGAAATAGCCAAGGCTCAGAGATGTTTGGAGATGATGACAAGCGG 3'

I30 Asense B
5'P AAAATacagtctcagttcaccgatgcccggaaaatACAGTCTCAGTTCACCGATGCCCAGAAGCATTACCAGACCCTGG 3'

B

GAAGACGA
CTTCTGCTATCG

TAGCCGACCTTGAGTTACATTACCAAGAGTTCATCAGAAATAGCCAAGGCTCAGAGATGTTTGGAGATGATGACAAGCGG
GCTGGAACTCAATGTAATGGTTCTCAAGTAGTCTTTATCGGTTCCGAGTCTCTACAAACCTCTACTACTGT

AAAATacagtctcagttcaccgatgcccggaaaatACAGTCTCAGTTCACCGATGCCCAGAAGCATTACCAGACCCTGG
TCGCCTTTTAtgtcagagtcaagtggctacgggccttttaTGTCAGAGTCAAGTGGCTACGGGTCTTCGTAATGGTCTGGGACCGGTA

CCATCAAGG
GTTCC

Figure 2.3. Generation of a 155 bp oligonucleotide duplex containing the 30 bp-insertion mutation (I608ins10). Four 5'P oligonucleotides **(A)** were used to generate the 155 bp insert containing the insertion mutation. Oligo I30 Sense A was annealed with oligo I30 AsenseB and oligo I30 Sense B was annealed with oligo I30 AsenseA to generate 2 compatible A/B duplexes **(B)**. The duplexes (B) are depicted in bold print with the I30 mutation highlighted in lowercase print. Bases in blue bold print are compatible with the 5' end of the vector and bases in red bold print are compatible with the 3' end of the vector. Bases in green bold print are compatible between the 2 A/B duplexes and used to join them.

A triple fragment ligation was performed to join the two duplexes (forming the 155 bp insert) and the vector. This ligation was performed using the following equation:

Mass of insert = ((i:v ratio) x length insert x mass of vector) / (length vector),

where an i:v (insert to vector) ratio of 10:1 was used; the length of the insert was 155 bp (formed by the two A/B duplexes) and 11 ng of vector with 6164 bp was used. Therefore, the calculated mass of insert was 2.84 ng and 1.42 ng of each duplex were ligated to 11 ng of vector using conditions described in 2.2.17.

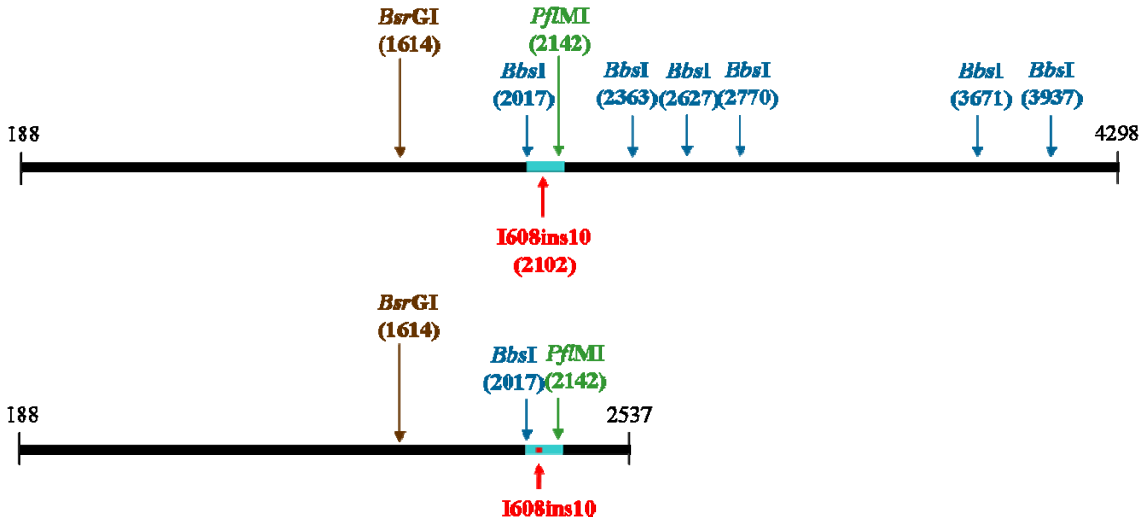

Figure 2.4. Generation of I608ins10-*DSPI*. Schematic of *DSP* fragment 1 cloned into pCRII-TOPO vector (nucleotides 118 to 4298) showing the location of the 30 bp insertion mutation (I608ins10) (nucleotide 2102, in red) and restriction sites for *Bsr*GI (in brown), *Bbs*I (in blue) and *Pfl*MI (in green) enzymes, used to generate the I608ins10 mutation (top diagram). *Bbs*I digest released nucleotides 2017 to 3937 and a fragment containing the insertion mutation and *Bbs*I compatible ends was inserted. The fragment released by *Bsr*GI and *Pfl*MI digest (containing I608ins10) was inserted into a vector containing wild type fragment 1, opened up with the same enzymes (bottom diagram).

This strategy was achieved in three steps due to the lack of unique restriction sites that would enable the insertion of the 155 bp duplex directly into the fragment 1-containing vector. First, fragment 1 was digested with the enzyme *Bbs*I releasing nucleotides 2017 to 3937 (see Figure 2.4). Second, the 155 nucleotide duplex containing the 30 bp insertion mutation and ends compatible with *Bbs*I- (2017 and 3937) digested fragments was ligated to the open vector. Third, the resulting vector was digested with the unique restriction enzymes *Bsr*GI (1614) and *Pfl*MI (2142) and the released fragment containing the insertion mutation was inserted into the original vector containing fragment 1 which was previously opened up with the same enzymes (Figure 2.4)

The flag tag was generated in a similar way. A 32 bp duplex consisting of annealed oligonucleotides (Figure 2.5) containing the flag tag-encoding sequence followed by a STOP codon (TAG) was generated as described above. The vector containing fragment 3 was digested with *Spe*I, the natural TAG termination codon was removed from fragment 3 using Mung Bean Nuclease (New England Biolabs) and the resulting fragments were digested with *Kpn*I. The 32 bp duplex, which had a blunt end

(compatible with the blunt extremity of the vector generated with the Mung Bean Nuclease) and a *Kpn*I compatible end, was then inserted.

All full length constructs were fully confirmed by sequencing analysis.

A

Flag Sense
5'P CCTACTActtgtcatcgtcgtccttgtagtcG 3'

Flag Asense
5'P CgactacaaggacgacgatgacaagTAGTAGGGTAC 3'

B

```
AAGCTCGGTAC
TTCGAGC

            CCTACTActtgtcatcgtcgtccttgtagtcG
        CATGGGATGATgaacagtagcagcaggaacatcagC

                                        TGCCC
                                        ACGGG
```

Figure 2.5. Generation of a 32 bp oligonucleotide duplex containing the flag tag-encoding sequence. Two 5'P oligonucleotides **(A)** were used to generate the 32 bp sequence encoding the flag tag followed by a STOP codon. Oligo Flag Sense was annealed with oligo Flag Asense to generate the 32 bp duplex **(B)**. The duplex (B) is depicted in bold print with the 3' overhang compatible with the vector depicted in purple bold print and the flag-encoding sequence highlighted in lowercase print.

2.4. Molecular Biology III – Protein methods

2.4.1. Antibodies

Primary antibodies used for western blot and immunocytochemistry and associated information including the working dilutions are listed in Table 2.7.

Table 2.7. Primary antibodies used for western blot and immunocytochemistry

Primary Antibody	Clone	Host	Working dilution WB	Working dilution Immunocytochemistry	Source
Mab anti-PG	PG5.1	Mouse	1:200	1:5	AbD Serotec (Serotec, Kidlington, UK)
Mab anti-PG	PG15F11	Mouse	1:200	----------	Abcam (Cambridge, UK)
Mab anti-DPI/DPII	11-5F	Mouse	1:250	1:100	Kind gift from Prof. David Garrod (Parrish *et al.*, 1987)
Pab anti-DPI	DP-1	Guinea pig	----------	1:250	Progen (Heidelberg, Germany)
Mab anti-β-actin	AC-15	Mouse	1:1,000	----------	Abcam
Mab anti-vinculin	hVIN-1	Mouse	1:40,000	----------	Sigma-Aldrich
Pab anti-DSC2	----------	Rabbit	1:1,000	----------	Progen
Mab anti-DSC3	Dsc3-U114	Mouse	1:250	----------	Progen
Mab anti-β-catenin	14	Mouse	1:2,000	----------	BD
Mab anti-PKP1	PP1-5C2	Mouse	1:100	----------	Progen
Mab anti-PKP2	Pkp2-518	Mouse	1:500	----------	Progen
Mab anti-PKP3	23E3/4	Mouse	1:500	----------	Abcam
Mab anti-keratin 14	LL002	Mouse	1:1,000	1:10	CRUK
Pab anti-DDDDK tag	DDDDK	Rabbit	1:500	1:500	Abcam
Mab anti-pan-cytokeratin	AE1/AE3	Mouse	----------	1:100	Dako (Glostrup, Denmark)
Mab anti-DSG3	5G11	Mouse	1:250	----------	Abcam
Mab anti-DSG1/2	DG3.10	Mouse	----------	1:250	Progen
Mab anti-DSG2	10G11	Mouse	1/50	----------	Progen

2.4.2. Western blotting

2.4.2.1. Protein preparation from frozen skin biopsies

Twenty cryosections from frozen skin biopsies samples (5 µm-thick) were scraped into 60 µl of 2x Laemmli buffer (Appendix E). Samples were heated to 100°C for 5 min and centrifuged at 15,700xg for 5 min before being subjected to SDS-polyacrylamide gel electrophoresis (SDS-PAGE) (see section 2.4.2.4) or stored at -80ºC.

2.4.2.2. Protein preparation from normal human atrium biopsies

Small fragments of redundant atrium tissue were obtained during cardiac surgery and transported to the lab in dry ice. These small fragments were solubilised into an appropriate volume of 2x Laemmli buffer (see Appendix E) and subsequently heated to 100°C for 5 min and centrifuged at 15,700xg for 5 min before being subjected to SDS-PAGE (section 2.4.2.4) or stored at -80ºC.

2.4.2.3. Protein preparation from cell extracts

Whole-cell protein extracts were prepared from HaCaT keratinocytes or from Phoenix amphotropic retroviral packaging cells (see section 2.5.2 for cell culture conditions). HaCaT keratinocytes were seeded at high density ($7x10^5$ cells/well of a 6-well dish) and total protein was extracted 24-48h later. Phoenix cells were grown to approximately 70% confluence before protein isolation. The cells were washed in PBS before lysis in boiling SDS sample buffer (see Appendix E). Cells were scraped and the cell lysate was transferred to microcentrifuge tubes and heated to 100°C for 5 min before being subjected to SDS-PAGE (section 2.4.2.4) or stored at -80ºC.

Protein lysates from the HpV immortalised human breast keratinocyte cell line K1 were prepared identically by Dr Andy South.

2.4.2.4. SDS-Polyacrylamide Gel Electrophoresis (PAGE) and transfer

2.4.2.4.1. Pre-cast gradient SDS-polyacrylamide gels and transfer

Whole cell lysates were resolved on NuPAGE Novex 4-12% Bis-Tris Mini Gels or NuPAGE Novex 3-8% Tris-acetate Mini Gels (Invitrogen), when western blotting for PG and DP respectively according to the manufacturer's specifications. Between 5-10 µl of protein sample and 12-15 µl of High Mark Pre-stained Molecular Weight Marker (Invitrogen) were loaded on the pre-cast SDS-polyacrylamide gels. The gel was run at 80-120 V until the desired separation was obtained. Proteins were subsequently transferred onto a Hybond – C Extra nitrocellulose membrane (GE Healthcare, Buckinghamshire, UK) in a wet transfer electrophoretic cell (Invitrogen) according to the manufacturer's specifications.

2.4.2.4.2. Preparation of SDS-polyacrylamide gels and transfer

A 10% separating polyacrylamide gel mixture was prepared and poured between two glass plates and 1.5 mm spacers in a gel electrophoresis apparatus (BioRad). The gel mixture was overlaid with 1 ml of isopropanol, and left to polymerise at RT for approximately 20 min. When the gel was polymerised, the isopropanol was washed away with ddH_2O. A 5% stacking gel mixture was prepared and cast with sample combs over the resolving gel, and left to polymerise at RT for approximately 30 min. Between 5-20 µl of protein sample as well as 10-12 µl of Full-range Rainbow Molecular Weight marker (GE Healthcare) were loaded on the SDS-polyacrylamide gel. The gel was run at 80-120 V in running buffer (Appendix E) until the desired separation was obtained.

Proteins were transferred onto a Hybond – C Extra nitrocellulose membrane (GE Healthcare) in a wet transfer electrophoretic cell (BioRad) with transfer buffer (Appendix E), usually at 80 V for 1.5h (or 10 V overnight). Quality of loading/transfer was assessed by staining of the membrane with ponceau stain (Appendix E) solution for 5 min, followed by de-stain in ddH_2O.

2.4.2.5. Immunoblotting and visualisation

Non-specific antibody binding to the membrane was prevented by incubating the membrane in 5% (w/v) non-fat milk TTBS (see Appendix E) for 30 min at RT. Blocked membranes were incubated at 4ºC overnight in 5% (w/v) non-fat milk TTBS containing the appropriate primary antibody at the suitable dilution. Following three 5 min washes in TTBS, membranes were incubated in 5% (w/v) non-fat milk TTBS containing the appropriate peroxidase-conjugated anti-mouse or anti-rabbit immunoglobulins (Dako) at a 1:1000 dilution, for 1h at RT. Membranes were subsequently washed again as described above, incubated in ECL or ECL Plus solution (GE Healthcare) for 5 min, sealed in a plastic sheet, and exposed to chemiluminescence sensitive film (GE Healthcare). The membrane was then washed in TTBS for 5 min and re-probed with an anti-vinculin or anti-β-actin primary antibody (Table 2.7) for 1h at RT. Vinculin and β-actin were used as controls for equal loading. Subsequent washes, incubation in anti-mouse secondary antibody and exposure were performed as described above.

2.5. Cell culture

2.5.1. Primary human keratinocyte culture conditions

First, 3T3 fibroblasts (primary mouse embryonic fibroblast cells) were grown in Dulbecco's Modified Eagles Medium (DMEM) supplemented with 5% (v/v) Foetal Bovine Serum (FBS; Biosera, East Sussex, UK) and 2 mM L-glutamine in a 5% CO_2 humidified incubator at 37^0C. When approximately 70-80% confluent, 3T3 cells were incubated for 3-4h in DMEM (supplemented with 5% (v/v) FBS (Biosera) and 2 mM L-glutamine) containing 7 μg/ml Mitomycin C to stop them from dividing. These cells were then washed in PBS and detached from the flask using 1 part 10x trypsin/EDTA to 3 parts versene. The trypsin was quenched with DMEM followed by centrifugation at 250x*g* for 5 min and re-suspension in DMEM:Ham's F12 (3:1) supplemented with 10% (v/v) FBS (Biosera), 2 mM L-glutamine, 100 U/ml penicillin, 100 μg/ml streptomycin and RM^+ (see Appendix E for RM^+ composition). Cells were then counted using a hematocytometer and 2 million cells were seeded in a 75cm^2 culture flask.

Second, primary NHK (6 million cells for a T75 flask) were inoculated in the flask containing the Mitomycin C treated 3T3 fibroblasts and incubated at 37°C in a 10% CO_2 humidified incubator. The medium was changed every 2-3 days and when necessary, more 3T3 cells were added. The keratinocytes were split once around 70% confluent. To split the keratinocytes, the 3T3 cells were first removed using versene and the keratinocytes were then detached using 1 part 10x trypsin/EDTA to 3 parts versene.

2.5.2. HaCaT and Phoenix culture conditions

The HaCaT spontaneously immortalised human keratinocyte cell line was cultured in DMEM:Ham's F12 (1:1) supplemented with 10% (v/v) FBS (Biosera), 2 mM L-glutamine, 100 U/ml penicillin, 100 µg/ml streptomycin and RM^+ (see Appendix E for RM^+ composition) and maintained at 37°C in a 5% CO_2 humidified incubator. When 80-90% confluent, cells were passaged (2.5.1) and re-seeded. Growth medium was changed every 2-3 days.

Culture of Phoenix cells was performed as described above, except that DMEM growth medium supplemented with 10% (v/v) FBS (Biosera), 100 U/ml penicillin, 100 µg/ml streptomycin and 2 mM L-glutamine was used.

2.5.3. Cryopreservation of cells

For cryopreservation, 80-90% confluent cells were detached from the culture dish with trypsin/EDTA as described (2.5.1), pelleted by centrifugation and resuspended in 90% FBS:10% DMSO. Vials were frozen slowly at -80°C for at least 24h and then transferred into liquid nitrogen for long term storage.

2.6. Retroviral transduction of HaCaT cells

2.6.1. Transient transfection of Phoenix cells

The Phoenix amphotrophic retroviral packaging cell line was used to generate viral particles as described previously (Kinsella & Nolan, 1996). These cells were seeded at a density of 1 million cells per well of a 6-well plate and transfected 24h later

with the appropriate DNA construct and FuGene 6 transfection reagent (Roche), at a ratio of 1:2.5. To this end, 25 µl of FuGene 6 were added dropwise to 200 µl of DMEM serum-free medium in a polystyrene tube and incubated for 5 min at RT. Subsequently, this mixture was added to another polystyrene tube containing 10 µg of DNA and incubated for 15 min at RT. Besides the plasmid constructs of interest, a *GFP*-pBabe control plasmid was used to follow expression, as well as a negative control where no DNA was added (mock control). The final mixture was added dropwise to cells in a 6-well plate containing 3 ml of DMEM complete medium and incubated at 37°C. When completely confluent, fresh DMEM medium was added to these cells, which were incubated at 32°C for 24h to allow virus production. The retrovirus-containing supernatant was then filtered using a 0.45 µm filter to remove cell debris and either directly used to infect target cells or snap frozen and kept at -80°C for long term storage. Fresh media was added again to Phoenix cells which were incubated at 32°C for another 24h to produce a second round of virus.

2.6.2. Infection of HaCaT cells with recombinant retroviruses

HaCaT cells were seeded at a density of $2x10^5$ cells per well of a 6-well plate 24h prior to retroviral infection. These cells were incubated in DMEM:Ham's F12 (1:1) supplemented with 10% (v/v) FBS (Biosera), 2 mM L-glutamine, 100 U/ml penicillin, 100 µg/ml streptomycin and RM^+ (see Appendix E for RM^+ composition) containing 5 µg/ml of polybrene (hexadimethrine bromide) for 10 min at 37°C to increase virus attachment to the cells. The polybrene-containing medium was replaced by 2 ml of retroviral supernatant containing 5 µg/ml of polybrene and centrifuged for 1h at 350x*g*. Cells were washed twice with PBS and incubated in DMEM:Ham's F12 (1:1) supplemented with 10% (v/v) FBS (Biosera), 2 mM L-glutamine, 100 U/ml penicillin, 100 µg/ml streptomycin and RM^+ (see Appendix E for RM^+ composition) at 37°C overnight. A second cycle of infection was performed and 24h later, cells were selected with 1 µg/ml puromycin until the mock control cells were all killed. Cells were switched to puromycin-free media at least 2 days before being harvested for experiments.

2.7. Transient siRNA mediated *DSP* knock-down

Transfection conditions were optimised using siGLO Cyclophilin B Control siRNA (Thermo Fisher Scientific). For transient down-regulation of *DSP* splice variants, siRNAs were designed using the custom siRNA design tool from Thermo Fisher Scientific, according to the manufacturer's specifications (see Appendix B). Table 2.8 summarises the characteristics of these siRNAs. The criteria used for siRNA design, as well as optimisations of transfection conditions, testing of the four designed siRNAs, optimisation of siI pool concentration and time course analysis of DPI down-regulation in HaCaT cells are described in Appendix B. The siRNA designated as siI/II (Table 2.8) was published previously (Wan *et al.*, 2007).

Transfections were performed according to the DharmaFECT general transfection protocol (Thermo Fisher Scientific) and optimised for a 6-well plate format. HaCaT cells were plated at a density of $2x10^5$ cell per well of a 6-well dish and incubated in complete antibiotic-free medium at 37°C, 24h prior to siRNA transfection. In separate polystyrene tubes, 10-100 nM of siRNA (final concentration) and 6 µl of DharmaFECT 1 were mixed in serum- and antibiotic-free media and incubated at RT for 5 min. The siRNA-containing medium was added to the tube containing the DharmaFECT 1 and these contents were mixed and incubated for 20 min at RT. Complete antibiotic-free media was added to the mix (transfection media). The culture media was then removed from the cells in the 6-well plate and 2 ml of transfection media were added to each well. Cells were incubated in transfection media for approximately 20h at 37°C and then this media was replaced by complete antibiotic-free medium. Cells were maintained in this media for 2-10 days and subsequently harvested for experiments. Cells transfected with a pool of four non-targeting (NT) siRNAs (on-target plus siControl non-targeting pool; Thermo Fisher Scientific) as well as cells incubated with DharmaFECT 1 transfection reagent only (mock) were used as negative controls.

Table 2.8. Characteristics of the siRNAs used

	siRNA	siRNA sequence	Target mRNA	Position in target mRNA*
siI pool	si1	GCGAAGGCGAGCTGAAGAA	DSPI/DSPIb	4077-4095
	si2	ATAAGGAGATCGAGAGACT	DSPI/DSPIb	4250-4268
	si3	GGCCTGTGGCTCTGAGATA	DSPI/DSPIb	4113-4131
	si4	AGATAGAACTGAAGCAGGT	DSPI/DSPIb	4154-4172
	siI/II	AACCCAGACTACAGAAGCAAT†	DSPI/DSPIb/DSPII	1633-1653
siDSPI 1/2	siDSPI 1	GAGCTTATCTGAAGAAATA	DSPI	4488-4506
	siDSPI 2	CGAACAGAGGAGAGCGTAA	DSPI	4651-4669

* Position of siRNAs according to the NCBI reference sequence NM_004415.2 (*DSPI*).
† Previously described in Wan *et al.* (2007)

2.8. Immunocytochemistry

For immunocytochemistry, cells were plated on coverslips at approximately 80% confluency in 12-well plates and grown overnight at 37°C. Cells were washed twice in PBS and fixed either in methanol:acetone (section 2.8.1) or in paraformaldehyde (PFA, section 2.8.2). Following fixation, cells were washed three times in PBS, then permeabilised in 0.1% Triton X-100 in PBS (PBST) for 5 min at RT, and finally blocked with 3%BSA in PBS (blocking buffer) for 30 min at RT. The cell-containing coverslips were then inverted onto a 50 µl drop of primary antibody-containing blocking buffer at the appropriate dilution and incubated for 1h at RT. Cells were washed three times in PBS and then incubated with the appropriate Alexa Fluor 488- (green) and/or 568- (red) conjugated goat anti-rabbit, mouse or guinea pig IgG secondary antibody (Invitrogen), at a 1:250 dilution in PBS, for 40 min at RT. DAPI was used as a nuclear stain at 100 ng/ml. Cells were mounted with Immu-mount (Thermo Fisher Scientific).

Immunfluorescence images were acquired with a Zeiss LSM 510 laser scanning confocal microscope (Carl Zeiss Ltd, Hertfordshire, UK). Images were processed using LSM image browser (Zeiss) and Adobe Photoshop (Dublin, Ireland).

2.8.1. Methanol:acetone fixation

Cells were washed twice with PBS and fixed in ice cold 1:1 methanol:acetone for 10 min at -20°C. This fixation method was used for staining with all primary antibodies used in this study, except for the anti-PG (PG5.1) antibody.

2.8.2. Paraformaldehyde (PFA) fixation

A fresh solution of 4% PFA in PBS (containing 0.8mM NaOH) was prepared each time. To this end, 2 g of PFA were dissolved in approximately 40 ml of boiling ddH_2O containing 20 µl of 2M NaOH. The solution was cooled to RT and 5ml of 10x PBS were added. Water was added to a final volume of 50 ml. Cells were washed twice with PBS and fixed in 4% PFA for 15 min. This fixation method was used for staining with the anti-PG primary antibody (PG5.1) (see Table 2.7).

2.9. Flexcell adhesion assay

The Flexcell FX-4000 Tension System (Flexcell, Hillsborough, NC) is a computer-regulated bioreactor that uses vacuum pressure to apply cyclic or static strain to cells cultured on flexible-bottomed culture plates. This system was used to subject a cell monolayer to mechanical stress. HaCaT cells were grown to approximately 80% confluency on BioFlex 6-well plates coated with pronectin (Flexcell) which contain a rubber membrane in each 35 mm well. Each plate was placed over the loading station containing 6 planar faced cylinders or posts. Each post (25 mm) is centred beneath the rubber membrane of each 35 mm well. Cells were subject to cyclic mechanical stretch with a frequency of 2Hz (i.e. two cycles of stretch and relaxation per second) and an elongation of amplitude ranging from 11 to 14% (i.e. increase in diameter across the silicone membrane from 11 to 14%). Cells were stretched for different periods of time, between 0h (unstretched) and 3h, and then prepared for immunocytochemistry as described (section 2.8). In order to stain the cells contained in each well of the 6-well dish with more than one antibody, the flexible rubber membrane was cut into 8 triangular fragments with a scalpel. Each of these cell-containing fragments was stained with a different antibody.

2.10. Statistical analysis

Statistical analyses were carried out using the two-tailed, paired t-test on Microsoft Excel. $p<0.05$ was significant; $p<0.01$ was highly significant; $p<0.001$was very highly significant.

– Chapter 3 –

Genetic Analysis of Patients with Recessive Skin Disease and Woolly Hair

3.1. Introduction

Three non-consanguineous patients originating from Argentina presented with a similar cutaneous phenotype. Their clinical and histopathological characteristics were suspected to be caused by a hereditary desmosomal defect. The focus of the work presented in this chapter was to investigate the genetic basis of disease in these patients to gain further insight into the mechanisms of this cutaneous disease. The following introductory sections describe clinical and histopathological findings which led to the hypothesis that this condition is a desmosomal disease. These findings were published elsewhere (Winik *et al.*, 2009), describing data determined prior to the work described here.

3.1.1. Clinical observations

Three non-consanguineous children (Figure 3.1A) from the province of Santiago del Estero in Argentina were examined at the Department of Dermatology at Tucuman Children's Hospital, over a period of four years. All three patients were born to healthy unrelated parents. Two of the patients originated from distant villages of the same county, whereas the third patient was from a separate county. The patients were aged between two and eleven years old.

All three patients had comparable skin phenotypes, which consisted of skin fragility with diffuse PPK, and woolly scalp hair (Figure 3.1B and C). They presented with blisters and erosions at sites of trauma since the first month of life (Figure 3.1C), and later development of hyperkeratotic palmoplantar plaques (Figure 3.1B) also associated with blisters and erosions. These lesions were present on the limbs, around the mouth and ears, in perianal and intergluteal folds and at the surface of the joints (Figure 3.1B and 3.1C) (Winik *et al.*, 2009). Each patient has been examined on up to nine occasions for cardiac abnormalities and all have presented with normal echocardiogram and normal resting electrocardiography. The eldest patient was 14 years old at the time of the last cardiac examination.

This clinical phenotype has features in common with the ectodermal dysplasia-skin fragility syndrome, which is caused by mutations in the *PKP1* gene. It also resembles some aspects of the Carvajal syndrome and Naxos disease, which are caused by mutations in *DSP* and *JUP*, respectively. However, the overall clinical picture of these patients is distinctive, and therefore the suggested clinical classification for this

novel genodermatosis is acantholytic ectodermal dysplasia due to similarities with ectodermal dysplasia-skin fragility syndrome (Winik *et al.*, 2009).

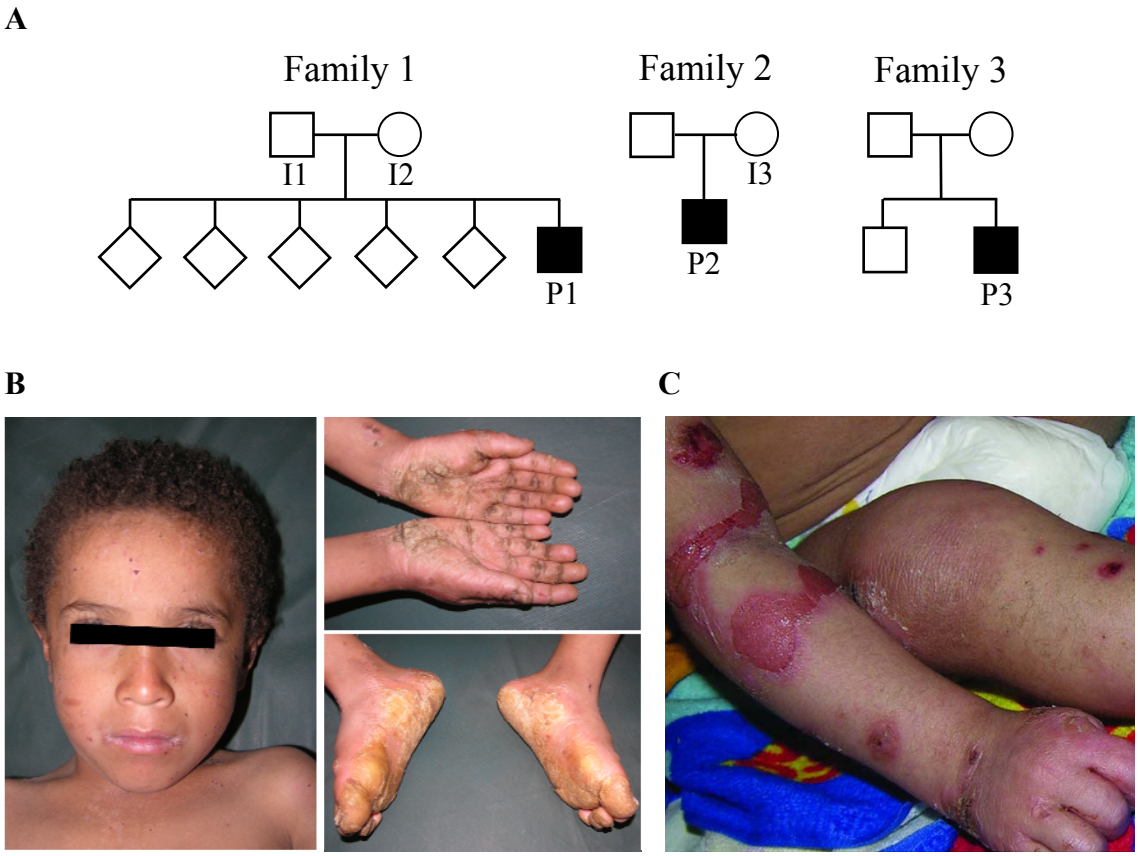

Figure 3.1. Pedigree structure of the three Argentinean families investigated in this study and clinical features showing distinct phenotype of skin fragility, PPK and woolly hair. (A) Filled symbols represent affected family members (P1, P2 and P3). Squares represent male and circles represent female individuals. I1, I2 and I3 code for investigated healthy family members. **(B)** Clinical phenotype of one affected patient. Diffuse PPK, erosions on the face and around the mouth and woolly scalp hair are shown. **(C)** Clinical features of another patient showing severe skin fragility and the extent of blistering in early months of life.

3.1.2. Histological, ultrastructural and immunohistochemical findings

Histological examination of affected skin from these patients showed thickening of the epidermis with hyperkeratosis and acanthosis (increased cell number). The intercellular spaces between keratinocytes of the spinous and granular layers in lesional skin were wider. Acantholysis within the upper spinous and granular layers, resulting in intra-epidermal clefts, was also observed (Figure 3.2A). Ultrastructurally, desmosomes were noted to be reduced in number and not fully developed. IFs were collapsed around the nuclei and their attachment to the desmosomal plaques was defective (Figure 3.2B). The split between keratinocytes occurred intracellularly, at the level of the inner dense

plaques (IDPs) of desmosomes. Desmosomes with discontinuous outer dense plaques (ODPs) were frequent (Figure 3.2C) (Winik *et al.*, 2009).

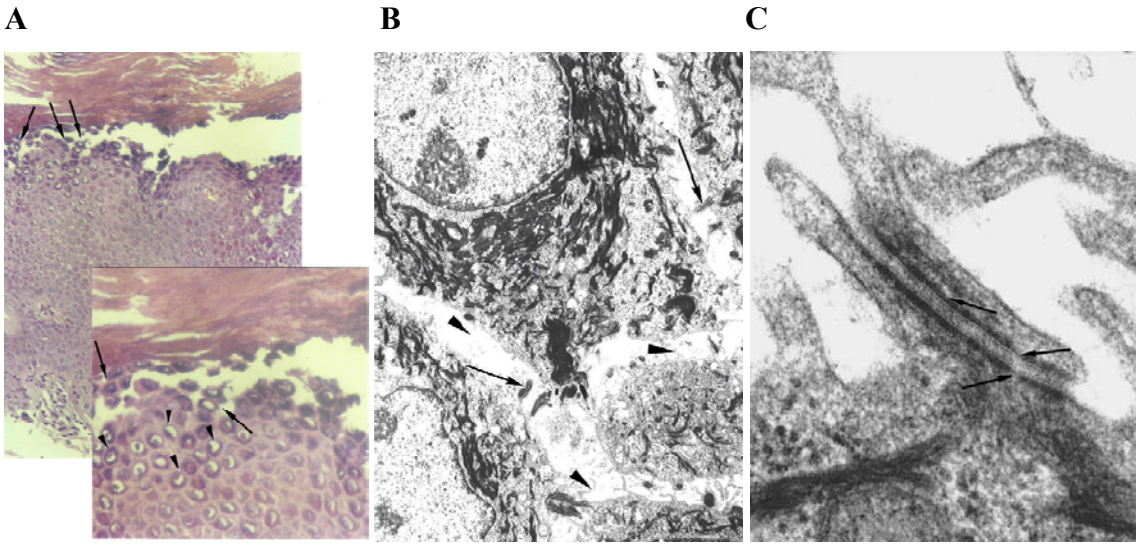

Figure 3.2. Histology and electron microscopy of affected skin. (A) Histology of affected skin stained with haematoxylin and eosin shows thickening of the epidermis with hyperkeratosis. Intercellular widening and acantholysis are observed in the upper spinous and granular layers (arrows). An increase in the cell cytoplasmic basophilia is also observed (arrowheads). **(B)** Ultrastructural analysis reveals intercellular widening (arrowheads) and poorly developed desmosomes (arrows). Clumped keratin IFs are observed in a perinuclear region with no clear insertions into desmosomes. The split between keratinocytes is observed intracellularly at the level of the IDPs **(C)** Poorly developed desmosome showing discontinuous ODPs (arrows). Figure courtesy of Dr. Beatrice Winik (Servicio de Microscopía Electrónica, INSIBIO, Universidad Nacional de Tucumán—CONICET, Tucumán, Argentina).

Immunohistochemistry of patients' skin with antibodies raised against desmosomal proteins demonstrated disrupted expression of both DP and DSG1, characterised by increased cytoplasmic staining compared to bright membrane bound immunoreactivity in normal control skin. More striking was the virtually absent PG staining in patient skin, compared to control skin. Moreover, the little amount of PG observed was not membrane bound, but mainly cytoplasmic. PKP1 and DSC 1-3 expression and localisation were normal. Immunostaining with antibodies raised against the adherens junction proteins E-cadherin and β-catenin also appeared normal (Cabral *et al.*, 2010).

3.1.3. Summary

The three patients described here presented with an identical, distinctive phenotype and all originated from Argentina. Therefore, it was hypothesised that all three patients inherited the same ancestral disease allele on both maternal and paternal chromosomes. Additionally, as the three affected children were born to healthy parents, *de novo* dominant mutations were not suspected. Histological and ultrastructural analysis of these patients' skin suggested a desmosomal disorder and immunofluorescence staining suggested the presence of mutations in PG, DP or DSG1. PG was the most likely candidate due to the very low immunoreactive signal observed by immunofluorescence staining of patient skin with a PG antibody, and to the discontinuous ODPs seen by electron microscopy. To gain further insight into the potential candidate genes for this disorder, a SNP genomic mapping array was first performed.

3.2. Results

3.2.1. SNP genomic mapping

Given that a recessive mode of inheritance was expected, a genome wide search for regions of common ancestry (homozygosity) was carried out in collaboration with Dr. Charles Main and Dr Richard Dobson. Common regions of genomic homozygosity were searched using the Illumina HumanHap550v3_A Genotyping BeadChip SNP mapping arrays. Scoring blocks of more than 20 consecutive homozygous SNPs common to all patients identified a region of 815 homozygous SNPs on chromosome 17 from positions 32 to 40 Mb (Figure 3.3). The next largest shared homozygous stretch on other autosomes was 94 SNPs on chromosome one (data not shown).

The homozygous region on chromosome 17 contains over 200 coding genes, among which a gene cluster encoding different keratins and the *JUP* gene encoding PG stood out. Given that ultrastructural data revealed defective desmosomal complexes with discontinuous ODPs (Winik *et al.*, 2009 and Figure 3.2C), PG was more likely to be abnormal than keratin IFs.

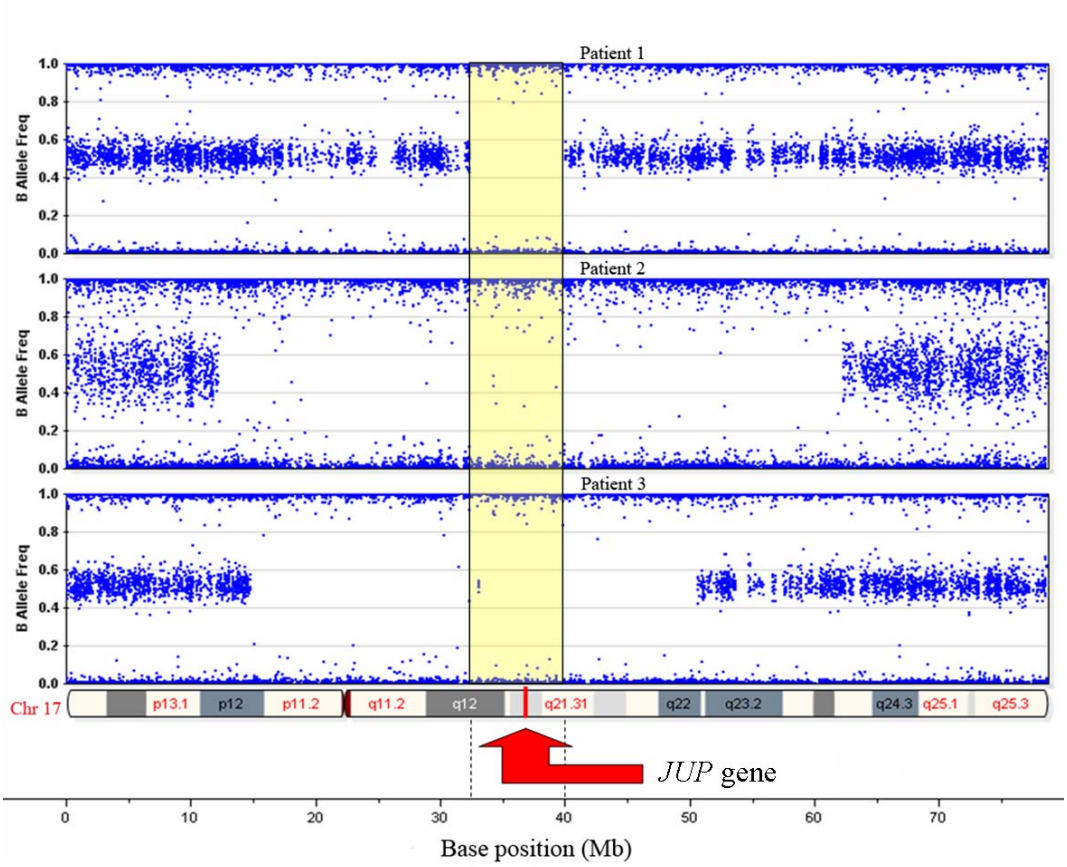

Figure 3.3. Allelic profile of chromosome 17 for the three affected individuals reveals a common 8 Mb region of homozygosity which includes the *JUP* gene. Scoring blocks of more than 20 consecutive SNPs which were homozygous in all three patients identified a major region of 815 homozygous SNPs from positions 32 to 40 Mb of chromosome 17. This 8 Mb region contains the gene encoding PG, *JUP*, which is the most likely candidate for the disease phenotype. Work done in collaboration with Dr. Charles Main and Dr Richard Dobson (Genome Centre, Barts and the London, Queen Mary's School of Medicine and Dentistry, University of London, London, UK).

3.2.2. Mutation analysis in the PG gene, *JUP*

The *JUP* gene was the most likely candidate within the 8 Mb region of homozygosity on chromosome 17. Exons eight to 14 of *JUP* had been screened for mutations in these patients prior to this study commencing (Dr. Andrew South). Therefore, genomic DNA from one patient was used to PCR amplify across the coding exons two to seven. Sequencing of these products identified a cytosine to adenine homozygous transversion at coding nucleotide 71, in the first coding exon of *JUP* (exon two). This substitution changes a serine amino acid codon, TCG, to a premature termination codon (PTC), TAG (c.71C>A, p.S24X). Further analysis revealed this homozygous change in the two remaining patients and heterozygous change in all three parental DNA samples studied (Figure 3.4A). The presence of this mutation destroys a

*Hinf*I restriction enzyme site and therefore its absence from 108 control chromosomes was confirmed either by PCR/*Hinf*I digest (Figure 3.4B), or by sequencing.

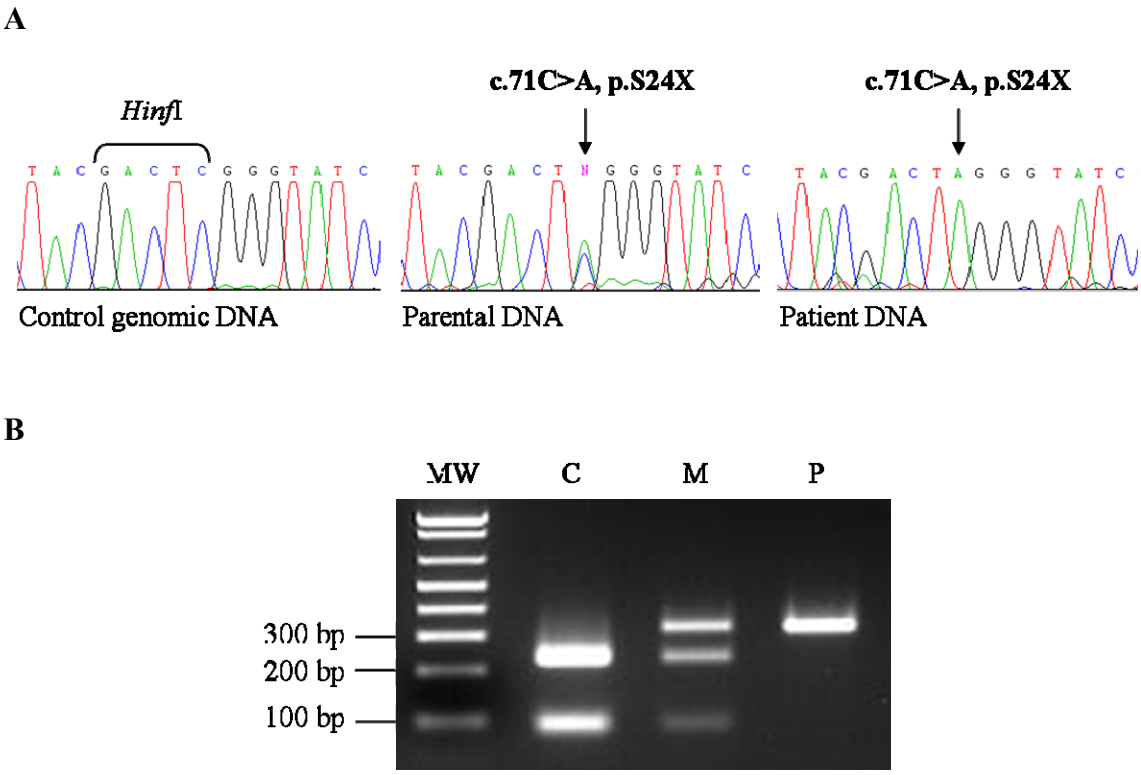

Figure 3.4. Identification of a nonsense mutation (c.71 C>A, p.S24X) in the *JUP* gene of three affected individuals and family members. (A) Electropherograms of control, parental and patient genomic DNA sequences within the second exon of *JUP*. Sequencing of patient DNA reveals a homozygous transversion from cytosine to adenine at coding position 71, which changes a serine amino acid codon, TCG, to a stop codon, TAG (c.71C>A, p.S24X). Unaffected parents are heterozygous carriers of this mutation. The *Hinf*I restriction site, which is destroyed by the mutation, is shown. **(B)** Verification of the mutation by PCR/*Hinf*I restriction enzyme digest of wild type and c.71C>A mutant *JUP*. Control (C) DNA shows complete digest (two fragments of 75 bp and 227 bp); DNA from a heterozygous c.71C>A carrier (mother, M) shows incomplete digest (one undigested fragment of 302 bp from the mutant allele and two digested fragments from the wild type allele); patient (P) DNA shows one undigested mutant fragment, indicating that the *Hinf*I site is ablated. MW = molecular weight marker.

3.2.3. RT-PCR from skin RNA and sequencing analysis

RT-PCR of total RNA from skin samples of one of the patients, his mother and a normal control was carried out to determine if mutant c.71C>A transcripts were readily detectable. Amplification across exons one to three of *JUP* with primers F1/R1 and F2/R2 (Figure 3.5A) showed the presence of *JUP* mRNA in the patient sample (Figure 3.5B), indicating that nonsense mediated mRNA decay (NMD) of mutant transcripts was not taking place. The c.71C>A mutant transcripts were expressed at higher levels than wild type transcripts (Figure 3.5A). Sequencing analysis of the PCR products

confirmed the presence of mutant transcripts in the patient sample as well as in the heterozygous maternal sample (Figure 3.5C) and no alternative 5' splicing was detected. Although this analysis is not quantitative it is clear from the sequencing data (Figure 3.5C) that the mutant mRNA is expressed at roughly equivalent levels to wild type mRNA in heterozygous carriers.

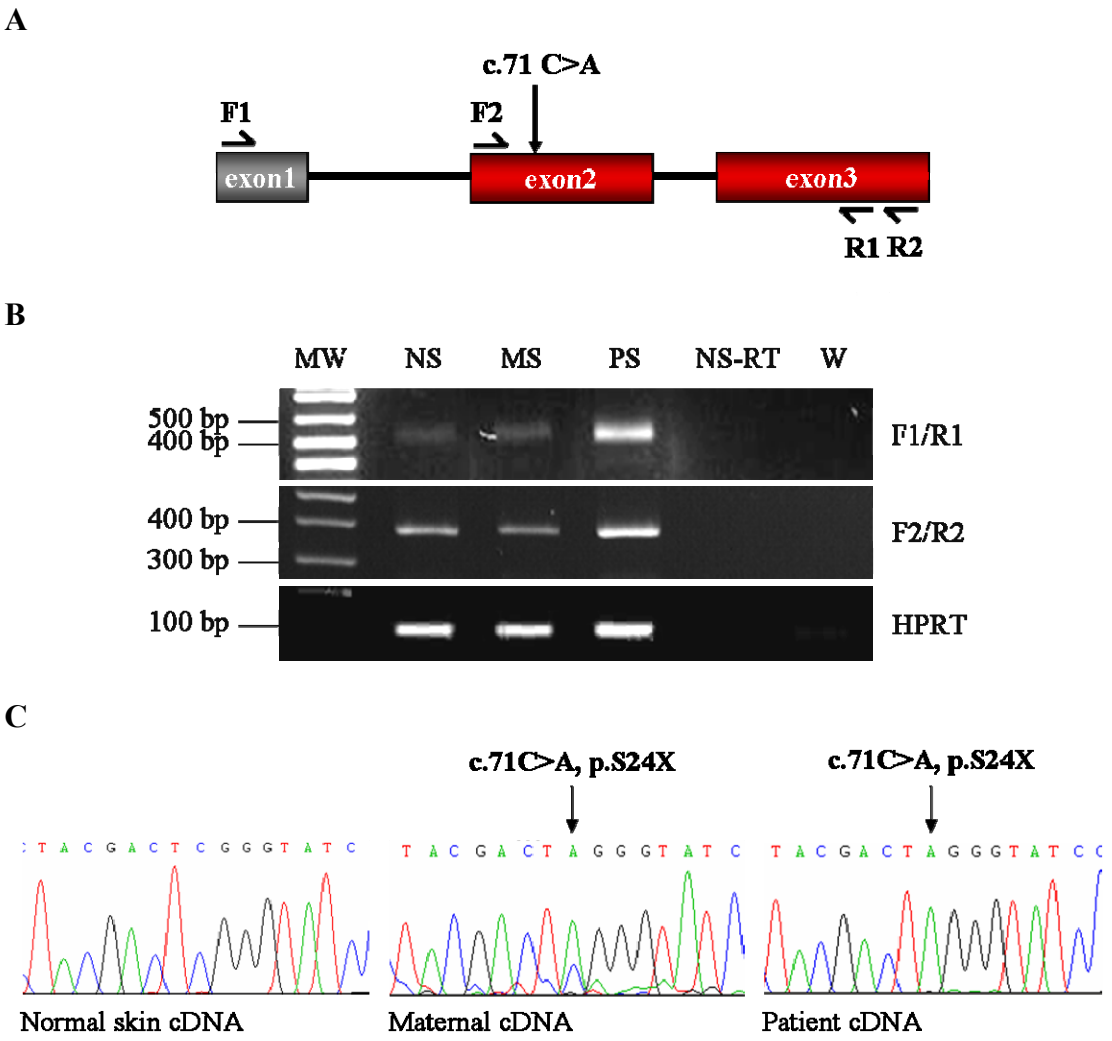

Figure 3.5. c.71C>A nonsense mutation results in detectable mutant transcript in patient skin. (A) Schematic diagram of exons one to three of the *JUP* gene, showing primer pairs used to amplify *JUP* cDNA (F1/R1 and F2/R2) and the relative location of c.71 C>A mutation (indicated with an arrow). Exon 1 (in grey) is non-coding. Primers F1/R1 and F2/R2 were designed to PCR amplify cDNA fragments of 465 bp and 375 bp, respectively. **(B)** RT-PCR of total RNA from normal control skin (NS), maternal skin (MS) and patient skin (PS) samples. Normal skin RNA in the absence of reverse transcriptase (NS-RT) and water (W) were used as internal negative controls. Primers to amplify the *hypoxanthine-guanine phosphoribosyltransferase* housekeeping gene (*HPRT*) were used as a control of cDNA abundance. **(C)** Sequencing analysis of RT-PCR products generated with primers F1/R1 and F2/R2 shows the presence of mutant transcript in both maternal and patient samples, indicating that normal 5' splicing is occurring.

3.2.4. Immunoblotting of skin proteins

PG expression was assessed by western blot of total skin proteins isolated from patient, mother and control samples, using an antibody mapped to the C-terminus of PG (PG 5.1, see Figure A1 in Appendix A). In the control sample, full length PG was observed at approximately 82 KDa, as expected. In the mother's sample, in addition to full length PG, a truncated protein was detected at a much lower expression level. The patient's sample only contained low levels of this truncated protein with no full length PG present. The truncated protein was not observed in the control sample (Figure 3.6A). Identical results were observed when using an N-terminal PG antibody (clone 15F11) which reacts with a C-terminally truncated PG protein containing only amino acids 1-144 (Sacco *et al.*, 1995) (see Figures A1 and A2 in Appendix A).

3.2.5. Identification of alternative translation initiation sites in the *JUP* mRNA

Three previous observations suggest that an N-terminally truncated PG protein is produced from the mutant transcript. Firstly, the c.71C>A nonsense mutation generates a PTC within the first coding exon of *JUP*. Secondly, the corresponding transcript is correctly 5' spliced, and thirdly a shorter mutant protein was detected by western blot. A possible explanation as to how this truncated protein is produced is by initiation of translation through an alternative start codon downstream of the PTC. Therefore, analysis of in-frame downstream AUG codons was undertaken to confirm whether this explanation was likely in this case.

Three potential alternative initiation sites for translation were found (Figure 3.6B). The first AUG codon downstream of the native translation start site, encoding methionine 43 (M43), is part of the strongest Kozak consensus sequence (Figure 3.6B). The Kozak consensus sequence is known to strongly facilitate translation initiation when containing the highly conserved nucleotides adenine at position -3 and guanine at position +4 (Kozak, 1981) (Figure 3.6B). Translation starting from the AUG codon encoding M43 would produce a protein with 703 amino acids, which would lack the first 42 amino acids of the wild type PG. This protein is calculated to be 5 KDa smaller than wild type PG, according to the protein molecular weight prediction of The Sequence Manipulation Suite bioinformatics program (http://www.bioinformatics.org/sms/index.html). The calculated molecular weights for the predicted N-terminally truncated protein (77KDa) and wild type PG (82KDa) correspond to those observed by western blot, based on the migration of the marker

proteins of known molecular weight. Therefore, these results suggest that the truncated PG protein is generated through the use of an in frame alternative site for translation initiation encoding M43 and lacks the first 42 amino acids. The N-terminally truncated mutant PG protein was designated as PGΔN42.

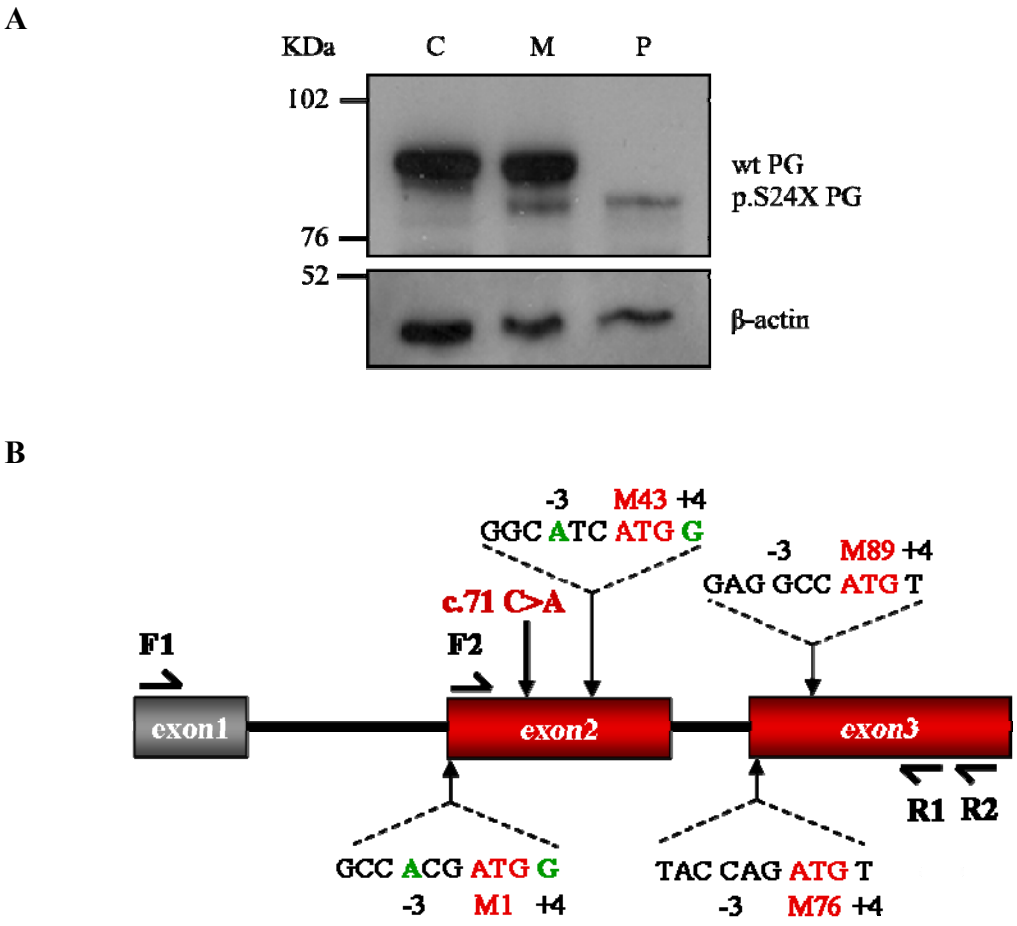

Figure 3.6. p.S24X mutation results in an N-terminally truncated protein, likely through alternative initiation of translation. (A) Western blotting of skin proteins from a normal control (C), maternal (M) and patient (P) samples with a C-terminal PG antibody (PG5.1) shows low levels of a truncated protein predicted to be 77 KDa (p.S24X PG) in both maternal and patient samples. Full length PG which is 82 KDa (wt PG) is observed in control and maternal skin samples. β-actin (42 KDa) was used as loading control. **(B)** Schematic diagram of *JUP* exons one to three showing primer pairs used to amplify *JUP* cDNA (F1/R1 and F2/R2), the site of the c.71C>A mutation (indicated with an arrow), the native Kozak consensus sequence of *JUP* and three possible alternative sites for translation initiation downstream of the mutation. The alternative AUG translation start codon encoding methionine 43 (M43) has the strongest Kozak sequence characterised by an adenine at conserved position -3 and a guanine at conserved position +4, as observed for the native Kozak sequence (M1). A truncated protein initiated from M43 is 703 amino acids, predicted to be 77 KDa which corresponds to the truncated protein seen by western blot.

3.3. Discussion

The goal of the work described in this chapter was to identify the disease causing genetic mutation in three non-consanguineous patients originating from the same region of South America. These patients were hypothesised to have a desmosomal disease caused by a common recessive mutation in a desmosomal gene.

During the course of this study, two additional sibling patients originating from Kuwait were identified, who presented with a very similar clinical phenotype to that of the Argentinean patients described here. This phenotype constitutes a novel genodermatosis designated as acantholytic ectodermal dysplasia. The Kuwaiti patients were found to carry a homozygous guanine to adenine transition at coding nucleotide 468, c.468G>A, in the 5' region of *JUP*. This mutation occurs in the last nucleotide of the second coding exon and is predicted to ablate splicing in this region (Cabral *et al.*, 2010) (see below). A PTC is found 18 nucleotides downstream of the mutation site which could lead to activation of the NMD pathway. Ultrastructural and immunohistochemical analysis of these patients' skin were performed (Cabral *et al.*, 2010) (discussed below), however, availability of biopsy material prevented detailed analysis of c.468G>A skin.

3.3.1. Clinical, histopathological and ultrastructural characteristics in acantholytic ectodermal dysplasia

3.3.1.1. Similarities between Argentinean and Kuwaiti patients

Both the Argentinean and Kuwaiti children have severe and widespread skin fragility, which was observed since the first month of life, with blisters and erosions in different sites of the body together with diffuse PPK and woolly hair (Figures 3.1B and 3.1C and 3.7A). The hair in Kuwaiti patients was predominantly sparse in contrast with the hair of Argentinean patients. No cardiac abnormalities were observed in any of the five children. All five patients were born to healthy parents. Histological analysis of these patients' skin revealed thickening of the epidermis, widening of intercellular spaces between suprabasal keratinocytes and loss of cell-cell contacts (Figure 3.7B). Immunohistochemistry of these patients' skin with antibodies raised against desmosomal proteins showed similar expression levels and localisation of these proteins in all patients. The distribution of DP and DSG1 was slightly disrupted but more

striking was the marked reduction of PG staining in patient skin compared to control skin (see section 3.1.2).

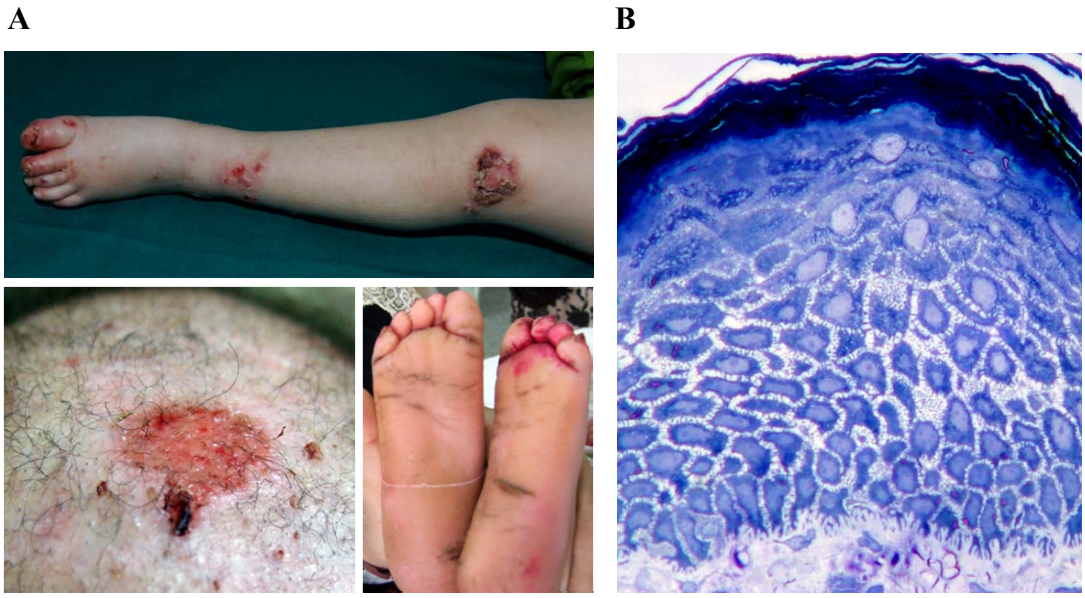

Figure 3.7. Clinical and histological features of the Kuwaiti patients. (A) The distinct phenotype of skin fragility, woolly (sparse) hair, and plantar keratoderma is shown in one affected patient from the Kuwaiti family. Figure courtesy of Prof. John McGrath. **(B)** Histology of lesional skin showing widening of spaces between suprabasal keratinocytes and loss of cell-cell adhesion. Figure courtesy of Dr. Beatrice Winik (Servicio de Microscopía Electrónica, INSIBIO, Universidad Nacional de Tucumán—CONICET, Tucumán, Argentina).

Skin transmission electron microscopy of Argentinean and Kuwaiti patients revealed very similar ultrastructural features (Cabral *et al.*, 2010) (see Figure 3.8). These included loss of inter-keratinocyte adhesion, most prominent in spinous layers, accompanied by some perinuclear aggregation of the keratin IF network. Desmosomes were under-developed and lacked defined insertions of keratin IFs. Instead of defined regions of homogenous electron density which are seen in normal desmosomes (i.e the IDP and ODP), these defective desmosomes showed a disorganised and heterogeneous combination of lighter and denser regions. This was particularly evident within the desmosomal inner plaques which frequently showed discontinuities (arrows, Figure 3.8).

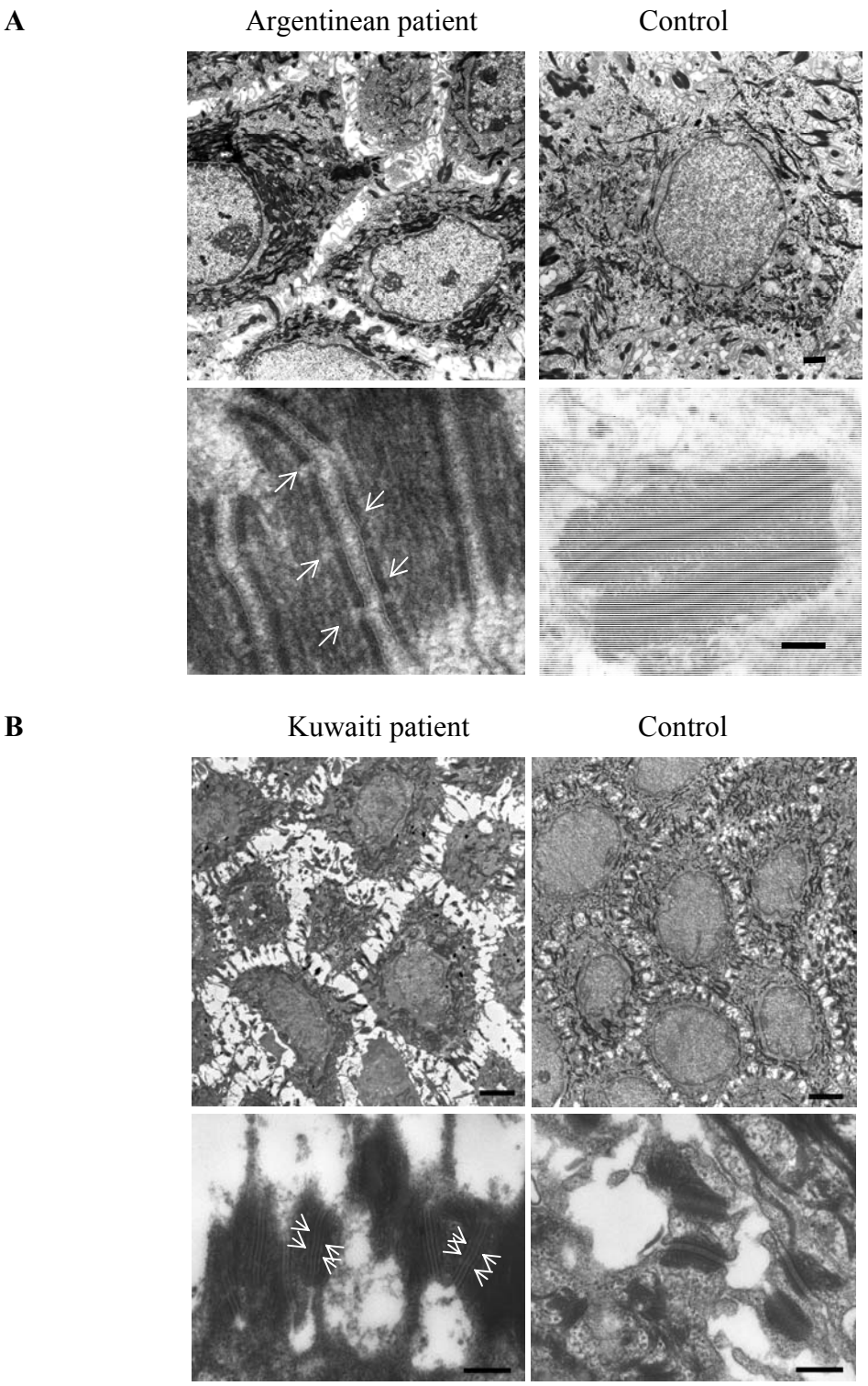

Figure 3.8. Electron microscopy of keratinocytes in the mid-spinous layer from acantholytic ectodermal dysplasia and control epidermis. Widening of intercellular spaces and underdeveloped desmosomes are observed in the epidermis of an Argentinean (**A**, left panels) and a Kuwaiti patient (**B**, left panels) compared with controls (**A** and **B**, right panels). The keratin IF network is not closely associated with cell membranes in patient skin and shows perinuclear aggregation (**A** and **B**, upper left panels) compared with controls (**A** and **B**, upper right panels). High magnification of patient skin (**A** and **B**, bottom left panels) reveals hypoplastic desmosomes with unclear sites of keratin IF insertion. Notably, disruption to the structural organization of the desmosomal inner plaques is evident (arrows). Scale bars: **(A)** 1μm, upper panels; 100nm lower panels; **(B)** 2.5μm, upper panels; 0.25μm, lower panels. Figure courtesy of Patricia Dopping-Hepenstal (National Diagnostic Epidermolysis Bullosa Laboratory, GSTS Pathology, St Thomas' Hospital, London, UK).

3.3.1.2. Similarities and differences between acantholytic ectodermal dysplasia patients and patients with other known genodermatosis

Interestingly, common clinical and histopathological characteristics are observed between patients with acantholytic ectodermal dysplasia (Argentinean and Kuwaiti patients described here) and patients with three different types of genodermatosis associated either with or without heart disease, namely ectodermal dysplasia-skin fragility syndrome, Carvajal syndrome and Naxos disease.

Patients with ectodermal dysplasia-skin fragility syndrome, which is caused by recessively inherited mutations in the *PKP1* gene (McGrath *et al.*, 1997; McGrath & Mellerio, 2010), also exhibit very severe skin fragility observed shortly after birth, with blisters and erosions in heals and soles. Later in life, severe hyperkeratosis, scaling and cracking of palms and soles are observed, as well as crusts and erosions in scalp and face, trunk and limbs. Patients with this condition usually have total loss of scalp hair, as well as eyebrows and eyelashes, in contrast with the Argentinean patients described here who have abundant curly hair. However, the Kuwaiti patients also showed sparse scalp hair (Figure 3.7A). Skin histological and ultrastructural features of patients with ectodermal dysplasia-skin fragility syndrome are very similar to those of the Argentinean and Kuwaiti patients, including thickening of the epidermis with widening of intercellular spaces and loss of cell-cell adhesion in suprabasal keratinocytes. Desmosomes are immature and reduced in number and their connections with IFs are defective (McMillan *et al.*, 2003).

Patients with Carvajal syndrome, which is caused by a homozygous nonsense mutation in *DSP* leading to truncation of the C-terminus of DP (Norgett *et al.*, 2000), also present with woolly hair and striate (focal) PPK (SPPK). In some instances blistering is observed on the trunk and extremities (Bolling & Jonkman, 2009). Additionally, Carvajal patients exhibit left ventricular dilated cardiomyopathy (LVDC), in contrast with patients with ectodermal dysplasia-skin fragility syndrome as well as the Argentinean and Kuwaiti patients who have no heart defects. Despite the clinical differences between Carvajal patients and the Argentinean or Kuwaiti patients, similar skin histopathological and ultrastructural features are observed between these two groups of patients. Carvajal patients' skin is thickened compared to normal skin and large intercellular spaces are seen between suprabasal keratinocytes. Acantholysis is observed in spinous layers, a feature which is not observed in Naxos patients (see below). Lesional palm skin also reveals clumping of desmosomes in suprabasal

keratinocytes, which are only present in infrequent sites of cell-cell adhesion. Immunohistochemistry of suprabasal layers of palmoplantar epidermis revealed condensed keratin filaments with membranous and perinuclear distribution, suggesting a collapsed IF network (Norgett *et al.*, 2000). Immunohistochemistry of Carvajal patients' hearts showed reduced DP and PG signal and loss of desmin attachment to desmosomal plaques (Kaplan *et al.*, 2004).

Naxos disease is another autosomal recessive disorder caused by a C-terminal truncating deletion in the *JUP* gene (McKoy *et al.*, 2000). Patients with this disorder have arrhythmogenic right ventricular cardiomyopathy (ARVC) associated with diffuse non-epidermolytic PPK (NEPPK) and woolly hair (Protonotarios *et al.*, 1986). Although this phenotype is similar to the one of patients with Carvajal syndrome, the cardiomyopathy in Naxos disease affects predominantly the right ventricle (ARVC), is generally less severe and appears later in adolescence. The hallmark of the cardiomyopathy in Naxos patients, or ARVC, is the presence of adipose depositions in the ventricles. This is not observed in the heart of Carvajal patients. Additionally, Naxos patients have a diffuse NEPPK whereas Carvajal patients have striate PPK (SPPK), which is a focal keratoderma. The skin phenotype shown by the Argentinean and Kuwaiti patients, which is a diffuse keratoderma with skin fragility, resembles more the Naxos skin phenotype but is however much more severe and shows additional blistering and erosions. Histological analysis of Naxos skin shows severe hyperkeratosis but in contrast with the patients described here, no skin blistering or erosions are observed (Coonar *et al.*, 1998). Although no detailed histopathology or electron microscopy analysis have been carried out in the skin of Naxos patients, intercellular widening appears to be a hallmark of desmosomal disease in general and is certainly common to the conditions described above.

Despite clinical and histopathological similarities between the Argentinean and Kuwaiti patients and patients with Carvajal, Naxos and ectodermal dysplasia-skin fragility syndromes, the Argentinean and Kuwaiti patients present with a distinct phenotype. However, a desmosomal adhesion defect in the skin is common to all these different groups of patients.

3.3.2. Candidate gene approach led to identification of homozygous nonsense mutation in *JUP*

Immunohistochemistry of the Argentinean patients' skin with antibodies raised against desmosomal components showed normal PKP1 and DSC1-3 staining, so a mutation in the genes encoding these proteins was not suspected. However, disrupted expression of DP, DSG1 and PG was observed, indicating that a mutation in any of these genes was likely. Moreover, PG expression was strikingly reduced, and the little PG observed was not membrane bound. These results, coupled with the homozygosity SNP array data, indicated that *JUP* was the most likely candidate gene for this genodermatosis. Therefore, a candidate gene approach was undertaken and a novel homozygous nonsense *JUP* mutation (c.71C>A, p.S24X) was found in all three patients and heterozygous family members.

3.3.3. p.S24X mutation results in detectable mutant transcript and reduced levels of truncated PG protein in the skin

The c.71C>A mutation generates a PTC in the first coding exon of *JUP*, 137 nucleotides upstream of the next exon-exon junction (Figure 3.5A). Therefore, it would be expected to activate the NMD pathway leading to degradation of the mutant transcript (Le Hir & Seraphin, 2008) (see section 3.3.4). However, RT-PCR and sequencing analysis revealed that the mutant transcript is normally produced and no abnormal 5' splicing events were detected. Although the RT-PCR was not quantitative, mRNA levels in patient skin were higher than those of control and maternal skin samples (Figure 3.5B). This increase could possibly reflect a mechanism of compensation for the low protein levels produced from the mutant allele (see 3.3.5), but further studies would be needed to confirm this hypothesis.

Western blotting of skin proteins revealed very low levels of expression of a truncated PG protein in both homozygous and heterozygous carriers of the mutant allele. The low expression levels of this truncated protein observed by western blot are consistent with the low levels of PG seen in the patients' skin by immunofluorescence (Cabral *et al.*, 2010; Winik *et al.*, 2009) (discussed in section 3.5.5).

3.3.4. Alternative initiation of translation generates an N-terminally truncated PG (PGΔN42)

The NMD pathway is a surveillance mechanism which ensures that mRNAs containing PTCs are rapidly degraded. It is currently accepted that in mammalian cells, NMD activation is dependent upon the assembly of protein exon junction complexes (EJCs), during mRNA splicing, 20-24 nucleotides upstream of each exon-exon junction. These EJCs stay associated with the mature mRNA until it reaches the cytoplasm, but are removed from the mRNA in ribosomes during the first round of translation. The presence of a PTC positioned more than 50-54 nucleotides upstream of an exon-exon junction will prevent the disassembly of at least one EJC downstream of the PTC. Retention of EJCs, which associate with other protein factors, will trigger NMD leading to the rapid degradation of mutant transcripts (Le Hir & Seraphin, 2008). Therefore generally only PTCs located downstream, or less than 50 nucleotides upstream of the next exon-exon junction will escape NMD.

As mentioned in section 3.3.3, the PTC in the c.71C>A mutant mRNA is located 137 nucleotides upstream of the next exon-exon junction and therefore should be targeted by the NMD pathway. However, exceptions to this rule have been observed, in particular when a PTC is located in close proximity to the translation initiation codon, which is the case in c.71C>A mutant mRNA. Work from different laboratories has shown that PTCs localised at the 5' end of the coding region inhibit mRNA destabilisation and this effect appears to overcome the previous rule. The mechanism used to circumvent NMD in these cases was shown to be by re-initiation of translation downstream of the stop codon (Howard *et al.*, 2004; Inacio *et al.*, 2004; Zhang & Maquat, 1997).

Analysis of in-frame AUG codons downstream of the c.71C>A mutation revealed three potential translation initiation sites. However, the first AUG codon downstream of the native translation start, encoding M43, is included in the strongest Kozak consensus sequence, identical to the Kozak sequence containing the M1-encoding AUG. Translation starting from the AUG codon encoding M43 would produce an N-terminally truncated protein in agreement with the results obtained by western blot (Figure 3.6A). These findings strongly suggest that translation of the PTC-containing *JUP* mRNA is initiating from this alternative start site and generates a truncated protein that lacks the first 42 amino acids (PGΔN42).

In agreement with other reports, evidence is shown here which supports alternative initiation of translation from mRNAs containing PTCs in close proximity to the first AUG (encoding M1), as a mechanism used by cells to overcome NMD. This mechanism may allow some level of phenotypic rescue compared to the damage predicted to be caused by the complete absence of PG in these patients. In support of this hypothesis, PG null mice die between embryonic days E10.5 and E16 with ruptured hearts and those that survive until birth exhibit severe epidermal blistering (Bierkamp *et al.*, 1996; Ruiz *et al.*, 1996). The fact that the Argentinean patients have a normal heart development may suggest that very low levels of the N-terminally truncated PG produce less harmful effects than complete absence of PG in the skin and heart. Likewise, very low levels of wild type PG in Kuwaiti patients might be less harmful than total absence of PG (see also section 3.3.7).

Wild type and c.71C>A mutant *JUP* constructs have been generated and PGΔN42 was shown to be efficiently translated in human dermal fibroblasts (see section 3.3.5). In order to confirm that translation of c.71C>A *JUP* mRNA starts at the AUG encoding M43, it would have been interesting to express wild type and c.71C>A *JUP* constructs as well as a c.71C>A *JUP* construct harbouring a nucleotide substitution in the ATG encoding M43 and investigate their initiation sites for translation. Translation from the latter construct would be expected not to occur or to start from an AUG codon downstream of the one encoding M43. Given that the Kozak consensus sequences in exon three are weaker than that of M43 (Figure 3.6B), translation from AUG codons downstream of M43 is likely to be reduced or absent. Therefore, if translation from M43 occurs, the band observed by western blot corresponding to PGΔN42 should disappear when the ATG encoding M43 is mutated. These results would ultimately confirm that in the presence of c.71C>A, the most favorable translation start site is the AUG encoding M43.

3.3.5. PGΔN42 is expressed at very low levels compared to wild type PG and is not incorporated into junctions

PGΔN42 is expressed in the skin at much lower levels then wild type PG. Furthermore, very little junction incorporation of PG was shown by immunohistochemistry in the patients' skin (Cabral *et al.*, 2010; Winik *et al.*, 2009). This difference in expression levels could be due to a decrease in translation efficiency or in protein stability. It was demonstrated by Dr. Andrew South that recombinant

PGΔN42 is efficiently translated in dermal fibroblasts (Cabral *et al.*, 2010), strongly suggesting that the reduced protein levels observed in patient skin are due to decreased protein stability, which could be caused by lack of junction incorporation.

It has been reported that in the absence of junction assembly in Madin-Darby canine kidney (MDCK) cells, the rate of metabolic turnover of desmosomal proteins is increased. For the glycoprotein components, this represents a dramatic increase in degradation and subsequent decrease in relative levels. These proteins are, however, synthesised and transported to the plasma membrane (Penn *et al.*, 1987). This evidence suggests that in the absence of junction assembly, the components are susceptible to accelerated proteolysis. It is possible, therefore, that PGΔN42 is less stable than wild type PG due to lack of junction incorporation and stabilisation by junctional binding partners. This could lead to increased PGΔN42 metabolic turnover in the skin.

Greatly reduced membrane bound PGΔN42 in the skin of patients homozygous for p.S24X indicates that PGΔN42 is hardly incorporated into adherens junctions or desmosomes. Immunofluorescence staining with E-cadherin and β-catenin antibodies in the epidermis of patients homozygous for p.S24X showed normal distribution of these adherens junction proteins (Cabral *et al.*, 2010). These results indicate that the lack of PG does not interfere with adherens junction assembly and function. Similar results have been observed in keratinocyte cultures established from the skin of PG knock-out (*JUP*$^{-/-}$) mice (Yin *et al.*, 2005). Given that PGΔN42 only differs from wild type PG in the first 42 amino acids, it is possible to conclude that these 42 amino acids are essential for PG incorporation into both desmosomes and adherens junctions of the skin.

The c.468G>A homozygous mutation is hypothesised to lead to activation of the NMD pathway and subsequent degradation of the mutant transcripts; however lack of patient biopsy material prevented confirmation of this event. If this is the case, it is possible to speculate that the reduced levels of PG in the Kuwaiti patients' skin might result from low levels of leaky splicing from the mutant donor splice site of the second coding exon (where the c.468G>A mutation lies). This would explain the low levels of PG immunoreactive signal and lack of junction incorporation observed by immunohistochemistry in the skin of Kuwaiti patients. Further studies will be needed to confirm this hypothesis.

3.3.6. Functional domains in the N-terminus of PG might account for lack of PGΔN42 junction incorporation

PG interacts with other proteins through its central arm-repeat and C-terminal domains (Holthofer *et al.*, 2007; see Figure 3.9). Arm-repeats one to three were found to be necessary for interactions with DSGs and DSCs (Chitaev *et al.*, 1998). This same region is also involved in binding to α-catenin (Chitaev *et al.*, 1998). Furthermore, the interaction with DSC1a is abolished when either end of the central arm-repeat domain is deleted, suggesting that the whole arm-repeat domain might be necessary for interaction with DSC1a (Witcher *et al.*, 1996). Interactions with E-cadherin are thought to be dependent upon arm-repeats four and five (Troyanovsky *et al.*, 1996b). A stretch of amino acids (K673-Q683) in the C-terminus of PG prevents interaction with DSGs because it interacts with upstream binding sites for DSGs and inhibits their activity (Troyanovsky *et al.*, 1996b).

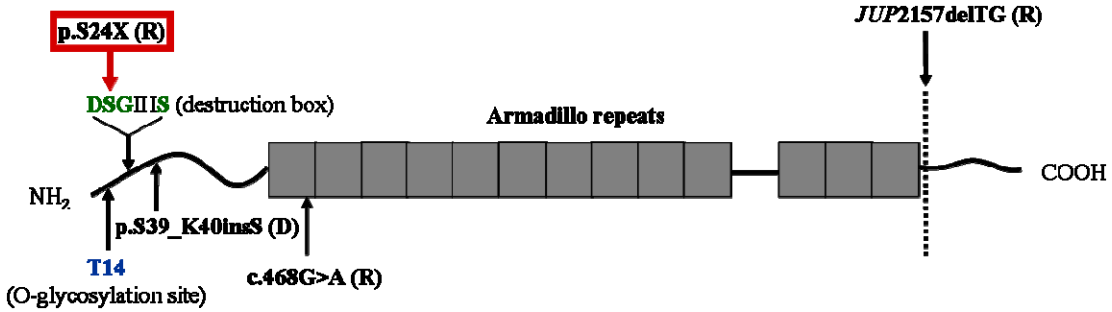

Figure 3.9. Schematic diagram of PG showing regulatory domains in the N-terminus and described mutations. Positions of p.S24X (boxed) as well as the three previously identified mutations are shown as well as the O-glycosylation site and the destruction box.

These findings suggest two interesting aspects. Firstly, overlapping PG binding sites exist for DSGs and α-catenin as well as for DSCs and E-cadherin. This might explain why PG forms mutually exclusive complexes either with α-catenin and classical cadherins in adherens junctions or with DSGs and DSCs in desmosomes (Aberle *et al.*, 1996; Chitaev *et al.*, 1998; Miravet *et al.*, 2003; Sacco *et al.*, 1995). Secondly, intramolecular interactions within PG might occur and might be important regulators of PG interactions (Wahl *et al.*, 2000; Zhurinsky *et al.*, 2000), explaining why sequences in the C-terminus of PG interfere with cryptic DSG binding sites which are located within arm-repeats 6-13 (Troyanovsky *et al.*, 1996a).

In light of these published studies, the known protein-protein interactions occur through regions which lie outside of the first 42 amino acids of PG. However, the lack of the first 42 amino acids of PG prevents its incorporation into both desmosomes and adherens junctions (see section 3.3.5). It is therefore possible that PGΔN42 has a different spatial conformation than wild type PG which could sterically hinder the association of binding partners, prevent its trafficking to junctions or interfere with intramolecular interactions. Furthermore, it was suggested by (Solanas *et al.*, 2004) that the N- and C-terminal domains of both PG and the closely related β-catenin have important regulatory functions which influence the affinity for different ligands. These authors showed that replacement of the central arm-repeat domain of β-catenin by that of PG generated a chimeric protein with the same ligand specificity as the native β-catenin.

PG is a target for both serine/threonine and tyrosine phosphorylation as well as for O-glycosylation (Yin & Green, 2004). Although the first 42 amino acids of PG are not known to participate in protein interactions, this region contains two possible regulatory sites of interest. The first is a consensus sequence for glycogen synthase kinase-3β (GSK-3β) phosphorylation, found within amino acids 22-39 of PG (Rubenstein *et al.*, 1997) (Figure 3.9). This GSK-3β phosphorylation site, also designated as destruction box, is highly conserved in PG, β-catenin and other proteins of the armadillo family, and it is well characterised in β-catenin (Aberle *et al.*, 1996). In the presence of axin, β-catenin and PG are phosphorylated by GSK-3β in residues within the destruction box, subsequently ubiquitinated and then degraded by the proteasome machinery. However, PG is less sensitive to degradation then β-catenin (Kodama *et al.*, 1999). The fact that PGΔN42 lacks this motif and is expressed at very low levels in the skin of these patients suggests degradation and turnover of PGΔN42 is not dependent on the destruction box sequence.

The second site of interest within the first 42 amino acids of PG is an O-glycosylation site. PG is known to be modified by the addition of O-N-acetylglucosamine (O-GlcNAc) at threonine 14 (Figure 3.9), close to the destruction box (Hatsell *et al.*, 2003). O-glycosylation is thought to be a mechanism to counteract phosphorylation and thus protect proteins from degradation by the proteasome (Hatsell *et al.*, 2003), however the effects of O-glycosylation in this particular residue of PG are not clear. Whether it is the lack of these two regulatory domains in the N-terminus of PG that prevents junction incorporation of PGΔN42 in the skin is not known.

It has also been reported that epithelial A-431 cells expressing a recombinant PG lacking the first 122 amino acids (PGΔN122), show an increase in the cytosolic pool of endogenous and ectopic PG (Gaudry *et al.*, 2001; Palka & Green, 1997b). Nevertheless, deletion of the N-terminus did not prevent ectopic or endogenous PG in these cell lines from incorporating into intercellular junctions. PGΔN122 was able to co-immunoprecipitate with classical and desmosomal cadherins. Also, PGΔN122 was able to bind to DSG1 and DP when these proteins were co-expressed in mouse L-fibroblasts (which do not form desmosomal junctions), but whether PGΔN122 was able to localise to junctions as wild type PG does was not described (Kowalczyk *et al.*, 1997). Given that the mutant PGΔN42 still harbours amino acids 43-122 and is not efficiently incorporated into junctions, it is possible that this region is preventing junction incorporation of PGΔN42 in the skin of these patients.

3.3.7. PGΔN42 and c.468G>A enable normal heart development in contrast with previously published *JUP* mutations

Two human mutations have been previously reported in the *JUP* gene both causing cardiomyopathy (Asimaki *et al.*, 2007; McKoy *et al.*, 2000), in contrast with p.S24X and c.468G>A (Cabral *et al.*, 2010). The first mutation is a homozygous two bp deletion (*JUP*2157delTG) causing a C-terminal truncation associated with autosomal recessive syndromic ARVC (Naxos disease) (McKoy *et al.*, 2000) (see section 1.7.2.2). The second mutation is a heterozygous insertion of three bp leading to insertion of a serine residue after amino acid 39 (p.S39_K40insS) and causes dominant non-syndromic ARVC (Asimaki *et al.*, 2007) (this mutation does not affect the skin).

The possibility of PGΔN42 and c.468G>A patients developing cardiomyopathy later in life cannot be ruled out, as the eldest patient to be examined by a cardiologist was 14 years old. Naxos patients usually develop cardiomyopathy in adolescence or early adulthood (Protonotarios & Tsatsopoulou, 2005), however in a study of Naxos patients minor cardiac abnormalities were identified in one five-year-old individual (Protonotarios *et al.*, 2001), and all homozygous individuals over the age of 13 met "Task Force" criteria for ARVC classification (McKenna *et al.*, 1994). None of the five patients described here exhibit cardiac abnormalities. In addition, unlike heterozygous carriers of the Naxos disease allele, individuals heterozygous for either mutant allele do not present with woolly hair (Protonotarios *et al.*, 2001). These observations coupled

with the lack of skin blistering in Naxos patients, indicate that the two *JUP* mutations described here cause a separate phenotype.

3.3.8. ARVC pathology and mechanisms

Although ARVC is known to be a disease mainly caused by defects in desmosomal genes, the molecular mechanism underlying the fibrofatty replacement of ventricular myocytes and consequent arrhythmias is not clear. Myocyte degradation and fibrofatty replacement could be a result of weakened cell adhesion or a defect in cell signalling or both, one leading to the other.

The p.S39_K40insS mutation (see section 3.3.7) was proposed to cause cardiomyopathy through the creation of additional binding partners in the N-terminus and/or disruption of normal function resulting in reduced stability of mutant PG. The authors identified reduced PG levels in the patient's heart tissue. Additionally, human embryonic kidney (HEK293) cells expressing a p.S39_K40insS mutant construct showed that the mutant protein was preferentially ubiquitinated and located for the most part in the cytoplasm. Increased proliferation and decreased apoptosis were also observed in these cells expressing the mutant protein (Asimaki *et al.*, 2007). Therefore, an insertion of a single amino acid into the N-terminus of PG allows normal skin development yet compromises heart whilst reduced levels of PG leads to skin disease with normal heart development. This observation supports the notion that ARVC in patients harbouring p.S39_K40insS results from a dominant negative effect of the mutant PG protein. This is interesting in light of the absence of NMD activation in the skin of PGΔN42 patients. If this is also the case in the heart of these patients, then reduced levels of PG in cardiomyocytes is supposedly more favourable than complete absence of PG or a dominant negative effect. Figure 3.9 shows the four mutations discovered so far in *JUP* as well as known PG regulatory domains.

Cell-cell junctions in the intercalated disc of the heart muscle were shown by immune oelectron microscopy to contain a combination of both desmosomal and adherens junction proteins (Franke *et al.*, 2006) (see section 1.3.2.2.2). Therefore, their composition is different from the typical desmosomes and adherens junctions observed in epithelial tissues. It is possible that some of the requirements for junction incorporation in the intercalated disc, such as binding affinity for other proteins, are different from those of epithelial junctions. The data shown here supports this idea in that it suggests the first 42 amino acids to be essential for junction incorporation in the

skin, but not in the heart. Since PG knock-out mice die from embryonic day E10.5 onwards due to severe heart defects, PG is important for normal murine heart development. However, it is also possible that PG is not essential for the formation of heart junctions in humans and is compensated for by other proteins in these junctions.

Recently, a mechanism for the pathology of ARVC has been proposed based on PG signalling (Garcia-Gras *et al.*, 2006). These authors showed that conditional ablation of DP in cardiomyocytes leads to translocation of PG into the nucleus and reduction in canonical Wnt/β-catenin signaling (see section 1.3.2.2.1). Suppression of this signaling pathway is known to cause a switch from myogenesis to adipogenesis and fibrogenesis and these authors showed increased expression levels of genes associated with adipogeneses and fibrosis in DP-null cardiomyocytes. These findings suggest that the fibrofatty replacement of cardiomyocytes seen in ARVC might result from altered Wnt/β-catenin signaling due to increased levels of non-junctional PG, as opposed to an adhesion defect. In light of these findings, PGΔN42 might still contribute to normal signalling functions in the heart, allowing normal Wnt signalling to occur, even if it has altered adhesion properties. One possible explanation for the lack of heart phenotype in c.468G>A is that PG is greatly reduced and therefore cannot interfere with canonical Wnt signaling.

Further functional studies will be necessary to unveil the role of PGΔN42 in keratinocyte and cardiomyocyte biology; nevertheless results shown here suggest the functional properties of PG and the domains which are important in normal function and development of skin and heart differ considerably.

3.3.9. PG as a diagnostic test for ARVC

A new diagnostic test for ARVC has been proposed based on reduction of PG expression in immunohistochemical analysis of endomyocardial biopsy samples (Asimaki *et al.*, 2009b). These authors tested myocardium tissue samples for PG expression in 11 individuals with ARVC, 10 control individuals and 15 individuals with distinct types of cardiomyopathy (hypertrophic, dilated, or ischemic). All individuals with ARVC, but not control individuals or individuals with other types of cardiomyopathy showed reduced levels of PG immunoreactive signal in the heart.

If PGΔN42 expression levels and localisation are similar in the skin and heart, the results shown here suggest that a diagnostic test for ARVC based on the observation

of reduced levels of PG might not be suitable. Likewise, the low levels of PG in the skin of c.468G>A patients and lack of heart phenotype support this hypothesis, if these patients also have low levels of PG in the heart. Given that cardiac biopsy samples from neither patient were available, it is not possible to definitely answer this question; however lack of PG immunostaining in the skin is certainly not an indicator of ARVC pathology.

Another study described a patient who died of cardiomyopathy and whose heart tissue showed fibrofatty replacement in both ventricles, characteristic of ARVC. This patient carried compound heterozygous mutations in the region encoding the C-terminus of DP. Interestingly, immunofluorescence microscopy of this patient's heart showed PG expression levels that were similar to those of control heart tissue (Mahoney *et al.*, 2009). These results indicate that individuals with ARVC may not present with reduced PG expression levels in the heart, supporting the hypothesis that reduced levels of PG in the heart might not be the most adequate diagnosis for ARVC.

3.4. Summary

This chapter describes a novel homozygous nonsense mutation, p.S24X, in the *JUP* gene. As hypothesised, this mutation was found in three non-consanguineous patients from Argentina and heterozygous family members. p.S24X causes a distinct clinical phenotype, designated as acantholytic ectodermal dysplasia, which consists of skin fragility, PPK and woolly hair but normal heart development. A homozygous splice site mutation in *JUP*, c.468G>A, was found in a parallel study leading to the same clinical phenotype in patients form Kuwait. pS24X was shown to result in very low levels of a N-terminally truncated protein, PGΔN42, which does not incorporate into skin junctions *in vivo*. c.468G>A also results in very low levels of PG in patient skin. These results demonstrate that PG is necessary for maintenance of skin integrity and the lack of heart disease in these patients suggests that normal levels of PG might not be essential for normal heart development in children.

– Chapter 4 –

Identification of DPIb – A Novel Desmoplakin Splice Variant

4.1. Introduction

In order to study the molecular mechanisms of DP in cultured human keratinocytes, *DSP* cDNA constructs had first to be generated (see section 1.9.1). During the process of cloning *DSPI*, a novel *DSP* isoform generated through alternative pre-mRNA splicing of the *DSP* gene was discovered, which had not been previously reported. This chapter describes the identification and characterisation of this novel *DSP* isoform. The generation and expression of wild type- and I608ins10-*DSPI* constructs and subsequent functional studies will be described in Chapter 5.

4.1.1. Alternative pre-mRNA splicing

Alternative pre-mRNA splicing is a mechanism of post-transcriptional regulation of gene expression which occurs in approximately 75% of human genes (Johnson *et al.*, 2003). This mechanism allows human cells to synthesize over 90,000 proteins out of approximately 26,000 coding genes, by generating multiple isoforms from a single pre-mRNA transcript (Ast, 2004). These alternative splice variants are differentially expressed according to tissue types and developmental stages. Among the mechanisms that contribute to protein diversity, alternative splicing is considered to be the most powerful contributor to the functional complexity of the human genome (Black, 2000).

Pre-mRNA splicing is the mechanism whereby non-coding introns are excised and exons are joined to form a mature mRNA transcript. This process involves sequential phosphodiester transfer reactions which are catalysed by a large ribonucleoprotein complex, the spliceosome. Alternative splicing allows different combinations of exons to be joined together. There are four main sub-types of alternative splicing, namely exon skipping, alternative 5' splice site selection, alternative 3' splice site selection and intron retention (Ast, 2004). Three consensus sequences within each introns are required for splicing to occur: the 5' and 3' splice sites (donor and acceptor sites, respectively), which flank each intron, and a branch point which is located more than 18 nucleotides upstream of the 3' splice site and more than 48 nucleotides downstream of the 5' splice site. The donor and acceptor splice sites almost always include the nucleotides GU at the 5' end and AG at the 3' end of the intron, characteristic of canonical splicing, and regulate assembly of the spliceosome complex (Matlin *et al.*, 2005).

It has been extremely challenging to decipher the "splicing code" due to the complex network of regulatory steps which coordinate the final splicing event (Moore & Silver, 2008). Although the relative strength of splice sites influences the frequency of exon selection, this requirement is not sufficient to define an exon; many "pseudo-exons" flanked by strong splice sites exist that are not spliced. Besides the consensus splice site sequences, other more variable regulatory elements are known to be involved in defining both constitutive and alternative exons. These auxiliary sequences are known as exon and intron splicing enhancers and silencers (ESE/ISE and ESS/ISS, respectively) and can have positive or negative effects in splicing events. In addition to these sequences within the pre-mRNA, there are cellular factors (RNA or protein) which are additional players in splicing regulation. Different combinations of RNA-binding proteins, including serine/arginine-rich (SR) proteins and heterogeneous nuclear ribonucleoproteins (hnRNPs), can interact with regulatory elements close to splice sites and promote or inhibit their use. Another level of regulation includes many post-transcriptional and post-translational mechanisms which regulate RNA-binding protein expression and cellular localisation. These mechanisms are in turn dependent upon different signalling pathways, tissue-specific factors and developmental stages (for reviews about mechanisms of splicing regulation see Moore & Silver (2008) and Matlin *et al.* (2005)).

Due to this large complexity, different approaches have been undertaken to gain further insight into the understanding of alternative splicing regulation, which together may enable prediction of the splicing pattern of each individual pre-mRNA. The traditional approach consists of genetic and biochemical studies in individual model systems to characterise regulatory sequences in pre-mRNAs (*cis*-acting regulatory elements) and protein factors (*trans*-acting elements) which together regulate splicing events. Although this approach is important and necessary, it is not sufficient to understand the complex nature of splicing regulation. Global scale approaches are also being used which enable genome-wide identification of *cis*- and *trans*-acting regulatory elements, splice variants in different organisms and cell types, pre-mRNAs which are regulated by individual *trans*-acting factors, as well as signalling pathways, developmental stages or differentiation stages which influence splicing events (Matlin *et al.*, 2005; Moore & Silver, 2008).

4.1.1.1. Alternative splicing within the DSP gene

As mentioned in Chapter 1 the *DSP* gene, like the majority of human genes, is subject to alternative pre-mRNA splicing. This gene gives rise to two known transcripts, *DSPI* and *DSPII*. *DSPI* results from use of the constitutive donor splice site at the exon23/intron 23 junction and is translated into a 332 KDa protein. *DSPII* is produced due to in frame alternative 5' splice site selection in exon 23, which lies upstream of the constitutive one (Figure 4.2B), producing a protein 72 KDa shorter than DPI. The 3' or acceptor splice site within the intron 23/exon 24 junction is common to both splice variants. No other DP isoforms were known prior to this study.

While DPI proteins are present in all desmosome-bearing tissues, expression of DPII is variable; this shorter isoform is widely expressed in epithelial tissues, but barely detectable in cardiac muscle (Green & Hobbs, 2006; Uzumcu *et al.*, 2006). In this chapter, the expression profiles of the previously unknown *DSPIb* isoform were investigated in different tissues and keratinocytes cell lines to assess whether they are similar or differ from those of the known *DSPI* and *DSPII* isoforms. DPIb protein levels were also investigated in two keratinocyte cell lines.

4.2. Results

4.2.1. cDNA amplification of a novel *DSP* alternative transcript, *DSPIb*, in primary normal human keratinocytes

With the purpose of generating a wild type *DSPI* cDNA construct, three overlapping RT-PCR reactions were performed using total RNA from primary normal human keratinocytes (NHK). Amplification of *DSPII* was excluded by using the forward oligonucleotide 2F (depicted in red, Figure 4.1A) which hybridises specifically with *DSPI*. PCR amplification of the first and third fragments generated cDNA products which migrated according to the expected sizes. However, amplification of the middle fragment (fragment 2) with the primer pair 2F/2R (depicted in red, Figure 4.1A) generated a single PCR product of approximately 850 bp (Figure 4.1B). This fragment was shorter than the expected 2196 nucleotide fragment of *DSPI* mRNA, based on the NCBI database (accession number NM_004415.2).

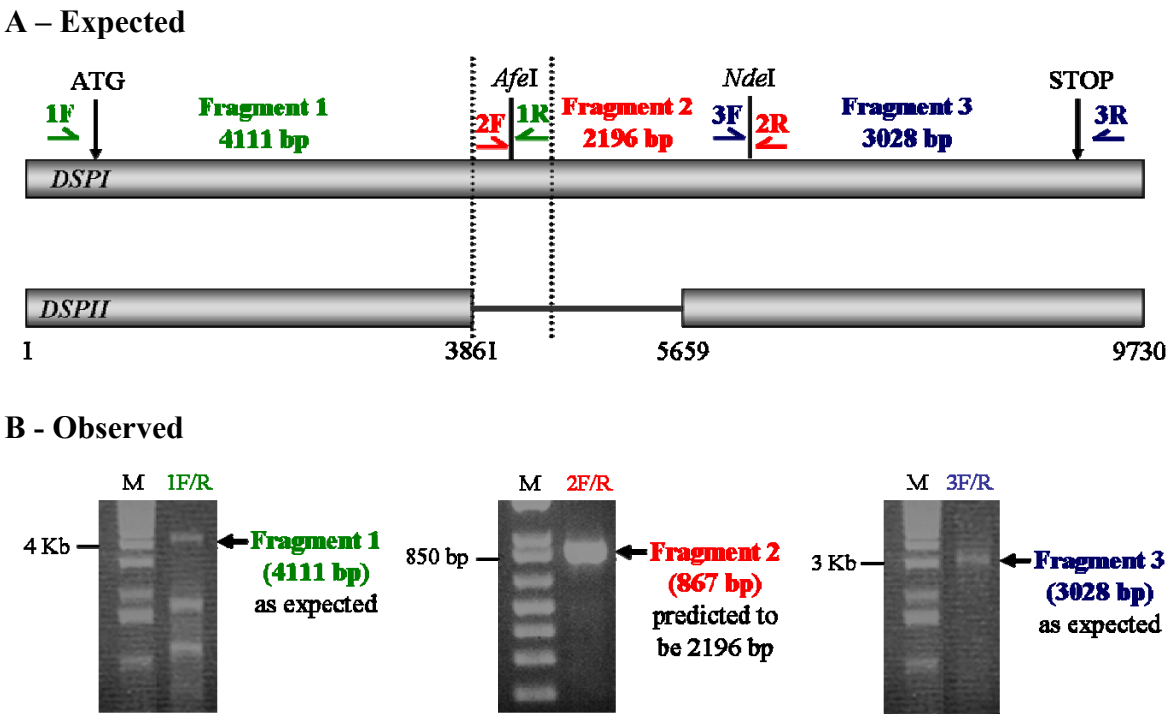

Figure 4.1. Initial *DSPI* cloning strategy led to identification of a novel *DSP* splice variant. **(A)** Schematic diagram of *DSPI* cDNA showing three primer pairs used to PCR amplify three overlapping fragments. Primers 1F/1R (in green), 2F/2R (in red) and 3F/3R (in blue) were used to amplify fragment 1 (predicted to be 4111 bp), fragment 2 (predicted to be 2196 bp) and fragment 3 (predicted to be 3028 bp), respectively. The *DSPII* cDNA is shown to illustrate that primer 2F (in red) was designed to hybridise specifically with *DSPI* cDNA and not with *DSPII* (see discontinuous vertical lines). **(B)** RT-PCR products following agarose gel electrophoresis, corresponding to each of the three amplified fragments. The PCR reaction that generated fragment 1 also resulted in two other fragments, probably due to non-specific binding of primers 1F/1R. Note that fragment 2 is observed at approximately 850 bp in contrast with the predicted size of 2196 bp. M = molecular weight marker.

Sequencing analysis of this PCR product confirmed that it comprises 867 bp. Alignment of the sequence traces with the wild type sequence of *DSPI* revealed homology at both ends, but a 1329 bp region was missing in the centre (Figure 4.2A). As the difference between the *DSPI* and *DSPII* transcripts is 1797 nucleotides, and because the forward primer (2F) used to amplify this fragment does not have sequence homology with *DSPII*, these results demonstrated the presence, at the mRNA level, of a novel *DSP* splice variant in primary NHK.

A

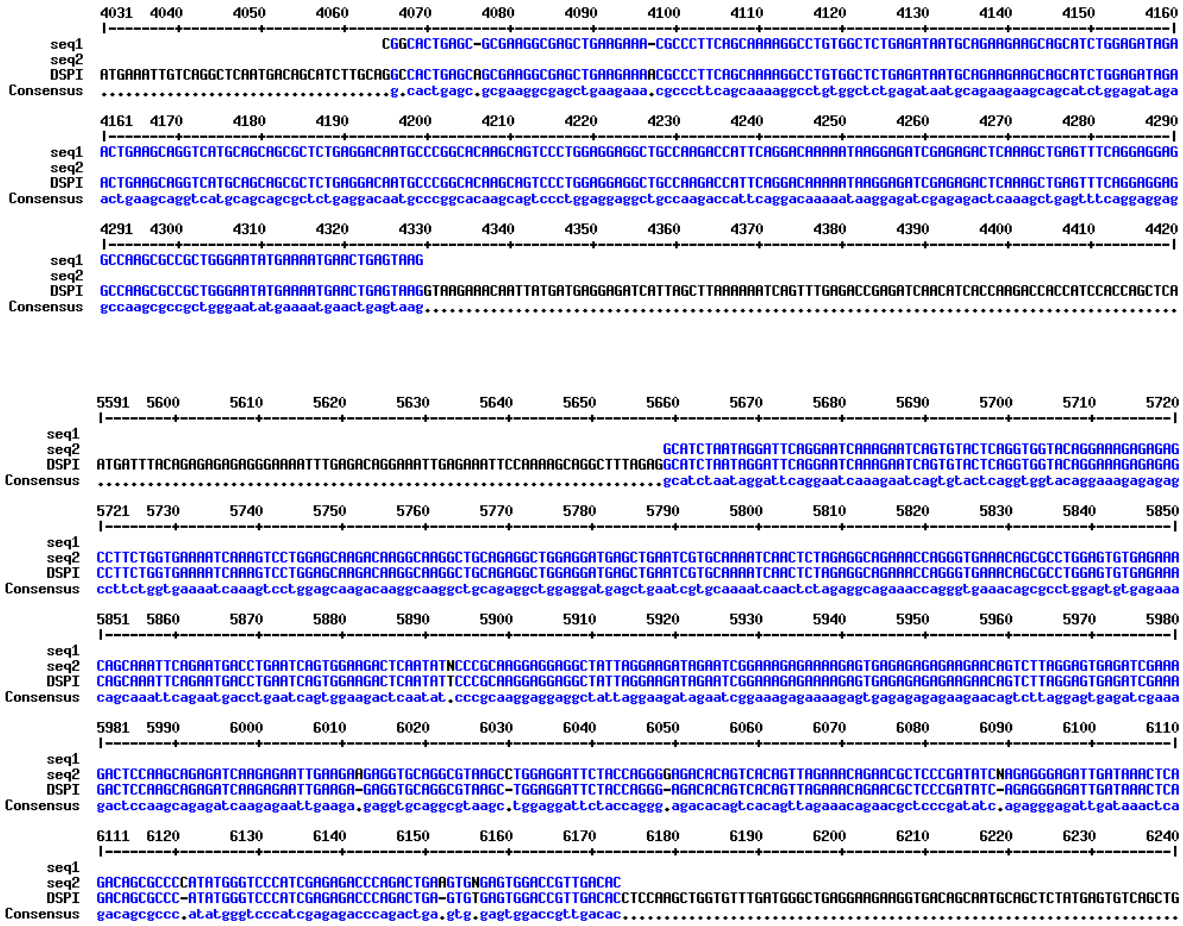

B

Figure 4.2. *DSPIb* is generated through the use of a novel alternative 5' splice site in the *DSP* gene. (A) Sequence alignment (using the Multalin Interface Page, http://bioinfo.genotoul.fr/multalin/multalin.html) of PCR amplified fragment 2 (see Figure 4.1) with the wild type sequence of *DSPI* reveals that the novel splice variant lacks a region from position 4330 to 5658 (position numbers according to accession number NM_004415.2 of NCBI database). **(B)** Genomic illustration of exons 22 to 24 of the *DSP* gene, showing sequences of three alternative donor splice sites in exon/intron 23 which produce the *DSPI*, *DSPIb* and *DSPII* isoforms. The donor splice site that generates *DSPIb* is nearly identical to the one that produces *DSPII*. The conserved nucleotides are illustrated in red.

The newly identified *DSP* transcript is composed of 7284 coding nucleotides and was designated as *DSPIb*. The genomic and mRNA sequences of *DSPI* and *DSPII* present in the NCBI database (accession numbers NM_004415.2 and NM_001008844.1, respectively) were examined and compared with the *DSPIb* sequence. This analysis revealed that *DSPIb* is generated due to the use of an in-frame alternative donor splice site in exon 23, located 468 bp downstream of that of *DSPII* and 1329 bp upstream of that of *DSPI* (Figure 4.2B). The alternative donor splice sites which originate *DSPI* and *DSPII* were also examined and compared to that of *DSPIb*. Interestingly, it was found that the 5' alternative splice sites of *DSPII* and *DSPIb* share 90% of the sequence (9 out of 10 bp, Figure 4.2B) according to the genomic structure of *DSP* described by Whittock *et al.* (1999). The acceptor splice site is common to all three splice variants.

4.2.2. Splice prediction and EST analysis

As *DSPIb* and *DSPII* are generated due to the use of alternative donor splice sites in exon 23, two different splice site predictor programs were used to investigate whether additional 5' alternative splice sites were predicted in this region.

Analysis of the whole *DSPI* mRNA sequence using the Splice Site Prediction by Neural Network (Reese *et al.*, 1997) revealed only two 5' alternative splice sites close to the *DSPI/DSPIb*-specific region (in exon 23), both of which had the highest possible score (1.00). The first one is the donor splice site which originates *DSPII* (starting at nucleotide 3855) and the second gives rise to *DSPIb* (starting at nucleotide 4323) (highlighted in blue, Figure 4.3A).

Analysis of nucleotides 3852 to 5174 using the Alternative Splice Site Predictor (ASSP) (Wang & Marin, 2006) showed the alternative 5' splice sites that originate *DSPII* (starting at nucleotide 3852) and *DSPIb* (starting at nucleotide 4320), also both with the highest score within this region (13 and 12, respectively, highlighted in blue, Figure 4.3B). This program also revealed six additional alternative donor sites within this region, four of which would give rise to in-frame splice variants intermediate in size between *DSPIb* and *DSPI*, assuming that the constitutive acceptor site common to all three isoforms is used (Figure 4.3B, highlighted in yellow and Figure 4.2B). These results suggest there might be additional *DSP* splice variants. However, it is noteworthy that the constitutive donor splice site for *DSPI* is identified by the ASSP program with a score of only 8.7 compared with 13.2 for the donor splice site of *DSPII*, and is not even

predicted by the Neural Network program. This suggests that splice predictions by these programs do not include all the variables that contribute to the final splicing event *in vivo* (see section 4.1.1) and might not always be a direct indicator of the likelihood of a splicing event.

Expressed sequence tag (EST) analysis was also performed to determine the number of transcripts representing the different regions of *DSP* as well as to investigate the existence of ESTs unique to *DSPIb* and *DSPII* on the NCBI EST-database. To this end, the 5' and 3' ends of *DSP* as well as five 50 bp stretches in different regions of the *DSP* mRNA were blasted against the NCBI human EST-database.

As shown in Figure 4.3D, a similarly high number of ESTs is found within the 5' end (comprising 3861 nucleotides) and 3' end (comprising 4071 nucleotides) of *DSP* (102 and 99 ESTs, respectively, depicted in purple), which are regions common to all three splice variants. Likewise, 50 bp stretches in three *DSPI*- (or *DSPI/DSPIb*-) specific regions (depicted in orange, yellow and green, Figure 4.3D) were also represented by a high and similar number of ESTs (31, 37 and 36 ESTs, respectively). In contrast, only 5 ESTs were found to span the *DSPII*-specific exon 23/24 junction (orange/green junction, Figure 4.3D) and only 1 EST spans the *DSPIb*-specific exon 23/24 junction (yellow/green junction, Figure 4.3D). Comparison between the *DSPII*-specific junction (orange/green junction, Figure 4.3D) and the corresponding *DSPI* junctions depicted in orange and green (Figure 4.3D) suggests a *DSPII*:*DSPI* ratio of 1:6 and 1:7, respectively. In a similar way, comparison between the *DSPIb*-specific junction (yellow/green junction, Figure 4.3D) and the corresponding *DSPI*-specific junctions depicted in yellow and green (Figure 4.3D) suggests a *DSPIb*:*DSPI* ratio of 1:37 and 1:36, respectively. Figure 4.3C depicts the alignment of part of the *DSPIb*-specific EST with the *DSPI* cDNA sequence. This clone lacks nucleotides 4330 to 5658, which is a feature of *DSPIb*.

A (Neural Network)

Start	End	Score	Exon Intron
128	142	0.61	ggcccag**gt**agcgag
360	374	0.45	ctacgag**gt**gaccag
1587	1601	0.69	gaacttg**gt**aaacaa
1751	1765	0.98	gcaagtg**gt**acgtga
2580	2594	0.93	atgcaca**gt**aagggc
3855	3869	1.00	ggcaaag**gt**aagaaa
4323	4337	1.00	gagtaag**gt**aagaaa
6016	6030	0.71	tgcaggc**gt**aagctg
6142	6156	0.76	actgagt**gt**gagtgg
6813	6827	0.88	aaagaag**gt**cagtta
7008	7022	0.61	tgacgag**gt**tggtga
7629	7643	0.42	gaaacag**gt**gcagac
8040	8054	0.95	tgaatca**gt**aagtaa
8179	8193	0.73	acagaag**gt**atagag
8212	8226	0.42	atcacgg**gt**cagagg

B (ASSP)

Start	End	Score	Exon Intron
3852	3871	13.23	gctggcaaag**gt**aagaaacc
4320	4339	12.01	actgagtaag**gt**aagaaaca
4656	4675	6.02	agaggagagc**gt**aagatata
4724	4743	7.44	agatagaaag**gt**taaaacaa
4802	4821	4.77	aaagggtcca**gt**atgacctg
4857	4876	5.97	caaactgaag**gt**tcaggagc
4986	5005	5.16	gaagcagaag**gt**ggaagagg
5155	5174	6.28	aagaagagga**gt**gaggatga

C

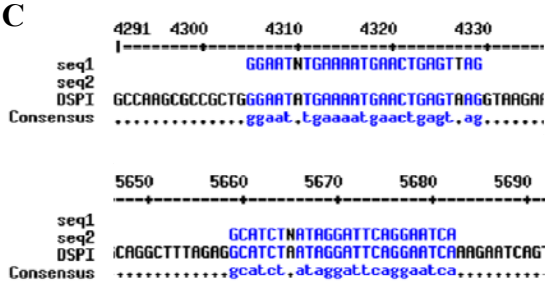

D

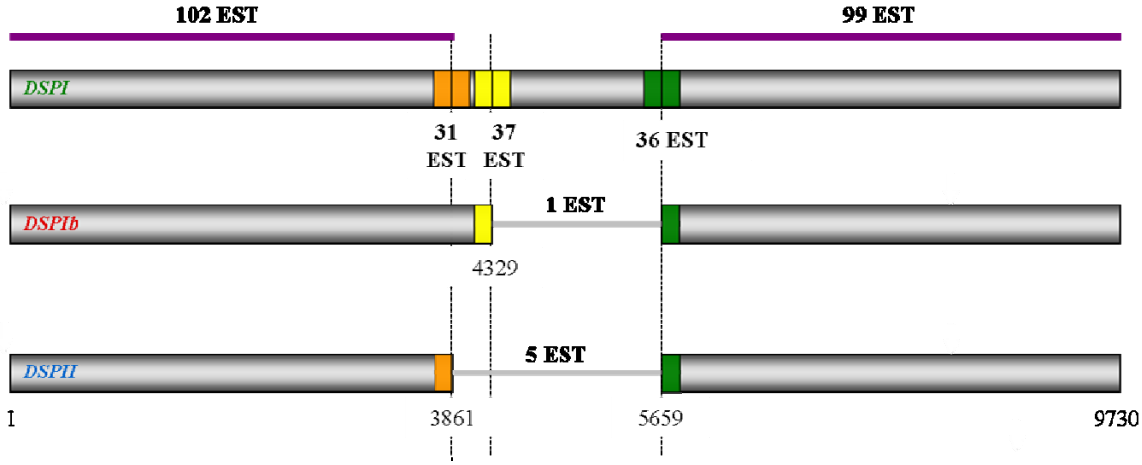

Figure 4.3 Alternative splice prediction and EST analysis in *DSP*. Alternative splice site predictions within *DSPI* cDNA from nucleotides **(A)** 1-9730 using the Splice Site Prediction by Neural Network (http://www.fruitfly.org/seq_tools/splice.html) and **(B)** 3852-5174 using the Alternative Splice Site Predictor (ASSP, http://www.es.embnet.org/~mwang/assp.html). **(A and B)** The predicted 5' alternative splice sites which originate *DSPII* and *DSPIb* are highlighted in blue. Exon/intron boundaries are shown in bold. **(B)** Four predicted in-frame alternative donor splice sites within nucleotides 3852-5174, which would generate *DSP* splice variants intermediate in size between *DSPI* and *DSPIb*, are highlighted in yellow. **(C)** Sequence alignment (using the multalin interface page, http://bioinfo.genotoul.fr/multalin/multalin.html) of part of the *DSPIb*-specific EST (accession number AI525952) with *DSPI* shows that this clone lacks nucleotides 4330 to 5658, which is characteristic of *DSPIb* **(D)** Schematic diagram of *DSP* splice variants showing ESTs found in the NCBI database. 5' and 3' regions (depicted in purple) are represented by 102 and 99 ESTs, respectively. The *DSPIb*- and *DSPII*-specific junctions (yellow/green and orange/green) are spanned by 1 and 5 ESTs, respectively. The corresponding *DSPI*-specific junctions are represented by 37 (yellow) and 31 (orange) ESTs, respectively. The *DSPI*-specific exon 23/24 junction (green) is represented by 36 ESTs. Each coloured square comprises 25 bp on each side of the dashed line.

Overall, the splice predictions and EST analysis of this central alternatively spliced region of *DSP* suggest some interesting points. Firstly, that *DSPIb* is a third *DSP* splice variant which is represented by only 1 EST, possibly due to its low expression level when compared to that of *DSPI*, in the cells or tissues where these ESTs were found. Identification of the *DSPIb*-specific EST is an independent confirmation of *DSPIb* existence. Secondly, that a reduced amount of information is available about the *DSPIb*- and *DSPII*-specific regions, as well as other potential splicing events in this region. These suggestions were taken as reasons to investigate this region further.

4.2.3. Expression profiles of alternative *DSP* transcripts in different tissues and different regions of the heart

To examine *DSPIb* mRNA expression levels in different types of tissue, an RT-PCR based method was designed to specifically amplify and distinguish between each of the *DSP* transcripts (Figure 4.4A). The reverse primer (depicted in grey, Figure 4.4A) hybridises with the 5' end of exon 24 and the three forward primers anneal with different regions of exon 23. The first primer (depicted in green, Figure 4.4A) is *DSPI*-specific, as the other isoforms lack the 3' portion of exon 23, where this primer anneals. The second primer (depicted in red, Figure 4.4A) can anneal with both *DSPI* and *DSPIb*, but generates PCR products of different sizes, the shortest of which will correspond to *DSPIb*. Likewise, the third primer (depicted in blue, Figure 4.4A) can amplify all isoforms, but the shortest product corresponds to *DSPII*. By shortening the PCR extension time in each reaction, it was possible to amplify only the required smaller fragments. Also, because the distance between each primer and the corresponding exon 23/24 border was different, the required fragments had different sizes, each one representative of one *DSP* isoform. Figure 4.4B shows the three resulting PCR products amplified from primary NHK cDNA.

Using the same set of primers and PCR conditions, the different *DSP* splice variants were amplified from a human multiple tissue cDNA panel and a human cardiovascular cDNA panel. The multiple tissue panel included different types of epithelial as well as non-epithelial tissues. The cardiovascular cDNA panel comprised various regions of the adult heart and aorta, as well as foetal heart. Primers which amplified the housekeeping gene g*lyceraldehyde-3-phosphate dehydrogenase* (*G3PDH*) were used as a control of cDNA abundance.

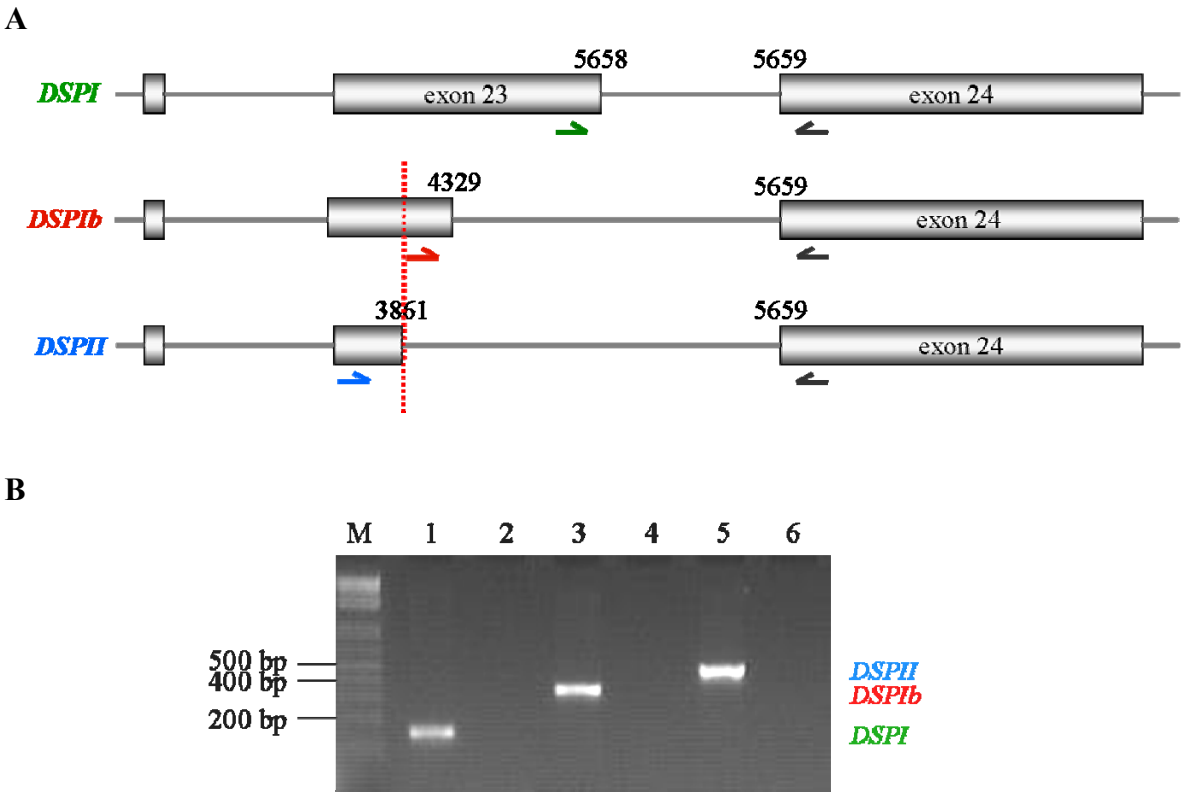

Figure 4.4. RT-PCR based method to specifically amplify each of the *DSP* splice variants from NHK. (A) Schematic diagram of *DSP* isoforms showing primers used to specifically amplify and distinguish between the different isoforms. The reverse primer (*DSP*R, depicted in grey) is common to all isoforms. Three different forward primers (*DSPI*F in green, *DSPIb*F in red and *DSPII*F in blue) were designed to specifically amplify *DSPI* (179 bp), *DSPIb* (383 bp) and *DSPII* (530 bp), respectively. **(B)** RT-PCR products and respective negative water controls amplified from *DSPI* (lanes 1 and 2), *DSPIb* (lanes 3 and 4) and *DSPII* (lanes 5 and 6) RNA from primary NHK. M = molecular weight marker.

All three *DSP* isoforms were shown to be expressed throughout the majority of epithelial tissues with similar expression patterns. They were predominant in the lung, liver and prostate. Low levels of expression of the three isoforms were also seen in the brain but not in skeletal muscle (Figure 4.4A). All three isoforms were also expressed throughout the various compartments of the heart. However, *DSPIb* was the only isoform to be detected in the aorta. The three *DSP* isoforms showed different expression patterns in the different cardiac compartments and aorta. *DSPI* was mostly expressed in the left and right ventricle and foetal heart, whereas *DSPIb* was mainly present in the aorta, right auricle, left atrium as well as in the right ventricle and foetal heart. *DSPII* expression was predominant in the right auricle, left atrium and right ventricle (Figure 4.5B).

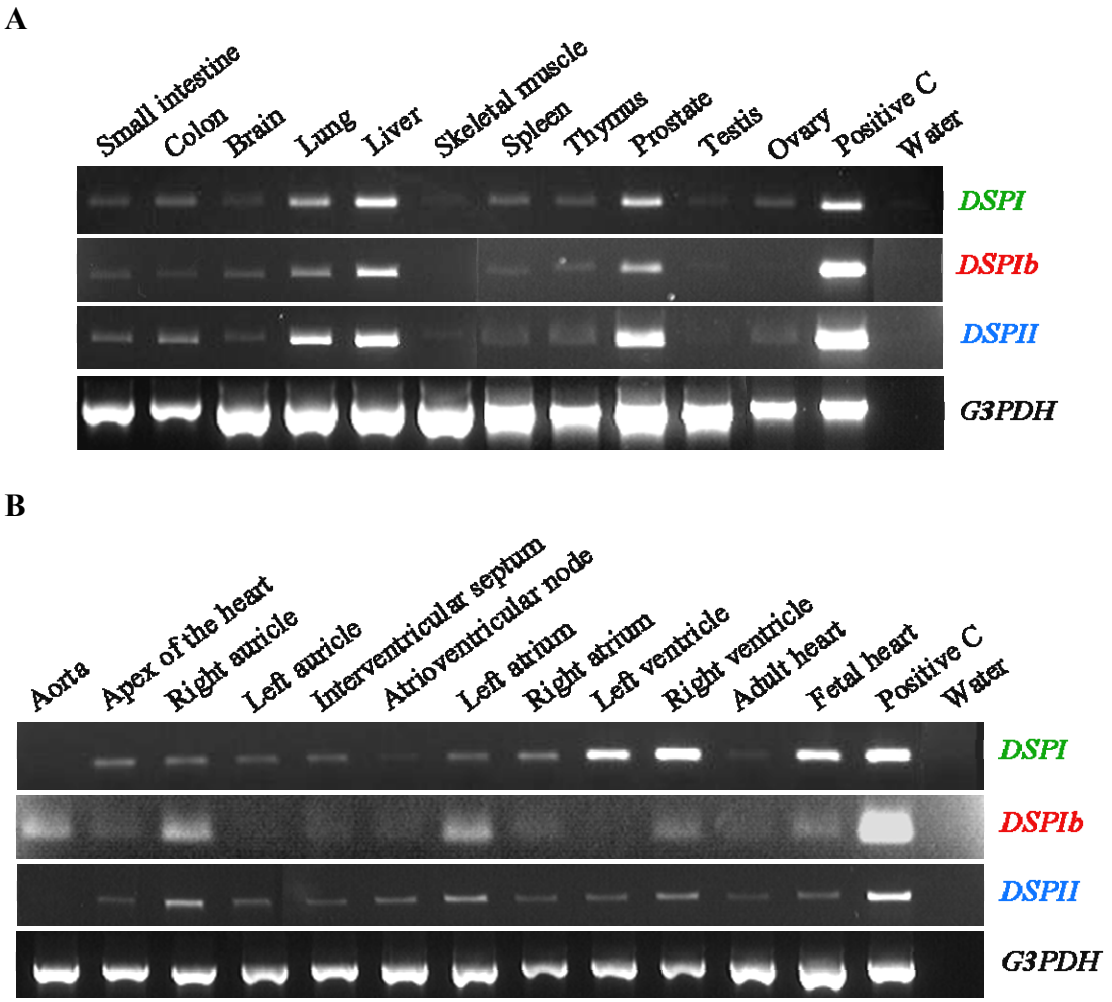

Figure 4.5. *DSPIb* transcript is expressed in several epithelial tissues and in various compartments of the heart and the only *DSP* isoform detected in the aorta. (A) Specific amplification of the different *DSP* transcripts across different types of tissue using a human multiple tissue cDNA panel. *DSPIb* (383 bp) was shown to be expressed throughout the majority of epithelial tissues with similar expression patterns to those of *DSPI* (179 bp) and *DSPII* (530 bp). **(B)** *DSPIb* was the only isoform detected in the aorta. *DSPI* was mostly expressed in the left and right ventricle and foetal heart, whereas *DSPIb* was mainly present in the aorta, right auricle, left atrium as well as in the right ventricle and foetal heart. *DSPII* was expressed at higher levels in the right auricle, left atrium, and right ventricle. Primers to amplify the *G3PDH* gene (983 bp according to NM_002046.3) were used as a control of cDNA abundance. Water = negative control.

Expression of *DSPIb* mRNA in normal human skin and in normal human keratinocyte cell lines was also investigated using the RT-PCR strategy described above. Total RNA isolated from normal skin and from cell lines was reverse transcribed and the resulting cDNA was used as template to amplify all three isoforms with the set of primers depicted in Figure 4.4A. As shown in Figure 4.6, all three isoforms were detected in normal skin, in the spontaneously immortalised human skin keratinocyte cell line HaCaT and in the HpV immortalised human breast keratinocyte cell line K1.

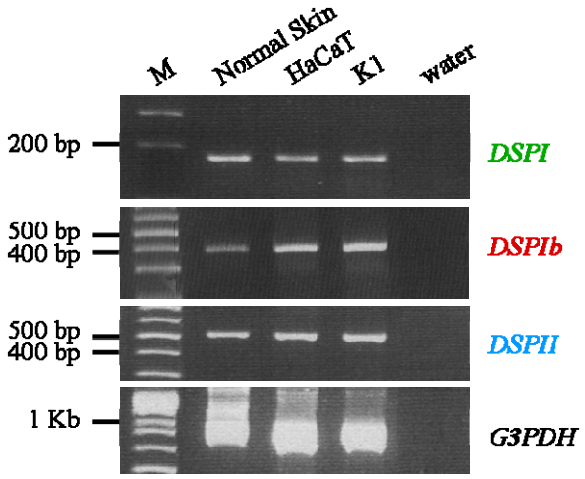

Figure 4.6. *DSPIb* mRNA is expressed in normal skin as well as in normal human keratinocyte cell lines. RT-PCR of total RNA from normal skin shows expression of *DSPI* (179 bp), *DSPIb* (383 bp) and *DSPII* (530 bp). All three isoforms are also expressed in the spontaneously immortalised normal keratinocyte cell line HaCaT and in the HpV immortalised normal breast keratinocyte cell line K1. Primers to amplify the *G3PDH* gene (983 bp according to NM_002046.3) were used as a control of cDNA abundance. M = molecular weight marker; water = negative control.

4.2.4. mRNA and protein quantification of DP splice variants in human keratinocyte cell lines

Quantitative RT-PCR with SYBR Green was performed in collaboration with Clare Cole (Department of Surgery & Molecular Oncology, University of Dundee, Ninewells Hospital & Medical School, Dundee, UK) to analyse the mRNA levels of the different *DSP* splice variants relative to *DSPI* in HaCaT, K1 and NHK keratinocytes (Figure 4.7B). The cDNA primers described in section 4.2.3 were used for this purpose. The *DSPIb*:*DSPI* mRNA ratios were found to be similar among HaCaT, K1 and NHK cells (1:20, 1:33 and 1:14, respectively). These ratios are within the same order of magnitude as the *DSPIb*:*DSPI* ratios calculated based on the EST analysis (see section 4.2.2).

Expression of DPIb at the protein level was also examined in HaCaT and K1 cells in order to determine whether translation of *DSPIb* was observed in these cell lines. Additionally, the expression levels of DPIb were compared to those of DPI and DPII. Total DP was assessed in whole cell extracts using a C-terminal DP antibody (clone 11-5F, see Table 2.7) (Parrish *et al.*, 1987) which detects both DPI and DPII. Samples were separated by 3-8% gradient SDS-PAGE over a period of six to seven hours, in order to resolve these high molecular weight proteins. DPI and DPII were observed at 332KDa and 260KDa, respectively, as expected. Two additional

immunoreactive bands were detected with sizes between those of DPI and DPII (Figure 4.7A). *DSPIb* mRNA is 468 bp longer than *DSPII*. This difference corresponds to 156 amino acids and approximately 19KDa, according to the protein molecular weight prediction of The Sequence Manipulation Suite bioinformatics program (http://www.bioinformatics.org/sms/index.html). Based on the migration of the marker proteins of known molecular weight, the immunoreactive band immediately above DPII is predicted to be approximately 19KDa larger than DPII and is therefore the most likely to correspond to DPIb (279KDa, Figure 4.7A).

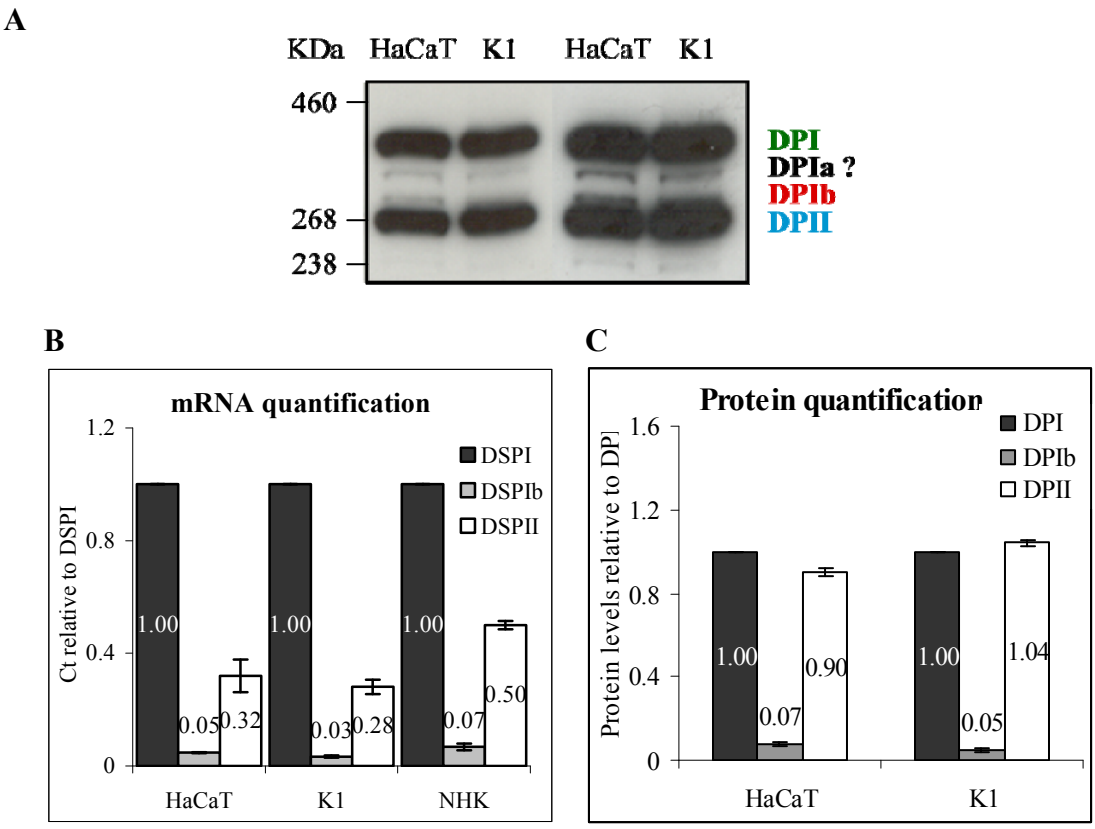

Figure 4.7. Western blot and quantitative RT-PCR analysis of DP splice variants. (A) Western blot of HaCaT and K1 total proteins with a C-terminal DP antibody (11-5F) directed against DPI and DPII. Left panel = low exposure, right panel = high exposure. DPI and DPII are observed at 332KDa and 260KDa, respectively. Two additional immunoreactive bands are observed between DPI and DPII. The band directly above DPII is calculated to be 279KDa and to correspond to DPIb, based on its predicted number of amino acids (2428 amino acids) and on the migration of the molecular weight marker (KDa). The band directly below DPI could correspond to a fourth DP splice variant, to a break down product of DPI or to western blot artefacts. This band was provisionary designated as DPIa. **(B)** SYBR Green quantitative RT-PCR using forward primers *DSPI*F, *DSPIb*F and *DSPII*F and the reverse primer *DSPI*R was performed to amplify *DSPI*, *DSPIb* and *DSPII*, respectively, from HaCaT, K1 and NHK keratinocytes. The mRNA expression levels (mean±SEM) of *DSPIb* and *DSPII* are shown relative to *DSPI* levels (n=3). Ct refers to threshold cycle. **(C)** Protein quantification (mean±SEM) of DPIb and DPII relative to DPI in HaCaT and K1 cells using densitometry analysis (n=2).

The identity of both this band and the one directly below DPI needed however to be investigated further, as they could represent breakdown products of DPI, could be the result of non-specific binding of the DP antibody or artefacts arising from the western blot procedure and the fact that the SDS-PAGE gels had to be run for long periods of time (see section 4.2.5). The band directly below DPI was provisionary designated as DPIa.

Densitometry measurements of the western blot using an image analysis program (Image J, v.1.34s) were used to calculate the protein levels of DPI, DPIb and DPII in HaCaT and K1 cells (Figure 4.7C). These protein levels are presented as a fold change of DPI protein levels for each sample. DPIb expression levels (relative to DPI) were similar between HaCaT and K1 cells and lower then DPII levels in both cell lines. DPIb:DPI ratios of 1:14 in HaCaT cells and 1:25 in K1 cells were observed. These ratios were similar to the mRNA *DSPIb*:*DSPI* ratios, suggesting that DPIb is efficiently translated.

4.2.5. Confirmation that DPIb is a novel splice variant

Two experiments were carried out to confirm that the immunoreactive band observed by western blot above DPII corresponds to DPIb and is a novel DP splice variant. First, to address whether the endogenous protein predicted to be DPIb in HaCaT cells is the same size as a recombinant DPIb protein, a full length *DSPIb* cDNA construct was over-expressed in HaCaT cells and western blots were performed (section 4.2.5.1). Second, RNAi technology was used to selectively down-regulate different DP isoforms and ultimately prove that DPIb is a splice variant and not a DP breakdown product (section 4.2.5.2).

4.2.5.1. Over-expression of recombinant DPIb proteins in HaCaT cells

4.2.5.1.1. Generation of a pBabe-DSPIb expression vector

A *DSPIb* cDNA construct was generated from primary NHK RNA. Due to the large size of the *DSPIb* coding region (8401 bp), three overlapping fragments were PCR amplified across two restriction enzyme sites, using primer pairs described in section 4.2.1 (Figures 4.1A and 4.8A). The resulting PCR products are shown in Figure 4.1B.

Because of non-specific hybridisation of primers 1F/1R (Figure 4.1B) the largest PCR product (which was of the expected size) was excised from the gel and purified.

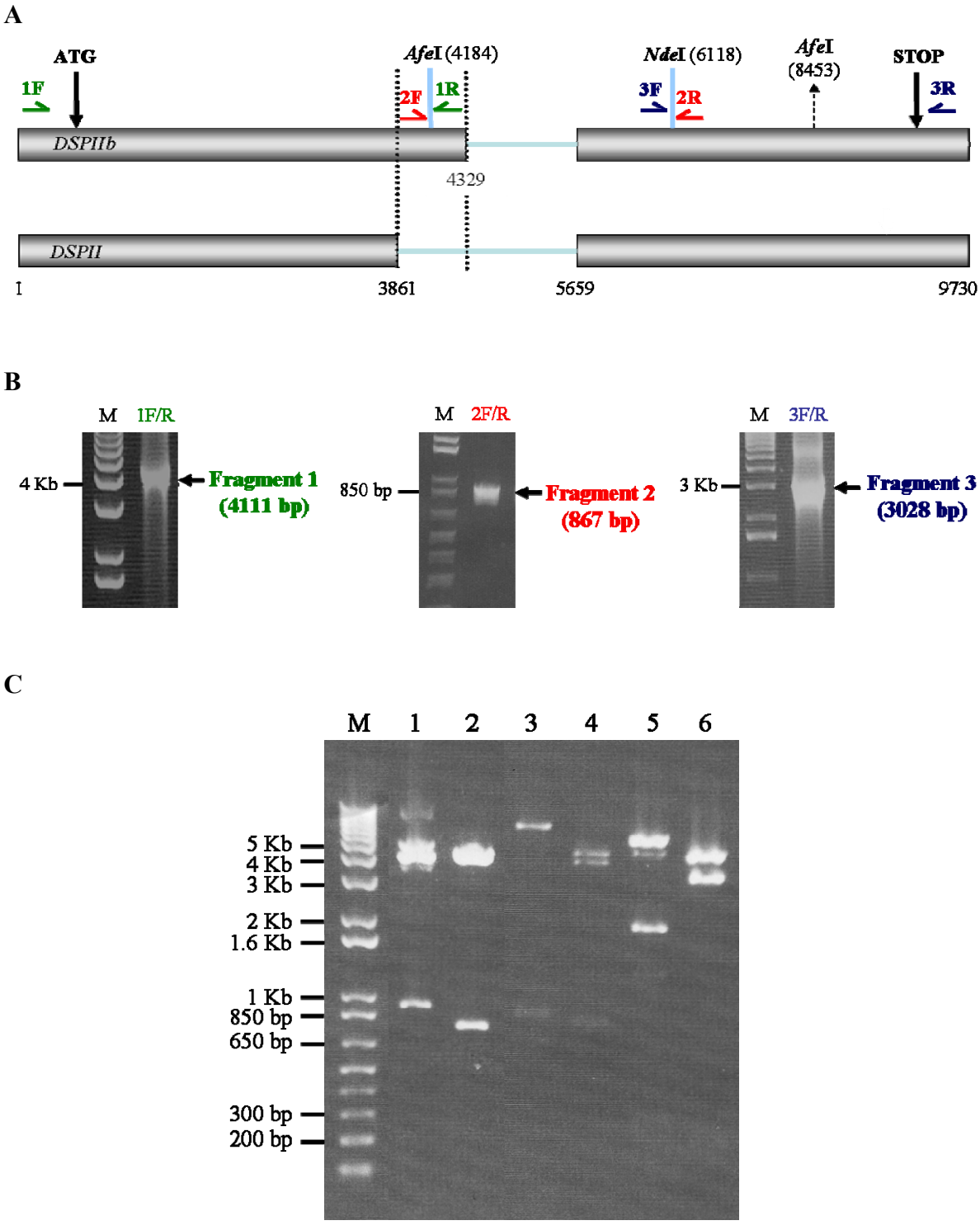

Figure 4.8. Cloning of *DSPIb* into the pCRII-TOPO cloning vector (continues).

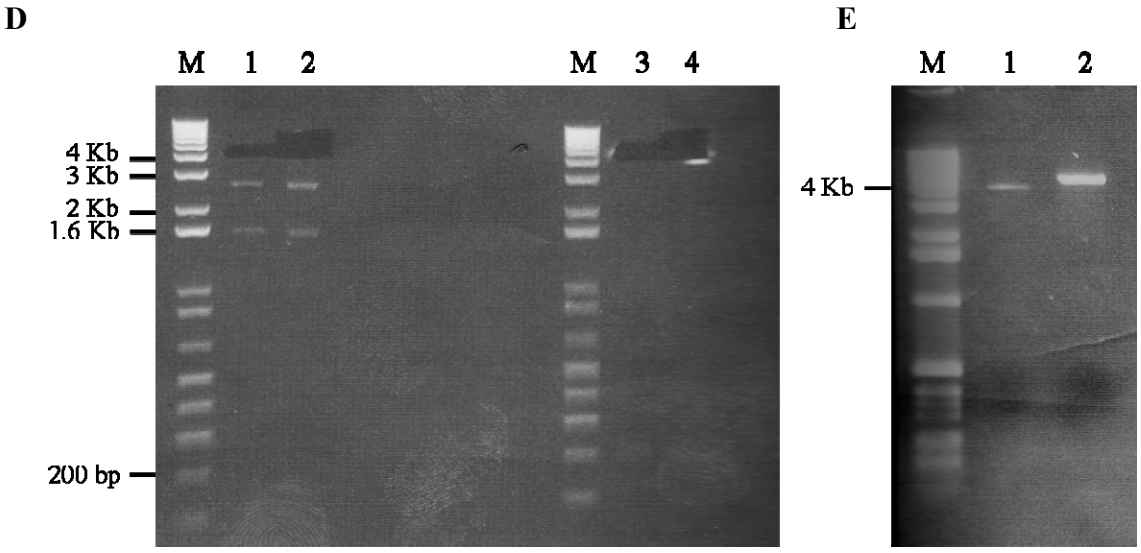

Figure 4.8. Cloning of *DSPIb* into the pCRII-TOPO cloning vector. (A) Schematic diagram of the cloning strategy used to generate the *DSPIb* construct. Primers 1F/1R (in green), 2F/2R (in orange) and 3F/3R (in blue) were used to amplify fragment 1 (4111 bp), fragment 2 (867 bp) and fragment 3 (3028 bp), respectively, by RT-PCR of total RNA isolated from primary NHK. **(B)** RT-PCR products of the three fragments following TA cloning into the pCRII-TOPO cloning vector. **(C)** Restriction enzyme digests of the cloned fragments: fragment 2 with *Eco*RI (3955 bp and 885 bp, lane 1) and *Eco*RV (4110 bp and 730 bp, lane 2); fragment 1 with *Hind*III (6423 bp, 852 bp and 809 bp, lane 3) and *Spe*I/*Xba*I (3885 bp, 3416 bp and 783 bp, lane 4); fragment 3 with *Hind*III (5037 bp, 1733 bp and 231 bp, lane 5) and EcoRI (3955 bp, 2882 bp and 164 bp, lane 6). **(D)** Fragment 1 in pCRII-TOPO cloning vector digested with *Afe*I, *Not*I and *Nco*I (4030 bp, 2503 bp and 1551 bp, lanes 1 and 2). The 4030 bp band corresponds to fragment 1 and was recovered from the gel. Fragment 2 in pCRII-TOPO vector digested with *Afe*I and *Not*I (4665 bp and 175 bp). The 4665 bp band corresponds to *pCRII*-TOPO vector containing fragment 2 and was recovered from the gel. **(E)** Fragment 1 (lane 1) and fragment 2 in pCRII-TOPO vector (lane 2) after gel purification and prior to ligation.

Each of the three fragments was TA cloned into a shuttle vector. Following transformation of competent bacteria, positive clones were selected. To confirm the presence of the desired insert, a diagnostic PCR was performed on boiled bacterial lysates using the same primers which amplified the original fragment to be cloned. The resulting PCR products are shown in Figure 4.8B. Plasmid DNA from bacterial cultures of clones containing the required fragment was isolated and restriction enzyme digests were performed to confirm the presence of the right inserts and to determine their orientation (Figure 4.8C). Finally, the three fragments were joined together following specific restriction digests. Figures 4.8D and 4.8E show an example of part of this procedure, which involves digest of the vectors containing fragments 1 and 2, excision of the required bands from an agarose gel and ligation to generate a vector containing both fragments 1 and 2. Full length *DSPIb* cDNA was then sub-cloned into the pBabe-puro retroviral expression vector and confirmed by sequencing analysis (for more details see Chapter 2).

4.2.5.1.2. Generation of a HaCaT stable cell line over-expressing DSPIb

Phoenix amphotropic retroviral packaging cells were transiently transfected with either the pBabe-*DSPIb* construct or a pBabe-*GFP* control plasmid. Whole cell DP proteins from transfected Phoenix cells were assessed by immunoblotting using the DP C-terminal antibody (11-5F). Expression of recombinant DPIb proteins was observed in the pBabe-*DSPIb* transfected Phoenix cells, which migrated at approximately 279KDa, as expected. This immunoreactive band was not observed in the pBabe-*GFP* transfected Phoenix cells (Fig.4.9A).

Following puromycin selection (see Chapter 2), transfected Phoenix cells were grown to confluency and allowed to produce virus. HaCaT cells were then transduced with pBabe-*DSPIb* and pBabe-*GFP* containing virus.

4.2.5.1.3. *HaCaT endogenous DPIb proteins migrate alongside recombinant DPIb proteins on SDS-PAGE*

Total DP proteins from transduced HaCaT cells were assessed by western blot with the DP C-terminal antibody (Figure 4.9B). As expected, recombinant DPIb proteins were observed in pBabe-*DSPIb* transduced HaCaT cells at approximately 279KDa. Recombinant DPIb proteins were expressed at higher levels than endogenous DPIb proteins present in pBabe-*GFP* transduced cells. Although these endogenous DPIb proteins were barely detectable on the western blot depicted in Figure 4.9B, a higher exposure of the same blot (Figure 4.9C) shows their presence in pBabe-*GFP* transduced HaCaT cells. Moreover, this blot shows that the immunoreactive band representing recombinant DPIb proteins migrates alongside the immunoreactive band predicted to correspond to endogenous DPIb in pBabe-*GFP* transduced cells.

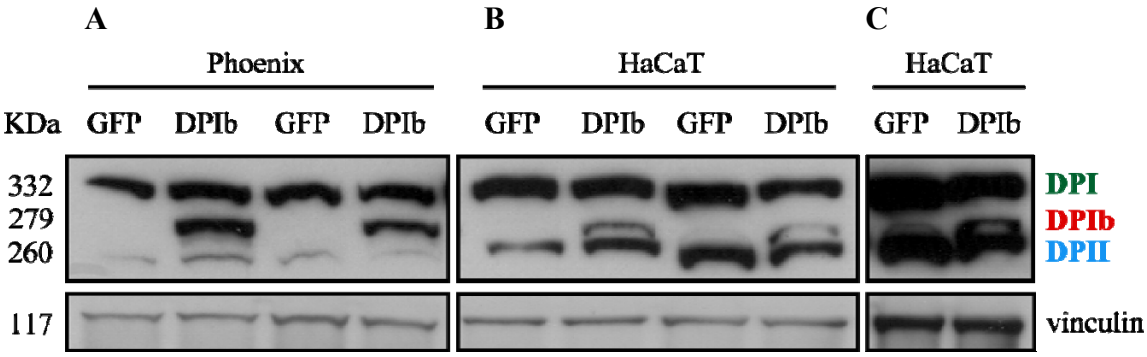

Figure 4.9. Potential DPIb proteins endogenously expressed in HaCaT cells are the same size as recombinant DPIb proteins over-expressed in HaCaT cells. Western blot of total proteins from Phoenix **(A)** and HaCaT cells **(B)** with a DP C-terminal antibody (11-5F) which detects DPI (332 KDa) and DPII (260KDa). **(A)** Phoenix cells were transiently transfected with a pBabe-*GFP* control vector (GFP) and the pBabe-*DSPIb* construct (DPIb). Recombinant DPIb expression is observed in pBabe-*DSPIb* transfected cells at approximately 279 KDa, but not in pBabe-*GFP* transfected cells. **(B)** HaCaT cells transduced with the pBabe-*DSPIb* construct (DPIb) show expression of recombinant DPIb at higher levels than those of the endogenous putative DPIb band in pBabe-*GFP* transduced cells (GFP). **(C)** Higher exposure of the same blot shows recombinant DPIb proteins migrate alongside endogenous potential DPIb proteins. Vinculin (117KDa) was used as loading control. The predicted molecular weight of each isoform is indicated on the left (KDa).

4.2.5.2. siRNA mediated knock-down of DSP splice variants in HaCaT cells confirms identity of DPIb

To further confirm that DPIb is represented by the immunoreactive band observed directly above DPII on western blots, three different groups of siRNAs were used which target: (1) the *DSPI*-specific region (si*DSPI* 1 and si*DSPI* 2); (2) a region common to both *DSPI* and *DSPIb* (si2, si3 and si4); and (3) a region in exon 11 common to all three splice variants (siI/II), respectively. Figure 4.10A depicts these siRNA sequences and targeting sites within the alternative *DSP* mRNAs. siRNAs si2, si3 and si4 were pooled and the pool was designated as siI. siRNAs si*DSPI* 1 and si*DSPI* 2 were used individually and also as a pool and this pool was designated si*DSPI* 1/2. siRNA siI/II was previously published (Wan *et al.*, 2007). Individual siRNAs and respective pools, as well as the transfection conditions used are described in Chapter 2.

Following si*DSPI* 1 or si*DSPI* 2 transfection into HaCaT cells, DPI was expected to be down-regulated but DPIb and DPII to remain unaffected. Likewise, siI transfection should result in DPI and DPIb down-regulation whilst leaving DPII intact. In contrast, if the immunoreactive band predicted to be DPIb was a breakdown product of DPI, then this band would also be down-regulated with *DSPI*-specific siRNAs. Transfection of HaCaT cells with siI/II should lead to down-regulation of all three isoforms, including DPIb, and if so the immunoreactive band predicted to be DPIb

would be confirmed to be DP-specific and not a result of non-specific binding of the DP antibody. Therefore, this experiment was conducted to demonstrate that the immunoreactive band observed above DPII is DP-specific (and not non-specific antibody cross reactivity) and to exclude the possibility of it being a break-down product of DPI.

As expected, the band directly above DPII was observed in control cells and in cells transfected with si*DSPI* 1 and si*DSPI* 2. This band was not observed in cells transfected with siI or siI/II (Figure 4.10C and 4.10D). To confirm that recombinant DPIb proteins are also down-regulated with the same siRNAs that down-regulate endogenous DPIb, stable HaCaT cell lines over-expressing either GFP or recombinant DPIb were transfected with the different siRNAs. Similarly to endogenous DPIb, recombinant DPIb proteins are expressed in cells transfected with the *DSPI*-specific siRNA pool (si*DSPI* 1/2) and are down-regulated with siRNAs specific to both *DSPI* and *DSPIb* mRNAs (siI) (Figure 4.10D). In cells transfected with siI/II all immunoreactive bands were down-regulated including the fourth band directly below DPI. Interestingly, in contrast with the DPIb immunoreactive band, the band directly below DPI (potential DPIa isoform, see section 4.2.4) is down-regulated with siRNAs which were thought to target only the DPI splice variant (si*DSPI* 1 and si*DSPI* 2) (Figure 4.10C and 4.10D). These results indicate that this band is either a breakdown product of DPI or a fourth DP splice variant, intermediate in size between DPI and DPIb.

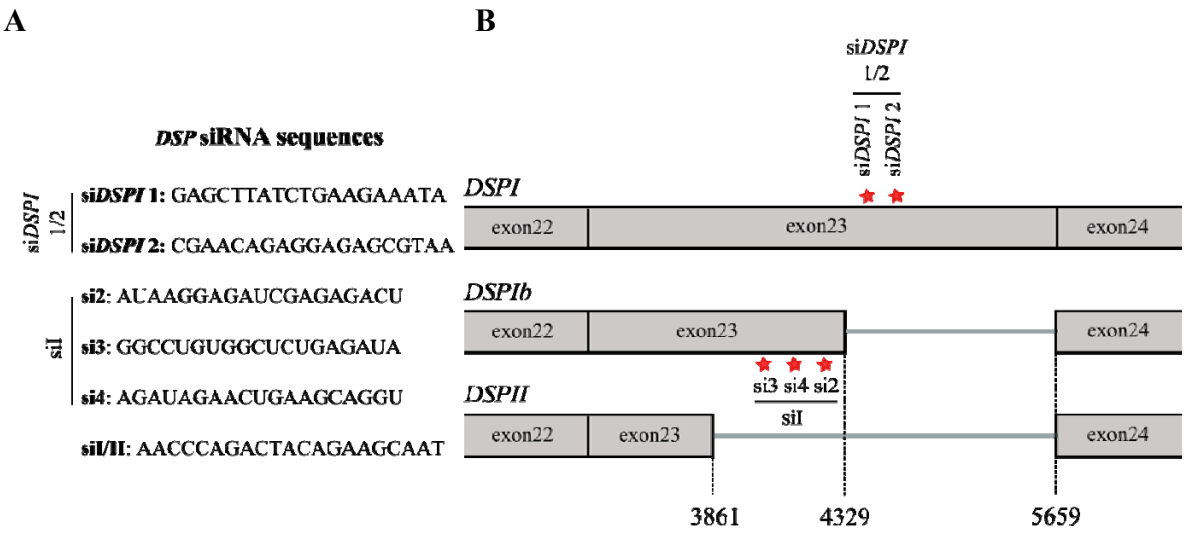

Figure 4.10. siRNAs directed against *DSP* splice variants show that DPIb is a novel DP splice variant and the immunoreactive band directly above DPII (continues).

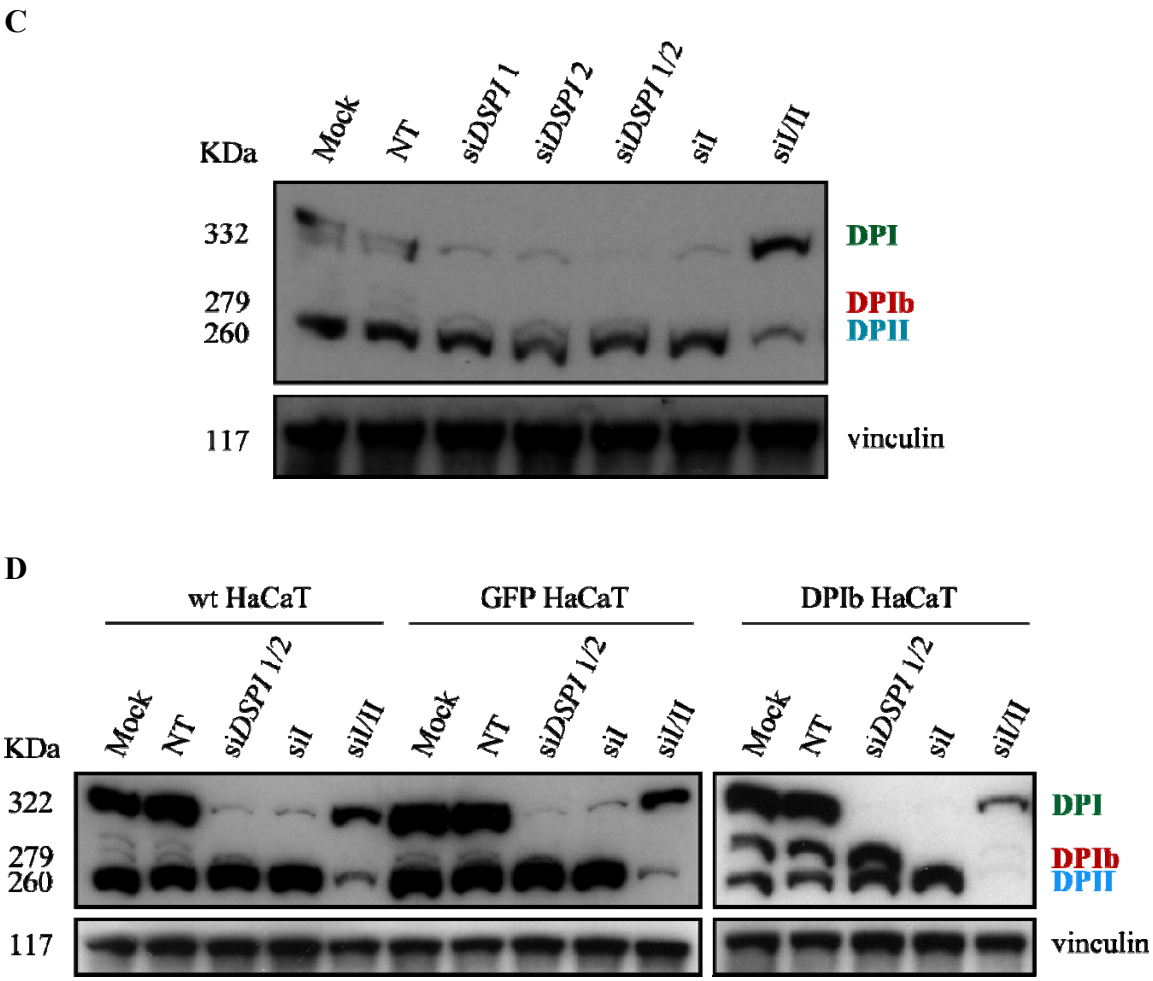

Figure 4.10. siRNAs directed against *DSP* splice variants show that DPIb is a novel DP splice variant and the immunoreactive band directly above DPII. (A) Sense strand sequences of six siRNAs directed against *DSP* splice variants. si*DSPI* 1 and si*DSPI* 2 siRNAs were designed to target *DSPI* only. A pool of these two siRNAs was also used which was designated si*DSPI* 1/2. si2, si3 and si4 were designed to target both *DSPI* and *DSPIb*. A pool of these three siRNAs (siI) was used. siI/II targets all three splice variants. **(B)** Schematic diagram of exons 22 to 24 of the *DSPI*, *DSPIb* and *DSPII* mRNAs showing the siRNA targeting sites (red stars). siI/II is not represented as it targets exon 11 which is common to all three splice variants. **(C)** Western blot of HaCaT whole cell lysates with the DP C-terminal antibody (11-5F). DPI (332KDa), DPIb (279KDa) and DPII (260KDa) are shown. Vinculin (117KDa) was used as loading control. The predicted molecular weight of each isoform is indicated on the left (KDa). The immunoreactive band directly above DPII (DPIb) is present in cells transfected with si*DSPI* 1, si*DSPI* 2 and the si*DSPI* 1/2 pool (which target *DSPI*) but is down-regulated in cells transfected with the siI pool (which targets *DSPI* and *DSPIb*) and with siI/II (which targets all three splice variants). In contrast, the band directly below DPI is down-regulated by all siRNAs. Mock refers to control cells that were incubated with DharmaFECT transfection reagent only**.** NT refers to control cells which were transfected with a pool of non-targeting siRNAs. **(D)** Western blot of whole cell lysates from wild type HaCaT cells and HaCaT cells transduced with either the pBabe-*GPF* or the pBabe-*DSPIb* construct. Both endogenous and recombinant DPIb proteins are down-regulated with siRNAs which target the predicted *DSPIb* sequence but not with siRNAs which are *DSPI*-specific.

This experiment confirms that DPIb is a novel splice variant of approximately 279 KDa and not a breakdown product of DPI or a result of non-specific antibody cross reactivity or other western blot artifacts.

4.2.6. Over-expression of DPIb in HaCaT cells does not change the expression level of other junctional or cytoskeletal proteins

To investigate whether over-expressing DPIb in HaCaT cells changes the expression levels of other desmosomal, adherens junctions or cytoskeletal proteins, western blots were performed on whole cell lysates from GFP and DPIb over-expressing cells (Figure 4.11A and B).

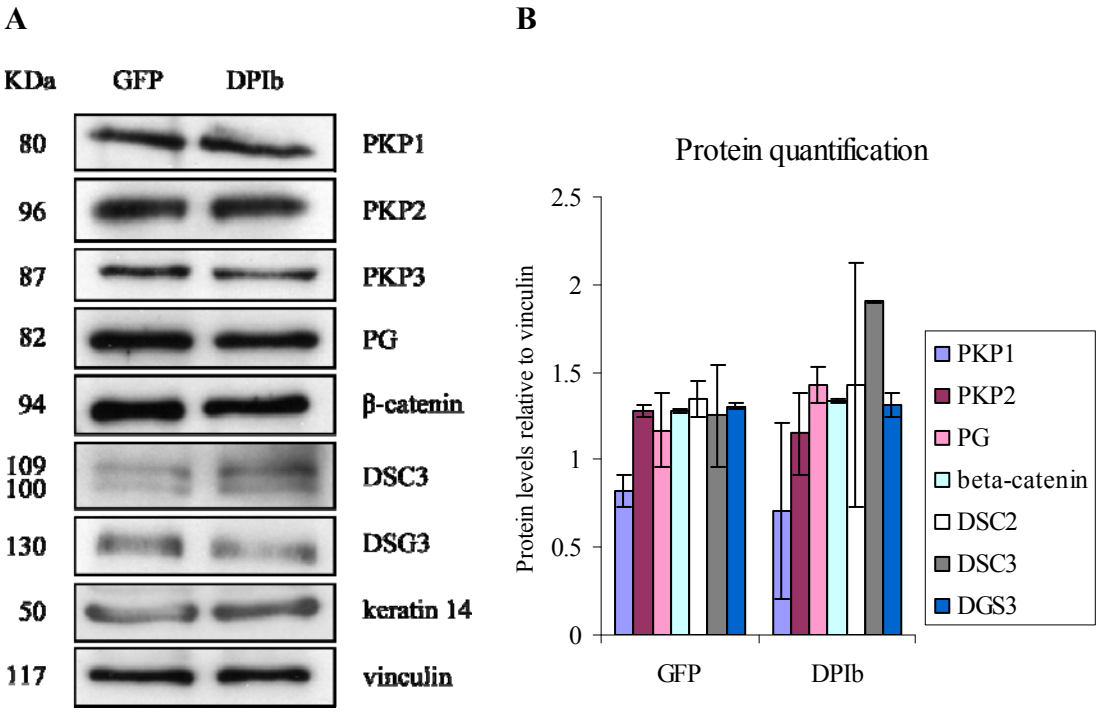

Figure 4.11. Over-expression of recombinant DPIb in HaCaT cells does not cause significant changes in the expression levels of other junctional or cytoskeletal proteins. (A) Western blots of whole cell lysates from HaCaT cells transduced with pBabe-*GFP* and pBabe-*DSPIb* plasmids. Antibodies raised against desmosomal (PKP1, PKP2, PKP3, PG, DSC3 and DSG3), adherens junctions (β-catenin) and IF (keratin 14) proteins were used. No major changes were observed in expression levels of these proteins between GFP and DPIb over-expressing cells. The predicted molecular weight of each protein is indicated on the left (KDa). **(B)** Protein quantification (mean±SEM) of junctional molecules relative to vinculin (loading control) in GFP and DPIb overexpressing HaCaT cells using densitometry analysis (n=2).

No significant changes were observed in the expression levels of the DP binding partners PKP1, PKP2, PKP3, PG or keratin 14 between GFP and DPIb over-expressing

cells. The expression levels of the basal desmosomal cadherins DSC3 and DSG3, as well as the adherens junction protein β-catenin were also not significantly altered (Figure 4.11A and B).

4.2.7. Normal human atrium expresses DPI and low levels of a smaller DP immunoreactive band

DP expression is prominent in epithelial and cardiac tissues (Green & Hobbs, 2006) (see Chapter 1) and DPIb was observed to be expressed at the mRNA level in normal human atrium, predominantly in the left atrium (Figure 4.5B). Therefore, expression of DPIb proteins in human atrium was investigated by western blot. Whole cell lysates from normal human atrium were resolved alongside total cell lysates from HaCaT cells in SDS-PAGE and subsequently blotted with the C-terminal DP antibody (11-5F) (Figure 4.12A). DPI was observed in human atrium, which migrated alongside the DPI immunoreactive band of HaCaT cells. Below this band, another immunoreactive band was observed at low levels compared to those of DPI. However, due to the fact that these high molecular weight DP isoforms are very similar in size and difficult to resolve in SDS-PAGE, it was not clear whether this band is the same size as DPIb or the potential DPIa splice variant observed in HaCaT cells on western blot above the DPIb immunoreactive band (see section 4.2.4). DPII was barely detected in human atrium (Figure 4.12).

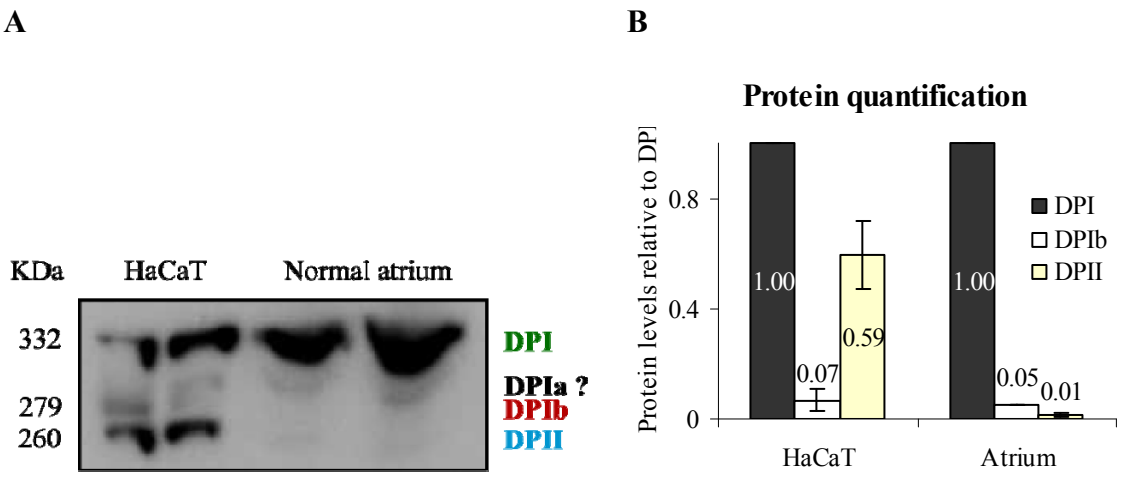

Figure 4.12. Expression of DP splice variants in normal human atrium. (A) Western blot of total proteins from HaCaT cells (first and second lanes) and normal human atrium (third and fourth lanes). The predicted molecular weight of each protein is indicated on the left (KDa). DPIb (279KDa) is observed in HaCaT cells, along with DPI (332 KDa) and DPII (260KDa). Expression of DPI is observed in the normal human atrium at 332 KDa. Below DPI, low levels of another immunoreactive band are observed. DPII is barely detectable in this tissue. **(B)** Protein quantification (mean±SEM) of DP isoforms relative to DPI in HaCaT cells and human atrium using densitometry analysis (n=2).

4.2.8. Mapping of the putative DPIa splice variant

The immunoreactive band observed on western blot directly below DPI (which was provisionary designated as DPIa, see section 4.2.4) was down-regulated with siRNAs which were thought to be *DSPI*-specific (section 4.2.6). These results indicate that this band is either a breakdown product of DPI or a fourth DP splice variant. If this band represents a DP isoform, then its corresponding mRNA has to be longer than 8401 (which corresponds to *DSPIb*) and shorter than 9730 (which corresponds to *DSPI*) nucleotides in length. If this isoform, like the others, is produced due to the use of an in frame alternative donor splice site in exon 23, then its exon 23/24 junction has to lie between nucleotides 4329 and 5659 (Figure 4.13A). This boundary would have to lie downstream of the region where si*DSPI* 1 (nucleotides 4488-4506) and si*DSPI* 2 (nucleotides 4651-4669) siRNAs hybridise, as the putative DPIa isoform is down-regulated when using these siRNAs (Figure 4.10 and 4.13A).

Four alternative donor splice sites were predicted by the ASSP predictor program, which would originate four in-frame alternative DP isoforms intermediate in size between DPIb and DPI and which could be detected with the DP C-terminal antibody (Figure 4.3B). This observation supports the hypothesis that this fourth DP specific immunoreactive band could be a DP isoform. Of these four in-frame 5' splice

sites, only the three that lie downstream of si*DSPI* 2 (i.e, downstream of nucleotide 4669, see Figures 4.13A and 4.3B) could represent the fourth immunoreactive band predicted to be DPIa.

To investigate whether it was possible to PCR amplify this putative *DSP* splice variant, a pair of primers was designed. The forward primer was expected to hybridise with a region in exon 23 just downstream of the *DSPIb* exon 23-24 border and upstream of the target site for the siRNA si*DSPI* 1 (Figure 4.13A). The reverse primer hybridised within the 5' end of exon 24. RT-PCR amplification of primary NHK using this primer pair was performed. When an annealing temperature of 56°C and extension time of 60 seconds was used, the only PCR product observed was a 1.3 Kb fragment, which corresponds to *DSPI* mRNA (Figure 4.13B). The annealing temperature was then decreased to 53°C and the extension time was shortened in 10 second increments to favor amplification of the shorter product (Figure 4.13C). Under these conditions, for extension times of 30 and 40 seconds, two bands were observed, the 1.3 Kb *DSPI*-specific band and a ~500 bp band (lanes 5 and 6, Figure 4.13C). For extension times of 10 and 20 seconds, the ~500 bp band was the only band observed (lanes 2 and 3, Figure 4.13C) and no PCR products were obtained when the extension step was omitted (lane 1, Figure 4.13C). Although the ~500 bp band was predicted to correspond to the potential *DSPIa* isoform, sequencing analysis of this PCR product revealed that it consisted of a *DSPIb* fragment, even though the forward primer was designed not to hybridise with *DSPIb* (Figure 4.13A). Therefore, the only possible explanation is if the forward primer was hybridising to a homologous sequence upstream of the *DSPIb* junction. This was demonstrated by the alignment with five mismatched bases of the forward primer with the *DSPI/DSPIb* specific region (Figure 4.13D).

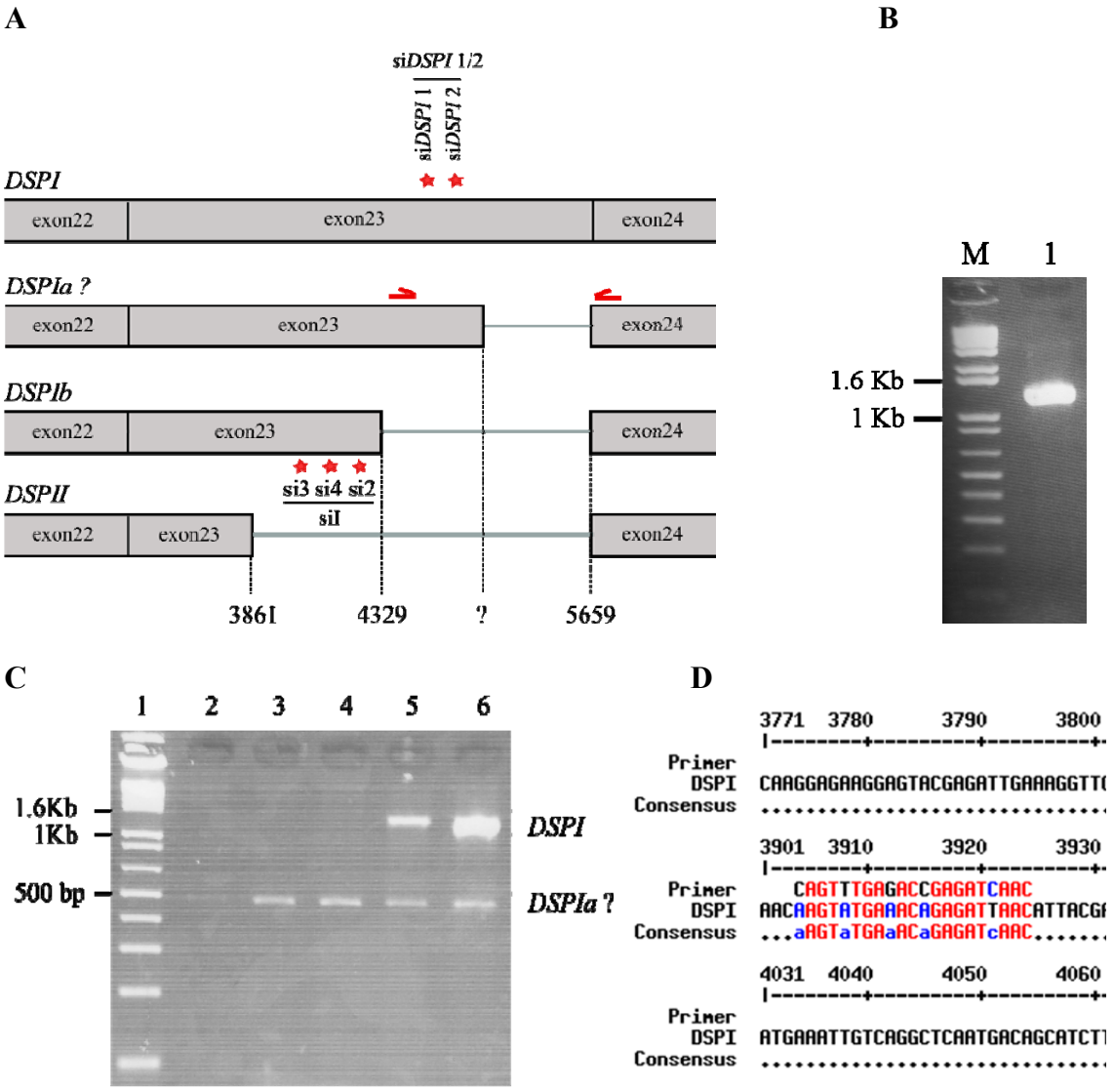

Figure 4.13. Strategy used to map the putative DPIa splice variant. (A) Schematic diagram of exons 22 to 24 of *DSPI*, *DSPIb* and *DSPII* mRNAs showing si*DSPI* 1 and si*DSPI* 2 siRNA targeting sites (red stars) and a primer pair designed to map the putative *DSPIa* splice variant. RT-PCR amplification of NHK RNA with the primer pair depicted in red results in **(B)** a 1.3 Kb *DSPI*-specific fragment (lane 1), when annealing temperature of 56°C and extension time of 60 secs are used in the PCR cycle and **(C)** the 1.3 Kb fragment as well as a ~500 bp fragment predicted to correspond to *DSPIa* when annealing temperature of 53°C and extension times of 30 secs (lane 5) and 40 secs (lane 6) are used, and only the ~500 bp fragment when the same annealing temperature and extension times of 20 secs (lane 4) and 10 secs (lane 3) are used. No PCR products are observed when the extension time step is omitted (lane 2). M (lane 1) = molecular weight marker. **(D)** Alignment of the forward primer with *DSPI* mRNA using the blast program multalin reveals that it hybridises with nucleotides 3904-3924 (instead of the required nucleotides 4372-4392) with 5 mismatches and amplifies a 472 bp product which corresponds to *DSPIb*. The expected product of ~ 500 bp corresponding to the putative *DSPIa* splice variant could not be amplified under these conditions.

Under the PCR conditions described here, and even though the extension time of the PCR cycle was reduced in an attempt to favour amplification of the desired shorter fragment, it was only possible to amplify *DSPI* and/or *DSPIb* cDNA. Although the

forward primer used here hybridised with mismatches to a homologous region upstream of the desired region, the fact that this primer pair did not amplify the putative *DSPIa* isoform suggests this isoform is not present in NHK. These results suggest that the fourth immunoreactive band observed with the DP antibody is a breakdown-product of DPI and not a DP splice variant.

4.3. Discussion

4.3.1. *DSPIb* is a novel alternative transcript produced from the *DSP* gene

In this chapter, the existence of a third alternative *DSP* transcript, *DSPIb*, identified from primary NHK cDNA whilst generating recombinant *DSP*, is described for the first time. As shown by sequencing analysis, this splice variant is produced by an in-frame splicing event using a third alternative 5' (donor) splice site in exon 23, 468 bp downstream of that of *DSPII*. Therefore, this alternative transcript is 468 nucleotides longer then *DSPII*, but still lacks 1329 nucleotides which are present in the *DSPI* transcript (Figure 4.4A).

All three splice isoforms are generated through canonical splicing, with the intronic flanking sequences following the GU-AG rule (see section 4.1.1). Furthermore, the 5' splice sites in exon 23 used to generate *DSPIb* and *DSPII* are virtually identical (nine out of ten nucleotides are conserved; Figure 4.2B), suggesting similar strengths for these consensus sequences. However, these consensus sequences appear to confer different specificity for the splicing machinery, as discussed below.

4.3.2. Splice prediction and EST analysis suggest there might be additional novel splice variants besides *DSPIb*

Alternative splice site predictions within the *DSPI* coding region were performed using two different programs. The donor splice site that generates *DSPIb* was predicted by both programs with a score similar to that of the corresponding splice site that generates *DSPII* (highlighted in blue, Figure 4.3A and 4.3B). This is not surprising, as the sequences of these two donor splice sites are virtually identical. In addition to the 5' splice sites that generate *DSPIb* and *DSPII*, one of the programs (ASSP) suggested six alternative donor splice sites within the *DSPI* specific region (Figure 4.3B). Four of these six donor sites would generate splice variants in-frame with *DSPI*, *DSPIb* and *DSPII*, if the common acceptor splice site on exon 24 is used. Additionally, under these circumstances, the potential additional splice variants would only differ from each other and from *DSPI*, *DSPIb* and *DSPII* in the central alternatively splice region. These results suggest that besides DPIb, there might be additional DP splice variants, that

could be detected with the C-terminal DP antibody (11-5F), which was though to be worthwhile investigating.

EST analysis of *DSP* splice variants also revealed interesting results. Firstly, one EST spanning the *DSPIb* exon23/24 junction was found on the NCBI human EST database, which represents further independent evidence that the *DSPIb* transcript exists, has been shotgun cloned and is expressed in a prostate tumour cell line (cells where the mRNA that generated this EST was extracted from). Secondly, the fact that only one *DSPIb*-specific EST and five *DSPII*-specific ESTs were found in the database, compared to 31-37 ESTs in *DSPI*-specific regions suggests that *DSPIb* and *DSPII* are expressed at lower levels than that of *DSPI* in the cells or tissues used to construct the cDNA library. These results were also suggested by quantitative RT-PCR, where *DSPIb*:*DSPI* mRNA ratios of 1:20, 1:33 and 1:14 and *DSPII*:*DSPI* ratios of 1:3, 1:4 and 1:2 were found in HaCaT, K1 and NHK cells, respectively (sections 4.2.2 and 4.2.4 and see also section 4.3.4).

4.3.3. *DSPIb* transcript is expressed in epithelial, brain and heart tissue and the only *DSP* isoform detected in the aorta

As revealed by RT-PCR using a commercially available multiple tissue panel, *DSPIb* is expressed along with *DSPI* and *DSPII* in a range of epithelial tissues including simple columnar (small intestine and colon), simple squamous (lung and spleen), simple cuboidal (liver, thymus) and stratified (prostate) epithelium. Among these tissues, all three *DSP* isoforms were most abundant in the lung, liver and prostate. Additionally, little expression of all three isoforms was observed in the brain.

Because this RT-PCR method is non-quantitative, it is only possible to compare the relative expression of each isoform across the range of tissues. A direct comparison between the three isoforms in each tissue is not possible, because these relative levels will also depend upon the efficiency of primer pairs and PCR conditions used in each case. mRNA expression profiles of *DSPI*, *DSPIb* and *DSPII* across the range of tissues were comparable, i.e. tissues that showed highest expression of *DSPI* also had highest levels of *DSPIb* and *DSPII*. Very subtle variations to this pattern were observed in some tissues. For instance, *DSPIb* was expressed at slightly higher levels in the brain compared to the colon or small intestine, in contrast with *DSPI* and *DSPII*, which were expressed in the brain at lower levels than in the colon or small intestine (Figure 4.5A). This divergence supports the observation that distinct splicing specificities can occur in

the presence of virtually identical consensus splice sites. These results further suggest that a single differing nucleotide within the 5' splice site of *DSPIb* could be important to confer splicing specificity.

Using a cardiovascular cDNA panel, expression of *DSPIb* at the mRNA level was observed in diverse compartments of adult heart, as well as in foetal heart. Similar expression profiles were observed in the heart for *DSPIb* and *DSPII*, which however differed from that of *DSPI*. Surprisingly, *DSPIb* was the only isoform detected in the aorta. The identical expression profiles for *DSPIb* and *DSPII* in the heart suggest similar splicing specificity for these two splice variants. However, the fact that only *DSPIb* was detected in the aorta suggests that despite the virtually identical splice sites, there are further more subtle levels of regulation which confer differing splicing specificities. As described before by many authors, splicing regulation is a very complex mechanism depending not only upon the relative strength of consensus sequences in the pre-mRNA, but also upon the many levels of regulation of RNA-binding proteins, which in turn depend upon signalling pathways, tissue-specific factors and differentiation stages (Matlin *et al.*, 2005; Moore & Silver, 2008). An example of tissue-specific regulation of splice isoform expression is shown by the high expression of DPII in the skin, whereas it is virtually absent in the heart(Angst *et al.*, 1990; Uzumcu *et al.*, 2006). It is therefore possible to conclude based on previous observations and results shown here that consensus sequences in the pre-mRNA molecule are important, but not sufficient, to predict which alternative splice variant will be preferentially expressed in a specific tissue or cell at a specific time point. It is also important to mention that other levels of post-transcriptional (as well as post-translational) regulation may also be involved in the relative expression levels of splice variants, such those affecting mRNA (and protein) stability.

In agreement with results shown here, both DPI and DPII have been shown to be expressed in simple and stratified epithelia (Angst *et al.*, 1990). Additionally, DPI is known to be an obligatory component of desmosomes and therefore present in all desmosome-bearing tissues, including skin, heart, lymph nodes and meninges (Green & Hobbs, 2006). Some of these tissues contain desmosome-like junctions that differ in ultrastructure from epithelial desmosomes. Complexus adherents are an example of this type of junction which are present in vascular and lymphatic endothelial cells and contain VE-cadherin together with DP and PG as well as several adherens junction and tight junction proteins (Moll *et al.*, 2009). Cardiomyocyte cell junctions also contain a

mixture of desmosomal and adherens junction proteins which localise to the "area composita" of the intercalated disc connecting cardiomyocytes (Borrmann *et al.*, 2006); see Chapter 1). Although these junctions are known to contain DPI, expression of DPII was observed at the mRNA level but barely detectable at the protein level (Uzumcu *et al.*, 2006). As shown here, *DSPIb* is also expressed at the mRNA level in epithelial, brain and heart tissue.

A similar RT-PCR method to specifically amplify *DSPI* and *DSPII* has been described, where the same cardiovascular cDNA panel was used (Uzumcu *et al.*, 2006). In this report, *DSPI* was shown to be ubiquitously expressed throughout all regions of the heart, including the aorta, in contrast with the observations described here. However, the primer pair used by this group to specifically detect *DSPI* amplifies an 800 bp region (from positions 3268 to 4068 according to accession number NM_004415.2 of the NCBI database) which is common to both *DSPI* and *DSPIb* (Figure 4.4A). Therefore, the reported *DSPI* expression across the different regions of the heart is a combination of *DSPI* and the previously unknown *DSPIb* isoform. This explains the differences between the published *DSPI* expression profile in the heart and the data presented here, and it is therefore plausible that *DSPIb* is the only transcript present in the aorta. Moreover, it is possible that, if synthesised, DPIb has a specific function in the aorta which may not be fully accomplished by DPI or DPII.

4.3.4. *DSPIb* transcript is expressed in human skin as well as HaCaT, K1 and NHK keratinocytes

DSPIb mRNA was also detected in normal human skin and keratinocyte cell lines along with *DSPI* and *DSPII*, using the same RT-PCR method. Taken together, these results demonstrate that a third *DSP* splice variant, *DSPIb*, is physiologically expressed at the mRNA level in normal skin and in other simple and stratified epithelia, in cardiac tissue, as well as in human keratinocyte cell lines and in primary NHK in culture, where it was first identified. This indicates that expression of *DSPIb* in cultured keratinocytes is not a result of aberrant splicing due to adaptation of these cells in culture.

Quantification of mRNA expression of the three *DSP* isoforms revealed that the levels of *DSPIb* (relative to *DSPI*) are similar among NHK, HaCaT and K1 keratinocytes. The DPIb protein levels observed by western blot were also similar between HaCaT and K1 cells, suggesting that there is a correlation between mRNA and

protein levels of this isoform (Figure 4.7). These results suggest that DPIb is efficiently translated in HaCaT and K1 cells. The DPIb protein levels were very low compared to those of DPI and DPII in both HaCaT and K1 cells. Similarly, quantitative RT-PCR suggested that the mRNA levels of *DSPIb* are lower than those of *DSPI* and *DSPII*. However, the quantitative RT-PCR experimental conditions used here are not ideal to compare expression levels of different mRNAs in the same type of cell or tissue because different primer pairs may have different effects on the PCR reaction efficiency. A confirmation of these results using techniques such as TaqMan assay, northern blot or an RNase protection assay would be more adequate to directly compare the mRNA levels of the different isoforms in the same cell type.

4.3.5. Western blot of DP proteins in keratinocyte cell lines revealed an additional immunoreactive band which represents the novel DPIb splice variant

Immunoblotting of DP proteins from HaCaT and K1 cells revealed DPI and DPII as well as two additional immunoreactive bands with sizes between those of DPI and DPII. Based on the calculated size of DPIb, this isoform was hypothesised to correspond to the band directly above DPII. However, this immunoreactive band could also represent: (1) a breakdown product of DPI (hence recognised by the DP antibody); (2) a modification of the DPI or DPII isoforms (such as phosphorylation); (3) the result of non-specific binding of the DP antibody used; or (4) artefacts arising from the western blot process and the fact that SDS-PAGE gels were resolved for long periods of time.

To confirm the initial hypothesis and to exclude these other possibilities, two experiments were conducted. Firstly, recombinant DPIb was retrovirally expressed in HaCaT cells and immunoblotted alongside endogenous HaCaT DP proteins. This experiment showed that recombinant DPIb proteins migrate alongside the endogenous immunoreactive band above DPII. Secondly, RNAi technology was used to specifically knock-down DPI only (si*DSPI* 1 and si*DSPI* 2), both DPI and DPIb (siI) and all three isoforms (siI/II). This experiment was performed in both wild type HaCaT cells and in HaCaT cells over-expressing either GFP (control) or recombinant DPIb, to demonstrate that both endogenous and recombinant DPIb proteins behave in the same way. As expected, this experiment showed down-regulation of both endogenous and recombinant DPIb proteins in HaCaT cells transfected with siI and siI/II, but not with si*DSPI* 1 or si*DSPI* 2. Interestingly, this experiment also showed down-regulation of the

immunoreactive band below DPI with all three groups of siRNAs used. This result indicates that this immunoreactive band corresponds either to a fourth DP splice variant, which shares with DPI the region targeted by siRNAs si*DSPI* 1 and si*DSPI* 2, or to a breakdown product or a modified version of DPI.

DPIb is expressed at the protein level in HaCaT and K1 immortalised keratinocyte cell lines, as demonstrated by immunoblotting. Taken together, RNAi and recombinant expression clearly demonstrated that the 279KDa band is DP-specific and corresponds to DPIb proteins, as opposed to a breakdown product, a modified version or an artefact. Given the high molecular weight of DP isoforms and their proximity in size, these proteins had to be resolved for long periods of time by SDS-PAGE in order to detect DPIb with good resolution. This, coupled with the low expression level of DPIb in these cell lines compared to those of DPI and DPII, might be the reasons why DPIb has been previously missed. However, a previous study where expression of DPI and DPII was investigated by immunoblotting in cells derived from different epithelia showed weak expression of an immunoreactive band of similar size to DPIb in cells from human pharyngeal squamous cell carcinoma (stratified or pseudostratified epithelium) (Angst *et al.*, 1990).

4.3.6. Expression levels of other junctional and cytoskeletal proteins are unaltered by over-expression of DPIb in HaCaT cells

The expression levels of DP binding partners and other junctional proteins were investigated in HaCaT cells over-expressing DPIb and compared to vector only control cells (HaCaT cells transduced with pBabe-*GFP* control vector). Since DP is a crucial component of desmosomes and its down-regulation leads to decreased expression levels of some other desmosomal proteins (see Chapter 5), it was hypothesised that over-expressing a DP isoform would increase desmosome stability. However, no significant differences in the expression levels of other desmosomal and adherens junction proteins or keratin 14 were observed between DPIb and GFP over-expressing HaCaT cells (Figure 4.11). It would have been interesting to investigate whether DPIb has any effect on the expression level of other adherens junctions' proteins, such as E-cadherin and N-cadherin, given the interdependence between adherens junctions and desmosomes.

No phenotypic changes were observed either between wild type and DPIb expressing Phoenix cells. These cells are derived from human embryonic kidney cells (HEK293T cells). They are more dendritic in shape and less adhesive then keratinocytes

and their morphology, as observed by phase contrast microscopy, did not change when DPIb was over-expressed (data not shown).

A number of reasons might possibly explain the results observed. First, the pBabe mammalian expression vector is a low expression vector where transcription is driven by the LTR promoter. Therefore, the difference in DPIb protein levels between wild type HaCaT cells and cells expressing recombinant DPIb might not be sufficient to cause a detectable effect. Second, over-expression of DPIb might have some subtle effects on HaCaT and/or Phoenix cell-cell adhesion which were not detectable with the methods used in this study. For instance, DPIb expression might interfere with the solubility of some desmosomal proteins, such as PG or PKPs, without changing total protein levels or it might have signalling effects. Third, it is possible that, although no effects were observed with the experimental conditions used in this study, other conditions may exist where DPIb expression is important. The observation that DPII is widely expressed in epithelial tissues, in particular in the skin, but barely detectable at the protein level in human heart supports this hypothesis. Furthermore, the fact that *DSPIb* was the only *DSP* transcript observed in the aorta supports a biological role for this isoform. Fourth, it is not possible to rule out the hypothesis that DPIb has a redundant function similar to that of DPI or DPII. More studies will be necessary to understand the function (if any) of DPIb.

4.3.7. Normal human atrium expresses DPI and low levels of immunoreactive band which is not DPII

Expression of DP isoforms was investigated in normal human atrium. As shown by western blot, high levels of DPI were observed in this tissue but, in agreement with previous observations (Uzumcu *et al.*, 2006), DPII was virtually absent. In addition to DPI, a shorter immunoreactive band was detected, which was expressed at very low levels. Although total lysates from atrium tissue were resolved alongside total HaCaT cell lysates, it was not clear whether this immunoreactive band is the same size as DPIb or as the potential DPIa isoform. This could be due to the fact that it is difficult to compare the mobility of proteins isolated from different cell types, as different modifications (such as phosphorylation) could affect protein migration on SDS-PAGE. Further experiments would be needed to confirm these results. Nevertheless, it is tempting to speculate that this immunoreactive band corresponds to DPIb, given that

mRNA expression of this isoform was observed in human atrium (Figure 4.5B) and that it was not possible to prove the existence of DPIa (sections 4.2.8 and 4.3.8).

4.3.8. Mapping of potential DPIa isoform

As shown by western blot of HaCaT cell lysates, the immunoreactive band observed below DPI is down-regulated with siRNAs which were predicted to be *DSPI*-specific. This result, coupled with the prediction of four possible in-frame alternative splice variants (section 4.3.2 and Figure 4.3B) and the observation when western blotting protein lysates from human atrium of an additional immunoreactive band below DPI, led to an attempt to map a potential fourth *DSP* isoform. A pair of oligonucleotides was designed which could amplify both a *DSPI* and/or a *DSPIa* fragment with different sizes. Because *DSPI* is probably in far greater abundance then the proposed *DSPIa* in NHK, RT-PCR conditions were used which did not enable amplification of *DSPI* and even under these conditions it was not possible to amplify a *DSPIa*-specific product. Given that the product corresponding to the proposed *DSPIa* isoform is shorter than that of *DSPI*, it is possible to conclude that *DSPIa* either does not exist or is due to an alternative splicing event which maps to a different region. If the former hypothesis is the case then the immunoreactive band observed above DPI is either a breakdown product of DPI or simply a western blot artefact. The fact that no 5' splice sites other than the ones that originate *DSPIb* and *DSPII* were presented by the Neural Network splice predictor program (Figure 4.3A) supports the RT-PCR result and the conclusion that DPIa (if existent) does not map to this region.

4.3.9. Hypothesis regarding possible function of DPIb

The C-terminal domain of DP is responsible for mediating interactions with different types of IFs: vimentin in meninges and dendritic cells of lymph nodes, desmin in the myocardium and a variety of keratins in epithelial tissues (Fontao *et al.*, 2003; Kouklis *et al.*, 1994; Meng *et al.*, 1997; Stappenbeck *et al.*, 1993; Stappenbeck & Green, 1992). The N-terminal plakin domain is important for targeting DP to the junctional plaque through interactions with PG and PKPs (Bornslaeger *et al.*, 2001; Kowalczyk *et al.*, 1997). As the DPIb isoform shares these two domains with DPI and DPII, it probably interacts with the same binding partners in the desmosome.

The central α-helical rod domains of two or more DP molecules are predicted to form coiled-coil interactions with one another (Bornslaeger *et al.*, 1996). DP molecules have also been reported to interact with each other through head-head associations (Smith & Fuchs, 1998). These higher order aggregates of DP form a filamentous network within the IDP which interacts with other plaque proteins between the membrane and IFs. However, while interactions with binding partners are known to be facilitated by the N- and C-terminal domains of DP, the rod domain is only known to be important for self-associations. While the DPI splice variant contains the entire rod domain, DPII lacks two thirds of this domain, and thus is likely to form less-stable dimers through coiled-coil interactions (Green *et al.*, 1990). The functional consequences of shortening the rod domain are unknown, but it is thought that DPII may govern the thickness of the desmosomal plaque (North *et al.*, 1999).

The ratio between DPI and DPII varies among different tissues and different cell types; DPII, which is abundantly expressed in complex epithelial tissues, is expressed at lower levels in cells derived from some other epithelial tissues such as epidermoid carcinoma (vulva) and human bladder carcinoma (transitional epithelium) (Angst *et al.*, 1990) as well as in the heart (Uzumcu *et al.*, 2006). Interestingly, Phoenix cells which are derived from a simple cuboidal epithelium (kidney) also show lower DPII expression levels than HaCaT cells (see Figure 4.9). Therefore DPII could have a functional significance (yet to be understood) which might not be fully accomplished by DPI alone in some tissues. Although it probably shares overlapping functions with DPI, DPII might play a unique role in desmosome assembly and maintenance in these tissues (Angst *et al.*, 1990).

The novel DPIb isoform described here contains half of the rod domain. Therefore, it can be hypothesised that DPIb will form more stable self associations than DPII but less stable than DPI. DPIb might also be important to stabilise DPI and DPII and different isoforms might play different roles in the stabilisation and adhesive state of the desmosome, which could be important to modulate the strength of the plaques in different tissues or during development and wound healing. Although DPIb was expressed at low levels in HaCaT and K1 keratinocytes, it might possibly be up-regulated under certain conditions and/or take over the function of other splice variants, for instance in cases of a *DSPI*-specific mutation. Nine mutations have been reported so far within the rod domain. Two of these mutations (p.R1113X and p.R1934X) affect all three isoforms; another three (p.R1255K, p.R1267X and p.N1324fsZ23) affect DPI and

DPIb and four (p.R1775I, p.K1583R, p.L1654P and p.Q1446X) affect only DPI whilst leaving DPIb and DPII intact (Figure 1.8). It is interesting to note that all mutations affecting only DPI are missense mutations causing dominant ARVC possibly through a dominant negative effect on cardiac junctions, except for the nonsense mutation (Q1446X) which only caused cardio-cutaneous disease when in a compound heterozygous background (Figure 1.8). This contrasts with the p.R1113X nonsense mutation which affects all three isoforms and leads to dominant non-syndromic ARVC (Figure 1.8) and with the p.R1267X nonsense mutation (described in Chapter 5) which leads to complete absence of both DPI and DPIb and results in skin and heart disease. These observations suggest that some degree of compensation by DPIb and DPII might occur in invividuals heterozygous for the Q1446X mutation (carriers), which are completely healthy. In fact there is a suggestion of slight DPIb up-regulation in HaCaT cells with *DSPI* down-regulation (Figure 4.10). However, further studies would be needed to confirm this hypothesis. It is possible that a higher degree of up-regulation and compensation occurs under mechanical stress.

The majority of desmosomal genes are alternatively spliced and little is known about the role of some of these splice isoforms, such as DSC 'b' proteins or DPII. A large volume of research has been published using recombinant DPI, however recombinant DPII has not been used. The importance of DPI during development and in the adult has been highlighted by observations from mouse models and human diseases of skin, hair and heart (Green & Hobbs, 2006). Further work will be necessary to investigate in more detail the importance and function of the DPII and DPIb isoforms and to investigate differences in isoform-specific adhesion properties.

4.4. Summary

This chapter describes a novel DP splice variant, DPIb, which has a molecular weight intermediate between those of DPI and DPII. This novel isoform is generated through alternative splicing of the *DSP* gene, using a third alternative 5' splice site and the common 3' splice site which generates also DPI and DPII. *DSPIb* transcript is expressed in several epithelial and cardiovascular tissues and the only *DSP* isoform detected in the aorta. DPIb protein was observed by western blot in HaCaT and K1 keratinocytes which has been previously missed, probably due to its similarity in size to DPII. DPIb might partially compensate for DPI in patients with *DSPI* specific mutations.

– Chapter 5 –

Functional Studies of Desmoplakin Mutants

5.1. Introduction

Thirty-six different mutations have been published to date in the gene encoding DPI and DPII, leading to a variety of different cardio-cutaneous syndromes (Figure 1.8). Although there are *in vivo* and/or *in vitro* data on some of these *DSP* mutations, the molecular mechanisms that lead to skin and/or heart disease are not fully understood and it is not clear why mutations in the same gene can lead to such different phenotypes. Additionally, the functional significance of the DPII splice variant, and to what extent it can compensate for DPI defects, is not clear. The goals of the work presented in this chapter are to mimic three *DSP* mutations in HaCaT keratinocytes to investigate their molecular mechanisms. Additionally, an indirect goal using this approach is to gain further insight into the functional significance of DPI and DPII. Although all three mutations affect the DPIb splice variant (Chapter 4), the work described in this chapter was directed at investigating the functional differences between the DPI and DPII isoforms as these are the predominant isoforms expressed in skin.

Heterozygous mutations (nonsense and splice site mutations) resulting in DPI (DPIb) and DPII haploinsufficiency and causing non-syndromic SPPK (p.Q331X and 939+1G>A) were modelled by using a siRNA targeting all three *DSP* isoforms. A homozygous *DSPI/DSPIb*-specific nonsense mutation (p.R1267X) leading to absence of DPI (and DPIb) in the skin and causing PPK, woolly hair and early lethal cardiomyopathy was also modelled by using siRNAs targeting *DSPI/DSPIb*. These loss of function mutations were investigated to understand the differences between the dosage effect of total DP (including DPI and DPII) and the dosage effect of each isoform (DPI or DPII) as well as to gain further insight into isoform-specific functions. Heterozygous carriers of the *DSPI*-specific nonsense mutation, p.R1267X, who have reduced expression levels of the DPI isoform and normal expression levels of DPII, are totally normal (Uzumcu *et al.*, 2006); patients who have DPI/DPII haploinsufficiency have skin disease (Armstrong *et al.*, 1999; Whittock *et al.*, 1999); and the patient with absence of DPI and normal expression levels of DPII (homozygous carrier of the *DSPI*-specific nonsense mutation p.R1267X; (Uzumcu *et al.*, 2006) has skin and heart disease, even though the total amount of DP produced in this case is predicted to be equivalent to that of patients with DP haploinsufficiency. In addition, patients with SPPK caused by DP haploinsufficiency mutations show adhesion defects in the skin including hyper-proliferative epidermis with loss of cell-cell adhesion and widening of intercellular

spaces (see below). However, it is not clear whether the *DSPI*-specific nonsense mutation has the same effect on desmosomal adhesion (Uzumcu *et al.*, 2006).

The third mutation studied is a heterozygous insertion of 30 bp leading to the presence of 10 additional amino acids in the N-terminus of both DPI and DPII. This autosomal dominant mutation leads to skin disease coupled with a very severe cardiomyopathy similar to the nonsense mutation that leads to absence of the DPI isoform (p.R1267X, see above). A more detailed background description on these three different *DSP* mutations is given in the following introductory sections.

5.1.1. Nonsense and haploinsufficiency *DSP* mutations result in different expression levels of DPI and DPII and lead to cardiac and/or cutaneous disease

Uzumcu *et al.* (2006) described a Turkish patient with a Naxos-like syndrome characterised by recessively inherited arrhythmogenic dilated cardiomyopathy, epidermolytic PPK (EPPK) and woolly hair. The patient presented with a very severe and early onset heart disease involving both ventricles, which rapidly progressed to heart failure and death at the age of four. A homozygous nonsense mutation, p.R1267X (c.3799C>T), in *DSPI* was found to be associated with this phenotype. This C to T transition generates a PTC in a region of exon 23 which is specific to *DSPI*, but absent from *DSPII* mRNA. Immunohistochemistry and western blot analysis of protein from the patient's skin with antibodies specific to DPI only and to both DPI and DPII revealed that DPI is below detectable levels in this patient's skin. Semi-quantitative RT-PCR showed the mutant *DSPI* transcript is unstable and likely to be rapidly degraded by the nonsense mediated decay (NMD) pathway (see below) (Uzumcu *et al.*, 2006).

As described in section 3.3.4, NMD is a mechanism of mRNA surveillance which detects mRNAs containing PTCs and targets these mutant transcripts for rapid degradation. The presence of an exon junction complex (EJC) downstream of a PTC is identified by NMD factors and leads to the activation of the NMD pathway resulting in the rapid decay of the PTC-containing transcripts (Maquat, 2004; Silva & Romao, 2009). The p.R1267X *DSPI*-specific nonsense mutation generates a PTC 1581 nucleotides upstream of the next exon-exon junction, which is hypothesised to trigger the NMD pathway. This mutation will be designated as *DSPI*-nonsense mutation throughout this chapter.

Two heterozygous mutations in *DSP* were described leading to DP haploinsufficiency and associated with dominantly inherited striate PPK (SPPK). One of these mutations is a splice site transition (939+1G>A) causing retention of intron seven which contains a PTC (Whittock *et al.*, 1999). The other is a C>T transition in exon four which substitutes a glutamine amino acid by a PTC (p.Q331X) (Armstrong *et al.*, 1999). Both dominant mutations affect all known *DSP* isoforms transcribed from the mutant allele and lead to decay of the mutant transcripts possibly through activation of the NMD pathway. Therefore, a reduced amount of each isoform is expressed in patients harbouring these mutations compared to normal individuals (Wan *et al.*, 2004). There is variable penetrance in these SPPK patients suggesting other genetic and/or environmental factors may contribute to the severity of the keratoderma (Whittock *et al.*, 1999). Ultrastructural analysis of these patients' skin showed loss of cell-cell contacts, under-developed desmosomes and retraction of the keratin IF network towards the nucleus (Armstrong *et al.*, 1999; Wan *et al.*, 2004; Whittock *et al.*, 1999). Immunohistochemistry of these patients' skin showed decreased expression of PKP1, DSC1 and DSC3, especially in the spinous layer (Wan *et al.*, 2004). This group of *DSP* mutations leading to haploinsufficiency will be designated as haploinsufficiency mutation throughout the chapter.

To mimic the *DSPI*-nonsense and haploinsufficiency *DSP* mutations, RNAi technology was used. *DSPI* was specifically down-regulated in HaCaT cells to resemble the p.R1267X *DSPI*-nonsense mutation and both *DSPI* and *DSPII* were partially down-regulated to mimic the haploinsufficiency mutation. This approach was used to investigate whether down-regulation of DPI has the same effect in HaCaT cells as partial reduction of both DPI and DPII in terms of expression of other components of the desmosomal complex and of cell-cell adhesion properties.

5.1.2. Heterozygous 30 bp-insertion mutation in *DSP* results in cardio-cutaneous disease

An insertion mutation in *DSP*, p.I608ins10, was previously identified in the Centre for Cutaneous Research (Norgett *et al.*, 2006). This heterozygous insertion of 30 bp into exon 14 of *DSP* (resulting in the insertion of 10 extra amino acids into the N-terminus of the protein) was associated with dominant SPPK, woolly hair and cardiomyopathy with left and right ventricular involvement. The cardiomyopathy resulted in heart failure and death of this patient at the age of 18. This patient's father

had also died suddenly from arrythmogenic right ventricular dysplasia (ARVD). The patient had a noticeable skin phenotype since the third year of life, consisting initially of hyperkeratosis and fissuring of the skin on palms and soles, and woolly hair. Later on in adolescence, the hyperkeratosis was observed on the knees, elbows, shins and ankles, and the patient had absent molars and pre-molars. The hair was woolly and kinky and the frontal scalp had short sparse hairs. Immunofluorescence staining of patient skin biopsies revealed a discontinuous distribution of DP and PG around the cell membrane, with some cytoplasmic localization, especially in the basal and lower supra-basal layers of the epidermis. Keratin 1 staining showed a slight reduction in expression and desmosomal attachment, only apparent in the lower regions of the epidermis (Norgett *et al.*, 2006). This mutation will be designated as insertion mutation throughout the chapter.

To study the I608ins10 insertion mutation, *DSPI* was cloned and the pBabe-puro retroviral system was used to generate HaCaT stable cell lines over-expressing wild type and mutant pBabe-*DSP* constructs (see sections 2.2.1 and 2.2.2 in Chapter 2). The effect of this mutation on the localisation of DP and pan-cytokeratin proteins in HaCaT cells was investigated using immunocytochemistry. An adhesion assay was used to study the effect of this mutation in HaCaT keratinocytes.

5.1.3. Flexcell adhesion assay to study mechanical properties of DP mutant cells

The skin phenotype observed in patients harboring these three types of *DSP* mutations is prominent in sites exposed to intense and constant mechanical pressure, such as palms and soles. In the case of the patient harboring the insertion mutation, involvement of other sites that are subject to physical trauma such as the knees, elbows, shins and ankles is also observed. To reproduce the *in vivo* physiological environment of these sites of pressure or abrasion, HaCaT cell monolayers, either with reduced expression of DP isoforms or over-expressing the insertion mutation, were subject to repeated cycles of radial stretch and relaxation for different periods of time, using the Flexcell FX-4000 Tension System. This system is a computer-regulated bioreactor that works by applying cyclic or static vacuum pressure onto silicone deformable matrix coated wells of tissue culture plates where cells are seeded (Flexcell International Corporation, http://www.flexcellint.com/). This system allows investigation of physical and biochemical cellular changes in response to mechanical stress.

5.1.4. Summary

This chapter is focused on the study of three distinct *DSP* mutations – *DSPI*-specific nonsense, haploinsufficiency and insertion mutations – in HaCaT keratinocytes in order to gain a deeper understanding of their molecular mechanisms leading to disease. Additionally, this study is aimed to provide further understanding about the specific functions of DPI and DPII. Different approaches were undertaken to study the molecular mechanisms of these mutations according to the different *in vivo* observations. The *DSPI*-nonsense and haploinsufficiency mutations are hypothesised to influence the expression levels of other desmosomal proteins and also keratinocyte adhesion properties. The insertion mutation is hypothesised to result in the abnormal distribution of other desmosomal-associated proteins. All mutations affect palmoplantar epidermis in particular, which is continuously subject to mechanical stress. Therefore, the influence of the *DSPI*-nonsense and haploinsufficiency mutations on the expression levels of other junctional proteins was investigated in HaCaT cells by western blot and densitometry analysis; the insertion mutant was over-expressed in HaCaT cells and its effects were investigated by immunocytochemistry; the Flexcell adhesion assay was used to examine the effect of all three mutations in HaCaT intercellular adhesion.

5.2. Results

5.2.1. Transient siRNA down-regulation of DP isoforms in HaCaT keratinocytes mimics *DSPI*-nonsense and haploinsufficiency mutations

The *DSPI*-nonsense mutation targets both *DSPI* and *DSPIb* (DPIb is described in Chapter 4) mRNAs (Figure 5.1B). To faithfully mimic this mutation, siRNAs were designed to specifically target the 648 bp region, from nucleotides 3861 to 4329, which is common to both splice variants (Figure 5.1A and 5.1B). Three of four designed siRNAs were shown to be functional and were pooled together in subsequent experiments. The sequences and targeting sites of these three functional siRNAs (si2, si3 and si4) as well as the position of the *DSPI*-nonsense mutation (c.3799C>T; R1267X) are shown in Figure 5.1. Cells transfected with the pool of functional siRNAs (siI) used to mimic the *DSPI*-nonsense mutation in HaCaT cells were designated as siI cells (Figure 5.1A and 5.1B).

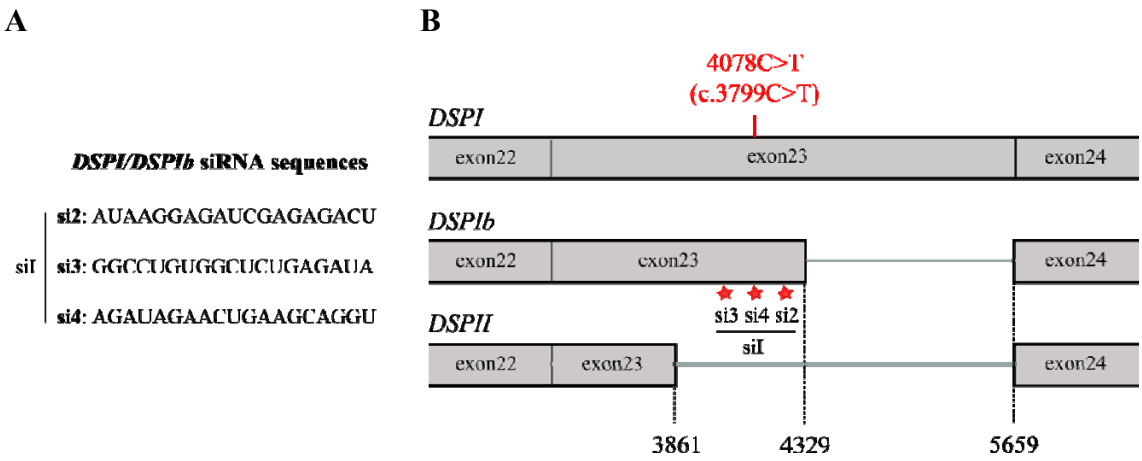

Figure 5.1. Nucleotide sequences of three siRNAs directed against *DSPI/DSPIb* and their targeting sites. (A) Sense strands of three individual siRNAs (si1, si2 and si3) designed to specifically target *DSPI* and *DSPIb* mRNAs. The three siRNAs were used as a pool designated as siI. **(B)** Schematic diagram of a portion of the *DSPI*, *DSPIb* and *DSPII* mRNAs including exons 22 to 24 and the position of the p.R1267X (c.3799C>T or 4078C>T) nonsense mutation. 4078C>T refers to nucleotide numbering commencing from the transcript's first nucleotide. Alternative donor splice sites around positions 5659, 4329 and 3861 (position numbers according to accession number NM_004415.2 of NCBI database) originate three different splice variants (*DSPI*, *DSPIb* and *DSPII* respectively). The p.R1267X mutation occurs in nucleotide position 4078 within a region common to both *DSPI* and *DSPIb* mRNAs, and therefore siRNAs were designed in this region to knock-down *DSPI* and *DSPIb* and mimic this mutation. The targeting sites of each individual siRNA are indicated with red stars.

A number of optimisations were performed prior to the siRNA experiments described in this chapter, including optimisation of transfection conditions, testing of the four designed siRNAs, optimisation of the siI pool concentration and time course analysis of DPI down-regulation in HaCaT cells. Optimisation of transfection conditions was carried out to find the highest transfection efficiency whilst maintaining cell viability. The four siRNAs were tested to determine which ones were functional, i.e. resulted in significant down-regulation of DPI. The concentration of siI pool was varied to determine the lowest concentration resulting in significant down-regulation of DPI in order to reduce off-target effects. A time course analysis was performed to determine the duration of DPI down-regulation. These optimisations, as well as the procedure used to design the four *DSPI* siRNAs, and respective results are described in Appendix B.

The haploinsufficiency mutation was mimicked using a siRNA that has been described by Wan *et al.* (2007), to down-regulate all *DSP* isoforms to about 50% in HaCaT cells. Cells transfected with this siRNA were designated as siI/II cells. A pool of four non-targeting (NT) siRNAs was used as a negative control (NT cells). A western blot showing down-regulation of DPI (which mimics the *DSPI*-nonsense mutation) in

siI cells and down-regulation of DPI and DPII (mimicking the haploinsufficiency mutation) in siI/II cells with a C-terminal DP antibody (11-5F, Parrish *et al.*, 1987) is depicted in Figure 5.2.

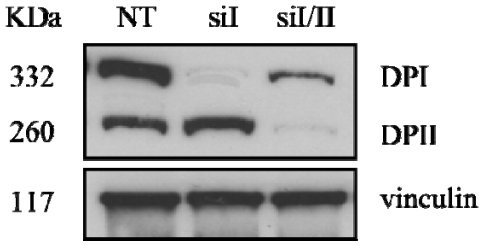

Figure 5.2. Western blot of DPI and DPII in HaCaT cells following siI and siI/II siRNA transfections to mimic the *DSPI*-nonsense and haploinsufficiency mutations, respectively. Total proteins from HaCaT cell lysates four days after transfection with non-targeting (NT) control siRNAs (lane 1), siI pool (lane 2) and siI/II siRNA (lane 3) with a C-terminal DP antibody (11-5F) which recognises both DPI (332KDa) and DPII (260KDa). Down-regulation of DPI with siI mimics the *DSPI*-nonsense mutation and down-regulation of DPI and DPII with siI/II mimics the haploinsufficiency mutation. Vinculin (117KDa) was used as loading control.

5.2.2. Characterisation of DPI and DPI/II down-regulation in HaCaT cells

5.2.2.1. Influence of DSPI-nonsense and DSP haploinsufficiency mutations on the expression levels of desmosomal associated proteins

The first goal of this chapter was to investigate the influence of the *DSPI*-nonsense and haploinsufficiency mutations on the expression levels of DP binding partners and other junctional proteins. This was performed by western blot and compared between the two DP knock-down situations and to the NT control cells.

Two independent siRNA knock down experiments were conducted and two to four replicate western blots were carried out for each protein in each experiment. Figures C1 and C2 (Appendix C) show representative western blots for each analysed protein in the first and second experiments, respectively. Protein levels, calculated from densitometry measurements of western blots using an image analysis program (Image J, v. 1.34s) are also graphically depicted for DPI and DPII, total DP (DPI+DPII expression levels), and for the proteins that showed reduced expression levels following DP knock-down (Figures C1 and C2, Appendix C). These protein levels were normalised to the loading control (vinculin) for each individual sample, and are presented as a fold change of the NT control for each western blot. For the DPI/DPII graphs (Figures C1C and C2C, Appendix C), DPI and DPII protein levels are presented as a fold change of the

DPI level of NT cells, as this reflects the DPI:II ratio that is present in wild type control cells. The t-test for matched pairs was used to compare the means of two samples in each western blot (Appendix C).

No detectable differences were observed in the expression levels of PKP2, PKP3, PG, β-catenin, keratin 14 and DSG3 between siI or siI/II (which mimic the *DSPI*-nonsense mutation and the haploinsufficiency mutation, respectively) and NT control cells, in any of the independent knock-down experiments. Variable results were observed for DSG2 expression levels between the two independent experiments (Figures C1A and C2B, Appendix C), and further experiments would be necessary to confirm these results.

Both independent knock-down experiments showed consistent results for the expression levels of PKP1, DSC2 and DSC3, which were reduced in siI and siI/II cells compared to NT cells. Therefore, the decision was made to pool western blot results from the two independent experiments for these three proteins as well as for DP. This procedure allowed for a larger number of data points to increase the confidence in the results. Figure 5.3 depicts protein levels of DP, PKP1, DSC2 and DSC3 calculated from the western blots of the two independent knock-down experiments.

Total DP expression levels were reduced, on average, to 50% in siI cells and to 40% siI/II cells when compared to NT control cells ($p<0.001$) (Figure 5.3A). Likewise, expression of PKP1, DSC2 and DSC3 was significantly reduced in siI and siI/II cells compared to NT cells (Figure 5.3B). Although the difference in total DP levels between siI and siI/II cells is not statistically significant (Figure 5.3A), the DPI and DPII expression levels between siI and siI/II cells changed significantly ($p<0.05$). The DPI:DPII ratios also changed from 1:8 in siI cells to 4:1 in siI/II cells (Figure 5.3A). Figure 5.3B shows that, similarly to the total DP levels, PKP1 and DSC2 levels are not significantly different between siI and siI/II cells. In contrast, DSC3 expression levels are significantly higher in siI/II cells than in siI cells ($p<0.05$). These results suggest that despite the intrinsic variability associated with all experimental procedures, PKP1 expression levels are not influenced by the DPI:DPII ratios. In contrast, DSC3 expression is influenced by the ratios of these DP isoforms, more than by total DP levels.

A

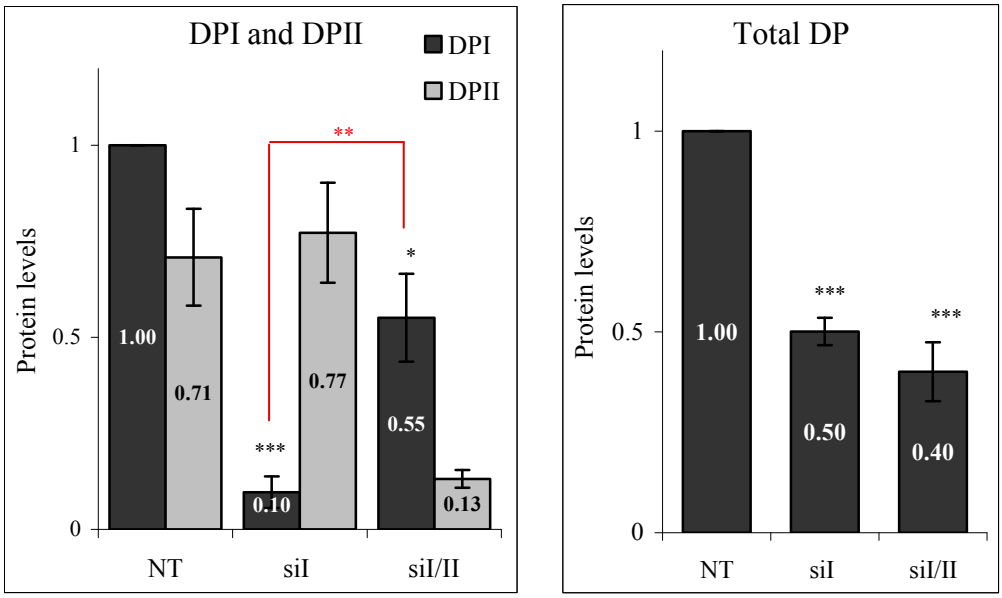

B

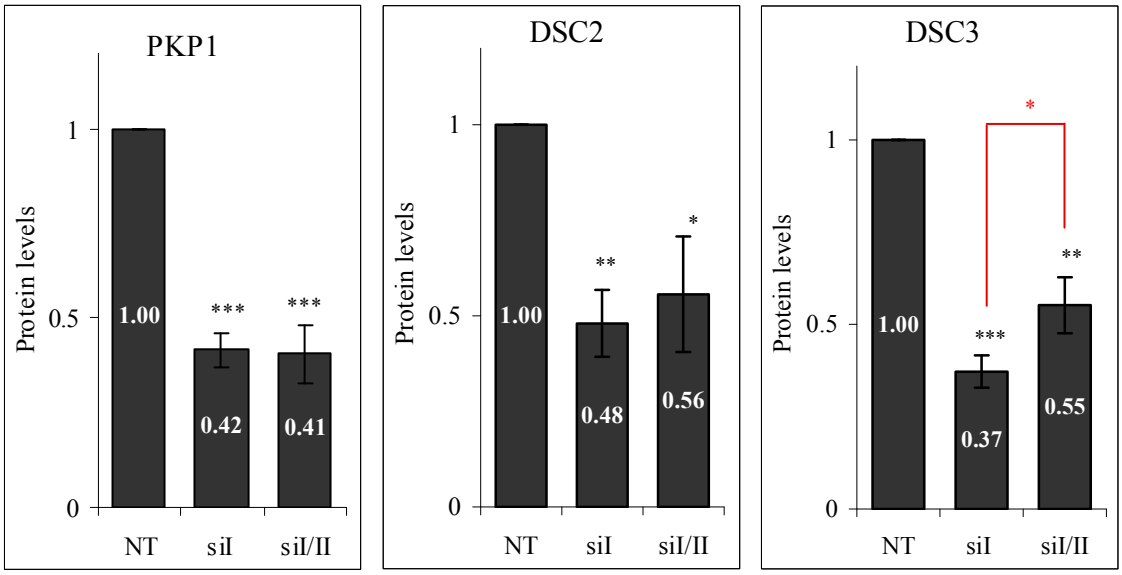

Figure 5.3. Protein levels of desmosomal proteins following *DSPI* and *DSPI/DSPII* knock-down suggests that DSC3 expression levels are influenced by the DPI:DPII ratios in contrast with PKP1. (A) Protein levels of DPI and DPII (n=6 blots) and of total DP (DPI+DPII) calculated from densitometry measurements of western blots (mean±SEM) and normalised to loading control (vinculin). DPI and DPII expression levels are presented as a fraction of the DPI levels of NT cells. Total DP expression levels are presented as a fraction of the DP levels of NT cells. **(B)** Protein levels (mean±SEM) of PKP1 (n=7 blots), DSC2 (n=5 blots) and DSC3 (n=6 blots) normalized to the loading control and presented as a fraction of the respective NT control levels. PKP1 levels do not change between siI and siI/II cells; in contrast DSC3 levels are significantly higher in siI cells than in siI/II cells. Statistical significance between siI or siI/II and NT following paired t-test is shown with black stars. Red stars represent statistical significance between siI and siI/II cells: * ($p<0.05$), ** ($p<0.01$), *** ($p<0.001$).

5.2.2.2. Influence of the DPI:DPII ratios on DSC3 and PKP1 expression

To confirm the previous results (section 5.2.2.1) which suggest that DSC3 expression is dependent on the DPI:DPII ratios in contrast with PKP1, the influence of DPI:DPII ratios on the expression levels of DSC3 and PKP1 was further investigated using different concentrations of siI and siI/II siRNAs. DPI expression was gradually reduced by increasing concentrations of the siI pool (lanes a-d, Figure 5.4A), and both this pool and increasing concentrations of siI/II were used to progressively down-regulate DPII whilst leaving DPI unchanged (lanes e-h, Figure 5.4A). Figure 5.4B shows total DP expression levels as well as DPI and DPII levels relative to NT cells (lane i, Figure 5.4A and 5.4B).

Figure 5.4C and 5.4D show that the DSC3 and PKP1 expression profiles differ considerably. Whilst DSC3 expression shows a progressively decreasing trend similar to DPI, PKP1 expression is relatively stable in lanes a-d and decreases by approximately half from lane d to lane e. This abrupt reduction parallels the reduction in the total DP levels from lanes d to e. These results suggest that DSC3 and PKP1 expression are differently affected by the DPI:DPII ratios.

To further investigate whether it is the DPI:DPII ratio that influence DSC3 expression levels rather than total DP levels, three additional replicate western blots were performed for DSC3 and PKP1 from HaCaT cells transfected with 2, 4 and 6 nM of siI (conditions b, c and d, Figures 5.4A and 5.4B). A representative western blot is shown in Figure C3 (Appendix C). Under these conditions, the total DP levels did not change significantly but the DPI:DPII ratios differed. Figure 5.4E shows protein levels of DSC3 and PKP1 (six western blots for each protein) under these conditions. A statistically significant difference in the levels of DSC3 is observed between conditions b and c and between b and d. However, the differences in PKP1 expression levels under these conditions are not statistically significant. These results suggest that DSC3 expression levels are more influenced by the DPI:DPII ratios whereas the expression levels of PKP1 are not.

A

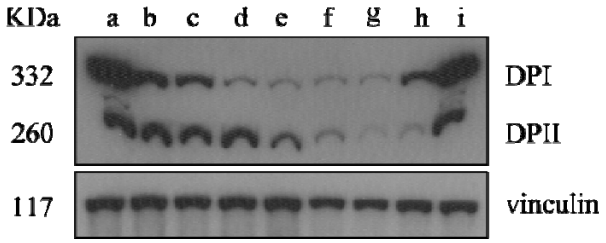

B

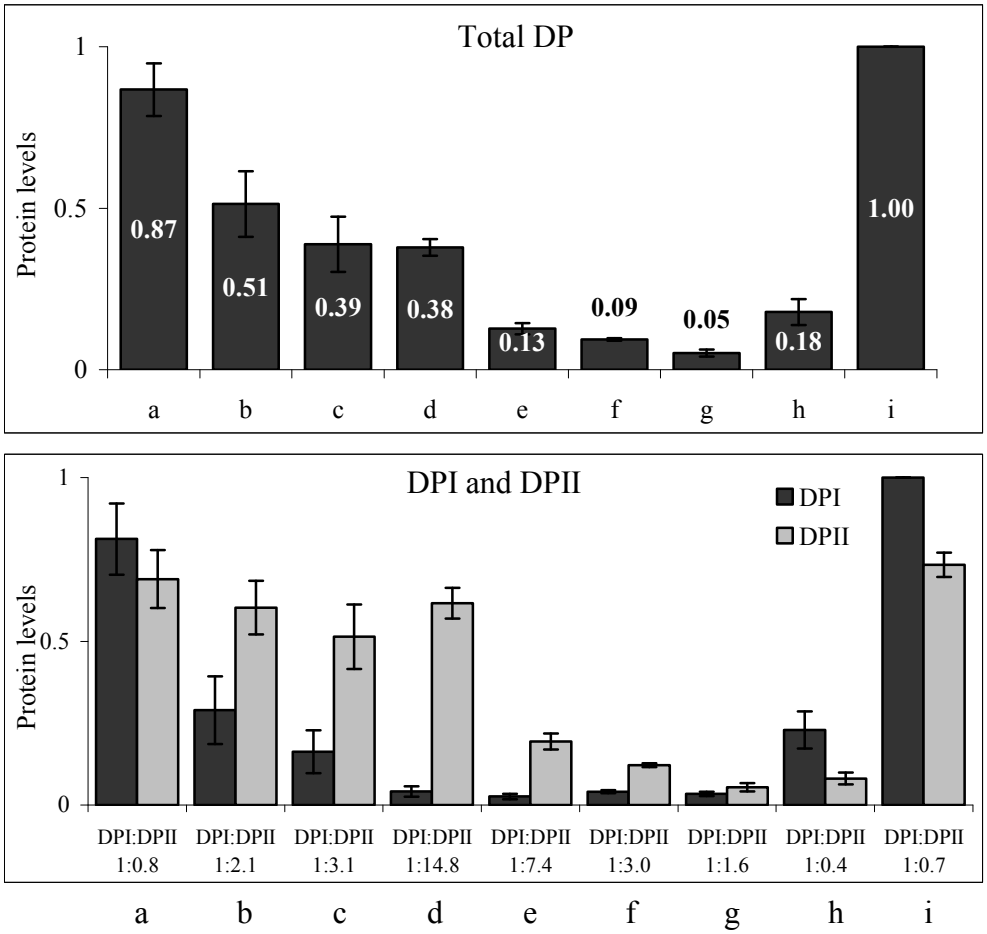

C

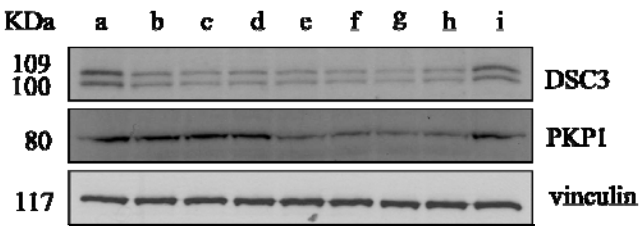

Figure 5.4. Variation of the DPI:DPII ratio has different effects on the expression levels of DSC3 and PKP1 (continues).

D

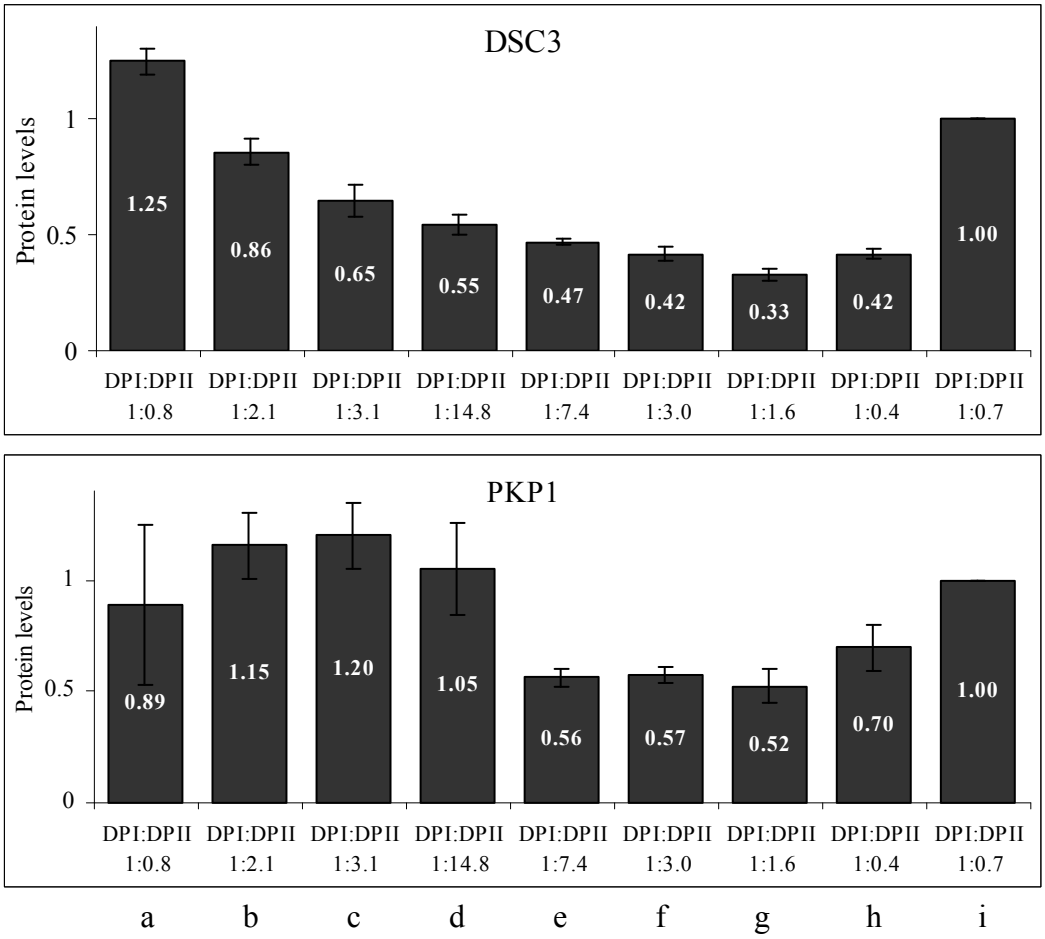

E

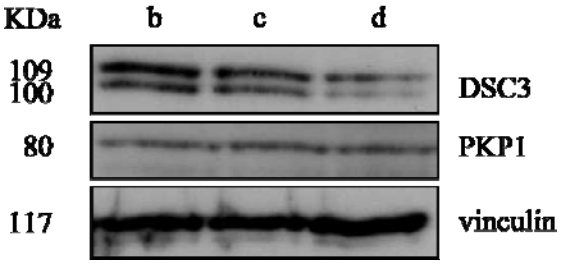

Figure 5.4. Variation of the DPI:DPII ratio has different effects on the expression levels of DSC3 and PKP1 (continues).

F

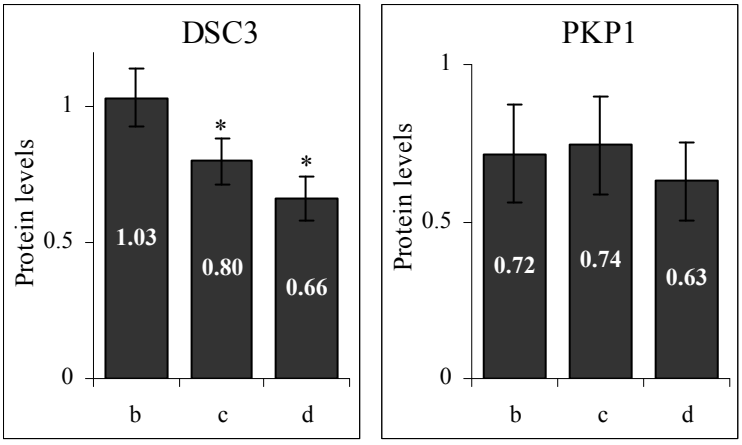

Figure 5.4. Variation of the DPI:DPII ratio has different effects on the expression levels of DSC3 and PKP1. **(A and C)** Western blots of desmosomal proteins from total HaCaT cell lysates, four days after transfection with 0 (a), 2 (b), 4 (c) and 16 (d) nM of siI and 16nM siI + 5 (e), 10 (f), 40 (g) and 100 (h) nM of siI/II. 140nM of NT pool (i) was used as negative control **(A)** DPI and DPII expression levels are shown. **(B)** Protein levels of DPI and DPII (n=3 blots) and of total DP (DPI+DPII) calculated from densitometry measurements (mean±SEM) and normalised to loading control. DPI and DPII levels are presented as a fraction of the DPI levels of NT cells (i). Total DP levels are presented as a fraction of DP levels of NT cells. **(C)** Protein levels of DSC3 and PKP1 are shown. Vinculin was used as loading control. **(D)** Protein levels (mean±SEM) of DSC3 (n=3 blots) and PKP1 (n=3 blots) normalized to the loading control and presented as a fraction of the respective NT control levels (i). **(E)** Representative western blot of HaCaT cells transfected with 2 (b), 4 (c) and 6 (d) nM of the siI pool. **(F)** Protein levels (mean±SEM) of DSC3 and PKP1 for conditions b, c and d (n=6 blots). Statistical significance between c or d and b following paired t-test: * ($p<0.05$).

5.2.3. Influence of *DSPI*-nonsense and haploinsufficiency mutations in HaCaT intercellular adhesion

The FX-4000T™ Cell Stretcher was used to investigate and compare the effects of mechanical stress in HaCaT cells transfected with siRNAs that mimic the *DSPI*-nonsense and DP haploinsufficiency mutations. Optimisations of this adhesion assay were first performed (see section D1, Apendix D) in order to find experimental conditions where NT control cells showed some degree of mechanical stress but remained attached to the culture dish. Under these conditions, DP knock down cells were predicted to have more altered mechanical properties than wild type cells.

Following these optimizations, siI and siI/II HaCaT cells (mimicking the *DSPI*-nonsense mutation and the haploinsufficiency mutation, respectively) were subjected to mechanical stretch with a frequency of 2 Hz (i.e. two cycles of stretch and relaxation per second) and an elongation of amplitude ranging from 11% to 14% (i.e. increase in diameter across the silicone deformable membrane from 11% to 14%). Cells were

stretched for 30 minutes, one hour and two hours. Western blots of siI/II and siI HaCaT cell lysates were performed with a DP C-terminal antibody (11-5F) to confirm that knock-down of DPI/DPII and DPI, respectively, had been successfully achieved prior to the stretch assay. Figures 5.5A and 5.5B demonstrate down-regulation of DPI and DPII in siI/II cells (which mimic the haploinsufficiency mutation) and Figures 5.6A and 5.6B show knock-down of DPI in siI cells (which mimic the *DSPI*-nonsense mutation), both before and after two hours of mechanical stretch.

Double immunocytochemistry of siI and siI/II cells was performed using antibodies raised against DPI (in green) and keratin 14, pan-cytokeratin, PG and DSG1/2 (in red) (Figures 5.5, 5.6 and D2, D3 and D4, Appendix D). DAPI stain was used to label the nuclei and care was taken to keep its intensity constant between control and knock down cells to reflect the same focal plane of cells across different conditions. However this was not possible at all times due to slight variability in DAPI staining across different samples. Before any stretch was applied (0h), NT control, siI and siI/II cells exhibited a normal network of keratin IFs (as shown by immunocytchemistry with keratin 14 and pan-cytokeratin antibodies) which extended from the nucleus to the cell periphery (Figures 5.5D, 5.5E and 5.6C). However, among some siI/II cells, widening of intercellular spaces were observed which were more pronounced in regions where there was no expression of DPI at cell-cell junctions (arrow heads, Figure 5.5D and 5.5E). Keratin IFs appeared slightly thicker and IF attachment appeared stronger in regions where DPI expression levels were higher. Despite the wider intercellular spaces and loosening of IF attachment, these cells still appeared connected to each other through intercellular junctions (Figure 5.5D and 5.5E).

Following a 30-minute-stretch, NT cells had slightly thicker and more compact keratin 14 IFs, particular around the nucleus (arrows, Figure 5.5D). These thicker IFs were more prominent in the perinuclear region of siI/II cells (arrows, Figure 5.5D). However, close to the cell membrane of siI/II cells keratin IFs were thinner, particularly along free edges (arrow head, Figure 5.5D). In contrast with NT cells, wider intercellular spaces were observed among these cells, particularly in regions where DPI was absent (arrow head, Figure 5.5D).

After a one-hour-stretch, NT cells showed thickening of the keratin 14 IFs which were denser around the nuclei (arrow, Figures 5.5D) and the DPI puncta at cell-cell contacts became elongated (arrow, Figure 5.5C). There was no longer a homogenous network of keratin IFs from the membrane to the nucleus of NT cells. These changes in

the keratin IF network were more prominent after two hours of stretch (arrows, Figures 5.5D and 5.5E). In contrast with NT cells, although some siI/II cells still showed thick IFs, most siI/II cells had IFs that appeared thinner and more fragile (Figure 5.5E) and in some cases even deformed and retracted towards the nucleus (arrow, Figure 5.5D). Large intercellular gaps were observed among some cells, particularly after two hours of stretch (arrow heads, Figure 5.5D and Figure D2B, Appendix D).

These results suggest that in contrast with NT cells which showed thickening of keratin IFs with increased exposure to mechanical stretch, siI/II cells exhibited thinner and more fragile filaments and wider intercellular spaces. These observations were prominent in siI/II cells that express lower levels of DPI.

Before stretch (0h), NT cells showed continuous immunofluorescence staining around the cell membrane with a PG antibody. In contrast, siI/II cells showed some discontinuous peripheral PG staining, mostly in regions with reduced DPI expression (arrows, Figure 5.5F). Following one and two hours of stretch, siI/II cells showed loss of cell-cell contacts (arrow heads, Figures 5.5E and 5.5F) and PG staining was only present at the less frequent sites of cell-cell adhesion (arrow, Figure 5.5F and Figure D3, Appendix D). A slight increase in intracellular PG staining was also observed in some siI/II cells compared to NT cells, predominantly following two hours of mechanical stretch (Figure 5.5F).

No major differences in DSG1/2 staining were observed between NT and siI/II cells either before or after stretch. These desmosomal cadherins remained associated with the cell membrane even after two hours of mechanical stress (Figure D4, Appendix D).

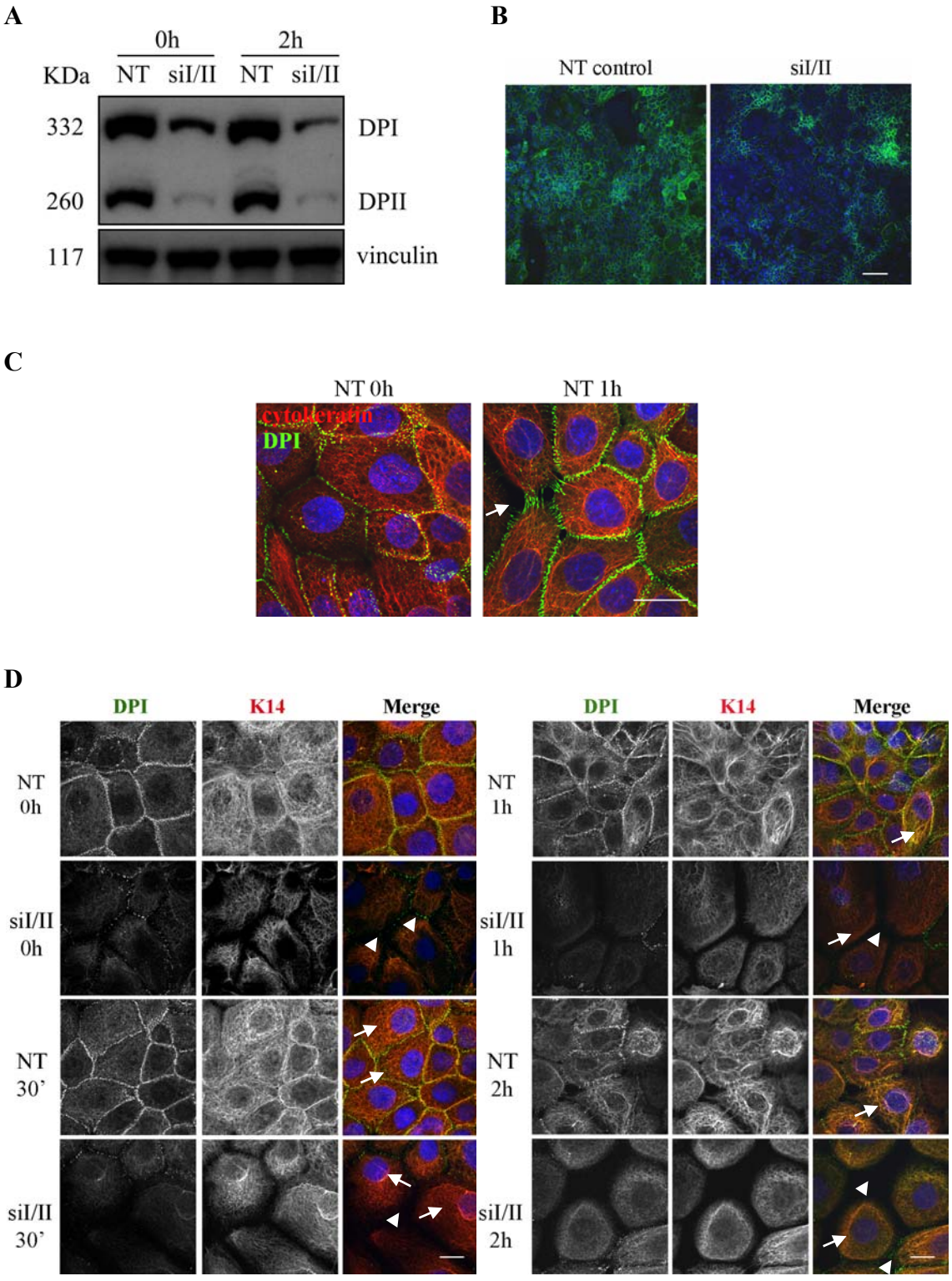

Figure 5.5. Mechanical stress causes reduced cell-cell adhesion in siI/II HaCaT cells (continues).

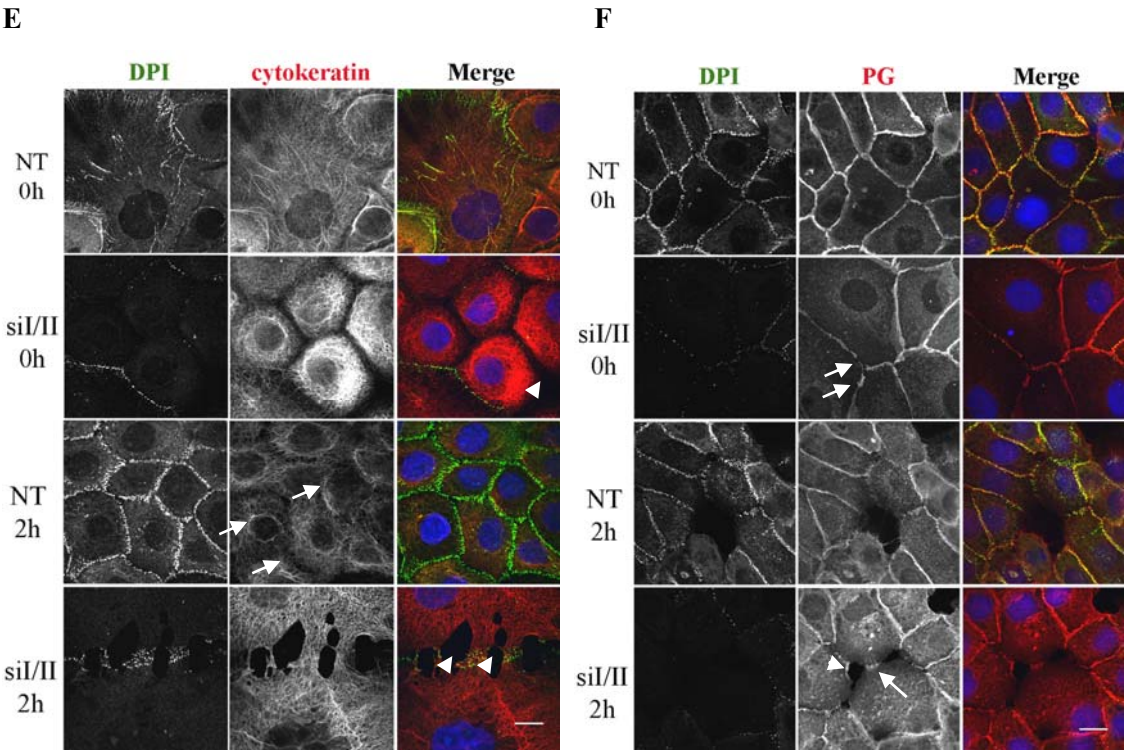

Figure 5.5. Mechanical stress causes reduced cell-cell adhesion in siI/II HaCaT cells. HaCaT cells transfected with a pool of four non-targeting siRNAs (NT control cells) and a siRNA which targets both *DSPI* and *DSPII* (siI/II) were subject to cyclic mechanical stress of frequency 2 Hz and amplitude 11-14% using the Flexcell FX-4000 Tension System for 0h (unstretched), 30 min, 1h and 2h. **(A)** Western blot of total proteins from NT and siI/II cells following 0h and 2h of stretch with a DP antibody (11-5F) that recognises both DPI (332KDa) and DPII (260KDa) shows reduction of DP levels in siI/II cells compared to NT control cells. Immunocytochemistry of NT and siI/II cells with 11-5F DP antibody **(B)** shows decrease in DP staining in siI/II cells compared to NT cells. Scale bar = 50µm. **(C)** Double immunocytochemistry of NT cells with antibodies against DPI (green) and keratin 14 (red) shows elongation of DP puncta along intercellular junctions (arrow) after 1h of stretch. Scale bar = 10 µm. Double immunocytochemistry of NT and siI/II cells with antibodies against DPI (green) and keratin 14 (red) before (0h) and after 30 min, 1h and 2h of stretch **(D)** and with antibodies against DPI (green) and pan-cytokeratin (red) **(E)** and DPI (green) and PG (red) **(F)** before and after 2h of stretch. siI/II cells show decrease of cell-cell adhesion with widening of intercellular spaces between keratinocytes following 2h of mechanical stress. Scale bar = 5µm.

Less evident morphological changes were displayed by siI cells (compared to NT cells) than siI/II cells following mechanical stretch (Figure D2A, Appendix D). Similarly to NT cells, thickening of keratin IFs was observed following one and two hours of stretch (Figure 5.6C). However, while siI/II cells showed thinner and more fragile IFs particularly along free edges after two hours of stretch, this was not observed in siI cells. Equally, although some widening of intercellular spaces was observed after one and two hours of stretch, these were less frequently seen than in siI/II cells (arrow heads, Figure 5.6 and Figure D2A, Appendix D).

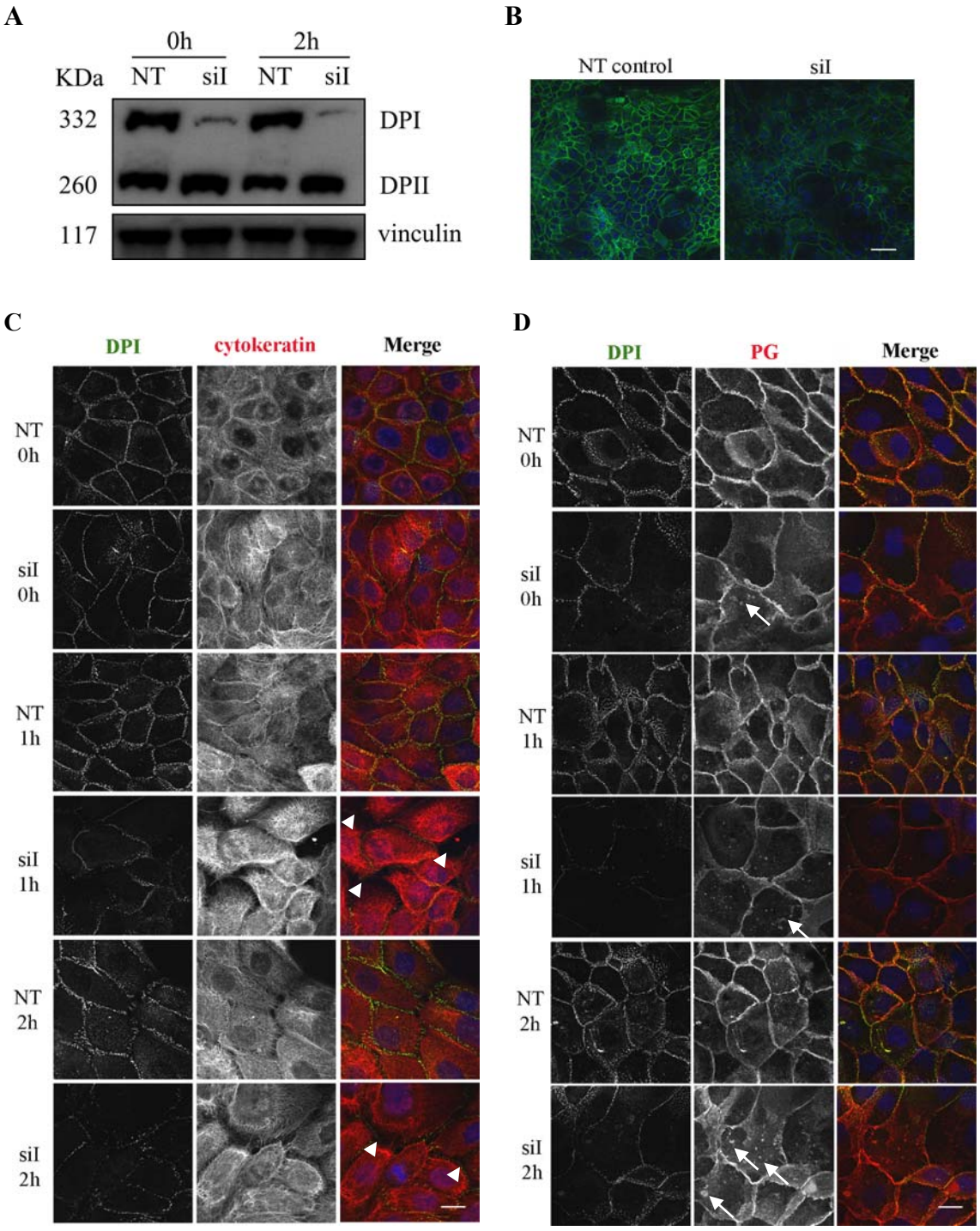

Figure 5.6. Mechanical stress causes reduced cell-cell adhesion in siI HaCaT cells. HaCaT cells transfected with a pool of four non-targeting siRNAs (NT control cells) and a pool of three siRNA which target *DSPI* and *DSPIb* (siI) were subject to cyclic mechanical stress of frequency 2 Hz and amplitude 11-14% using the Flexcell FX-4000 Tension System for 0h (unstretched) and 2h. **(A)** Western blot of total proteins from NT and siI cells following 0h and 2h of stretch with a DP antibody (11-5F) that recognises both DPI (332KDa) and DPII (260KDa). Immunocytochemistry of NT and siI cells with a DPI-specific antibody **(B)** shows decrease in DP staining in siI cells compared to NT control cells. Scale bar = 25 µm. Double immunocytochemistry of NT and siI cells with antibodies against DPI (green) and pan-cytokeratin (red) **(C)** and with antibodies against DPI (green) and PG (red) **(D)** before and after 2h of stretch. siI transfected cells show decrease in cell-cell adhesion however to a lesser extent compared to siI/II transfected cells. Scale bar = 5µm.

PG staining revealed a slight increase in cytoplasmic staining in siI cells compared to NT cells before stretch. This was progressively more evident in cells stretched for one and two hours, where cytoplasmic aggregates reactive with the PG antibody were observed (arrows, Figure 5.6D).

No obvious differences in localisation of the desmosomal proteins DSC2, DSC3, PKP2 and PKP3 and of the adherens junction proteins E-cadherin and β-catenin were observed among siI, siI/II cells and NT cells, either before or after mechanical stretch (data not shown).

Overall, these results suggest that the adhesive properties of desmosomes with approximately 50% of DPI and DPII (which mimic desmosomes with DP haploinsufficiency) are more impaired than those of desmosomes with DPI down-regulation (which mimic the *DSPI*-nonsense mutation).

5.2.4. Over-expression of recombinant I608ins10-DPI in HaCaT keratinocytes to mimic the *DSP* 30 bp-insertion mutation

5.2.4.1. Generation of wild type- and I608ins10-DSPI-flag expressing stable cell lines

HaCaT cells were transduced with virus containing pBabe-*DSPI*-flag, pBabe-I608ins10-*DSPI*-flag or pBabe-GFP control plasmid. The generation of the constructs as well as transduction conditions are described in Chapter 2. Recombinant DP protein expression was assessed by western blot using an antibody raised against the flag tag epitope (Table 2.7). As expected, flag tagged-DPI was observed in HaCaT cells transduced with pBabe-*DSPI*-flag and pBabe-I608ins10-*DSPI*-flag, but not in cells transduced with the pBabe-*GFP* control plasmid. Wild type HaCaT total lysates were also immunoblotted with the C-terminal DP antibody (11-5F) for comparison (Figure 5.7).

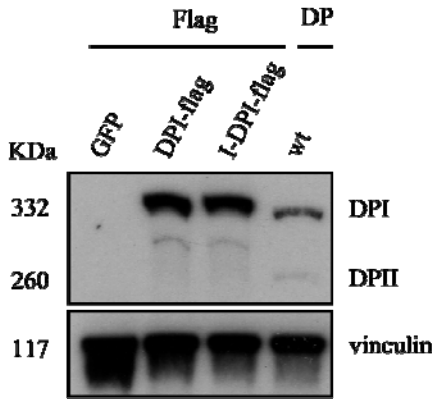

Figure 5.7. Recombinant DPI-flag and I608ins10-DPI-flag protein expression in HaCaT cells. Western blot of total lysates from HaCaT cells transduced with pBabe-*GFP* (lane 1), pBabe-*DSPI*-flag (lane 2) and pBabe-I608ins10-*DSPI*-flag (lane 3) constructs with an anti-flag antibody and wild type HaCaT cells with the 11-5F C-terminal DP antibody (lane 4). Flag tagged-DPI (~332 KDa) is observed in lanes 2 and 3 but not in lane 1, as expected. DPII (~260KDa) is observed only in wild type cells. Vinculin (117 KDa) was used as loading control. Lanes 2 and 3 express also an immunoreactive band shorter than DPI at a much lower level which resembles the putative DPIa protein referred to in Chapter 4 seen in most western blots immediately below DPI (Figures 4.7B, 4.10C, 4.10D and 4.12). As these cell lysates were immunoblotted with a flag antibody, the faint immunoreactive band cannot be a splice variant other then flag-tagged DPI. These results suggest that this faint band (and possibly DPIa) is either a western blot artefact, or a breakdown product of DPI.

5.2.5. Immunocytochemistry of wild type and I608ins10 mutant DPI in HaCaT cells

Immunocytochemistry of HaCaT cells transduced with pBabe-*DSPI*-flag, pBabe-I608ins10-*DSPI*-flag and pBabe-GFP control vector was performed to investigate the cellular localisation of wild type and I608ins10 mutant flag tagged-DPI proteins. As expected, GFP expressing control cells showed no reactivity with the anti-flag antibody. DPI-flag expressing cells show punctuate staining at the cell membrane, characteristic of DP proteins. In contrast, I608ins10-DPI-flag expressing cells show large DPI aggregates which localise to the cell membrane (Figure 5.8).

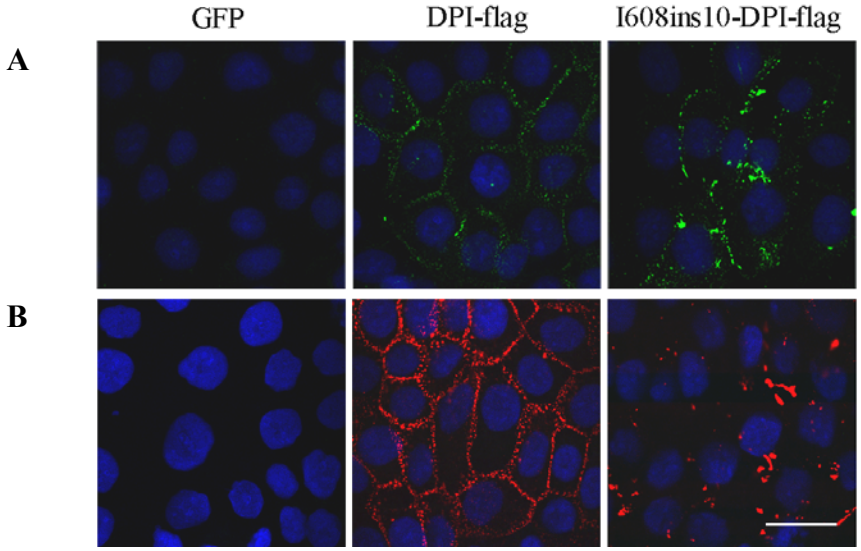

Figure 5.8. I608ins10-DPI-Flag proteins form large aggregates in HaCaT cells. Immunocytochemistry of HaCaT cells transduced with a pBabe-GFP control vector, pBabe-*DSPI*-flag and pBabe-I608ins10-*DSPI*-flag with an anti-flag primary antibody and a secondary antibody conjugated to Alexa Fluor 488 (green) **(A)** or 568 (red) **(B)**. GFP expressing cells show no reactivity with the flag antibody, wild type DPI-expressing cells show punctate membranous flag staining characteristic of DP proteins and I608ins10-DPI-expressing cells show large aggregates at the cell membrane. Scale bar = 20µm.

5.2.6. Effect of the I608ins10 *DSP* insertion mutation in intercellular adhesion

The Flexcell adhesion assay was used to investigate whether I608ins10-DPI recombinant proteins influence HaCaT intercellular adhesion. This assay was performed under the conditions described in section 5.2.3 for zero hours (before stretch) and two hours. HaCaT cells over-expressing wild type DPI-flag or I608ins10-DPI-flag were subject to double immunocytochemistry with DP (11-5F) or pan-cytokeratin (green) and flag (red) antibodies (Figure 5.9).

Double immunocytochemistry with DP and flag antibodies showed that junctional endogenous DP (green) and recombinant wild type DPI-flag (red) co-localise (Figure 5.9). This result indicates that recombinant flag-tagged DPI proteins localise to desmosomes similarly to endogenous DPI. I608ins10-DPI-flag aggregates also localise to the cell membrane. This result suggests that these large mutant DPI aggregates are still able to traffic to the cell membrane.

Double immunocytochemistry with flag and pan-cytokeratin antibodies revealed that the I608ins10-DPI-flag aggregates are still able to co-localise with keratin IFs at intercellular junctions (Figure 5.9). Although the keratin IFs appeared slightly thicker following two hours of physical stretch, no major differences were observed between DPI-flag and I608ins10-DPI-flag expressing cells (Figure 5.9). These results suggest

that the mechanical properties of I608ins10-DPI-flag proteins are similar to those of DPI-flag proteins.

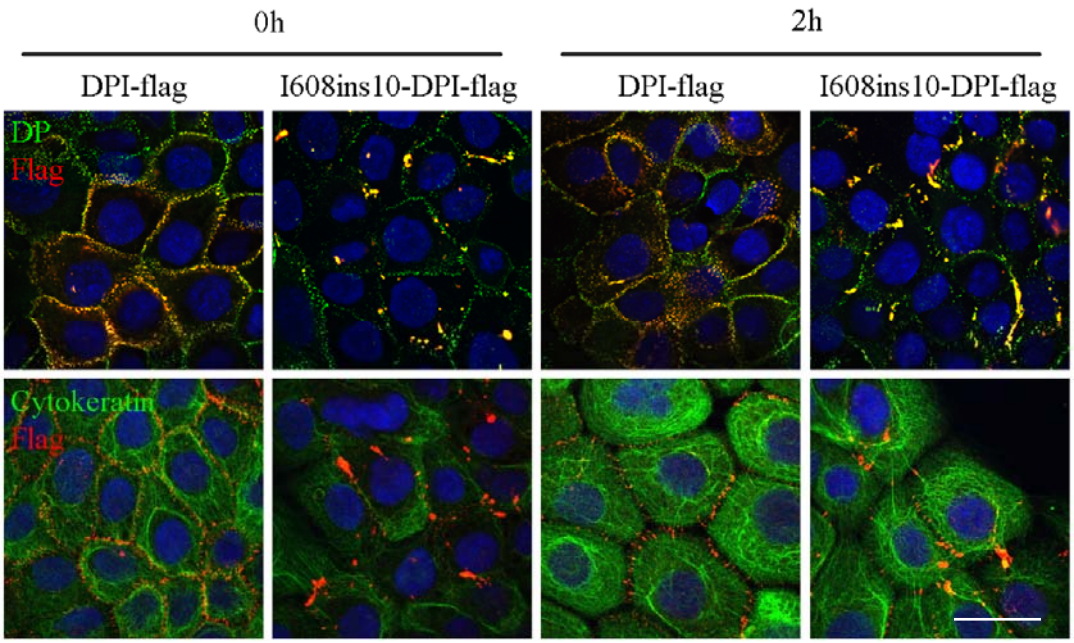

Figure 5.9. I608ins10-DPI-Flag proteins do not appear to influence HaCaT cell-cell adhesion. HaCaT cells over-expresisng DPI-flag and I608ins10-DPI-flag proteins were subject to cyclic mechanical stress of frequency 2 Hz and amplitude 11-14% using the Flexcell FX-4000 Tension System for 0h (unstretched) and 2h. Double immunocytochemistry of these cells with antibodies raised against DP (11-5F, green) and flag (red) and with antibodies raised against flag (red) and pan-cytokeratin (green) show that large I608ins10-DPI-flag aggregates are cell membrane bound and co-localise with keratin IFs. I608ins10 mutant DPI proteins do not appear to influence HaCaT intercellular adhesion. Scale bar = 20μm.

5.2.7. Overview of the effects of the *DSP* mutations studied on HaCaT keratinocytes

Table 5.1 summarises the changes observed in the expression levels of desmosomal associated proteins and in HaCaT mechanical properties in cells expressing the three types of *DSP* mutations studied.

Table 5.1. Summary of the effects of three *DSP* mutations; *DSPI*-nonsense mutation, DP haploinsufficiency and 30 bp-insertion mutation, modeled in HaCaT keratinocytes.

***In vivo* observations in patients**			***In vitro* observations in HaCaT cells***					
Mutation studied	**Molecular outcome**	**Human phenotype**	**Method for modelling mutation**	**Effect on PKP1 expression**	**Effect on DSC2 expression**	**Effect on DSC3 expression**	**Effect on intercellular adhesion**	**Cytoplasmic localisation of PG**
c.3799C>T; p.R1267X	DPI knock-out	EPPK, woolly hair, cardiomyopathy	siRNA DPI knock-down	↓	↓	↓↓	↓	↑
c.991C>T; p.Q331X 939+1G>A	DPI+DPII haploinsufficiency	SPPK	siRNA DPI/DPII partial down-regulation	↓	↓	↓	↓↓	↑
c.1823_1824 ins30 bp; I608ins10	Insertion of 10 aa in the N-terminus of DPI/DPII	SPPK, woolly hair, cardiomyopathy	Over-expression of DPI-I608ins10-flag construct	–	–	–	no detectable effect	–

*The *DSPI*-specific nonsense mutation (p.R1267X) modeled by down-regulation of DPI, and the DP haploinsufficiency mutations modeled by partial down-regulation of DPI/DPII in HaCaT cells result in decreased expression of PKP1 and DSC2 (↓). Down-regulation of DPI results in a higher reduction of DSC3 protein levels (↓↓) compared to those of DSC2 (↓). The haploinsufficiency mutation causes reduction in HaCaT intercellular adhesion to a higher extent (↓↓) than the *DSPI*-specific nonsense mutation (↓). Both mutations cause increase in cytoplasm localisation of PG. The insertion mutation modelled by over-expression of a DPI-I608ins10-flag construct in HaCaT cells causes no effect on intercellular adhesion but leads to formation of DP aggregates at the cell membrane. – refers to not investigated.

.

5.3. Discussion

The focus of this chapter was to investigate the mechanisms by which DPI and DPII contribute to tissue architecture and normal function, by studying the role of three different types of *DSP* mutations associated with skin and heart disease.

Over the past 13 years, an increasing number of monogenic diseases that are caused by mutations in genes encoding desmosomal proteins have been revealed. Although the genetic defects leading to these diseases are known, the molecular pathogenic mechanisms are, for the most part, not completely understood. There are still a large number of difficult questions that remain unanswered. Firstly, it is not clear why mutations in *DSP* can give rise to different clinical presentations in patients. Some *DSP* mutations are restricted to skin, others affect only the heart and some other mutations result in a combination of skin and heart disease (Figure 1.8). Additionally, varying degrees of severity are observed in skin and heart manifestations depending on the type of mutation. Secondly, another complicated issue is the lack of correlation between the functional domain of DP encoded by the region where the mutation occurs and the resulting clinical outcome. For instance, mutations in regions encoding the central rod domain as well as the N- and C-terminal domains can lead to ARVC, whereas mutations in regions coding for the N-terminus of the protein can cause skin disease only, a combination of skin and hair abnormalities and also a combination of skin, hair and heart disease. Thirdly, it is interesting that mutations in different genes can result in similar phenotypes, suggesting that different desmosomal proteins have overlapping functions and may be involved in overlapping pathways. A fourth question that prompted the work described here is whether the different DP splice variants have different adhesion and/or signalling properties and whether DPI:DPII ratios influence normal desmosome function.

5.3.1. Clinical and histopathological manifestations of *DSPI*-nonsense, *DSP* haploinsufficiency, and *DSP* insertion mutations

The first two types of *DSP* mutations studied in this chapter include a haploinsufficiency mutation effecting both DPI and DPII and a homozygous *DSPI*-specific nonsense mutation (p.R1267X) leading to loss of the DPI splice variant. The haploinsufficiency mutations resulted in a more severe SPPK while the *DSPI*-nonsense mutation caused a relatively mild EPPK (Armstrong *et al.*, 1999; Uzumcu *et al.*, 2006;

Whittock *et al.*, 1999). Additionally, in contrast with the haploinsufficiency mutants, the *DSPI*-specific nonsense mutation led also to a very severe heart condition with early onset and rapid progression which resulted in death of this patient at four years of age (Uzumcu *et al.*, 2006).

Previous reports have described histopathological features of SPPK lesional skin in patients with the *DSP* haploinsufficiency (Armstrong *et al.*, 1999; Wan *et al.*, 2004; Whittock *et al.*, 1999). Histological analyses revealed thickening of the epidermis and impaired cell-cell adhesion, with widening of intercellular spaces in suprabasal layers. Immunofluorescence microscopy of these patients' epidermis showed reduced expression and abnormal localisation of PKP1 in the spinous layer. DSC1 and DSC3 expression levels were also markedly reduced, particularly in the spinous layer. Ultrastructural analysis of spinous layers revealed reduced cell-cell contacts and desmosomes with variable morphological appearances. In some regions, connections between keratinocytes were maintained by rudimentary desmosomes that displayed underdeveloped cytoplasmic plaques and lack of association with the IF network, which appeared retracted towards the nucleus. In other regions where keratinocytes remained closely connected, desmosomes had a normal appearance both in size and structure, with well developed cytoplasmic plaques, clear electron dense midlines and insertion of IFs. In some regions an abnormal clustering of normal as well as less electron dense, underdeveloped desmosomes was also observed. The number of desmosomes was shown by morphometric analysis to be significantly reduced in suprabasal layers and this phenomenon was observed both in lesional and non-lesional SPPK epidermis (Armstrong *et al.*, 1999; Wan *et al.*, 2004; Whittock *et al.*, 1999).

Skin immunohistochemistry of the patient with the *DSPI*-specific nonsense mutation revealed complete absence of DPI but apparently normal expression and localisation of DPII, PG and keratin 1. The structural appearance of this non-lesional epidermis appeared normal; however no ultrastructural analysis was performed on this patient's skin. Therefore, changes in desmosome ultrastructure, size, number or distribution might be present, as seen in the epidermis of patients with *DSP* haploinsufficiency mutations.

The third *DSP* mutation studied in this chapter was a dominant insertion of 30 bp in the region encoding the N-terminus of DP. The patient harbouring this mutation had SPPK accompanied by hyperkeratosis on the knees, elbows, shins and ankles, and absent molars and pre-molars. The patient also had a very severe bi-ventricular

cardiomyopathy which resulted in heart failure at the age of 18. Immunofluorescence microscopy of patient epidermis revealed a discontinuous distribution of DP and PG around the cell membrane with some cytoplasmic localisation, particularly in the lower layers of the epidermis. Keratin 1 staining in the patient skin was comparable to that of normal skin, showing only a slight decrease in expression levels and desmosomal attachment in the lower regions of the epidermis (Norgett *et al.*, 2006).

Taken together, these observations suggest different molecular mechanisms and clinical outcomes for these three types of *DSP* mutations.

5.3.2. DP down-regulation results in decreased expression levels of PKP1, DSC2 and DSC3

Previous reports have shown down-regulation of desmosomal components in HaCaT cells upon DPI/DPII knock-down and in primary keratinocytes derived from SPPK skin (Wan *et al.*, 2004; Wan *et al.*, 2007). The first question of this chapter was whether down-regulation of *DSPI* (without targeting *DSPII*) would cause similar effects on HaCaT cells. This experiment was performed not only to study the *DSPI*-specific loss of function mutation, but also to gain further insight into the functional significance of the DPII splice variant.

In a previous study, western blotting and densitometry analysis of total lysates from primary keratinocytes derived from SPPK lesional skin revealed reduced expression levels of DPI and DPII. DPI expression was reduced to a higher extent than DPII compared to control cells (Wan *et al.*, 2004). Here, DPI expression levels were reduced to 55% and DPII expression levels to 18% in siI/II HaCaT cells compared to NT control cells (Figure 5.3A). Despite the difference between DPI:DPII ratios observed in HaCaT cells here (4:1) and in the previous report in primary SPPK keratinocytes (approximately 1:3; Wan *et al.*, 2004), a significant reduction in PKP1 and DSC3 expression was observed; 41% and 55% in HaCaT cells (Figure 5.3B) and 56% and 17% in keratinocytes derived from SPPK skin, respectively (Wan *et al.*, 2004). These results suggest that independently of the DPI:DPII ratios, reduction of total DP expression levels results in decreased expression of PKP1, DSC2 and DSC3. This trend is also observed when siI (*DSPI* knock-down) and siI/II (*DSPI* and *DSPII* knock-down) HaCaT cells, which have different DPI:DPII ratios (Figure 5.3A), are compared. Cells with DPI:DPII ratios of 1:8 (siI cells) and 4:1 (siI/II cells) show significantly reduced

expression levels of PKP1 (42% and 41%, respectively) and DSC3 (37% and 55%, respectively).

As mentioned above, Wan *et al.*(2007) have investigated the expression levels of desmosomal proteins in HaCaT cells following DP down-regulation with the same siRNA that was used here (siI/II). In this study, reduced expression levels of DSG1/2, DSC2/3 and PKP1/3 were observed. Reduced levels of DSC2/3 and PKP1 were also observed here in agreement with this study. However, in contrast with the report by Wan *et al.*(2007), no changes in expression levels of PKP3 or DSG3 were observed in any of the two independent knock-down experiments, and DSG2 expression was reduced in one experiment but not in the other (see Appendix C). The reason for this discrepancy is unclear, but might be related to the efficiency of DP down-regulation or to the number of replicate western blots performed in each case. In Wan *et al.*(2007) the levels of PKP2 expression were slightly reduced in siI/II cells compared to control cells; however these changes were not statistically significant. Here, the levels of PKP2 were unchanged between siI/II and NT cells in both siRNA independent experiments. Despite this variability, the results obtained here and elsewhere (Wan *et al.*, 2007) for the levels of expression of DSC2, DSC3 and PKP1 upon DPI/DPII down-regulation were consistent observations.

5.3.3. Influence of the DPI:DPII ratios on expression levels of PKP1 and DSC3

A reduction in expression levels of PKP1, DSC2 and DSC3 is observed upon DP knock-down (both in siI and siI/II cells). However, comparison between siI and siI/II cells revealed that, in contrast with PKP1, DSC3 expression is influenced by the DPI:DPII ratios. This result is shown by the statistically significant difference in DSC3 expression levels between siI cells (37%) and siI/II cells (55%) ($p<0.05$, Figure 5.3B). This increase in DSC3 expression levels from siI to siI/II cells occurs even though total DP levels are higher in siI than in siI/II cells, suggesting that DPI has more influence than DPII in regulating the levels of expression of DSC3. The fact that PKP1, DSC2 and DSC3 are down-regulated to some extent upon DP knock-down independently of the DPI:DPII ratio suggests that DPII can compensate partially but not totally for the lack of DPI.

To confirm these results, HaCaT cells expressing a gradient of decreasing levels of DPI and constant levels of DPII, as well as decreasing levels of DPII with constant

levels of DPI were generated (Figure 5.4A). Under these conditions, the expression profiles of PKP1 and DSC3 were considerably different. The DSC3 expression profile showed a trend that was similar to that of DPI, whereas the trend shown by the PKP1 expression profile was more similar to that of total DP (Figure 5.4B and 5.4D). These trends were confirmed by performing three additional replicate western blots for conditions b, c and d (Figure 5.4E), which correspond to DPI:DPII ratios of approximately 1:2, 1:3 and 1:15, respectively. Under these conditions, PKP1 expression does not vary significantly whereas DSC3 expression levels significantly decrease when the DPI:DPII ratio decreases.

It is not clear why down-regulation of DP leads to decreased expression of PKP1, DSC2 and DSC3 but not PKP2, PKP3, DSG3 or PG (Figures C1 and C2, Appendix C). However, it is interesting that down-regulation of PKP1 and DSC3 was also observed in cultured primary keratinocytes of DP-associated SPPK (Wan *et al.*, 2004). The effect of DP haploinsufficiency on the expression levels of DSC2 was not investigated in this previous study (Wan *et al.*, 2004). No detectable differences were observed in protein levels of PG and DSG3 between cultured primary keratinocytes of DP-associated SPPK and normal keratinocytes (Wan *et al.*, 2007). Overall, these results are consistent with the results obtained here.

Loss of function mutations in the gene encoding PKP1 have been shown to cause ectodermal dysplasia-skin fragility syndrome (sections 1.7.2 and 3.3.1.2), characterised by severe skin fragility and blistering, thickening of palmoplantar epidermis and abnormalities of hair development (Lai-Cheong *et al.*, 2007). Although patients harboring *DSP* haploinsufficiency mutations or the *DSPI*-nonsense mutation do not present with skin fragility and blistering, skin disease involving PPK is a common feature of all these patients. These observations suggest that overlapping roles might exist between DP and PKP1 in the skin, involved in normal skin architecture and perhaps in the maintenance of the balance between proliferation and differentiation of epidermal keratinocytes. The fact that interactions between PKP1a and DPI have been identified in HaCaT cells (Hofmann *et al.*, 2000) supports this hypothesis. Recently, a homozygous single bp deletion in the gene encoding DSC2 has been reported, causing PPK, woolly hair and ARVC (Simpson *et al.*, 2009). This phenotype is similar to the one caused by the *DSPI*-nonsense mutation. DSC2 and DP might, therefore, also be involved in common pathways which, when disrupted, result in similar clinical outcomes. Although no direct interactions between these two proteins have been

reported, they co-localise within the desmosome and are linked via PG and PKPs. Another report described a heterozygous splice site mutation in the gene encoding DSC2, causing non-syndromic ARVC due to the loss of protein synthesis from the mutant allele (Heuser *et al.*, 2006). These results suggest that the dose of DSC2 is important for normal cardiac function, but not for normal skin function, as this patient did not have cutaneous abnormalities (Bolling & Jonkman, 2009; Heuser *et al.*, 2006). However, it is interesting that both the haploinsufficiency and *DSPI*-nonsense mutations studied here caused reduced expression of DSC2 in HaCaT keratinocytes and resulted in skin disease, in contrast with the patient with a DSC2 mutation. Recently, the first mutation in the gene encoding DSC3 was reported. This is a homozygous nonsense mutation causing hair loss and the development of skin vesicles (Ayub *et al.*, 2009). The skin phenotype of these patients appears more severe then the skin phenotype of the patients described here, possibly because of complete loss of DSC3 expression in the skin due to NMD. However, loss of DSC3 synthesis in these patients was not confirmed (Ayub *et al.*, 2009).

Overall, these results suggest that the mechanisms leading to cardio-cutaneous disease might not always be straightforward and a combination of factors might influence the resulting clinical phenotype. Desmosomal proteins have functions in common but probably also diverging functions which might partially overlap with those of direct or indirect binding partners.

5.3.4. Influence of DPI and DPII in HaCaT intercellular adhesion

The Flexcell adhesion assay revealed some interesting adhesion properties and responses to mechanical stress of normal, siI and siI/II HaCaT cells.

In response to cyclic mechanical stretch in this experimental situation, normal HaCaT cells exhibit thickening and wrinkling of its keratin IFs and condensation of bundles, particularly in perinuclear regions. Additionally, DPI puncta at the cell membrane became elongated suggesting that desmosomes impart some level of elasticity and resilience to the cells which involves at least DPI. Following two hours of mechanical stretch these cells no longer show a normal homogenous network of IFs as seen in unstretched cells. This effect is also observed in siI cells following one and two hours of cyclic stretch. Although some siI/II cells also exhibit thickening of keratin IFs around the nucleus, close to the cell membrane these filaments are thinner and appear

more fragile particularly along free edges. These results suggest that the position of cells within a colony might influence the extent or speed with which cells are affected by the mechanical impact. Deformation and retraction of thin keratin IFs in siI/II cells is prominent after two hours of stretch, especially in regions where no junctional DPI is observed, and coincides with increased intercellular gaps among these cells.

These results suggest, firstly, an important role for keratin IFs in maintenance of structural support and stress resilience in these cells. These cytoskeletal filaments have the ability to reorganise during cycles of stretch and relaxation to better absorb physical stress. Secondly, as DP is the protein primarily responsible for anchorage of the keratin IF cytoskeleton to the cell membrane, it is not surprising that when DP expression levels are lower, the keratin IF attachment to the desmosome might be less strong, leading eventually to IF deformation and retraction when the levels of physical stress are above a certain threshold. This is probably the reason why areas where desmosomes lack or have reduced levels of DP are more prone to adhesion defects. The IF network of one cell is connected to IF networks of many other cells through desmosomes. If part of this chain is broken or weakened, as in the case of weakened IF-desmosome connections, then desmosomal connections between cells might also be weakened resulting eventually in loss of cell-cell adhesion.

Two other studies support these ideas. In one, keratinocyte cell lines expressing a keratin 14 mutation that causes epidermolysis bullosa simplex were exposed to repeated stretch and relaxation cycles using the Flexcell system (Russell *et al.*, 2004). Although the stretch conditions and cell lines in this study were different, these authors observed some cellular responses which resemble the ones observed here. First, normal cells after mechanical stretch showed thickening and compaction of keratin IFs. Second, keratin mutant cells showed IFs that were unable to withstand the levels of mechanical stretch used, and thus collapsed and fragmented. As a consequence, cell junctions started disassembling. In a similar way, the mutations in *DSP* studied here lead to decreased levels of DP which cause weakened IF-desmosome attachment resulting in decreased cell-cell adhesion. It is possible therefore, as suggested by (Russell *et al.*, 2004), that loss of IF tension is the driving force for desmosome disassembly because of its importance in maintaining desmosomal junctions. Norgett *et al.* (2000) also support this idea by showing that a recessive mutation in the C-terminus of DP which compromises IF attachment leads to loss of cell-cell adhesion and large intercellular spaces among keratinocytes.

It is not clear why cells with down-regulation of DPI (siI cells) showed less adhesion defects than cells with DPI/DPII haploinsufficiency (siI/II cells). These trends are simply qualitative, as no quantification of cells with loss of contacts with other cells was performed. However, these trends resemble some aspects of the *in vivo* phenotypes of patients harbouring these mutations. In particular, IFs that are unable to withstand mechanical stress and show condensation and retraction towards the nucleus as well as widening of intercellular spaces and loss of cell-cell adhesion are characteristic of SPPK epidermis (see section 5.1.1) (Armstrong *et al.*, 1999; Wan *et al.*, 2004; Whittock *et al.*, 1999; Whittock *et al.*, 2000). The patient harbouring the *DSPI*-nonsense mutation presents with a less severe keratoderma than the patients with DP haploinsufficiency. Both phenotypes are prominent in palms and soles, suggesting they are observed only in sites of pressure or abrasion. This probably explains why siI and siI/II cells only showed a phenotype when induced by mechanical stretch.

Immunocytochemistry of HaCaT siI and siI/II cells before and after stretch was also performed with antibodies against PG, and DSG1/2. PG staining in stretched siI/II cells was only observed at the cell membrane in regions where cells were still connected and a slight increase in cytoplasmic staining was observed in these cells. It is possible that PG stays attached to IFs when these retract towards the nucleus after mechanical stretch. No major differences in PG staining were observed between siI and NT cells, suggesting that IF detachment in these cells was not enough to cause PG re-localisation. These results contrast with data from (Garcia-Gras *et al.*, 2006) who have shown that siRNA down-regulation of DP in atrial cardiomyocyte cell lines causes PG re-localisation to the nucleus, which subsequently leads to increased expression of adipogenic and fibrogenic genes. PG was not observed in the nucleus of siI or siI/II keratinocytes, suggesting different roles for DP in keratinocytes and cardiomyocytes. These differences might be related to the different environments these different types of cells are exposed to, or to the different types of mechanical stress perhaps leading to activation of different signalling pathways. DSG1/2 staining was similar in siI, siI/II and NT cells before and after stretch, suggesting that DSGs stay associated with desmosomes (or half-desmosomes) after exposure to mechanical stress.

5.3.5. I608ins10 mutant DPI forms abnormal aggregates at the cell membrane

Immunocytochemistry of HaCaT cells over-expressing I608ins10 mutant, flag tagged-DPI proteins using an anti-flag antibody revealed the presence of atypical

aggregates that localised to the cell membrane. The molecular composition of these aggregates is unknown. It would have been interesting to perform double immunocytochemistry in these cells using a flag antibody in conjunction with antibodies targeting PG, PKP 2/3 or DSGs/DSCs to investigate whether these proteins co-localise with mutant DPI proteins, but time did not permit these experiments. The DPI aggregates formed by the mutant proteins in HaCaT keratinocytes resemble observations from *in vivo* skin of the patient harbouring this mutation, which include discontinuous membranous staining for DP and PG (Norgett *et al.*, 2006). These observations suggest that PG co-localises with mutant DP proteins, but further studies are needed to clarify this.

I608ins10 results in the insertion of 10 new amino acids into the N-terminus of DPI and DPII. Although the N-terminal domain of DP is involved in interactions with PG and the PKPs, the DP binding sites for these proteins lie within the first 584 amino acids. As the mutation affects the region just downstream of the stretch encoding the first 584 amino acids, mutant DPI might still be able to interact with PG and the PKPs. Likewise, the mutation might result in a conformational change that prevents DP from interacting with some of its binding partners or it may generate new binding sites for additional binding partners.

I608ins10 mutant DPI was shown to retain the ability to co-localise with keratin IFs at the cell membrane. This is not surprising as the amino acids that are necessary for IF binding lie within the C-terminus of DP (Green & Hobbs, 2006). Additionally, supporting these results, keratin 1 staining in the skin of the patient harbouring this mutation was comparable to normal skin. No major adhesion defects were observed in HaCaT cells over-expressing these mutant DPI proteins (Norgett *et al.*, 2006). Likewise, no loss of cell-cell contacts was seen in the skin of this patient. Nevertheless, immunohistochemistry was only performed in this patient's non-lesional skin and it is possible that adhesion defects occur when the skin is exposed to mechanical stress. The results shown here in mutant HaCaT cells exposed to cyclic stretch suggest, however, that the main defects caused by this mutation are not structural defects leading to loss of desmosomal cell-cell adhesion. Further studies will be necessary to understand the defects caused by this mutation and the nature of the junctional mutant-DPI aggregates.

5.3.6. Insights into the functional significance of DPI and DPII in skin and heart

Both the *DSPI*-specific nonsense mutation (p.R1267X) and the *DSP* haploinsufficiency mutations affect the skin, but only the former leads to heart disease. The reason for this is probably because the DPII splice variant is virtually absent in the heart (see Chapter 4; Uzumcu *et al.*, 2006) and hence cannot compensate for the lack of DPI, as probably occurs to some extent in the skin. Therefore, as p.R1267X results in complete absence of DPI likely through activation of the NMD pathway, assuming this also occurs in the heart, this patient will have very low levels of DP. This said, it is interesting that this patient survived until four years of age in contrast with what is seen in DP knock-out mice which die before birth (Gallicano *et al.*, 1998). These observations suggest pathophysiological differences between humans and mice.

The functional studies performed with these mutations suggest that they affect the skin by causing reduced inter-keratinocyte adhesion due to a dosage defect of DP splice variants. This was particularly prominent in cells with *DSP* haploinsufficiency. Although the DPI:DPII ratios in DP haploinsufficient cells are predicted to be similar to those of wild type cells, the total amount of DP does not seem to be enough to maintain normal skin function, in particular in palms and soles which are areas subject to constant physical assaults. This amount of DP seems to be enough, however, for normal heart function. The observation that p.R1267X still affects the skin, although 100% of DPII is still expressed in this tissue, suggests that compensation of DPII for the lack of DPI is only partial. Both these mutations resulted in decreased expression levels of some desmosomal components, DSC3, DSC2 and PKP1, and decreased cell-cell adhesion, in agreement with observations in SPPK skin (Wan *et al.*, 2004). The difference in DSC3 expression levels between siI and siI/II cells suggests that the different DP splice variants might have some specific functions that are not redundant and cannot be completely compensated for by another splice variant. The fact that DPII cannot totally compensate for the lack of DPI in the patient with the *DSPI*-nonsense mutation supports this hypothesis.

In contrast with the previous mutations, the dominant insertion mutation (I608ins10) does not seem to cause adhesion defects in keratinocytes, as suggested by *in vitro* (here) and *in vivo* (Norgett *et al.*, 2006) studies. This mutation affects the N-terminus of the DP protein and interactions with PKPs or PG, which are involved in targeting DP to the desmosomal plaque, might be affected. Further studies will be necessary to unveil the pathogenic mechanism of this mutation. However, the fact that it

causes a very severe heart disease suggests that it affects interactions with DP binding partners in the heart. The observation of bright membranous aggregates in cells expressing this mutant, which are still able to co-localise with keratin IFs at the cell membrane suggests a dominant negative effect. Table 5.1 summarises the effects of the three modelled *DSP* mutations in HaCaT keratinocytes.

5.4. Summary

In this chapter, the functional consequences of three different types of *DSP* mutations causing PPK associated or not with cardiomyopathy were studied in HaCaT keratinocytes and compared with each other (Table 5.1).

Mutations causing DP haploinsufficiency (modelled in siI/II cells) and DPI down-regulation (*DSPI*-nonsense mutation modelled in siI cells) were found to result in decreased expression levels of PKP1, DSC2 and DSC3 in this experimental system, as previously observed in keratinocytes derived from SPPK skin. Significant differences in DSC3 expression levels were observed between siI and siI/II cells, suggesting that DPI and DPII have different influences in DSC3 expression. Besides DPI and DPII common (redundant) functions, there might be isoform-specific functions which may account for the phenotypic variation of *DSP* mutations. Both haploinsufficiency and nonsense mutations resulted in decreased HaCaT cell-cell adhesion, as shown with the Flexcell adhesion assay, which was however more pronounced in DP haploinsufficient cells, consistent with previous *in vivo* observations.

Over-expression of recombinant DPI harbouring a 30 bp insertion mutation, I608ins10, in HaCaT cells resulted in the formation of large junctional aggregates, not observed in wild type DPI over-expressing cells. No adhesion defects were observed in cells expressing this insertion mutation, in contrast with the other two mutations studied, suggesting a different molecular mechanism for this mutation. Further studies are needed to clarify this mechanism.

– Chapter 6 –

Final Discussion and Future Work

6.1. Background

Desmosomes are crucial links between neighbouring cells, whereby several proteins cooperate to support tissues such as the epidermis and the myocardium. These tissues need to be flexible and at the same time resistant to stress. Although the precise roles of desmosomes as adhesion structures and as signalling centres are not entirely defined, it is currently accepted that these junctions perform both structural and signalling functions. They are involved not only in physical adhesion but also in tissue differentiation and morphogenesis (Garrod & Chidgey, 2008; Getsios *et al.*, 2004b; Green & Simpson, 2007). Mouse models as well as human genetic and autoimmune disease involving desmosomal components provide us with clues as to some of these functions.

This thesis is focused on the effects of human genetic mutations in desmosomal components and on the contributions of different DP splice variants to desmosomal function. Mutations affecting most of the major desmosomal proteins, including the desmosomal cadherins and plaque proteins (of the armadillo and plakin families) as well as in the desmosomal-associated IF proteins, can lead to cardio-cutaneous diseases. The molecular mechanisms of these mutations in the development of disease are continuously being uncovered and provide valuable information about the importance of these intercellular junctions.

6.2. Homozygous nonsense mutation in *JUP* results in skin fragility, PPK and woolly hair but normal heart development

Two mutations in the gene encoding PG, *JUP*, have been previously published and in both instances individuals who harbour these mutations suffer from ARVC, with or without skin abnormalities (Table 6.1). Here, a novel homozygous nonsense mutation in the first coding exon of *JUP* was identified with leads to skin fragility and PPK but, in contrast with previous mutations, results in normal heart development (Table 6.1). This clinical phenotype is designated as acantholytic ectodermal dysplasia and can also be caused by a recessively inherited *JUP* mutation, c.468G>A predicted to affect splicing. This predicted splice site mutation was found in Kuwaiti patients during the course of this study (Table 6.1).

Table 6.1. Currently known mutations in the gene encoding PG, *JUP*, and corresponding modes of inheritance and human phenotypes.

***JUP* mutations**	**Mode of inheritance**	**Human phenotype**
*JUP*2157delTG	Recessive	Naxos disease: diffuse NEPPK, woolly hair and ARVC
S39_K40insS	Dominant	ARVC
S24X	Recessive	Acantholytic ectodermal dysplasia: skin fragility, diffuse PPK and woolly hair
c.468G>A	Recessive	Acantholytic ectodermal dysplasia: skin fragility, diffuse PPK and woolly hair

The two *JUP* mutations described here are thought to lead to skin disease through a common molecular mechanism involving three main steps. First, both mutations result in remarkably low levels of PG (wild type or PGΔN42, see Chapter 3) in patient skin which is barely present at intercellular junctions. Second, these low levels of PG in the skin affect the ultrastructure of desmosomes, although they do not appear to interfere with normal adherens junction structure or function. Finally, the low levels of PG in the skin of these patients lead to an adhesion defect resulting in the clinical features of skin fragility which is aggravated by mechanical stress. These mutations cause a more severe skin disease than the mutation causing Naxos disease (which results in PG C-terminal truncation), including blistering and acantholysis which are not observed in the skin of Naxos patients. The less severe phenotype in the skin of Naxos patients could be due to partial functionality of the truncated PG protein. Therefore, although both types of mutations lead to skin disease, the severity of the phenotype might vary in response to different functional levels of the mutant proteins.

It is interesting that there is no evidence of heart abnormalities in the patients described here, despite the very low levels of PG. However, given that the oldest patient was only 14 years-old at the time of the last cardiac examination, the possibility of developing cardiomyopathy later in life cannot be ruled out. ARVC in Naxos patients is probably not related to low expression levels of the C-terminally truncated PG, as suggested by western blot which showed equivalent levels of PG in normal heart and in the heart of a Naxos patient (McKoy *et al.*, 2000). This observation together with observations described here and elsewhere (Mahoney *et al.*, 2009) suggest that low expression levels of PG in the heart may not be a suitable diagnostic test for ARVC as suggested by Asimaki *et al.* (2009) (see Chapter 3). Mahoney *et al.* (2009) described a

patient with compound heterozygous *DSP* mutations affecting the C-terminus of both DPI and DPII and leading to heart failure but who showed bright PG immunoreactivity at the cardiac intercalated discs. ARVC in this patient is suggested to result from defective DP-IF attachments. ARVC in Naxos patients could be due to altered binding properties of the mutant PG caused by the presence of five additional amino acids in its C-terminus (McKoy *et al.*, 2000). ARVC caused by the dominant insertion mutation, S39_K40insS, appears to be related to the creation of additional binding partners. The lack of a heart phenotype in the patients described here suggests four different hypotheses. First, PG might not be essential for normal heart development, and the fact that heart intercellular junctions are formed by a mixture of desmosomal and adherens junction proteins may allow for compensation for lack of PG by other junctional molecules. However, even if PG does not contribute with normal adhesion properties within junctions, its correct signalling functions in the heart might still be important. In this respect, the presumably low levels of PG in the heart of the patients described here might still contribute to normal signalling in contrast with other cases where aberrant signalling of PG is suggested to lead to ARVC (Garcia-Gras *et al.*, 2006). Therefore, the mutant PG proteins expressed by the patients described here are proposed to contribute to normal Wnt/β-catenin signalling functions in the heart, thereby allowing normal heart development. The second and third hypotheses are, assuming that PG is essential for normal heart development, that cardiomyopathy might still develop in these patients later in life or PGΔN42 has different binding partners in skin and heart and is therefore incorporated into heart junctions and stabilised leading to normal heart function. A fourth hypothesis is that the lack of heart phenotype is due to incomplete penetrance of ARVC (which means that not all patients with this mutation will develop the disease), which has been reported to be below 50% (Vatta *et al.*, 2007).

Further studies will be necessary to test these hypotheses and fully understand the lack of heart phenotype in these patients, including determining PGΔN42 binding partners in keratinocytes and cardiomyocytes, investigating whether PGΔN42 is incorporated into cardiomyocyte junctions and the testing of PGΔN42 signalling properties in both types of cells.

6.3. Identification of a third alternative DP splice variant and its possible functions

In Chapter 4, the identification of a novel DP splice variant, DPIb, was described. *DSPIb* mRNA was detected in a range of epithelial and cardiovascular tissues as well as in the brain, and was the only transcript observed in the aorta. DPIb protein expression was observed in HaCaT and K1 keratinocytes and western blot analysis of human atrium suggested presence of this novel isoform. Although DPIb was expressed at low levels compared to those of DPI and DPII in the cell and tissue types tested here (as suggested by western blot and qRT-PCR), the possibility that it is expressed at higher levels in other tissues cannot be excluded. Supporting this hypothesis is the observation of virtually absent DPII protein in heart tissue (Uzumcu *et al.*, 2006 and Figure 4.12) whereas the DPII expression level observed in the skin is similar to that of DPI (Uzumcu *et al.*, 2006). Given the fact that *DSPIb* was the only transcript detected in the aorta, it is hypothesised that this tissue will express higher levels of DPIb than the levels observed in the cells and tissues tested here, but further studies will be needed to confirm this hypothesis. As the size of DPIb is close to that of DPII, the function of DPIb might be similar to that of DPII. DPIb might be able to provide some degree of compensation for defects in DPI or in the case of DPI absence, in the same way as DPII can partially compensate for the lack of DPI (see below). This is not the case in cells harbouring the *DSPI*-nonsense mutation (p.R1267X) because this mutation also causes DPIb knock-down (see Chapter 5). Further studies will be necessary to understand the functions of DPIb and also the functions of DPII, which are for the most part unknown.

A possible way to dissect the functions of DPIb and DPII within the desmosome would be to generate an *in vitro* reconstitutional model of the desmosome where a desmosomal cadherin (e.g. DSG1), together with PG, a PKP (e.g. PKP1) and either DPIb or DPII would be co-expressed in a cell line that does not express desmosomal proteins (e.g. L-fibroblasts). Subsequently, immunocytochemistry could be performed to determine the localisation (and co-localisations) of these proteins, as well as co-immunoprecipitation studies to determine interactions among these proteins. These experiments were previously described in studies where the interactions between the N-terminus of DPI and the desmosomal plaque proteins were determined (Kowalczyk *et al.*, 1997; Kowalczyk *et al.*, 1999). However, these experiments were only performed

using DPI. Although DPII has now been cloned (see section 2.2.1 in Chapter 2), time did not permit experiments using this construct.

Western blotting proteins with a C-terminal DP antibody suggested the presence of a fourth DP splice variant in HaCaT cells, which was provisionary designated as DPIa. This immunoreactive band was demonstrated to be down-regulated with siRNAs which were thought to be *DSPI*-specific. However, attempts to amplify this potential isoform at the mRNA level with primers flanking the known *DSP* alternatively spliced region in exon 23 failed to amplify this fourth splice variant. These results suggested that the immunoreactive band observed by immunoblotting between DPI and DPIb is a breakdown product of DPI or a western blot artefact.

6.4. Insights into the molecular mechanisms of three different DP mutants

Three different *DSP* mutations were studied as described in Chapter 5. The first mutation leads to DPI and DPII haploinsufficiency resulting in SPPK in patients (Armstrong *et al.*, 1999; Whittock *et al.*, 1999), and was predicted to result in reduced desmosomal adhesion, deficient IF attachment and widening of intercellular spaces, as previously demonstrated *in vivo* by electron microscopy and immunohistochemistry in patient skin (Armstrong *et al.*, 1999; Wan *et al.*, 2004; Whittock *et al.*, 1999). The second mutation is a *DSPI*-specific nonsense mutation which is predicted to activate the NMD pathway leading to complete absence of DPI in the patient (Uzumcu *et al.*, 2006). This mutation results in skin and heart disease but little was known to date about its molecular mechanisms. These two mutations were modelled in HaCaT keratinocytes using siRNA transfections and their effect on the expression levels of other junctional proteins and in intercellular adhesion were investigated.

In this *in vitro* experimental system, both *DSPI*-nonsense and DP haploinsufficiency mutations resulted in reproducible reduction of DSC3, DSC2 and PKP1 expression levels compared to control cells. Moreover, the *DSPI*-nonsense mutation (modelled in siI transfected cells, Chapter 5) results in significantly lower levels of DSC3 compared to the haploinsufficiency mutation (modelled in siI/II transfected cells, Chapter 5). No significant differences in the expression levels of PKP1 and DSC2 were observed between siI and siI/II transfected cells. These results suggest that DSC3 expression is influenced by the DPI:DPII ratios, in contrast with PKP1 and

DSC2. Furthermore, these experiments suggested that DPI has more influence on the expression levels of DSC3 than DPII. This is an interesting observation in light of possible functional differences between the DPI and DPII isoforms, and suggests that although DPII can partially compensate for DPI, the latter might have a specific role in stabilising DSC3 within the desmosome, but further studies are needed to confirm this. The re-constitutional model of the desmosome described in section 6.3 could be a possible starting point to confirm and further investigate these observations.

As expected, in this experimental system the haploinsufficiency mutation resulted in reduced cell-cell adhesion and IF attachment in an *in vitro* adhesion assay. Adhesion defects were less prominent in cells mimicking the *DSPI*-nonsense mutation, which is consistent with *in vivo* observations which show that the skin of patients harbouring this mutation has an apparently normal structure (Uzumcu *et al.*, 2006). It is interesting to note that more pronounced adhesion defects are observed in cells with DP haploinsufficiency than in cells with DPI down-regulation despite the lower levels of DSC3 in the latter case. These results suggest that the adhesion defects in DP haploinsufficient cells are not directly dependent on the expression levels of DSC3.

The third mutation studied here results in the insertion of 10 amino acids into the N-terminus of DP. The N-terminus is involved in targeting DP to the desmosome via interactions with PG, PKPs 1-3 and DSC1a. As the insertion mutation occurs downstream of the critical region for DP's interactions with PG, PKPs 1-3 and DSC1a, this mutation is not expected to cause disruption of these protein-protein interaction. A recombinant DPI protein harbouring these 10 extra amino acids was over-expressed in HaCaT cells and shown to form abnormal aggregates in these cells. These aggregates still appeared associated with keratin IFs at the cell membrane and no obvious adhesion defects were observed in these cells when subject to mechanical stretch. Further studies will be necessary to investigate the molecular nature of these DP aggregates and whether the insertion mutation results in higher affinity of DPI for known binding partners, for instance due to a conformational change of the protein, or generates new protein-protein interactions. Possible experiments in cells over-expressing this mutant include co-localisation studies between DPI and known binding partners such as PG, PKPs and DSC1a as well as immunoprecipitation studies to determine protein interactions. It would have been interesting to also study the effects of this mutation in the DPII protein and whether these effects are similar or differ from those related to DPI. Additionally, the effects of this mutation *in vivo*, including clumping of DP and

PG at cell borders, are observed predominantly in the lower layers of the epidermis whereas the upper layers, which are more exposed to mechanical stress, appear to have a normal structure and distribution of these proteins (Norgett *et al.*, 2006). Considering these results obtained prior to the work described here, it would be interesting to investigate the direct or indirect effects of this mutant in signal transduction. A strong first candidate would be PG, as its signalling activity has been suggested to be involved in the development of disease, such as in the case of ARVC (Garcia-Gras *et al.*, 2006). A speculative hypothesis for the mechanism of disease caused by this insertion mutation is that DP has higher affinity for PG (possibly through interactions with novel binding partners expressed only in the lower layers of the epidermis) and therefore less PG is available to perform normal signalling (and balance β-catenin signalling). β-catenin over-expression has been shown to cause hyper-proliferation and hair follicle differentiation (Gat *et al.*, 1998). Therefore increased Wnt/β-catenin signalling might be responsible for the keratinocyte hyper-proliferation observed in the skin of this patient and the woolly hair. However, ARVC has been associated with decreased Wnt/β-catenin signalling and increased PG signalling in cardiomyocytes causing a switch from myogenesis to adipogenesis and fibrosis (Garcia-Gras *et al.*, 2006). Although it is not clear whether the insertion mutation indirectly leads to increased or decreased Wnt/β-catenin signalling, it is tempting to speculate that it leads to an imbalance between PG and β-catenin signalling. Further studies will be needed to clarify this mechanism.

6.5. Desmosome associated genetic disease and unresolved questions

Mutations affecting all of the main desmosomal proteins expressed in the heart have been associated with cardiomyopathies, PKP2 being the most common target. The vast majority of these mutations are inherited in an autosomal dominant fashion, however, variable penetrance is observed. Autosomal recessive mutations in PKP2, PG, DP, and DSC2, predominantly associated with syndromic cardiomyopathies (except for PKP2) have also been reported (Table 6.2). These observations suggest that in the heart, because there is only one representative of each protein sub-family (i.e. PKP2, DSC2, DSG2) together with the constitutive PG and DP, there might be less compensatory mechanisms by similar proteins in case of mutation in any of these main components.

Table 6.2. Desmosomal associated genetic disease and corresponding affected proteins and human clinical phenotypes.

	Genetic disease	Affected proteins	Clinical features	References
Heart defects	ARVC	DP, PG, DSC2, DSG2, PKP2	Fibrofatty replacement of the right ventricular myocardium resulting in arrhythmias and sudden cardiac death (may envolve both ventricles)	(Gerull *et al.*, 2004); (Pilichou *et al.*, 2006); (Rampazzo *et al.*, 2002); (McKoy *et al.*, 2000); (Syrris *et al.*, 2006)
	Dilated cardiomyopathy (DC)	DP, DSG2	Dilation of ventricles leads to impared myocardial function and heart failure	(Posch *et al.*, 2008); (Norgett *et al.*, 2000)
Skin	SPPK	DP, DSG1, DSC2	Focal thickening of the palmoplantar epidermis with a striated pattern characterised by linear hyperkeratosis on the digits	(Simpson *et al.*, 2009); (Rickman *et al.*, 1999); (Armstrong *et al.*, 1999)
	EPPK	DP, K1	Diffuse thickening of the palmoplantar epidermis associated with perinuclear vacuolisation, cytolysis and blistering	(Uzumcu *et al.*, 2006); (Terron-Kwiatkowski *et al.*, 2006)
	Skin fragility, PPK and alopecia/sparce hair with or without cardiomyopathy	DP, PG, PKP1	PPK and fragile skin that blisters and peels	(Tanaka *et al.*, 2009); (Asimaki *et al.*, 2009a); (Cabral *et al.*, 2010); (McGrath *et al.*, 1997)
	Acantholytic epidermolysis bullosa	DP	Skin fragility, SPPK, alopecia, lack of nails and cardiomyopathy	(Jonkman *et al.*, 2005)
	Woolly hair, PPK with or without cardiomyopathy	DP, PG, DSC2	Kinky and wiry hair scalpe hair which has a wool-like appearance, PPK and heart disease	(Whittock *et al.*, 2002b); (Norgett *et al.*, 2000); (McKoy *et al.*, 2000); (Cabral *et al.*, 2010); (Simpson *et al.*, 2009)
	Hypotrichosis	DSG4	Sparse, thin hair with atrophic hair follicles, impaired hair keratinization and epidermal hyperproliferation	(Kljuic *et al.*, 2003)
	Hypotrichosis with skin vesicles	DSC3	Sparse and fragile hair with normal hair follicles	(Ayub *et al.*, 2009)

In contrast, mutations in the genes encoding DSC1, DSG3 and PKP3 have not been associated with human disease, even though these proteins are abundantly expressed in the skin. This observation suggests that mutations in the genes encoding these proteins either do not disrupt the skin because these proteins are compensated for by other similar proteins or they cause other diseases that have not yet been found.

The fact that more mutations have been found in genes encoding desmosomal proteins that are expressed in the upper epidermal layers highlights the importance of these proteins (such as DSG1, DSC1 and PKP1) in the maintenance of epidermal integrity and resistance to mechanical stress. However, the hypothesis that disease-causing mutations in the genes encoding DSC1, DSG3 and PKP3 will be discovered in the future cannot be excluded.

Mutations in the gene encoding PG have been associated with both skin and heart disease, however, only four mutations have been uncovered so far compared to 36 in the gene encoding DP. The fact that 36 *DSP* mutations leading to disease are now described highlights the importance of this plakin protein within the desmosome. It is likely that more mutations will be discovered in the *JUP* gene.

Mutations in *DSP* result in a variety of different phenotypes involving skin and heart disease (Table 6.2). This is not surprising as, together with PG, DP is expressed in all desmosome-containing tissues and is therefore a crucial component of these junctions. Interestingly, desmosomes and other junctions have been shown to be interdependent. Expression and localisation of connexin 43, a major gap junction protein, are impaired in desmosome-related cardiomyopathies, although this is also observed in other types of heart disease (Asimaki *et al.*, 2009b); adherens junctions are disrupted in keratinocytes derived from the epidermis of conditional (epidermis-specific) DP knock-out mice (Vasioukhin *et al.*, 2001); and β-catenin appears to partially compensate for the lack of PG in keratinocytes derived from PG knock-out mice (Acehan *et al.*, 2008; Bierkamp *et al.*, 1999). Therefore, although the initial defect may be specific to desmosomal components, it can ultimately lead to disruption of related adherens and gap junctions as part of the disease manifestation.

It is interesting that *DSP* mutations resulting in haploinsufficiency can lead to skin disease only, SPPK (Chapter 5), but can also result in ARVC without skin disease, as shown by a patient harbouring a *DSP* nonsense mutation (W233X) in the N-terminus of DP (Yang *et al.*, 2006). As illustrated by the work done in cardiac-specific *DSP* haploinsufficient mice and in *DSP* knock down cardiomyocytes, PG is able to translocate to the nucleus and up-regulate genes involved in the development of ARVC (Garcia-Gras *et al.*, 2006). This process might be dependent on the dosage of DP that is present at junctions to stabilise PG, which might vary according to different haploinsufficiency-causing mutations and their efficiency on the activation of the NMD pathway. Additionally, manifestation of the ARVC phenotype is aggravated by

endurance training and therefore different degrees of training might influence the development and severity of the heart disease (Bolling & Jonkman, 2009). It is also interesting to note that in other cases, DP haploinsufficiency does not result in an observable phenotype which shows variable penetrance (Whittock *et al.*, 2002b). Likewise, heterozygous DP knock-out mice were indistinguishable form wild type mice (Gallicano *et al.*, 1998). These observations suggest that in humans the dosage of DP is important for the maintenance of epidermal integrity.

The most deleterious mutations found so far in *DSP* led to a cardio-cutaneous syndrome called lethal acantholytic epidermolysis bullosa in one patient (Chapter 1). Clinically, this patient mimics the conditional epidermis-specific DP knock-out mouse (Bolling & Jonkman, 2009; Jonkman *et al.*, 2005; Vasioukhin *et al.*, 2001). The affected child was a compound heterozygote for C-terminally truncating mutations affecting both DPI and DPII and died 10 days after birth of heart failure. The skin phenotype of this patient was extremely severe including skin fragility and displacement of large masses of skin, total alopecia and lack of nails. This phenotype is thought to be caused by a severe adhesion defect due to the lack of DP-mediated IF attachment to desmosomes. This is suggested by ultrastructural analysis of patient skin which shows a split between cells at the level of the cytoplasmic side of the desmosomal inner dense plaque (IDP) (Jonkman *et al.*, 2005). This patient showed a much more severe skin phenotype then the Carvajal patients harbouring the 7901delG homozygous mutation. The latter mutation results in the truncation of the C-terminal tail of DP which lacks the C plakin repeat domain (PRD; see Figure 1.8) (Norgett *et al.*, 2000). In contrast, the compound heterozygous mutations referred to above result in two C-terminally truncated DP proteins, of which one lacks the entire C-terminal domain and the other retains only the A PRD. These results suggest two important points. Firstly, as previously suggested by *in vitro* studies (Choi *et al.*, 2002), these observations suggest that the combination of more than one PRD is more efficient for IF binding than individual PRDs (in this particular comparison, presence of PRDs A plus B appears to be more favourable then presence of PRD A alone). Secondly, the dosage of partially functional DP molecules might also contribute to the resulting phenotype, since the patient with the compound heterozygous mutations expresses reduced levels (~50%) of DP molecules containing the A PRD whereas the Carvajal disease-associated mutation results in 100% of DP molecules containing PRDs A plus B. These two points might explain why in Carvajal patients the skin phenotype is exacerbated by mechanical stress, whereas the patient with acantholytic epidermolysis bullosa shows a very severe

skin fragility and loss of barrier function that appears to occur independently of mechanical stress.

6.5.1. Common pathways in desmosome associated disease

The desmosomal associated genetic disease results in a phenotypic convergence into two major disease manifestations; the skin fragility and/or PPK which can be associated or not with hair abnormalities, and the desmosomal-associated cardiomyopathy. The epidermal hyperproliferation (which is associated with most desmosomal mutations affecting the skin) might be a result of loss of cell-cell adhesion leading to transmission of cell signals towards increased proliferation in a wound healing-like response. It might also be a result of signal transduction imbalance resulting in decreased cell-cell adhesion. Additionally, it might be initiated by different processes, depending on the type of mutation and the target gene, despite resulting in similar clinical manifestations. Similarly, the cardiac phenotype might be caused by altered Wnt/β-catenin signalling resulting in fibrofatty replacement of cardiac myocytes in a wound healing-like process; it might also be caused by loss of cell-cell adhesion or both, one process leading to the other. As the desmosome is a complex of interacting proteins, it is not surprising that defects in different components lead to similar clinical phenotypes, as the affected proteins are involved in common pathways and/or in overlapping interactions. More interesting is the fact that mutations in the same desmosomal component can give rise to different phenotypes, but this might be due to different dosages of the mutant protein in question, different composition of skin and heart desmosomes, different levels of mechanical stress, different genetic backgrounds among other variations. Clinically, it is important to regard PPK in combination with woolly hair (or alopecia) as a "warning signal" for the development of cardiomyopathy, as suggested by Norgett *et al.* (2006).

6.6. Conclusions

Two general conclusions, which are open to discussion, are proposed in this thesis. Firstly, although there are common pathways leading to disease of the desmosome which results in cardio-cutaneous syndromes, the initial stages differ, according to the molecular defect and the protein in question. The understanding of these initial variations or different molecular mechanisms leading to a common

phenotype is crucial to unveil the range of functions preformed by each individual protein of the desmosome and how these functions are altered in disease. Further, this understanding might be valuable to develop methods to specifically target the initial stages (original problems) in attempts to prevent or cure desmosomal associated disease. Secondly, because skin and heart desmosomes are slightly different in composition and because skin and heart are different tissues themselves and perform different functions, the mechanisms leading to disease might also differ between these tissues. Therefore the same protein might be subject to different regulation, might perform different functions and their associated defects might lead to different outcomes, even though the molecular mechanisms of disease may sometimes overlap.

More specific conclusions can be drawn from the work described in this thesis, some of which support and reinforce previous observations. Firstly, two novel recessively inherited *JUP* mutations are described, associated with skin disease without heart involvement for the first time. The resulting PG proteins in these cases are expressed in the skin at extremely low levels and are barely incorporated into epidermal junctions, leading to the development of skin fragility associated with PPK and woolly hair. These proteins are, however, proposed to contribute with normal (Wnt/β-catenin) signalling functions in the heart thereby allowing normal heart development, but further studies are necessary to conform this hypothesis. Secondly, a novel DP splice variant, DPIb, is shown to be expressed in a variety of epithelial tissues as well as in the brain, cardiac tissue and aorta at the mRNA level and in keratinocyte cell lines at the protein level. Although the functions of this novel isoform remain uncertain, the awareness of its existence is important as it might play a particular role in other tissues or compensate for defects in DPI. Finally, three different *DSP* mutations which cause skin disease associated or not with cardiomyopathy, were studied. siRNA mediated DPI down-regulation (which mimicked the *DSPI*-specific nonsense mutation causing skin and heart disease) and DPI/DPII down-regulation (which mimicked the DP haploinsufficiency mutations leading to SPPK) caused decreased expression levels of DSC2, DSC3 and PKP1 in an experimental system using HaCaT keratinocytes. Further, statistically significant differences in the expression levels of DSC3 were observed between the two siRNA-mediated knock-down situations. These differences, coupled with a suggestion of less prominent adhesion defects in the DPI-knock down cells suggest that DPI and DPII are not completely redundant isoforms. A 30 bp-insertion mutation was genetically engineered in a *DSPI*-construct and the recombinant protein was shown to form large aggregates at the cell membrane of HaCaT cells. Overall, these

results suggest that different *DSP* mutations have different molecular mechanisms leading to final common pathways that end in phenotypic convergence.

Bibliography

Aberle H., Bierkamp C., Torchard D., Serova O., Wagner T., Natt E., Wirsching J., Heidkamper C., Montagna M., Lynch H. T., and et al. (1995). The human plakoglobin gene localizes on chromosome 17q21 and is subjected to loss of heterozygosity in breast and ovarian cancers. *Proc Natl Acad Sci U S A* **92:** 6384-8.

Aberle H., Schwartz H., Hoschuetzky H., and Kemler R. (1996). Single amino acid substitutions in proteins of the armadillo gene family abolish their binding to alpha-catenin. *J Biol Chem* **271:** 1520-6.

Acehan D., Petzold C., Gumper I., Sabatini D. D., Muller E. J., Cowin P., and Stokes D. L. (2008). Plakoglobin is required for effective intermediate filament anchorage to desmosomes. *J Invest Dermatol* **128:** 2665-75.

Al-Amoudi A., Chang J. J., Leforestier A., McDowall A., Salamin L. M., Norlen L. P., Richter K., Blanc N. S., Studer D., and Dubochet J. (2004). Cryo-electron microscopy of vitreous sections. *Embo J* **23:** 3583-8.

Alberts B., Johnson A., Lewis J., Raff M., Roberts K., and Walter P. (2002). Cell Junctions, Cell Adhesion, and the Extracellular Matrix. *In* "Molecular Biology of the Cell", pp. 950-1009, Garland Science.

Alcalai R., Metzger S., Rosenheck S., Meiner V., and Chajek-Shaul T. (2003). A recessive mutation in desmoplakin causes arrhythmogenic right ventricular dysplasia, skin disorder, and woolly hair. *J Am Coll Cardiol* **42:** 319-27.

Anderson E. M., Birmingham A., Baskerville S., Reynolds A., Maksimova E., Leake D., Fedorov Y., Karpilow J., and Khvorova A. (2008). Experimental validation of the importance of seed complement frequency to siRNA specificity. *Rna* **14:** 853-61.

Angst B. D., Nilles L. A., and Green K. J. (1990). Desmoplakin II expression is not restricted to stratified epithelia. *J Cell Sci* **97** 247-57.

Armstrong D. K., McKenna K. E., Purkis P. E., Green K. J., Eady R. A., Leigh I. M., and Hughes A. E. (1999). Haploinsufficiency of desmoplakin causes a striate subtype of palmoplantar keratoderma. *Hum Mol Genet* **8:** 143-8.

Asimaki A., Syrris P., Ward D., Guereta L. G., Saffitz J. E., and McKenna W. J. (2009a). Unique epidermolytic bullous dermatosis with associated lethal cardiomyopathy related to novel desmoplakin mutations. *J Cutan Pathol* **36:** 553-9.

Asimaki A., Syrris P., Wichter T., Matthias P., Saffitz J. E., and McKenna W. J. (2007). A novel dominant mutation in plakoglobin causes arrhythmogenic right ventricular cardiomyopathy. *Am J Hum Genet* **81:** 964-73.

Asimaki A., Tandri H., Huang H., Halushka M. K., Gautam S., Basso C., Thiene G., Tsatsopoulou A., Protonotarios N., McKenna W. J., Calkins H., and Saffitz J. E. (2009b). A new diagnostic test for arrhythmogenic right ventricular cardiomyopathy. *N Engl J Med* **360:** 1075-84.

Ast G. (2004). How did alternative splicing evolve? *Nat Rev Genet* **5:** 773-82.

Ayub M., Basit S., Jelani M., Ur Rehman F., Iqbal M., Yasinzai M., and Ahmad W. (2009). A homozygous nonsense mutation in the human desmocollin-3 (DSC3) gene underlies hereditary hypotrichosis and recurrent skin vesicles. *Am J Hum Genet* **85:** 515-20.

Bass-Zubek A. E., and Green K. J. (2007). Biochemical characterization of the desmosome. *J Invest Dermatol* **127:** E4-E5.

Basso C., Czarnowska E., Della Barbera M., Bauce B., Beffagna G., Wlodarska E. K., Pilichou K., Ramondo A., Lorenzon A., Wozniek O., Corrado D., Daliento L., Danieli G. A., Valente M., Nava A., Thiene G., and Rampazzo A. (2006). Ultrastructural evidence of intercalated disc remodelling in arrhythmogenic right

ventricular cardiomyopathy: an electron microscopy investigation on endomyocardial biopsies. *Eur Heart J* **27:** 1847-54.

Basso C., Thiene G., Corrado D., Angelini A., Nava A., and Valente M. (1996). Arrhythmogenic right ventricular cardiomyopathy. Dysplasia, dystrophy, or myocarditis? *Circulation* **94:** 983-91.

Bauce B., Basso C., Rampazzo A., Beffagna G., Daliento L., Frigo G., Malacrida S., Settimo L., Danieli G., Thiene G., and Nava A. (2005). Clinical profile of four families with arrhythmogenic right ventricular cardiomyopathy caused by dominant desmoplakin mutations. *Eur Heart J* **26:** 1666-75.

Beausoleil S. A., Jedrychowski M., Schwartz D., Elias J. E., Villen J., Li J., Cohn M. A., Cantley L. C., and Gygi S. P. (2004). Large-scale characterization of HeLa cell nuclear phosphoproteins. *Proc Natl Acad Sci U S A* **101:** 12130-5.

Beffagna G., Bauce B., Lorenzon A., Nava A., Smaniotto G., De Bortoli M., Basso C., Thiene G., Thiene G. A., and Rampazzo A. (2008). Compound genotypes of two mutated genes in arrhythmogenic right ventricular cardiomyopathy. *Eur Heart J* **29 (Suppl.1):** 162.

Beffagna G., Occhi G., Nava A., Vitiello L., Ditadi A., Basso C., Bauce B., Carraro G., Thiene G., Towbin J. A., Danieli G. A., and Rampazzo A. (2005). Regulatory mutations in transforming growth factor-beta3 gene cause arrhythmogenic right ventricular cardiomyopathy type 1. *Cardiovasc Res* **65:** 366-73.

Bierkamp C., McLaughlin K. J., Schwarz H., Huber O., and Kemler R. (1996). Embryonic heart and skin defects in mice lacking plakoglobin. *Dev Biol* **180:** 780-5.

Bierkamp C., Schwarz H., Huber O., and Kemler R. (1999). Desmosomal localization of beta-catenin in the skin of plakoglobin null-mutant mice. *Development* **126:** 371-81.

Bizzozero G. (1864). Delle cellule cigliate, del reticolo Malpighiano dell'epidermide. . *Annal Univ Med* **190:** 110-8.

Bizzozero G. (1870). Osservazioni sulla struttura degli epiteli pavimentosi stratificati. *Rend R Ist Lomb* **3:** 675.

Black D. L. (2000). Protein diversity from alternative splicing: a challenge for bioinformatics and post-genome biology. *Cell* **103:** 367-70.

Blanpain C., and Fuchs E. (2009). Epidermal homeostasis: a balancing act of stem cells in the skin. *Nat Rev Mol Cell Biol* **10:** 207-17.

Bolling M. C., and Jonkman M. F. (2009). Skin and heart: une liaison dangereuse. *Exp Dermatol* **18:** 658-68.

Bolling M. C., Pas H. H., de Visser M., Aronica E., Pfendner E. G., van den Berg M. P., Diercks G. F., Suurmeijer A. J., and Jonkman M. F. (2009). PLEC1 Mutations Underlie Adult-Onset Dilated Cardiomyopathy in Epidermolysis Bullosa Simplex with Muscular Dystrophy. *J Invest Dermatol*.

Bonne S., Gilbert B., Hatzfeld M., Chen X., Green K. J., and van Roy F. (2003). Defining desmosomal plakophilin-3 interactions. *J Cell Biol* **161:** 403-16.

Bornslaeger E. A., Corcoran C. M., Stappenbeck T. S., and Green K. J. (1996). Breaking the connection: displacement of the desmosomal plaque protein desmoplakin from cell-cell interfaces disrupts anchorage of intermediate filament bundles and alters intercellular junction assembly. *J Cell Biol* **134:** 985-1001.

Bornslaeger E. A., Godsel L. M., Corcoran C. M., Park J. K., Hatzfeld M., Kowalczyk A. P., and Green K. J. (2001). Plakophilin 1 interferes with plakoglobin binding to desmoplakin, yet together with plakoglobin promotes clustering of desmosomal plaque complexes at cell-cell borders. *J Cell Sci* **114:** 727-38.

Borradori L., and Sonnenberg A. (1996). Hemidesmosomes: roles in adhesion, signaling and human diseases. *Curr Opin Cell Biol* **8:** 647-56.

Borrmann C. M., Grund C., Kuhn C., Hofmann I., Pieperhoff S., and Franke W. W. (2006). The area composita of adhering junctions connecting heart muscle cells of vertebrates. II. Colocalizations of desmosomal and fascia adhaerens molecules in the intercalated disk. *Eur J Cell Biol* **85:** 469-85.

Boulais N., and Misery L. (2008). The epidermis: a sensory tissue. *Eur J Dermatol* **18:** 119-27.

Braun-Falco M. (2009). Hereditary Palmoplantar Keratodermas. *J Dtsch Dermatol Ges*.

Burgeson R. E., and Christiano A. M. (1997). The dermal-epidermal junction. *Curr Opin Cell Biol* **9:** 651-8.

Cabral R. M., Liu L., Hogan C., Dopping-Hepenstal P. J., Winik B. C., Asial R. A., Dobson R., Mein C. A., Baselaga P. A., Mellerio J. E., Nanda A., Boente M. D., Kelsell D. P., McGrath J. A., and South A. P. (2010). Homozygous Mutations in the 5' Region of the JUP Gene Result in Cutaneous Disease but Normal Heart Development in Children. *J Invest Dermatol*.

Calkins C. C., Hoepner B. L., Law C. M., Novak M. R., Setzer S. V., Hatzfeld M., and Kowalczyk A. P. (2003). The Armadillo family protein p0071 is a VE-cadherin- and desmoplakin-binding protein. *J Biol Chem* **278:** 1774-83.

Calkins C. C., and Setzer S. V. (2007). Spotting desmosomes: the first 100 years. *J Invest Dermatol* **127:** E2–3.

Carthew R. W., and Sontheimer E. J. (2009). Origins and Mechanisms of miRNAs and siRNAs. *Cell* **136:** 642-55.

Carvajal-Huerta L. (1998). Epidermolytic palmoplantar keratoderma with woolly hair and dilated cardiomyopathy. *J Am Acad Dermatol* **39:** 418-21.

Chen X., Bonne S., Hatzfeld M., van Roy F., and Green K. J. (2002). Protein binding and functional characterization of plakophilin 2. Evidence for its diverse roles in desmosomes and beta -catenin signaling. *J Biol Chem* **277:** 10512-22.

Cheng X., Den Z., and Koch P. J. (2005). Desmosomal cell adhesion in mammalian development. *Eur J Cell Biol* **84:** 215-23.

Chitaev N. A., Averbakh A. Z., Troyanovsky R. B., and Troyanovsky S. M. (1998). Molecular organization of the desmoglein-plakoglobin complex. *J Cell Sci* **111** 1941-9.

Chitaev N. A., Leube R. E., Troyanovsky R. B., Eshkind L. G., Franke W. W., and Troyanovsky S. M. (1996). The binding of plakoglobin to desmosomal cadherins: patterns of binding sites and topogenic potential. *J Cell Biol* **133:** 359-69.

Chitaev N. A., and Troyanovsky S. M. (1997). Direct Ca2+-dependent heterophilic interaction between desmosomal cadherins, desmoglein and desmocollin, contributes to cell-cell adhesion. *J Cell Biol* **138:** 193-201.

Choi H. J., Park-Snyder S., Pascoe L. T., Green K. J., and Weis W. I. (2002). Structures of two intermediate filament-binding fragments of desmoplakin reveal a unique repeat motif structure. *Nat Struct Biol* **9:** 612-20.

Choi H. J., and Weis W. I. (2005). Structure of the armadillo repeat domain of plakophilin 1. *J Mol Biol* **346:** 367-76.

Chu D. H. (2008). Development and Structure of Skin. *In* "Fitzpatrick's Dermatology in General Medicine, 7th Edition" (Wolff K., Goldsmith L., Katz S., Gilchrest B., Paller A., and Leffell D., Eds.), pp. 57-66, McGraw Hill.

Coonar A. S., Protonotarios N., Tsatsopoulou A., Needham E. W., Houlston R. S., Cliff S., Otter M. I., Murday V. A., Mattu R. K., and McKenna W. J. (1998). Gene for arrhythmogenic right ventricular cardiomyopathy with diffuse nonepidermolytic

palmoplantar keratoderma and woolly hair (Naxos disease) maps to 17q21. *Circulation* **97:** 2049-58.

Corrado D., and Thiene G. (2006). Arrhythmogenic right ventricular cardiomyopathy/dysplasia: clinical impact of molecular genetic studies. *Circulation* **113:** 1634-7.

Cowin P. (1994). Unraveling the cytoplasmic interactions of the cadherin superfamily. *Proc Natl Acad Sci U S A* **91:** 10759-61.

Cowin P., Kapprell H. P., and Franke W. W. (1985). The complement of desmosomal plaque proteins in different cell types. *J Cell Biol* **101:** 1442-54.

Cowin P., Kapprell H. P., Franke W. W., Tamkun J., and Hynes R. O. (1986). Plakoglobin: a protein common to different kinds of intercellular adhering junctions. *Cell* **46:** 1063-73.

Danieli G. A., and Rampazzo A. (2002). Genetics of arrhythmogenic right ventricular cardiomyopathy. *Curr Opin Cardiol* **17:** 218-21.

Delva E., Tucker D. K., and Kowalczyk A. P. (2009). The desmosome. *Cold Spring Harbor Perspect Biol* **1:** a002543.

Desai B. V., Harmon R. M., and Green K. J. (2009). Desmosomes at a glance. *J Cell Sci* **122:** 4401-7.

Editorial (2003). Whither RNAi? *Nat Cell Biol* **5:** 489-90.

Elbashir S. M., Harborth J., Lendeckel W., Yalcin A., Weber K., and Tuschl T. (2001). Duplexes of 21-nucleotide RNAs mediate RNA interference in cultured mammalian cells. *Nature* **411:** 494-8.

Fontaine G., Fontaliran F., Hebert J. L., Chemla D., Zenati O., Lecarpentier Y., and Frank R. (1999). Arrhythmogenic right ventricular dysplasia. *Annu Rev Med* **50:** 17-35.

Fontao L., Favre B., Riou S., Geerts D., Jaunin F., Saurat J. H., Green K. J., Sonnenberg A., and Borradori L. (2003). Interaction of the bullous pemphigoid antigen 1 (BP230) and desmoplakin with intermediate filaments is mediated by distinct sequences within their COOH terminus. *Mol Biol Cell* **14:** 1978-92.

Franke W. W., Borrmann C. M., Grund C., and Pieperhoff S. (2006). The area composita of adhering junctions connecting heart muscle cells of vertebrates. I. Molecular definition in intercalated disks of cardiomyocytes by immunoelectron microscopy of desmosomal proteins. *Eur J Cell Biol* **85:** 69-82.

Franke W. W., and Moll R. (1987). Cytoskeletal components of lymphoid organs. I. Synthesis of cytokeratins 8 and 18 and desmin in subpopulations of extrafollicular reticulum cells of human lymph nodes, tonsils, and spleen. *Differentiation* **36:** 145-63.

Fuchs E. (1990). Epidermal differentiation: the bare essentials. *J Cell Biol* **111:** 2807-14.

Fuchs E. (2007). Scratching the surface of skin development. *Nature* **445:** 834-42.

Fuchs E. (2009). The tortoise and the hair: slow-cycling cells in the stem cell race. *Cell* **137:** 811-9.

Fuchs E., and Raghavan S. (2002). Getting under the skin of epidermal morphogenesis. *Nat Rev Genet* **3:** 199-209.

Gallicano G. I., Kouklis P., Bauer C., Yin M., Vasioukhin V., Degenstein L., and Fuchs E. (1998). Desmoplakin is required early in development for assembly of desmosomes and cytoskeletal linkage. *J Cell Biol* **143:** 2009-22.

Garcia-Gras E., Lombardi R., Giocondo M. J., Willerson J. T., Schneider M. D., Khoury D. S., and Marian A. J. (2006). Suppression of canonical Wnt/beta-catenin signaling by nuclear plakoglobin recapitulates phenotype of arrhythmogenic right ventricular cardiomyopathy. *J Clin Invest* **116:** 2012-21.

Garrod D., and Chidgey M. (2008). Desmosome structure, composition and function. *Biochim Biophys Acta* **1778:** 572-87.

Garrod D. R., Berika M. Y., Bardsley W. F., Holmes D., and Tabernero L. (2005). Hyper-adhesion in desmosomes: its regulation in wound healing and possible relationship to cadherin crystal structure. *J Cell Sci* **118:** 5743-54.

Garrod D. R., Merritt A. J., and Nie Z. (2002). Desmosomal cadherins. *Curr Opin Cell Biol* **14:** 537-45.

Gat U., DasGupta R., Degenstein L., and Fuchs E. (1998). De Novo hair follicle morphogenesis and hair tumors in mice expressing a truncated beta-catenin in skin. *Cell* **95:** 605-14.

Gaudry C. A., Palka H. L., Dusek R. L., Huen A. C., Khandekar M. J., Hudson L. G., and Green K. J. (2001). Tyrosine-phosphorylated plakoglobin is associated with desmogleins but not desmoplakin after epidermal growth factor receptor activation. *J Biol Chem* **276:** 24871-80.

Geiger B., Bershadsky A., Pankov R., and Yamada K. M. (2001). Transmembrane extracellular matrix-cytoskeleton crosstalk. *Nat Rev Mol Cell Biol* **2:** 793-805.

Gerull B., Heuser A., Wichter T., Paul M., Basson C. T., McDermott D. A., Lerman B. B., Markowitz S. M., Ellinor P. T., MacRae C. A., Peters S., Grossmann K. S., Drenckhahn J., Michely B., Sasse-Klaassen S., Birchmeier W., Dietz R., Breithardt G., Schulze-Bahr E., and Thierfelder L. (2004). Mutations in the desmosomal protein plakophilin-2 are common in arrhythmogenic right ventricular cardiomyopathy. *Nat Genet* **36:** 1162-4.

Getsios S., Amargo E. V., Dusek R. L., Ishii K., Sheu L., Godsel L. M., and Green K. J. (2004a). Coordinated expression of desmoglein 1 and desmocollin 1 regulates intercellular adhesion. *Differentiation* **72:** 419-33.

Getsios S., Huen A. C., and Green K. J. (2004b). Working out the strength and flexibility of desmosomes. *Nat Rev Mol Cell Biol* **5:** 271-81.

Ghildiyal M., and Zamore P. D. (2009). Small silencing RNAs: an expanding universe. *Nat Rev Genet* **10:** 94-108.

Godsel L. M., Hobbs R. P., and Green K. J. (2008). Intermediate filament assembly: dynamics to disease. *Trends Cell Biol* **18:** 28-37.

Godsel L. M., Hsieh S. N., Amargo E. V., Bass A. E., Pascoe-McGillicuddy L. T., Huen A. C., Thorne M. E., Gaudry C. A., Park J. K., Myung K., Goldman R. D., Chew T. L., and Green K. J. (2005). Desmoplakin assembly dynamics in four dimensions: multiple phases differentially regulated by intermediate filaments and actin. *J Cell Biol* **171:** 1045-59.

Goossens S., Janssens B., Bonne S., De Rycke R., Braet F., van Hengel J., and van Roy F. (2007). A unique and specific interaction between alphaT-catenin and plakophilin-2 in the area composita, the mixed-type junctional structure of cardiac intercalated discs. *J Cell Sci* **120:** 2126-36.

Green K. J., and Gaudry C. A. (2000). Are desmosomes more than tethers for intermediate filaments? *Nat Rev Mol Cell Biol* **1:** 208-16.

Green K. J., and Hobbs R. (2006). Ties that Bind: Desmoplakin Keeps Us Together. *Progress in Dermatology* **40**.

Green K. J., and Jones J. C. (1996). Desmosomes and hemidesmosomes: structure and function of molecular components. *Faseb J* **10:** 871-81.

Green K. J., Parry D. A., Steinert P. M., Virata M. L., Wagner R. M., Angst B. D., and Nilles L. A. (1990). Structure of the human desmoplakins. Implications for function in the desmosomal plaque. *J Biol Chem* **265:** 2603-12.

Green K. J., and Simpson C. L. (2007). Desmosomes: new perspectives on a classic. *J Invest Dermatol* **127:** 2499-515.

Haake A., Scott G. A., and Holbrook K. A. (2001). Structure and function of the skin: overview of the epidermis and dermis *In* "The Biology of the Skin" (Freinkel R.K., and Woodley D.T., Eds.), pp. 19-45, Informa Healthcare.

Haegel H., Larue L., Ohsugi M., Fedorov L., Herrenknecht K., and Kemler R. (1995). Lack of beta-catenin affects mouse development at gastrulation. *Development* **121:** 3529-37.

Halata Z., Grim M., and Bauman K. I. (2003). Friedrich Sigmund Merkel and his "Merkel cell", morphology, development, and physiology: review and new results. *Anat Rec A Discov Mol Cell Evol Biol* **271:** 225-39.

Hammerling B., Grund C., Boda-Heggemann J., Moll R., and Franke W. W. (2006). The complexus adhaerens of mammalian lymphatic endothelia revisited: a junction even more complex than hitherto thought. *Cell Tissue Res* **324:** 55-67.

Hannon G. J. (2002). RNA interference. *Nature* **418:** 244-51.

Hartsock A., and Nelson W. J. (2008). Adherens and tight junctions: structure, function and connections to the actin cytoskeleton. *Biochim Biophys Acta* **1778:** 660-9.

Hatsell S., and Cowin P. (2001). Deconstructing desmoplakin. *Nat Cell Biol* **3:** E270-2.

Hatsell S., Medina L., Merola J., Haltiwanger R., and Cowin P. (2003). Plakoglobin is O-glycosylated close to the N-terminal destruction box. *J Biol Chem* **278:** 37745-52.

Hatsell S. J., and Kelsell D. P. (2000). The diffuse palmoplantar keratodermas. *Acta Dermatovenerologica Alpina, pannonica et adriatica* **9**.

Hatzfeld M. (1999). The armadillo family of structural proteins. *Int Rev Cytol* **186:** 179-224.

Hatzfeld M. (2007). Plakophilins: Multifunctional proteins or just regulators of desmosomal adhesion? *Biochim Biophys Acta* **1773:** 69-77.

Hatzfeld M., Green K. J., and Sauter H. (2003). Targeting of p0071 to desmosomes and adherens junctions is mediated by different protein domains. *J Cell Sci* **116:** 1219-33.

Hatzfeld M., and Nachtsheim C. (1996). Cloning and characterization of a new armadillo family member, p0071, associated with the junctional plaque: evidence for a subfamily of closely related proteins. *J Cell Sci* **109:** 2767-78.

Herrenknecht K., Ozawa M., Eckerskorn C., Lottspeich F., Lenter M., and Kemler R. (1991). The uvomorulin-anchorage protein alpha catenin is a vinculin homologue. *Proc Natl Acad Sci U S A* **88:** 9156-60.

Heuser A., Plovie E. R., Ellinor P. T., Grossmann K. S., Shin J. T., Wichter T., Basson C. T., Lerman B. B., Sasse-Klaassen S., Thierfelder L., MacRae C. A., and Gerull B. (2006). Mutant desmocollin-2 causes arrhythmogenic right ventricular cardiomyopathy. *Am J Hum Genet* **79:** 1081-8.

Hofmann I., Casella M., Schnolzer M., Schlechter T., Spring H., and Franke W. W. (2006). Identification of the junctional plaque protein plakophilin 3 in cytoplasmic particles containing RNA-binding proteins and the recruitment of plakophilins 1 and 3 to stress granules. *Mol Biol Cell* **17:** 1388-98.

Hofmann I., Mertens C., Brettel M., Nimmrich V., Schnolzer M., and Herrmann H. (2000). Interaction of plakophilins with desmoplakin and intermediate filament proteins: an in vitro analysis. *J Cell Sci* **113:** 2471-83.

Holthofer B., Windoffer R., Troyanovsky S., and Leube R. E. (2007). Structure and function of desmosomes. *Int Rev Cytol* **264:** 65-163.

Houben E., De Paepe K., and Rogiers V. (2007). A keratinocyte's course of life. *Skin Pharmacol Physiol* **20:** 122-32.

Howard M. T., Malik N., Anderson C. B., Voskuil J. L., Atkins J. F., and Gibbons R. J. (2004). Attenuation of an amino-terminal premature stop codon mutation in the

ATRX gene by an alternative mode of translational initiation. *J Med Genet* **41:** 951-6.

Huber A. H., Nelson W. J., and Weis W. I. (1997). Three-dimensional structure of the armadillo repeat region of beta-catenin. *Cell* **90:** 871-82.

Huber O. (2003). Structure and function of desmosomal proteins and their role in development and disease. *Cell Mol Life Sci* **60:** 1872-90.

Huber O., Korn R., McLaughlin J., Ohsugi M., Herrmann B. G., and Kemler R. (1996). Nuclear localization of beta-catenin by interaction with transcription factor LEF-1. *Mech Dev* **59:** 3-10.

Huen A. C., Park J. K., Godsel L. M., Chen X., Bannon L. J., Amargo E. V., Hudson T. Y., Mongiu A. K., Leigh I. M., Kelsell D. P., Gumbiner B. M., and Green K. J. (2002). Intermediate filament-membrane attachments function synergistically with actin-dependent contacts to regulate intercellular adhesive strength. *J Cell Biol* **159:** 1005-17.

Inacio A., Silva A. L., Pinto J., Ji X., Morgado A., Almeida F., Faustino P., Lavinha J., Liebhaber S. A., and Romao L. (2004). Nonsense mutations in close proximity to the initiation codon fail to trigger full nonsense-mediated mRNA decay. *J Biol Chem* **279:** 32170-80.

Ishii K., and Green K. J. (2001). Cadherin function: breaking the barrier. *Curr Biol* **11:** R569-72.

Jamora C., and Fuchs E. (2002). Intercellular adhesion, signalling and the cytoskeleton. *Nat Cell Biol* **4:** E101-8.

Jefferson J. J., Ciatto C., Shapiro L., and Liem R. K. (2007). Structural analysis of the plakin domain of bullous pemphigoid antigen1 (BPAG1) suggests that plakins are members of the spectrin superfamily. *J Mol Biol* **366:** 244-57.

Johnson J. M., Castle J., Garrett-Engele P., Kan Z., Loerch P. M., Armour C. D., Santos R., Schadt E. E., Stoughton R., and Shoemaker D. D. (2003). Genome-wide survey of human alternative pre-mRNA splicing with exon junction microarrays. *Science* **302:** 2141-4.

Jonkman M. F., Pasmooij A. M., Pasmans S. G., van den Berg M. P., Ter Horst H. J., Timmer A., and Pas H. H. (2005). Loss of desmoplakin tail causes lethal acantholytic epidermolysis bullosa. *Am J Hum Genet* **77:** 653-60.

Kang T. W., Lee J. S., Kim S. E., Oh S. W., and Kim S. C. (2010). Novel and recurrent mutations in Keratin 5 and 14 in Korean patients with Epidermolysis bullosa simplex. *J Dermatol Sci* **57:** 90-4.

Kaplan S. R., Gard J. J., Carvajal-Huerta L., Ruiz-Cabezas J. C., Thiene G., and Saffitz J. E. (2004). Structural and molecular pathology of the heart in Carvajal syndrome. *Cardiovasc Pathol* **13:** 26-32.

Kimura T. E., Merritt A. J., and Garrod D. R. (2007). Calcium-independent desmosomes of keratinocytes are hyper-adhesive. *J Invest Dermatol* **127:** 775-81.

Kimyai-Asadi A., Kotcher L. B., and Jih M. H. (2002). The molecular basis of hereditary palmoplantar keratodermas. *J Am Acad Dermatol* **47:** 327-43; quiz 344-6.

Kinsella T. M., and Nolan G. P. (1996). Episomal vectors rapidly and stably produce high-titer recombinant retrovirus. *Hum Gene Ther* **7:** 1405-13.

Kljuic A., Bazzi H., Sundberg J. P., Martinez-Mir A., O'Shaughnessy R., Mahoney M. G., Levy M., Montagutelli X., Ahmad W., Aita V. M., Gordon D., Uitto J., Whiting D., Ott J., Fischer S., Gilliam T. C., Jahoda C. A., Morris R. J., Panteleyev A. A., Nguyen V. T., and Christiano A. M. (2003). Desmoglein 4 in hair follicle differentiation and epidermal adhesion: evidence from inherited hypotrichosis and acquired pemphigus vulgaris. *Cell* **113:** 249-60.

Kodama S., Ikeda S., Asahara T., Kishida M., and Kikuchi A. (1999). Axin directly interacts with plakoglobin and regulates its stability. *J Biol Chem* **274:** 27682-8.

Kottke M. D., Delva E., and Kowalczyk A. P. (2006). The desmosome: cell science lessons from human diseases. *J Cell Sci* **119:** 797-806.

Kouklis P. D., Hutton E., and Fuchs E. (1994). Making a connection: direct binding between keratin intermediate filaments and desmosomal proteins. *J Cell Biol* **127:** 1049-60.

Kowalczyk A. P., Bornslaeger E. A., Borgwardt J. E., Palka H. L., Dhaliwal A. S., Corcoran C. M., Denning M. F., and Green K. J. (1997). The amino-terminal domain of desmoplakin binds to plakoglobin and clusters desmosomal cadherin-plakoglobin complexes. *J Cell Biol* **139:** 773-84.

Kowalczyk A. P., Hatzfeld M., Bornslaeger E. A., Kopp D. S., Borgwardt J. E., Corcoran C. M., Settler A., and Green K. J. (1999). The head domain of plakophilin-1 binds to desmoplakin and enhances its recruitment to desmosomes. Implications for cutaneous disease. *J Biol Chem* **274:** 18145-8.

Kowalczyk A. P., Palka H. L., Luu H. H., Nilles L. A., Anderson J. E., Wheelock M. J., and Green K. J. (1994). Posttranslational regulation of plakoglobin expression. Influence of the desmosomal cadherins on plakoglobin metabolic stability. *J Biol Chem* **269:** 31214-23.

Kozak M. (1981). Mechanism of mRNA recognition by eukaryotic ribosomes during initiation of protein synthesis. *Curr Top Microbiol Immunol* **93:** 81-123.

Lai-Cheong J. E., Arita K., and McGrath J. A. (2007). Genetic diseases of junctions. *J Invest Dermatol* **127:** 2713-25.

Le Hir H., and Seraphin B. (2008). EJCs at the heart of translational control. *Cell* **133:** 213-6.

Lechler T., and Fuchs E. (2007). Desmoplakin: an unexpected regulator of microtubule organization in the epidermis. *J Cell Biol* **176:** 147-54.

Leung C. L., Green K. J., and Liem R. K. (2002). Plakins: a family of versatile cytolinker proteins. *Trends Cell Biol* **12:** 37-45.

Lodish H., Berk A., Matsudaira P., Kaiser C. A., Krieger M., Scott M. P., Zipursky L., and Darnell J. (2003). Integrating Cells into Tissues. *In* "Molecular Cell Biology, 5th edition", pp. 197-243, W.H.Freeman & Co Ltd.

Maeda O., Usami N., Kondo M., Takahashi M., Goto H., Shimokata K., Kusugami K., and Sekido Y. (2004). Plakoglobin (gamma-catenin) has TCF/LEF family-dependent transcriptional activity in beta-catenin-deficient cell line. *Oncogene* **23:** 964-72.

Mahoney M. Y., Sadowski S., Brennan D., Pikander P., Saukko P., Wahl J., Aho H., Heikinheimo K., Bruckner-Tuderman L., Fertala A., Peltonen J., Uitto J., and Peltonen S. (2009). Compound Heterozygous Desmoplakin Mutations Result in a Phenotype with a Combination of Myocardial, Skin, Hair, and Enamel Abnormalities. *J Invest Dermatol*.

Maquat L. E. (2004). Nonsense-mediated mRNA decay: splicing, translation and mRNP dynamics. *Nat Rev Mol Cell Biol* **5:** 89-99.

Marcozzi C., Burdett I. D., Buxton R. S., and Magee A. I. (1998). Coexpression of both types of desmosomal cadherin and plakoglobin confers strong intercellular adhesion. *J Cell Sci* **111:** 495-509.

Matlin A. J., Clark F., and Smith C. W. (2005). Understanding alternative splicing: towards a cellular code. *Nat Rev Mol Cell Biol* **6:** 386-98.

McGrath J. A. (2005). Inherited disorders of desmosomes. *Australas J Dermatol* **46:** 221-9.

McGrath J. A., McMillan J. R., Shemanko C. S., Runswick S. K., Leigh I. M., Lane E. B., Garrod D. R., and Eady R. A. (1997). Mutations in the plakophilin 1 gene result in ectodermal dysplasia/skin fragility syndrome. *Nat Genet* **17:** 240-4.

McGrath J. A., and Mellerio J. E. (2010). Ectodermal dysplasia-skin fragility syndrome. *Dermatol Clin* **28:** 125-9.

McKenna W. J., Thiene G., Nava A., Fontaliran F., Blomstrom-Lundqvist C., Fontaine G., and Camerini F. (1994). Diagnosis of arrhythmogenic right ventricular dysplasia/cardiomyopathy. Task Force of the Working Group Myocardial and Pericardial Disease of the European Society of Cardiology and of the Scientific Council on Cardiomyopathies of the International Society and Federation of Cardiology. *Br Heart J* **71:** 215-8.

McKoy G., Protonotarios N., Crosby A., Tsatsopoulou A., Anastasakis A., Coonar A., Norman M., Baboonian C., Jeffery S., and McKenna W. J. (2000). Identification of a deletion in plakoglobin in arrhythmogenic right ventricular cardiomyopathy with palmoplantar keratoderma and woolly hair (Naxos disease). *Lancet* **355:** 2119-24.

McMillan J. R., Haftek M., Akiyama M., South A. P., Perrot H., McGrath J. A., Eady R. A., and Shimizu H. (2003). Alterations in desmosome size and number coincide with the loss of keratinocyte cohesion in skin with homozygous and heterozygous defects in the desmosomal protein plakophilin 1. *J Invest Dermatol* **121:** 96-103.

Meng J. J., Bornslaeger E. A., Green K. J., Steinert P. M., and Ip W. (1997). Two-hybrid analysis reveals fundamental differences in direct interactions between desmoplakin and cell type-specific intermediate filaments. *J Biol Chem* **272:** 21495-503.

Mertens C., Hofmann I., Wang Z., Teichmann M., Sepehri Chong S., Schnolzer M., and Franke W. W. (2001). Nuclear particles containing RNA polymerase III complexes associated with the junctional plaque protein plakophilin 2. *Proc Natl Acad Sci U S A* **98:** 7795-800.

Mertens C., Kuhn C., and Franke W. W. (1996). Plakophilins 2a and 2b: constitutive proteins of dual location in the karyoplasm and the desmosomal plaque. *J Cell Biol* **135:** 1009-25.

Miravet S., Piedra J., Castano J., Raurell I., Franci C., Dunach M., and Garcia de Herreros A. (2003). Tyrosine phosphorylation of plakoglobin causes contrary effects on its association with desmosomes and adherens junction components and modulates beta-catenin-mediated transcription. *Mol Cell Biol* **23:** 7391-402.

Miravet S., Piedra J., Miro F., Itarte E., Garcia de Herreros A., and Dunach M. (2002). The transcriptional factor Tcf-4 contains different binding sites for beta-catenin and plakoglobin. *J Biol Chem* **277:** 1884-91.

Moll R., Sievers E., Hammerling B., Schmidt A., Barth M., Kuhn C., Grund C., Hofmann I., and Franke W. W. (2009). Endothelial and virgultar cell formations in the mammalian lymph node sinus: endothelial differentiation morphotypes characterized by a special kind of junction (complexus adhaerens). *Cell Tissue Res* **335:** 109-41.

Moon R. T., Bowerman B., Boutros M., and Perrimon N. (2002). The promise and perils of Wnt signaling through beta-catenin. *Science* **296:** 1644-6.

Moore M. J., and Silver P. A. (2008). Global analysis of mRNA splicing. *Rna* **14:** 197-203.

Morgenstern J. P., and Land H. (1990). Advanced mammalian gene transfer: high titre retroviral vectors with multiple drug selection markers and a complementary helper-free packaging cell line. *Nucleic Acids Res* **18:** 3587-96.

Norgett E. E., Hatsell S. J., Carvajal-Huerta L., Cabezas J. C., Common J., Purkis P. E., Whittock N., Leigh I. M., Stevens H. P., and Kelsell D. P. (2000). Recessive mutation in desmoplakin disrupts desmoplakin-intermediate filament interactions and causes dilated cardiomyopathy, woolly hair and keratoderma. *Hum Mol Genet* **9:** 2761-6.

Norgett E. E., Lucke T. W., Bowers B., Munro C. S., Leigh I. M., and Kelsell D. P. (2006). Early death from cardiomyopathy in a family with autosomal dominant striate palmoplantar keratoderma and woolly hair associated with a novel insertion mutation in desmoplakin. *J Invest Dermatol* **126:** 1651-4.

Norman M., Simpson M., Mogensen J., Shaw A., Hughes S., Syrris P., Sen-Chowdhry S., Rowland E., Crosby A., and McKenna W. J. (2005). Novel mutation in desmoplakin causes arrhythmogenic left ventricular cardiomyopathy. *Circulation* **112:** 636-42.

North A. J., Bardsley W. G., Hyam J., Bornslaeger E. A., Cordingley H. C., Trinnaman B., Hatzfeld M., Green K. J., Magee A. I., and Garrod D. R. (1999). Molecular map of the desmosomal plaque. *J Cell Sci* **112:** 4325-36.

North A. J., Chidgey M. A., Clarke J. P., Bardsley W. G., and Garrod D. R. (1996). Distinct desmocollin isoforms occur in the same desmosomes and show reciprocally graded distributions in bovine nasal epidermis. *Proc Natl Acad Sci U S A* **93:** 7701-5.

Nuber U. A., Schafer S., Stehr S., Rackwitz H. R., and Franke W. W. (1996). Patterns of desmocollin synthesis in human epithelia: immunolocalization of desmocollins 1 and 3 in special epithelia and in cultured cells. *Eur J Cell Biol* **71:** 1-13.

O'Keefe E. J., Erickson H. P., and Bennett V. (1989). Desmoplakin I and desmoplakin II. Purification and characterization. *J Biol Chem* **264:** 8310-8.

Odland G. F. (1958). The fine structure of the interrelationship of cells in the human epidermis. *J Biophys Biochem Cytol* **4:** 529-38.

Orban T. I., and Izaurralde E. (2005). Decay of mRNAs targeted by RISC requires XRN1, the Ski complex, and the exosome. *Rna* **11:** 459-69.

Palka H. L., and Green K. J. (1997a). Roles of plakoglobin end domains in desmosome assembly. *J Cell Sci* **110 (Pt 19):** 2359-71.

Palka H. L., and Green K. J. (1997b). Roles of plakoglobin end domains in desmosome assembly. *J Cell Sci* **110:** 2359-71.

Parrish E. P., Steart P. V., Garrod D. R., and Weller R. O. (1987). Antidesmosomal monoclonal antibody in the diagnosis of intracranial tumours. *J Pathol* **153:** 265-73.

Penn E. J., Burdett I. D., Hobson C., Magee A. I., and Rees D. A. (1987). Structure and assembly of desmosome junctions: biosynthesis and turnover of the major desmosome components of Madin-Darby canine kidney cells in low calcium medium. *J Cell Biol* **105:** 2327-34.

Pilichou K., Nava A., Basso C., Beffagna G., Bauce B., Lorenzon A., Frigo G., Vettori A., Valente M., Towbin J., Thiene G., Danieli G. A., and Rampazzo A. (2006). Mutations in desmoglein-2 gene are associated with arrhythmogenic right ventricular cardiomyopathy. *Circulation* **113:** 1171-9.

Posch M. G., Posch M. J., Geier C., Erdmann B., Mueller W., Richter A., Ruppert V., Pankuweit S., Maisch B., Perrot A., Buttgereit J., Dietz R., Haverkamp W., and Ozcelik C. (2008). A missense variant in desmoglein-2 predisposes to dilated cardiomyopathy. *Mol Genet Metab* **95:** 74-80.

Proksch E., Brandner J. M., and Jensen J. M. (2008). The skin: an indispensable barrier. *Exp Dermatol* **17:** 1063-72.

Proksch E., and Jensen J.-M. (2007). Skin as an Organ of Protection. *In* "Fitzpatrick's Dermatology in General Medicine, 7th Edition" (Wolff K., Goldsmith L., Katz S., Gilchrest B., Paller A., and Leffell D., Eds.), pp. 383-395, McGraw Hill.

Protonotarios N., and Tsatsopoulou A. (2005). Naxos disease. *Indian Pacing Electrophysiol J* **5:** 76-80.

Protonotarios N., Tsatsopoulou A., Anastasakis A., Sevdalis E., McKoy G., Stratos K., Gatzoulis K., Tentolouris K., Spiliopoulou C., Panagiotakos D., McKenna W., and Toutouzas P. (2001). Genotype-phenotype assessment in autosomal recessive arrhythmogenic right ventricular cardiomyopathy (Naxos disease) caused by a deletion in plakoglobin. *J Am Coll Cardiol* **38:** 1477-84.

Protonotarios N., Tsatsopoulou A., Patsourakos P., Alexopoulos D., Gezerlis P., Simitsis S., and Scampardonis G. (1986). Cardiac abnormalities in familial palmoplantar keratosis. *Br Heart J* **56:** 321-6.

Rampazzo A., Nava A., Malacrida S., Beffagna G., Bauce B., Rossi V., Zimbello R., Simionati B., Basso C., Thiene G., Towbin J. A., and Danieli G. A. (2002). Mutation in human desmoplakin domain binding to plakoglobin causes a dominant form of arrhythmogenic right ventricular cardiomyopathy. *Am J Hum Genet* **71:** 1200-6.

Reese M. G., Eeckman F. H., Kulp D., and Haussler D. (1997). Improved splice site detection in Genie. *J Comput Biol* **4:** 311-23.

Rickman L., Simrak D., Stevens H. P., Hunt D. M., King I. A., Bryant S. P., Eady R. A., Leigh I. M., Arnemann J., Magee A. I., Kelsell D. P., and Buxton R. S. (1999). N-terminal deletion in a desmosomal cadherin causes the autosomal dominant skin disease striate palmoplantar keratoderma. *Hum Mol Genet* **8:** 971-6.

Ross R., DiGiovanna J. J., Capaldi L., Argenyi Z., Fleckman P., and Robinson-Bostom L. (2008). Histopathologic characterization of epidermolytic hyperkeratosis: a systematic review of histology from the National Registry for Ichthyosis and Related Skin Disorders. *J Am Acad Dermatol* **59:** 86-90.

Rubenstein A., Merriam J., and Klymkowsky M. W. (1997). Localizing the adhesive and signaling functions of plakoglobin. *Dev Genet* **20:** 91-102.

Rubinfeld B., Souza B., Albert I., Muller O., Chamberlain S. H., Masiarz F. R., Munemitsu S., and Polakis P. (1993). Association of the APC gene product with beta-catenin. *Science* **262:** 1731-4.

Rudini N., and Dejana E. (2008). Adherens junctions. *Curr Biol* **18:** R1080-2.

Ruiz P., Brinkmann V., Ledermann B., Behrend M., Grund C., Thalhammer C., Vogel F., Birchmeier C., Gunthert U., Franke W. W., and Birchmeier W. (1996). Targeted mutation of plakoglobin in mice reveals essential functions of desmosomes in the embryonic heart. *J Cell Biol* **135:** 215-25.

Russell D., Andrews P. D., James J., and Lane E. B. (2004). Mechanical stress induces profound remodelling of keratin filaments and cell junctions in epidermolysis bullosa simplex keratinocytes. *J Cell Sci* **117:** 5233-43.

Sacco P. A., McGranahan T. M., Wheelock M. J., and Johnson K. R. (1995). Identification of plakoglobin domains required for association with N-cadherin and alpha-catenin. *J Biol Chem* **270:** 20201-6.

Sadot E., Simcha I., Iwai K., Ciechanover A., Geiger B., and Ben-Ze'ev A. (2000). Differential interaction of plakoglobin and beta-catenin with the ubiquitin-proteasome system. *Oncogene* **19:** 1992-2001.

Schaffer J. (1920). Vorlesungen ber Histologie und Histogenese. *Leipzig, Germany: W Engelmann,* **69**.

Schmidt A., and Jager S. (2005). Plakophilins--hard work in the desmosome, recreation in the nucleus? *Eur J Cell Biol* **84:** 189-204.

Schmidt A., Langbein L., Pratzel S., Rode M., Rackwitz H. R., and Franke W. W. (1999). Plakophilin 3--a novel cell-type-specific desmosomal plaque protein. *Differentiation* **64:** 291-306.

Schmidt A., Langbein L., Rode M., Pratzel S., Zimbelmann R., and Franke W. W. (1997). Plakophilins 1a and 1b: widespread nuclear proteins recruited in specific epithelial cells as desmosomal plaque components. *Cell Tissue Res* **290:** 481-99.

Sen-Chowdhry S., Syrris P., Prasad S. K., Hughes S. E., Merrifield R., Ward D., Pennell D. J., and McKenna W. J. (2008). Left-dominant arrhythmogenic cardiomyopathy: an under-recognized clinical entity. *J Am Coll Cardiol* **52:** 2175-87.

Shibata T., Gotoh M., Ochiai A., and Hirohashi S. (1994). Association of plakoglobin with APC, a tumor suppressor gene product, and its regulation by tyrosine phosphorylation. *Biochem Biophys Res Commun* **203:** 519-22.

Shimizu H., Masunaga T., Ishiko A., Kikuchi A., Hashimoto T., and Nishikawa T. (1995). Pemphigus vulgaris and pemphigus foliaceus sera show an inversely graded binding pattern to extracellular regions of desmosomes in different layers of human epidermis. *J Invest Dermatol* **105:** 153-9.

Silva A. L., and Romao L. (2009). The mammalian nonsense-mediated mRNA decay pathway: to decay or not to decay! Which players make the decision? *FEBS Lett* **583:** 499-505.

Simpson M. A., Mansour S., Ahnood D., Kalidas K., Patton M. A., McKenna W. J., Behr E. R., and Crosby A. H. (2009). Homozygous mutation of desmocollin-2 in arrhythmogenic right ventricular cardiomyopathy with mild palmoplantar keratoderma and woolly hair. *Cardiology* **113:** 28-34.

Skerrow CJ., and Matoltsy AG. (1974a). Chemical characterization of isolated epidermal desmosomes. . *Cell Biol* **63:** 524–30.

Skerrow CJ., and Matoltsy AG. (1974b). Isolation of epidermal desmosomes. *Cell Biol* **63:** 515-23.

Smith E. A., and Fuchs E. (1998). Defining the interactions between intermediate filaments and desmosomes. *J Cell Biol* **141:** 1229-41.

Solanas G., Miravet S., Casagolda D., Castano J., Raurell I., Corrionero A., de Herreros A. G., and Dunach M. (2004). beta-Catenin and plakoglobin N- and C-tails determine ligand specificity. *J Biol Chem* **279:** 49849-56.

South A. P. (2004). Plakophilin 1: an important stabilizer of desmosomes. *Clin Exp Dermatol* **29:** 161-7.

South A. P., Wan H., Stone M. G., Dopping-Hepenstal P. J., Purkis P. E., Marshall J. F., Leigh I. M., Eady R. A., Hart I. R., and McGrath J. A. (2003). Lack of plakophilin 1 increases keratinocyte migration and reduces desmosome stability. *J Cell Sci* **116:** 3303-14.

Stappenbeck T. S., Bornslaeger E. A., Corcoran C. M., Luu H. H., Virata M. L., and Green K. J. (1993). Functional analysis of desmoplakin domains: specification of the interaction with keratin versus vimentin intermediate filament networks. *J Cell Biol* **123:** 691-705.

Stappenbeck T. S., and Green K. J. (1992). The desmoplakin carboxyl terminus coaligns with and specifically disrupts intermediate filament networks when expressed in cultured cells. *J Cell Biol* **116:** 1197-209.

Stappenbeck T. S., Lamb J. A., Corcoran C. M., and Green K. J. (1994). Phosphorylation of the desmoplakin COOH terminus negatively regulates its interaction with keratin intermediate filament networks. *J Biol Chem* **269:** 29351-4.

Stuhrmann M., Bukhari I. A., and El-Harith el H. A. (2004). Naxos disease in an Arab family is not caused by the Pk2157del2 mutation. Evidence for exclusion of the plakoglobin gene. *Saudi Med J* **25:** 1449-52.

Syed S. E., Trinnaman B., Martin S., Major S., Hutchinson J., and Magee A. I. (2002). Molecular interactions between desmosomal cadherins. *Biochem J* **362:** 317-27.

Syrris P., Ward D., Evans A., Asimaki A., Gandjbakhch E., Sen-Chowdhry S., and McKenna W. J. (2006). Arrhythmogenic right ventricular dysplasia/cardiomyopathy associated with mutations in the desmosomal gene desmocollin-2. *Am J Hum Genet* **79:** 978-84.

Tanaka A., Lai-Cheong J. E., Cafe M. E., Gontijo B., Salomao P. R., Pereira L., and McGrath J. A. (2009). Novel truncating mutations in PKP1 and DSP cause similar skin phenotypes in two Brazilian families. *Br J Dermatol* **160:** 692-7.

Terron-Kwiatkowski A., van Steensel M. A., van Geel M., Lane E. B., McLean W. H., and Steijlen P. M. (2006). Mutation S233L in the 1B domain of keratin 1 causes epidermolytic palmoplantar keratoderma with "tonotubular" keratin. *J Invest Dermatol* **126:** 607-13.

Teuliere J., Faraldo M. M., Shtutman M., Birchmeier W., Huelsken J., Thiery J. P., and Glukhova M. A. (2004). beta-catenin-dependent and -independent effects of DeltaN-plakoglobin on epidermal growth and differentiation. *Mol Cell Biol* **24:** 8649-61.

Thiene G., Nava A., Corrado D., Rossi L., and Pennelli N. (1988). Right ventricular cardiomyopathy and sudden death in young people. *N Engl J Med* **318:** 129-33.

Tiso N., Stephan D. A., Nava A., Bagattin A., Devaney J. M., Stanchi F., Larderet G., Brahmbhatt B., Brown K., Bauce B., Muriago M., Basso C., Thiene G., Danieli G. A., and Rampazzo A. (2001). Identification of mutations in the cardiac ryanodine receptor gene in families affected with arrhythmogenic right ventricular cardiomyopathy type 2 (ARVD2). *Hum Mol Genet* **10:** 189-94.

Tomari Y., and Zamore P. D. (2005). Perspective: machines for RNAi. *Genes Dev* **19:** 517-29.

Troyanovsky R. B., Chitaev N. A., and Troyanovsky S. M. (1996a). Cadherin binding sites of plakoglobin: localization, specificity and role in targeting to adhering junctions. *J Cell Sci* **109** 3069-78.

Troyanovsky R. B., Chitaev N. A., and Troyanovsky S. M. (1996b). Cadherin binding sites of plakoglobin: localization, specificity and role in targeting to adhering junctions. *J Cell Sci* **109 (Pt 13):** 3069-78.

Troyanovsky S. M., Eshkind L. G., Troyanovsky R. B., Leube R. E., and Franke W. W. (1993). Contributions of cytoplasmic domains of desmosomal cadherins to desmosome assembly and intermediate filament anchorage. *Cell* **72:** 561-74.

Troyanovsky S. M., Troyanovsky R. B., Eshkind L. G., Leube R. E., and Franke W. W. (1994). Identification of amino acid sequence motifs in desmocollin, a desmosomal glycoprotein, that are required for plakoglobin binding and plaque formation. *Proc Natl Acad Sci U S A* **91:** 10790-4.

Tselepis C., Chidgey M., North A., and Garrod D. (1998). Desmosomal adhesion inhibits invasive behavior. *Proc Natl Acad Sci U S A* **95:** 8064-9.

Uitto J., Richard G., and McGrath J. A. (2007). Diseases of epidermal keratins and their linker proteins. *Exp Cell Res* **313:** 1995-2009.

Uzumcu A., Norgett E. E., Dindar A., Uyguner O., Nisli K., Kayserili H., Sahin S. E., Dupont E., Severs N. J., Leigh I. M., Yuksel-Apak M., Kelsell D. P., and Wollnik B. (2006). Loss of desmoplakin isoform I causes early onset cardiomyopathy and heart failure in a Naxos-like syndrome. *J Med Genet* **43:** e5.

Vasioukhin V., Bowers E., Bauer C., Degenstein L., and Fuchs E. (2001). Desmoplakin is essential in epidermal sheet formation. *Nat Cell Biol* **3:** 1076-85.

Vatta M., Marcus F., and Towbin J. A. (2007). Arrhythmogenic right ventricular cardiomyopathy: a 'final common pathway' that defines clinical phenotype. *Eur Heart J* **28:** 529-30.

Virata M. L., Wagner R. M., Parry D. A., and Green K. J. (1992). Molecular structure of the human desmoplakin I and II amino terminus. *Proc Natl Acad Sci U S A* **89:** 544-8.

Wahl J. K. r., Nieset J. E., Sacco-Bubulya P. A., Sadler T. M., Johnson K. R., and Wheelock M. J. (2000). The amino- and carboxyl-terminal tails of (beta)-catenin reduce its affinity for desmoglein 2. *J Cell Sci* **113:** 1737-45.

Wallis S., Lloyd S., Wise I., Ireland G., Fleming T. P., and Garrod D. (2000). The alpha isoform of protein kinase C is involved in signaling the response of desmosomes to wounding in cultured epithelial cells. *Mol Biol Cell* **11:** 1077-92.

Wan H., Dopping-Hepenstal P. J., Gratian M. J., Stone M. G., McGrath J. A., and Eady R. A. (2003). Desmosomes exhibit site-specific features in human palm skin. *Exp Dermatol* **12:** 378-88.

Wan H., Dopping-Hepenstal P. J., Gratian M. J., Stone M. G., Zhu G., Purkis P. E., South A. P., Keane F., Armstrong D. K., Buxton R. S., McGrath J. A., and Eady R. A. (2004). Striate palmoplantar keratoderma arising from desmoplakin and desmoglein 1 mutations is associated with contrasting perturbations of desmosomes and the keratin filament network. *Br J Dermatol* **150:** 878-91.

Wan H., South A. P., and Hart I. R. (2007). Increased keratinocyte proliferation initiated through downregulation of desmoplakin by RNA interference. *Exp Cell Res* **313:** 2336-44.

Wang M., and Marin A. (2006). Characterization and prediction of alternative splice sites. *Gene* **366:** 219-27.

Werner S., and Grose R. (2003). Regulation of wound healing by growth factors and cytokines. *Physiol Rev* **83:** 835-70.

Whittock N. V., Ashton G. H., Dopping-Hepenstal P. J., Gratian M. J., Keane F. M., Eady R. A., and McGrath J. A. (1999). Striate palmoplantar keratoderma resulting from desmoplakin haploinsufficiency. *J Invest Dermatol* **113:** 940-6.

Whittock N. V., Eady R. A., and McGrath J. A. (2000). Genomic organization and amplification of the human plakoglobin gene (JUP). *Exp Dermatol* **9:** 323-6.

Whittock N. V., Smith F. J., Wan H., Mallipeddi R., Griffiths W. A., Dopping-Hepenstal P., Ashton G. H., Eady R. A., McLean W. H., and McGrath J. A. (2002a). Frameshift mutation in the V2 domain of human keratin 1 results in striate palmoplantar keratoderma. *J Invest Dermatol* **118:** 838-44.

Whittock N. V., Wan H., Morley S. M., Garzon M. C., Kristal L., Hyde P., McLean W. H., Pulkkinen L., Uitto J., Christiano A. M., Eady R. A., and McGrath J. A. (2002b). Compound heterozygosity for non-sense and mis-sense mutations in desmoplakin underlies skin fragility/woolly hair syndrome. *J Invest Dermatol* **118:** 232-8.

Williamson L., Raess N. A., Caldelari R., Zakher A., de Bruin A., Posthaus H., Bolli R., Hunziker T., Suter M. M., and Muller E. J. (2006). Pemphigus vulgaris identifies plakoglobin as key suppressor of c-Myc in the skin. *Embo J* **25:** 3298-309.

Winik B. C., Asial R. A., McGrath J. A., South A. P., and Boente M. C. (2009). Acantholytic ectodermal dysplasia: clinicopathological study of a new desmosomal disorder. *Br J Dermatol* **160:** 868-74.

Witcher L. L., Collins R., Puttagunta S., Mechanic S. E., Munson M., Gumbiner B., and Cowin P. (1996). Desmosomal cadherin binding domains of plakoglobin. *J Biol Chem* **271:** 10904-9.

Wolf A., Keil R., Gotzl O., Mun A., Schwarze K., Lederer M., Huttelmaier S., and Hatzfeld M. (2006). The armadillo protein p0071 regulates Rho signalling during cytokinesis. *Nat Cell Biol* **8:** 1432-40.

Woodley D., and Chen M. (2001). The basement membrane zone. *In* "The Biology of the Skin" (Freinkel R.K., and Woodley D.T., Eds.), pp. 133-152, Informa Healthcare.

Wozniak M. A., Modzelewska K., Kwong L., and Keely P. J. (2004). Focal adhesion regulation of cell behavior. *Biochim Biophys Acta* **1692:** 103-19.

Yamada S., Pokutta S., Drees F., Weis W. I., and Nelson W. J. (2005). Deconstructing the cadherin-catenin-actin complex. *Cell* **123:** 889-901.

Yang Z., Bowles N. E., Scherer S. E., Taylor M. D., Kearney D. L., Ge S., Nadvoretskiy V. V., DeFreitas G., Carabello B., Brandon L. I., Godsel L. M., Green K. J., Saffitz J. E., Li H., Danieli G. A., Calkins H., Marcus F., and Towbin J. A. (2006). Desmosomal dysfunction due to mutations in desmoplakin causes arrhythmogenic right ventricular dysplasia/cardiomyopathy. *Circ Res* **99:** 646-55.

Yin T., Getsios S., Caldelari R., Godsel L. M., Kowalczyk A. P., Muller E. J., and Green K. J. (2005). Mechanisms of plakoglobin-dependent adhesion: desmosome-specific functions in assembly and regulation by epidermal growth factor receptor. *J Biol Chem* **280:** 40355-63.

Yin T., and Green K. J. (2004). Regulation of desmosome assembly and adhesion. *Semin Cell Dev Biol* **15:** 665-77.

Yu C. C., Yu C. H., Hsueh C. H., Yang C. T., Juang J. M., Hwang J. J., Lin J. L., and Lai L. P. (2008). Arrhythmogenic right ventricular dysplasia: clinical characteristics and identification of novel desmosome gene mutations. *J Formos Med Assoc* **107:** 548-58.

Zhang J., and Maquat L. E. (1997). Evidence that translation reinitiation abrogates nonsense-mediated mRNA decay in mammalian cells. *Embo J* **16:** 826-33.

Zhurinsky J., Shtutman M., and Ben-Ze'ev A. (2000). Plakoglobin and beta-catenin: protein interactions, regulation and biological roles. *J Cell Sci* **113:** 3127-39.

The 59th Annual Meeting of The American Society of Human Genetics [online]. Available at:
http://www.ashg.org/2009meeting/abstracts/fulltext/

The Sequence Manipulation Suite [online]. Available at:
http://www.bioinformatics.org/sms/index.html

Multalin Interface Page [online]. Available at:
http://bioinfo.genotoul.fr/multalin/multalin.html

Splice Site Prediction by Neural Network [online]. Available at:
http://www.fruitfly.org/seq_tools/splice.html

Alternative Splice Site Predictor [online]. Available at:
http://www.es.embnet.org/~mwang/assp.html

National Center for Biotechnology Information
http://www.ncbi.nlm.nih.gov/

Appendices

Appendix A. Genetic analysis in patients with recessive skin disease and woolly hair

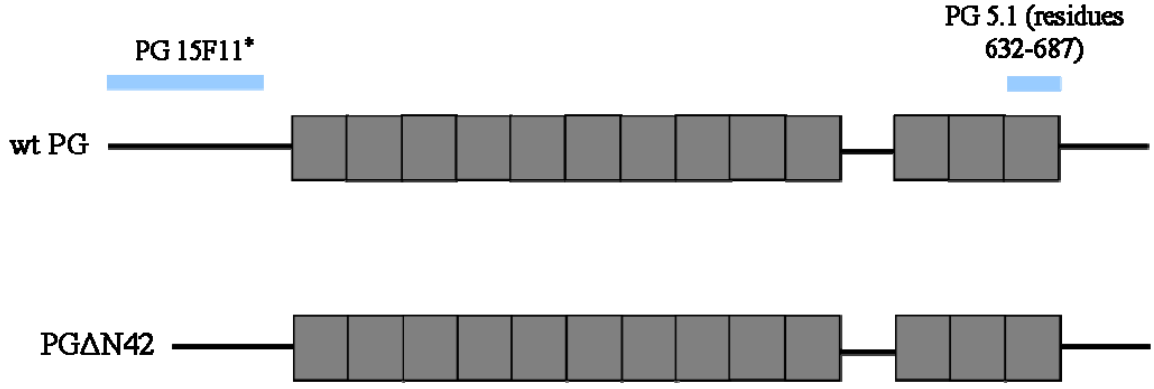

*15F11 antibody reacts with a C-terminally truncated PG protein which contains only amino acids 1-144 (Sacco et al., 1995)

Figure A1. Schematic diagram of epitope recognition sites for the two anti-PG antibodies used in this study in relation to wild type PG and PGΔN42. The epitope of the mouse monoclonal antibody PG 5.1 maps to the C-terminus at the extreme end of repeat 13 (amino acids 632-687) of PG. The mouse monoclonal antibody 15F11 was raised against full length *Gallas* PG and was shown to react with residues 1-144 (Sacco *et al.*, 1995).

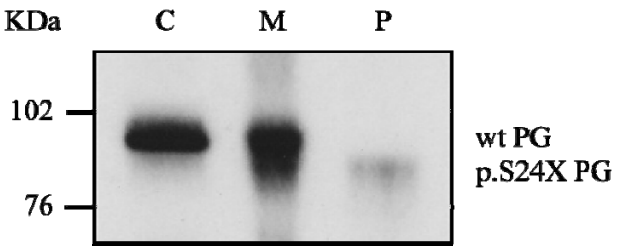

Figure A2. Mutant protein PGΔN42 is recognized with an N-terminal PG monoclonal antibody, 15F11. Western blotting of skin proteins isolated from a normal control (C), maternal (M) and patient A (P) samples with the monoclonal N-terminal antibody 15F11 shows reduced levels of truncated PGΔN42 in both maternal (M) and patient (P) samples. Wild type PG is observed in control (C) and maternal (M) samples.

Appendix B: Optimisations of siRNA knock-down experiment for transient down-regulation of DP isoforms

B1. Transient down-regulation of DPI with synthetic siRNAs in HaCaT keratinocytes

B1.1. Optimisation of the siRNA transfection conditions

Lipid-based transfections using the DharmaFECT transfection reagent (Thermo Fisher Scientific) were performed to deliver siRNAs into HaCaT cells. Transfection conditions were first optimised in HaCaT cells, prior to *DSP* siRNA transfections, in order to find the highest transfection efficiency. To accomplish this, siGLO Cyclophilin B Control siRNA (Thermo Fisher Scientific) was complexed with three different volumes of DharmaFECT transfection reagent – 2, 4 and 6 µl – (as suggested by the manufacturer) to deliver a final concentration of 100 nM siRNA per well of a 6-well plate. siGLO Cyclophilin B Control siRNA is a stable, fluorescent form of Cyclophilin B (peptidylprolyl isomerase B or PPIB) which provides positive correlation of fluorescent uptake with transfection efficiency and gene silencing activity. The uptake of the control siGLO siRNA was visualised using the Cy3 filter on a fluorescence microscope after approximately 20 hours.

As shown in Figure B1, cells appeared healthy and remained viable following a 20 hour-incubation with up to 6µl of DharmaFECT. Toxicity was observed after 24 hours of incubation with DharmaFECT (2, 4 and 6µl) and therefore fresh media was always added to the cells 20 hours post-transfection in subsequent experiments. The amount of siGLO uptake, as judged by the red fluorescence levels, increased progressively with increasing volumes of DharmaFECT, and was highest when cells were transfected with 6µl of DharmaFECT. No fluorescence was observed when the cells were incubated with DharmaFECT only or with siGLO only (negative controls). These results indicated that 6µl was the optimum volume of DharmaFECT to deliver siRNAs to HaCaT cells plated at a density of $1x10^5$ cells/ml, since the maximum uptake of siRNA was achieved with minimum cell toxicity. These transfections conditions were used in all subsequent experiments.

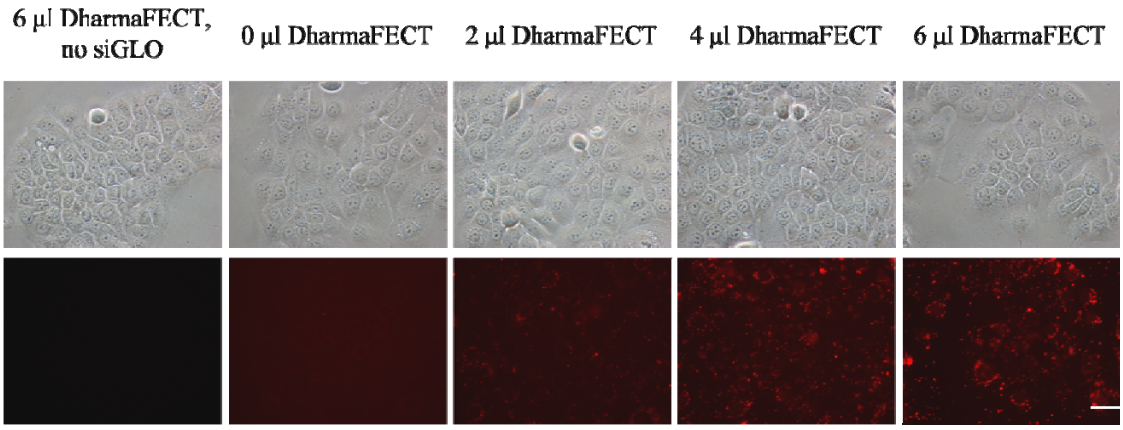

Figure B1. Optimisation of siRNA transfection conditions in HaCaT cells with siGLO Cyclophilin B Control siRNA and different volumes of DharmaFECT transfection reagent. Cells were incubated with a final concentration of 100 nM of siGLO Cyclophilin B Control siRNA which was first complexed with 0, 2, 4 or 6 µl of DharmaFECT transfection reagent. Cells that were incubated with 6 µl of DharmaFECT had the highest uptake of the fluorescently labelled siGLO control siRNA whilst cell toxicity was not observed. Scale bar = 20 µm.

B1.2. siRNA design for down-regulation of DPI (and DPIb)

To mimic the p.R1267X nonsense mutation, siRNAs had to be specifically designed to target the 648 bp coding region, from nucleotides 3582 to 4050, which is the only region common to both *DSPI* and *DSPIb* and absent from *DSPII* mRNAs. The Thermo Fisher Scientific si*DESIGN* Center was used for this purpose which offered 50 top- scoring candidates (Table B1).

Four siRNAs (si1, si2, si3 and si4, Figure B2) were chosen from the 50 top-scoring candidates (Table B1) based on two criteria. Firstly, siRNAs with the highest "minimum number of mismatches" of the 19-nucleotide sense and anti-sense strands to a sequence record other than the required target (as determined by BLAST analysis) were chosen. Secondly, within the siRNAs with the highest "minimum number of mismatches" for sense and anti-sense strands, the four siRNAs with highest scores were selected (84, 82 and 80). Figure B2 depicts the four siRNAs (si1-si4) chosen to knock-down *DSPI* (and *DSPIb*) mRNA, and their target sites.

Table B1. Fifty top-scoring candidate *DSPI/DSPIb* siRNAs provided by the Thermo Fisher Scientific **si*DESIGN* Centre.** The chosen four siRNAs based on scoring and number of mismatches of the sense and antisense strands are shaded in blue.

Sense Strand Sequence	Start Pos.	GC %	Score	Low Seed Freq?	Min # Mis-matches (α-sense)	Min # Mis-matches (sense)	Requires Sense Mods?
ctgagataatgcagaagaa	204	37	86	No	2	**2**	**No**
gcgaaggcgagctgaagaa	157	58	84	No	3	**3**	**No**
ataaggagatcgagagact	330	42	84	No	3	**>3**	**Yes**
ccaagaccattcaggacaa	309	47	83	No	2	**3**	**No**
ggcctgtggctctgagata	193	58	82	No	3	**3**	**No**
cttagaaaccagcttgata	62	37	81	No	2	**2**	**No**
agataatgcagaagaagca	207	37	81	No	1	**3**	**Yes**
agatagaactgaagcaggt	234	42	80	No	3	**3**	**Yes**
aaggagatatccatgcaaa	23	37	79	No	3	**3**	**Yes**
gaaaccagcttgatagact	66	42	79	No	3	**3**	**Yes**
aaataaggagatcgagaga	328	37	79	Yes	1	**3**	**Yes**
gatgaaattgtcaggctca	110	42	76	No	1	**3**	**Yes**
gcaaaaggcctgtggctct	187	58	76	No	3	**2**	**No**
agtttcaggaggaggccaa	357	53	76	No	2	**1**	**Yes**
aggagatatccatgcaaaa	24	37	75	No	3	**3**	**No**
gggaaaatcgagatctgaa	90	42	75	No	3	**3**	**No**
agaaaacgcccttcagcaa	172	47	75	No	2	**3**	**No**
ggagatcgagagactcaaa	334	47	75	No	3	**3**	**No**
agatctgaaggatgaaatt	100	32	74	No	2	**3**	**No**
aaggagatcgagagactca	332	47	74	No	2	**2**	**Yes**
tcgagagactcaaagctga	339	47	74	No	3	**3**	**Yes**
atcgagatctgaaggatga	96	42	73	No	2	**3**	**Yes**
gagatctgaaggatgaaat	99	37	73	No	3	**2**	**No**
ggatgaaattgtcaggctc	109	47	73	No	2	**3**	**No**
gccaagaccattcaggaca	308	53	73	No	2	**3**	**No**
agaccaccatcaaggagat	12	47	72	No	2	**2**	**No**
cctgtggctctgagataat	195	47	72	No	3	**3**	**No**
gggaatatgaaaatgaact	384	32	72	No	3	**3**	**No**
aggatgaaattgtcaggct	108	42	71	No	2	**3**	**Yes**
gaaggcgagctgaagaaaa	159	47	71	No	1	**3**	**No**
tggagatagaactgaagca	231	42	71	No	2	**3**	**Yes**
tgaagcaggtcatgcagca	243	53	71	No	2	**2**	**Yes**
gcctgtggctctgagataa	194	53	70	No	3	**3**	**No**
gagataatgcagaagaagc	206	42	70	No	2	**3**	**Yes**
cagcagcgctctgaggaca	257	63	70	No	2	**2**	**Yes**
ccgctgggaatatgaaaat	379	42	70	No	3	**3**	**No**
ccatcaaggagatatccat	18	42	69	No	2	**2**	**No**
aaaagaggatgattccaaa	40	32	69	No	1	**2**	**Yes**
atgaaattgtcaggctcaa	111	37	69	No	2	**3**	**Yes**
aaaacgcccttcagcaaaa	174	42	69	No	2	**3**	**Yes**
ccaccatcaaggagatatc	15	47	69	No	3	**2**	**No**
agaagaagcagcatctgga	216	47	69	No	2	**2**	**Yes**
tagaaaccagcttgataga	64	37	69	No	2	**3**	**Yes**
ttacgaagaccaccatcaa	6	42	69	No	3	**3**	**Yes**
gctgggaatatgaaaatga	381	37	69	No	3	**3**	**No**
cgaaggcgagctgaagaaa	158	53	68	No	2	**>3**	**No**
aaaccagcttgatagactt	67	37	68	No	3	**3**	**Yes**
aagaagcagcatctggaga	218	47	68	No	2	**2**	**Yes**
acaagcagtccctggagga	285	58	68	No	1	**2**	**Yes**
caagaccattcaggacaaa	310	42	68	No	2	**2**	**No**

An additional parameter to take into account when designing siRNAs is the seed complement frequency which ideally should be as low as possible. Given that none of the siRNAs offered by the si*DESIGN* Centre (except for one) had low seed frequency (Table B1) additional methodologies had to be used to reduce off-target signatures. Firstly, all four chosen siRNAs had chemical modifications (named by Thermo Fisher Scientific as ON-TARGET*plus* modifications) on their sense and antisense strands (even though some of them did not require sense modifications according to the si*DESIGN* Centre, see Table B1). Secondly, a pooling strategy was used (see B1.2) to reduce the concentration of each individual siRNA.

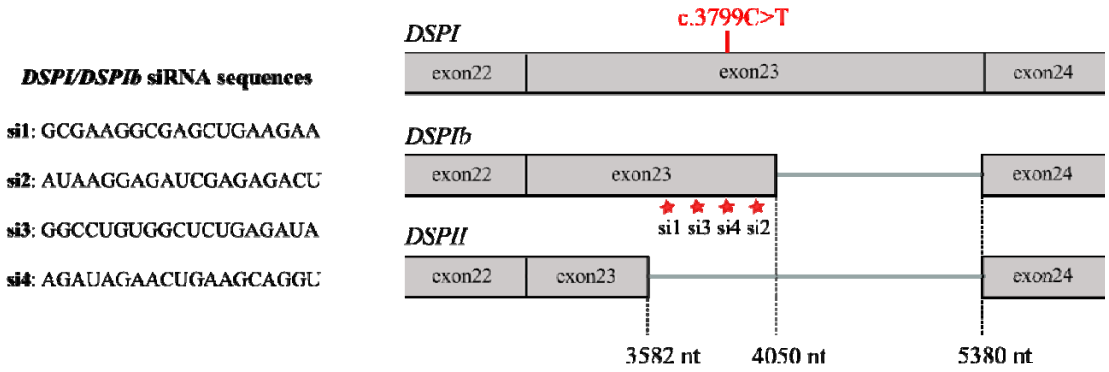

Figure B2. Nucleotide sequences of four siRNAs targeting *DSPI/DSPIb* and their targeting sites. (A) Sense strands of four individual siRNAs designed to specifically target *DSPI* and *DSPIb* mRNAs. **(B)** Schematic diagram of a portion of the *DSPI*, *DSPIb* and *DSPII* mRNAs including exons 22 to 24 and the position of the p.R1267X (c.3799C>T) nonsense mutation. Alternative donor splice sites around positions 5380, 4050 and 3582 (coding nucleotides) originate three different splice variants (*DSPI*, *DSPIb* and *DSPII* respectively). R1267X occurs in a region common to both *DSPI* and *DSPIb* mRNAs and therefore four siRNAs (si1 to si4) were design in this region to knock-down *DSPI* and *DSPIb* and mimic this mutation. The targeting regions of each individual siRNA are indicated with red stars.

B1.3. Three out of four designed siRNAs cause significant down-regulation of DPI/DPIb

In order to test the four chosen siRNAs, HaCaT cells were independently transfected with 100nM of each individual siRNA (si1, si2, si3 and si4) using the transfection conditions described in B1.1. Additionally, the four siRNAs were pooled at a final concentration of 100nM (sipool (1-4)), and a mock control consisting of cells incubated with DharmaFECT transfection reagent only (no siRNA) was included. Cells were assayed four days post-transfection for DP protein expression by western blot, using an antibody that recognises the C-terminus of DP (11-5F; see Table 2.6), which is common to all three splice variants. Vinculin was used as a control for equal loading

(Figure B3). DPI protein levels were determined using densitometry measurements of western blots and normalised to the loading control (vinculin) (Figure B3B). siRNAs si2, si3 and si4 caused between 87% (si2) and 95% (si3) down-regulation of DPI. Virtually 100% down-regulation of DPIb was also achieved with these duplexes. In contrast, si1 did not cause down-regulation of either DPI or DPIb. DPII expression levels following si1, si2 and si3 transfections were comparable to those of the mock control and following si4 transfection, DPII expression levels appeared to be slightly up-regulated. These results indicate that siRNAs si2, si3 and si4 as well as the sipool (1-4) target *DSPI* (and *DSPIb*) specifically in HaCaT cells, without causing down-regulation of DPII.

A

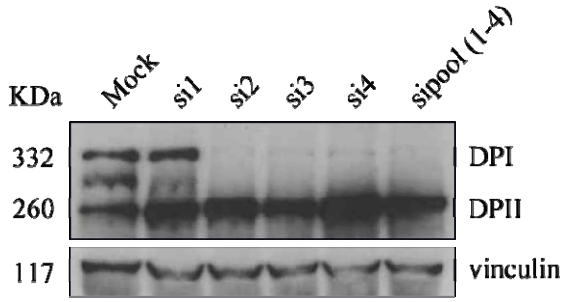

B

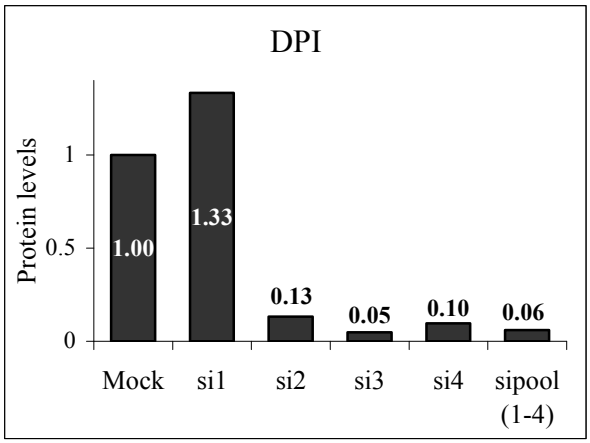

Figure B3. Three out of the four selected siRNAs result in over 85% knock-down of DPI/DPIb. (A) Western blot analysis of total HaCaT cell lysates from HaCaT cells transfected with 100nM of each of the four siRNAs (si1, si2, si3 and si4) designed to target *DSPI/DSPIb*, and with a pool containing 25nM of each siRNA (sipool (1-4), 100nM final concentration). siRNAs si2-4 lead to significant down-regulation of both DPI and DPIb, four days following transfection. Mock refers to cells that were incubated with DharmaFECT transfection reagent only. Positions of DPI (332KDa) and DPII (260KDa) and the loading control vinculin (117KDa) are indicated. DPIb is predicted to be 279KDa **(B)** DPI protein levels normalised to loading control and presented as a fraction of the DPI levels of Mock cells.

One possible way for attenuating off-target effects is by pooling functional and specific siRNA duplexes. This control strategy is particularly important in the present case where siRNAs with low seed frequency were not available. Each siRNA within the pool will be present as a fraction of the total siRNA concentration. Since each siRNA a unique off-target signature, reducing its concentration to a minimum reduces its likelihood of causing off-target effects by interacting with unintended mRNAs (Anderson *et al.*, 2008).

Another important control is a quantitative control by means of a siRNA titration. This is important because the RNAi components may be saturable, particularly the RISC complex (Editorial, 2003).

Since siRNA duplexes si2-4 were demonstrated to be functional, a pool containing 33.3nM of each of the three duplexes was first prepared (for a final concentration of approximately 100nM). This pool of siRNAs was designated as siI and cells transfected with this pool were designated siI cells. Then, the concentration of the pool was varied in a gradient from 100nM to 10nM (final concentrations). Western blotting of total lysates from HaCaT cells four days after transfection was carried out (Figure B4A) to assess DPI and DPIb expression levels. Densitometry measurements revealed over 95% down-regulation of DPI with 100nM, 70nM and 40nM of siI (Figure B4B). In contrast, only about 60% knock-down of DPI was observed with 10nM of siI. DPII expression levels in siI cells remained comparable to those of mock cells and normal untransfected cells, regardless of the concentration of siI. These results indicate that the knock down efficiency does not increase with siRNA concentrations above 40nM and suggest that this concentration is the threshold above which the RNAi machinery possible becomes saturated.

A

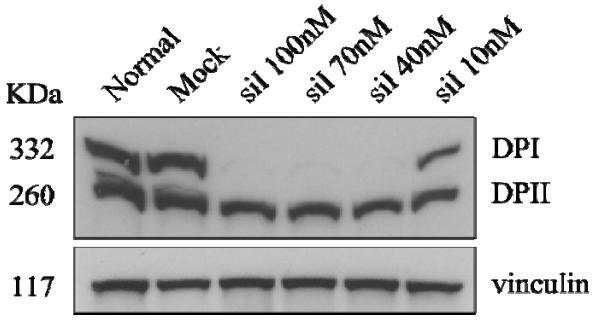

Figure B4. Quantitative control of the pool of siRNAs (siI) which includes si2, si3 and si4. (continues).

B

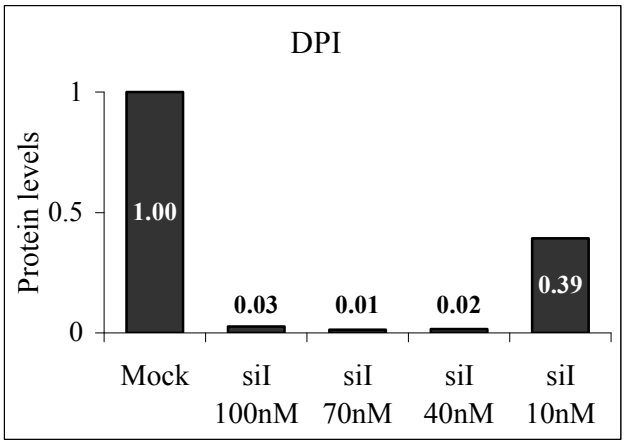

Figure B4. Quantitative control of the pool of siRNAs (siI) which includes si2, si3 and si4. (A) Western blot of proteins from total HaCaT cell lysates four days after transfection with different concentrations of the siI pool (from 100nM to 10nM). Normal refers to cells that have been incubated neither with transfection reagent nor with siRNA. Mock refers to cells that were incubated with DharmaFECT transfection reagent only. Positions of DPI (332KDa) and DPII (260KDa) and the loading control vinculin (117KDa) are indicated. DPIb is predicted to be 279KDa. **(B)** DPI expression levels normalised to loading control and presented as a fraction of the DPI levels of mock cells.

B1.4. Time-course analysis of DPI down-regulation

DPI and DPIb expression levels were monitored 2, 4, 6 and 8 days following transfection with siI by western blot (Figure B5A). Two days after transfection, a significant down-regulation of DPI and DPIb was observed. Four days following transfection, the overall protein levels are higher because a larger number of cells were assayed when compared to day two post-transfection. However, as shown by the loading control (vinculin), the amount of protein loaded on the gel was always comparable between mock and siI cells for each time point. A significant down-regulation of DPI and DPIb was also observed 4 and 6 days post-transfection, however, after 8 days DP expression starts reappearing. Densitometry analysis (Figure B5B) showed that while DPI was down-regulated by approximately 90% (when compared to mock cells for which DPI expression was taken as 100%) up to day 6 following transfection, only 40% of DPI knock-down was achieved 8 days post-transfection. In light of these results, in subsequent knock down experiments cells were always assayed 4 days following siRNA transfection because this time point allowed for a significant knock-down of DPI/DPIb and for a suitable cell density to work with.

A

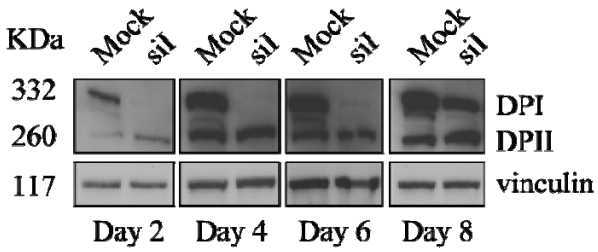

B

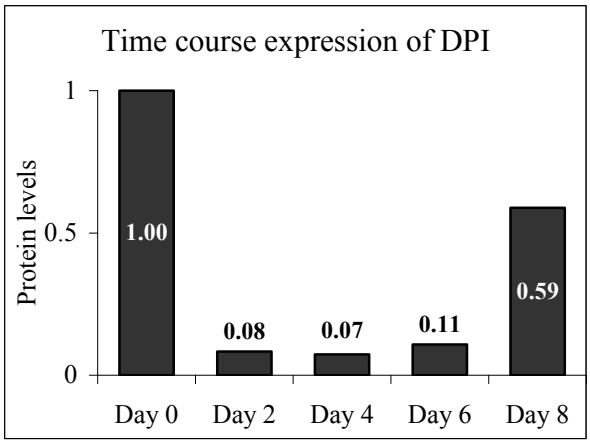

Figure B5. Time course expression of DPI. (A) Western blot analysis of proteins from total HaCaT cell lysates over a period of 8 days (2, 4, 6 and 8 days) following transfection with the siRNA pool (siI). Mock refers to cells that were incubated with DharmaFECT transfection reagent only. siI refers to cells that have been transfected with the siRNA pool including si2, si3 and si4. Positions of DPI (332KDa) and DPII (260KDa) and the loading control vinculin (117KDa) are indicated. DPIb is predicted to be 279KDa. **(B)** DPI expression levels normalised to loading control and presented as a fraction of the DPI levels of mock cells for each corresponding day. DPI expression on day 0 was taken as 1 for both mock and siI cells.

Appendix C: Functional studies of *DSPI*-nonsense and DP haploinsufficiency mutants

C1. Influence of *DSPI*-nonsense and *DSP* haploinsufficiency mutations on desmosomal protein expression: two independent experiments

Two independent *DSPI* and *DSPI/DSPII* knock-down experiments were performed and two to four replicate western blots were carried out for each protein of interest. For statistical analysis, the paired t-test was used to compare means of two samples. A paired t-test is classically used when measurements are taken from the same sample before and after some treatment. However, it can also be used to compare samples that are subjected to different conditions, provided the samples in each pair are identical otherwise. NT control cells are identical to siI and siI/II cells, except for the fact that they are transfected with different siRNAs. More importantly, each data point (densitometry value) in one set is inseparably linked with a data point in the other set because that data point is on the same western blot and therefore subject to the same experimental conditions. For these reasons, the paired t-test was found appropriate for these experiments.

In the first knock down experiment, HaCaT cells were transfected with 40nM (final concentration) of the siI pool of siRNAs (which mimic the *DSPI*-nonsense mutation) and with 40nM of the siI/II siRNA which targets all isoforms (mimicking the haploinsufficiency mutation). Control cells were transfected with the NT pool of siRNAs at a final concentration of 40nM. The total DP content was reduced to approximately one half when compared to the NT control, in both siI and siI/II cells (47% in siI cells and 43% in siI/II cells, on average). However the DPI:II ratios were different: approximately 1:4 in siI cells and approximately 5:1 in siI/II cells (Figures C1A and C1C).

No detectable changes were observed in the expression levels of PKP2 or PKP3, PG and DSG2 or DSG3 in siI or siI/II cells, when compared to the NT control cells (Figure C1A). In contrast, PKP1 and DSC2 were reduced to about one half and DSC3 was reduced by approximately one third in siI and siI/II cells (Figures C1B and C1D). A closer analysis of Figures C1B and C1D reveals that, on average, while PKP1 expression levels are similar between siI and siI/II cells, DSC2 and DSC3 levels are slightly higher in siI/II then in siI cells. These trends suggest that in contrast with PKP1,

the expression levels of DSC2 and DSC3 are influenced by the DPI:II ratios, as the levels of total DP are similar between siI and siI/II cells. Moreover, the expression levels of DSC2 and DSC3 are slightly higher when the DPI:DPII ratio is larger and decrease when the DPI:DPII ratio decreases (i.e, when DPI/II ratio is 1:4 (siI cells), the protein level of DSC3 is 33%; when DPI/II ratio is 5:1 (siI/II cells), the level of DSC3 is 40%) (Figures C1C and C1D).

In order to confirm these results, a second siRNA knock-down experiment was performed (Figure C2) in identical conditions, except that 100mM of the siI/II was used instead of 40nM. The concentration of the siI pool was 40nM as before and the NT pool was used at 100nM. Increasing the concentration of siI/II did not alter the efficiency of DP knock down: DPI and DPII expression levels were on average 54% and 12% respectively (compared to DPI expression levels of NT control cells) in the first siI/II knock-down experiment (Figure C1C) and 56% and 14% respectively in the second siI/II experiment (Figure C2C).

Although the same concentration of siI was used, the first experiment resulted, on average, in 85% down-regulation of DPI (Figure C1C) compared to 96% in the second experiment (Figure C2C). This difference probably reflects the inherent variability among transfections or western blots. Variability among transfections may result from slight differences in cell density at the moment of transfection and the clumping of cells may reduce transfection efficiency. Independent westerns blots are subject to slightly different conditions due to the inherent errors associated with sample loading on the SDS-PAGE gel or blot exposure times, which may account for the observed variability.

In the second knock-down experiment, the average total DP levels were 53% of NT control cells in siI cells and 38% in siI/II cells, compared to 47% and 43% respectively in the first experiment (Figures C1C and C2C). Even though in the first experiment the total DP levels in siI and siI/II cells were slightly lower than in the second experiment, the difference in total DP levels between the two knock down situations was comparable. The DPI:DPII ratios were 1:24 and 4:1, respectively, in the second experiment compared to 1:4 and 5:1 respectively in the first (Figures C1C and C2C). While the DPI:DPII ratios were comparable between the two experiments in siI/II cells, a much larger DPI:DPII ratio was observed in the first experiment in siI cells. This is possibly due to two circumstances. Firstly, as mentioned before, the first siI transfection was less efficient than the second (85% compared to 96% down-regulation

of DPI, Figures C1C and C2C). Secondly, different DPI:DPII ratios were also observed in NT control cells between the two knock-down experiments, because the expression levels of DPII were lower in the first experiment (55% of DPI expression levels) than in the second experiment (87% of DPI expression levels) (Figures C1C and C2C). Therefore, the lower expression levels of DPII in NT cells as well as in siI cells accounted for the larger DPI:DPII ratio observed upon the first siI transfection. These results suggest that the DPI:DPII ratio in wild type HaCaT cells is not always the same.

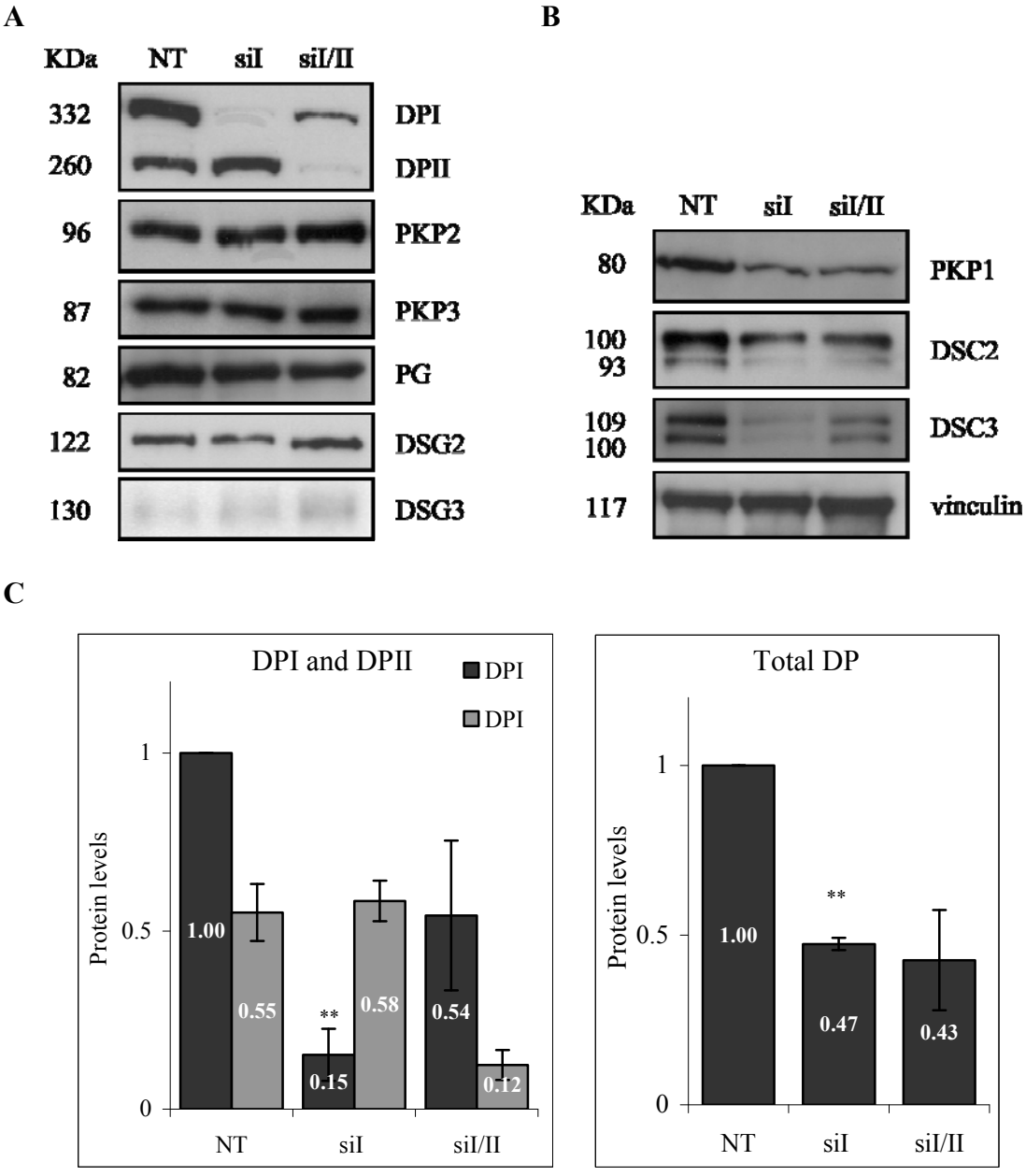

Figure C1. Western blot and protein quantification of desmosomal proteins following *DSPI* and *DSPI/DSPII* knock-down suggests that DSC2 and DSC3 expression levels are dependent upon the DPI:DPII ratios in contrast with PKP1(first knock-down experiment) (continues).

D

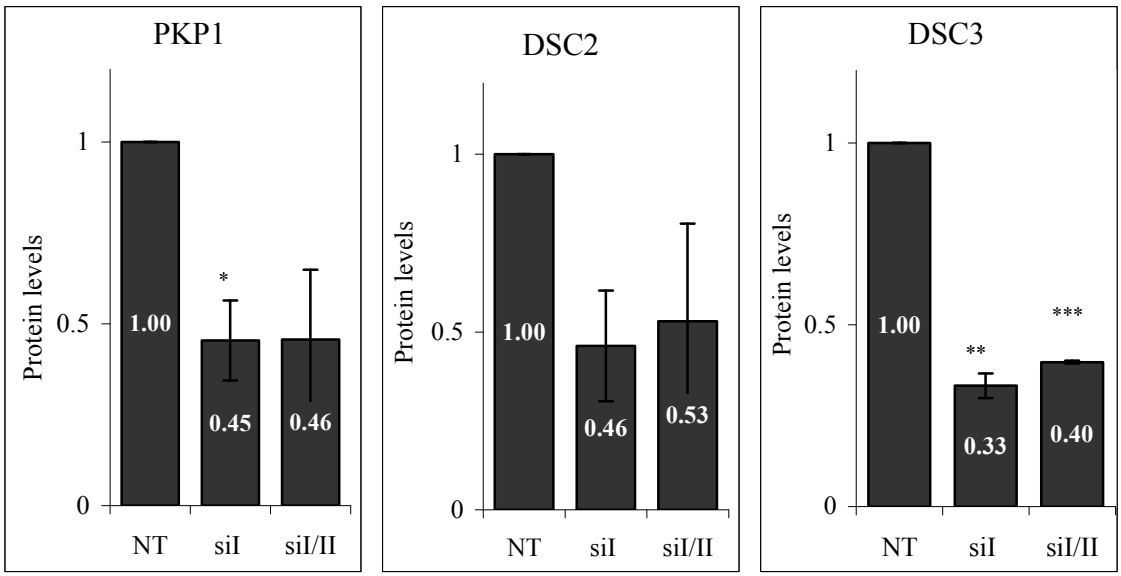

Figure C1. Western blot and protein quantification of desmosomal proteins following *DSPI* and *DSPI/DSPII* knock-down suggests that DSC2 and DSC3 expression levels are dependent upon the DPI:DPII ratios in contrast with PKP1 (first knock-down experiment). (A and B) Western blot of total proteins from HaCaT cells, four days after transfection with the siI pool, the siI/II siRNA and the NT control pool. The predicted molecular weight of each protein is indicated on the left (KDa). **(A)** DPI and DPII expression levels and proteins which levels did not change following siRNA transfection are shown. **(B)** PKP1, DSC2 and DSC3 show reduced expression levels following both siI and siI/II transfections compared to the NT control; however, DSC2 and DSC3 show lower expression levels in siI cells then in siI/II cells. Vinculin was used as a loading control. **(C)** Protein levels (mean±SEM) of DPI and DPII (n=3 blots) and total DP (DPI+DPII) normalised to loading control. DPI and DPII expression levels are presented as a fraction of the DPI levels of NT cells and total DP expression levels are presented as a fraction of the DP levels of NT cells. **(D)** Protein levels (mean±SEM) of PKP1 (n=3 blots), DSC2 (n=3) and DSC3 (n=3) normalized to the loading control and presented as a fraction of the respective NT control levels. PKP1 levels do not change between siI and siI/II cells; in contrast, DSC2 and DSC3 expression levels are higher in siI cells than in siI/II cells. Statistical significance between siI or siI/II and NT following paired t-test: * ($p<0.05$), ** ($p<0.01$), *** ($p<0.001$).

In agreement with the first knock-down experiment, no detectable differences were observed in the expression levels of PKP2, PKP3 and DSG3 in either siI or siI/II cells compared to NT control cells (Figure C2A). The expression levels of K14 and β-catenin were determined for the first time in this second knock-down experiment, and no major differences were observed between siI or siI/II cells and NT cells (Figure C2A). Similarly to the fist experiment, PKP1 expression levels were reduced to about 40% and did not change between siI and siI/II cells. DSC2 levels increased on average from 51% to 59%; and DSC3 levels increased from 41% to 71% (Figures C2B and C2D). The larger increase of DSC3 levels between siI and siI/II cells observed in this second experiment parallels the larger increase of DPI levels (4% to 56%, Figure C2C)

compared to the first experiment (15% to 54%, Figure C1C). These results confirmed that the levels of PKP1 remain approximately constant independently of the DPI:DPII ratios and of subtle changes in the levels of total DP. In contrast, DSC2 and to a larger extent DSC3 expression levels are affected by the DPI:DPII ratios and are higher when DPI levels are higher, even when the total DP content decreases slightly.

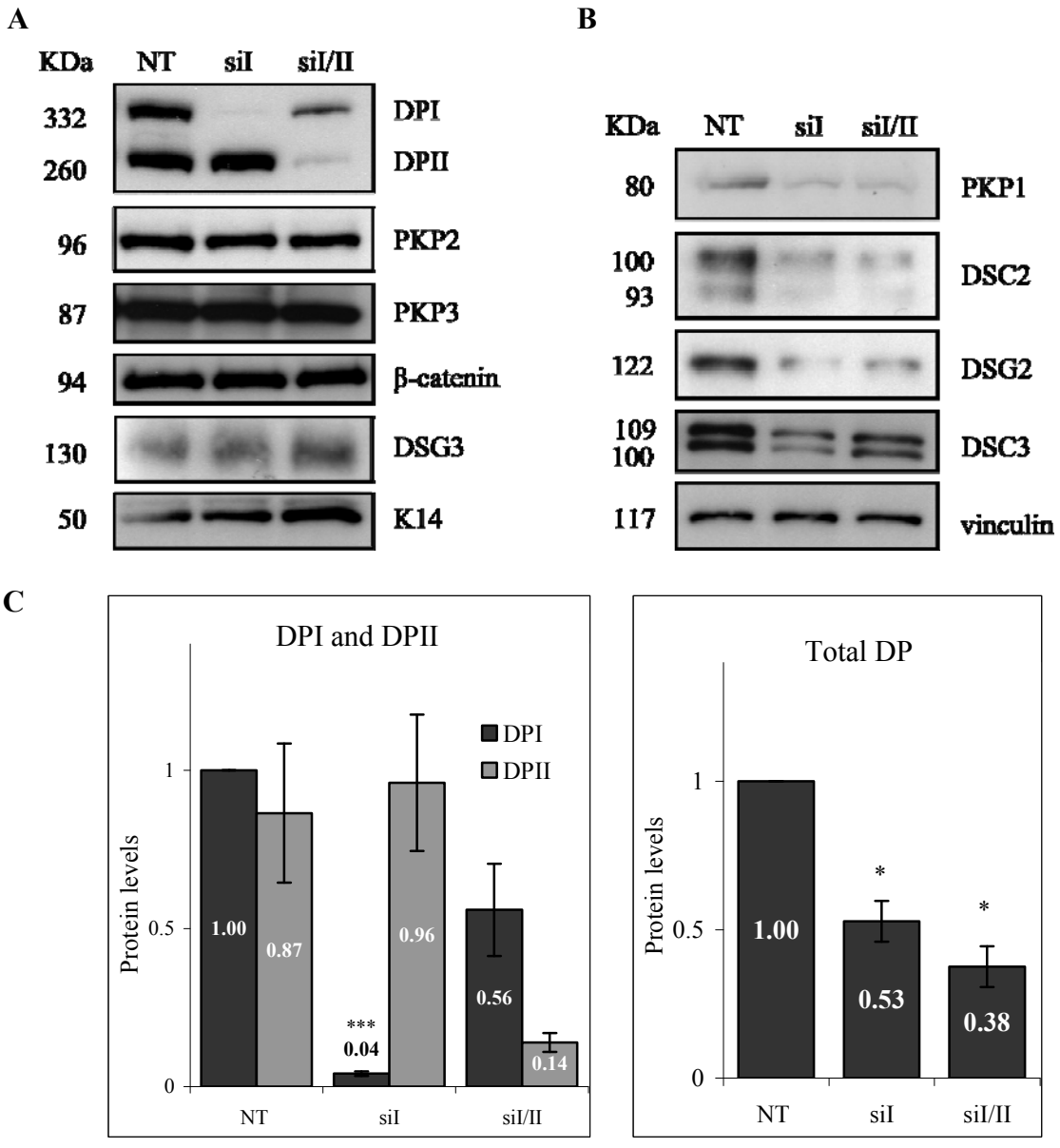

Figure C2. Western blot and protein quantification of junctional proteins following *DSPI* and *DSPI/DSPII* knock-down suggests that DSC2, DSG2 and DSC3 expression levels are dependent upon the DPI:DPII ratios in contrast with PKP1 (second knock-down experiment) (continues).

D

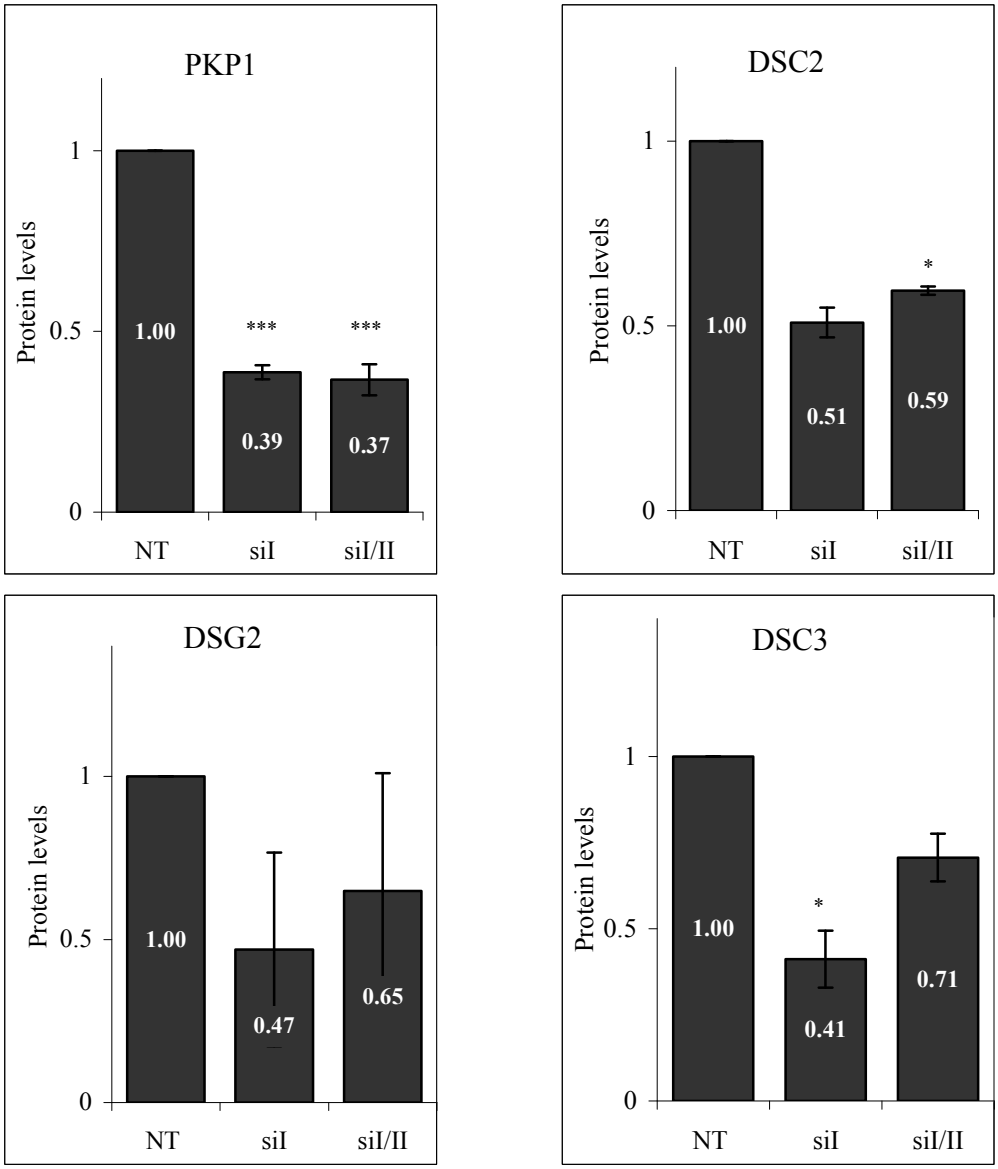

Figure C2. Western blot and protein quantification of junctional proteins following *DSPI* and *DSPI/DSPII* knock-down suggests that DSC2, DSG2 and DSC3 expression levels are dependent upon the DPI:DPII ratios in contrast with PKP1 (second knock-down experiment). (A and B) Western blot of total proteins from HaCaT cells, four days after transfection with the siI pool, the siI/II siRNA and the NT control pool. The predicted molecular weight of each protein is indicated on the left (KDa). **(A)** DPI and DPII expression levels and proteins which levels did not change following siRNA transfection are shown. **(B)** PKP1, DSC2, DSG2 and DSC3 show reduced expression following both siI and siI/II transfections compared to the NT control; however, DSC2, DSG2 and DSC3 show lower expression levels in siI cells then in siI/II cells. Vinculin was used as a loading control **(C)** Protein levels (mean±SEM) of DPI and DPII (n=3 blots) and of total DP (DPI+DPII) normalised to loading control. DPI and DPII expression levels are presented as a fraction of the DPI levels of NT transfected cells. Total DP expression levels are presented as a fraction of the DP levels of NT cells. **(D)** Protein levels (mean±SEM) of PKP1 (n=4 blots), DSC2 (n=2), DSG2 (n=2) and DSC3 (n=3) normalized to the loading control and presented as a fraction of the respective NT control levels. PKP1 levels do not change between siI and siI/II cells, in contrast DSC2 and DSC3 expression levels are higher in siI cells than in siI/II cells. Statistical significance between siI or siI/II and NT following paired t-test: * ($p<0.05$), *** ($p<0.001$).

A reduction in DSC2 and DSC3 expression levels was also observed in both siI and siI/II cells compared to NT cells by immunocytochemistry, confirming the results obtained by western blot (data not shown).

No major changes were observed in the expression levels of DSG2 in siI and siI/II cells in the first knock down experiment (two replicate western blots, Figure C1A); however, the second knock down experiment showed that the levels of DSG2 (two replicate western blots) decrease, on average, to 47% in siI cells and 65% in siI/II cells compared to NT cells (100%). This trend suggests that DSG2 expression levels, like those of DSC2 and DSC3, might also be affected by the DPI:DPII ratios. The discrepancy between the first and second knock-down experiments might reflect the variability among westerns blots, and a larger number of replicate western blots would be necessary to confirm the changes in the levels of expression of DGS2 between siI and siI/II cells. Additionally, this discrepancy might be due to the different DPI knock-down efficiencies in the two independent experiments, which accounted for differences in the DPI:DPII ratios in siI cells, as well as to natural changes in protein expression levels.

Appendix D: Flexcell adhesion assay

D1. Optimisation of the Flexcell adhesion assay

As described in section 5.1.3, the FX-4000T System was used to investigate morphological changes in cells with desmosome defects, in particular with *DSP* mutations, in response to mechanical stress.

To optimise the stretching conditions, normal HaCaT cells were subject to cyclic mechanical stretch with a frequency of 2 Hz (i.e. two cycles of stretch and relaxation per second) and an elongation of amplitude ranging from 11-14% (i.e. increase in diameter across the silicone membrane from 11 to 14%). Cells were stretched for 0, 1, 2 and 3 hours and then fixed and prepared for immunocytochemistry with an antibody raised against keratin 14 (LL002; see Table 2.6). Before any stretch was applied (0h), these cells showed a normal, well-formed network of keratin 14, which extended from the nucleus to the cell periphery (0h, Figure D1). Following 1 hour of stretch, thickening of the keratin IFs and more compact bundles were observed, particularly in the perinuclear region. These denser keratin IFs were more prominent after 2 hours of stretch (arrows, Figure D1). In contrast, following a 3-hour-stretch approximately 90% of the cells had lifted off the tissue culture dish, suggesting occurrence of cell death due to the prolonged mechanical stress. The few cells that remained adherent to the dish presented with keratin networks that appeared less dense than in non-stretched cells and more fragile, and fragmentation of filaments was observed in some of these cells, predominantly at free edges.

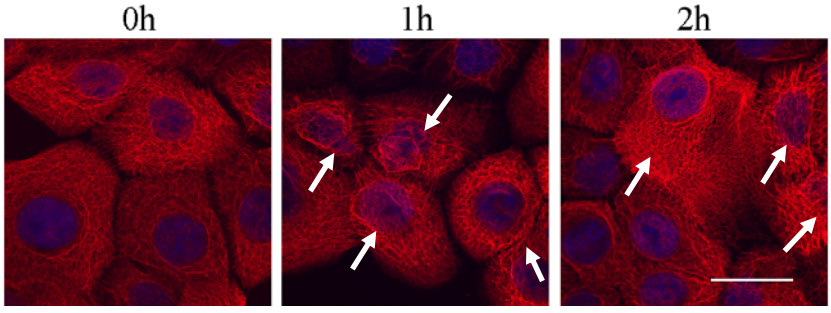

Figure D1. Mechanical stress induces thickening of keratin 14 IFs in normal HaCaT keratinocytes. For optimisation of the Flexcell adhesion assay, normal HaCaT cells were subject to 0h, 1h, 2h and 3h of mechanical stretch of 2 Hz frequency and amplitude ranging from 11 to 14%. Immunocytochemistry with a keratin 14 antibody shows a normal, well-formed network of keratin IFs before stretch (0h), which extended from the nucleus to the cell periphery. Thickening of keratin IFs is observed following 1h stretch which is intensified after 2h. Scale bar = 10µm.

D2. Effect of *DSPI*-nonsense and haploinsufficiency mutations in HaCaT intercellular adhesion

A

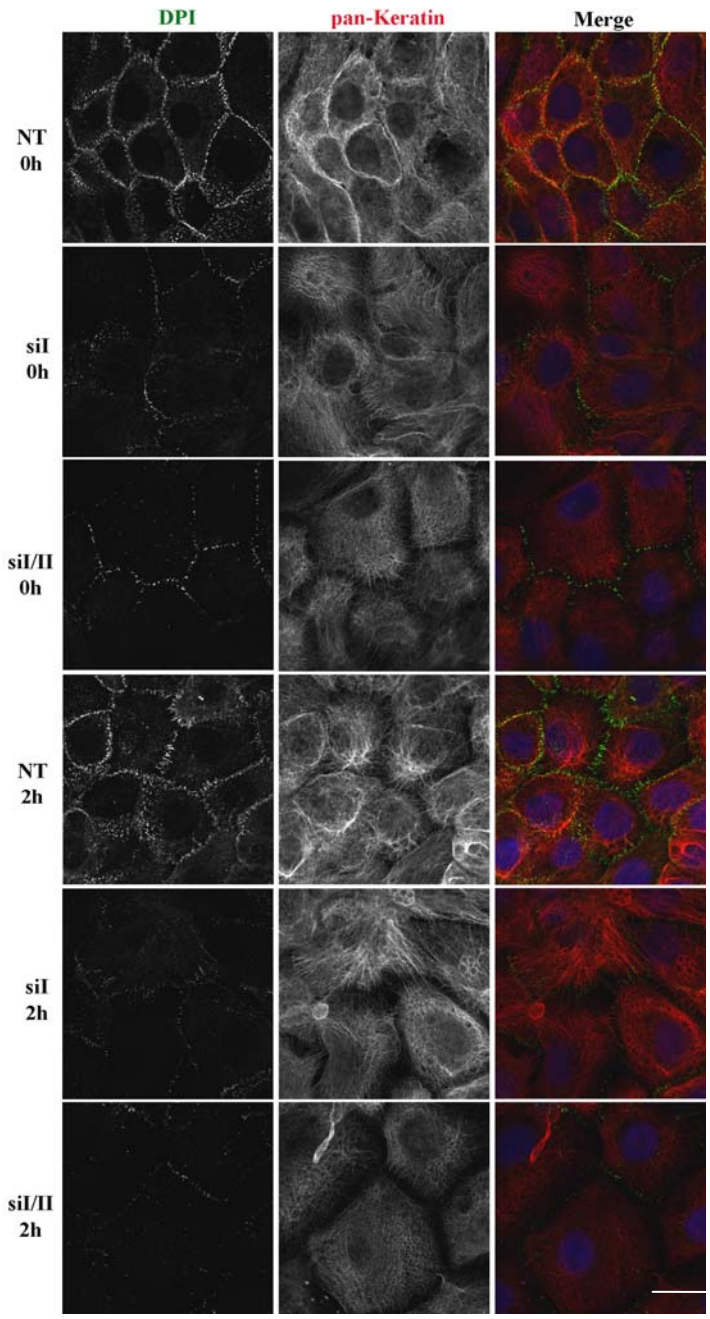

Figure D2. Mechanical stress causes reduced cell-cell adhesion in siI and siI/II HaCaT cells (continues).

B

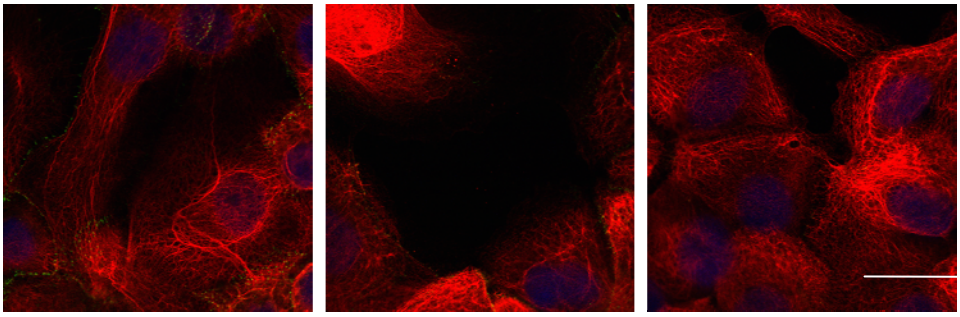

Figure D2. Mechanical stress causes reduced cell-cell adhesion in siI and siI/II HaCaT cells. HaCaT cells transfected with (1) a pool of four non-targeting siRNAs (NT control cells), (2) a pool of three siRNAs with target *DSPI* (siI) and (3) an siRNA which targets both *DSPI* and *DSPII* (siI/II) were subject to mechanical stress using the FX-4000T™ Cell Stretcher (Flexcell International, USA). Cyclic stretch at a frequency of 2 Hz and amplitude ranging from 11-14% was applied for 0h (unstretched) and 2h. Cells were stained with **(A and B)** monoclonal antibody DP-1 against human DPI (green) and monoclonal antibody AE1/AE3 against human pan-cytokeratin (red) **(B)** Different field views of siI/II cells stretched for 2h show loss of cell-cell contacts. Scale bar = 10μm.

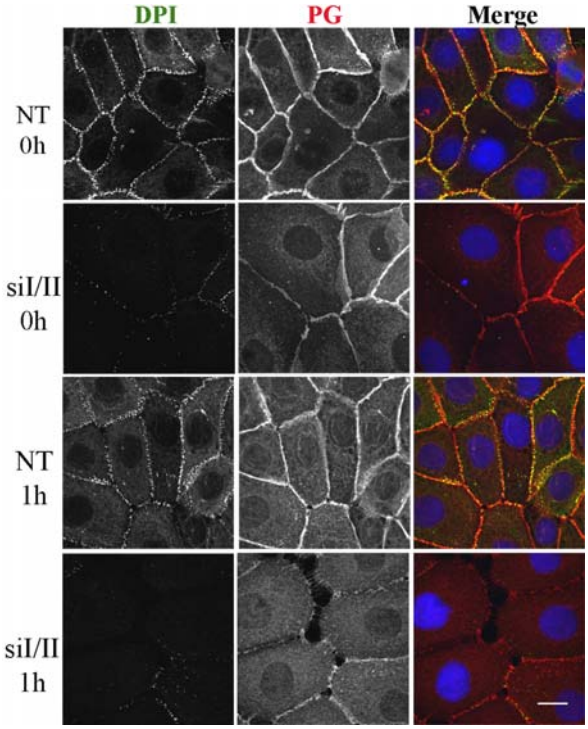

Figure D3. Mechanical stress causes reduced cell-cell adhesion and slight increase in PG cytoplasmic staining in siI/II HaCaT cells. HaCaT cells transfected with a pool of four non-targeting siRNAs (NT control cells) and a siRNA which targets both *DSPI* and *DSPII* (siI/II) were subject to cyclic mechanical stress of frequency 2 Hz and amplitude 11-14% using the FX-4000T™ Cell Stretcher for 0h (unstretched), and 1h. Double immunocytochemistry of NT and siI/II cells with antibodies against DPI (green) and PG (red) before and after 2h of stretch. siI/II transfected cells show decrease of cell-cell adhesion with widening of intercellular spaces between keratinocytes following 2h of mechanical stress. PG staining is only present in the infrequent sites of cell-cell adhesion. Scale bar = 5μm.

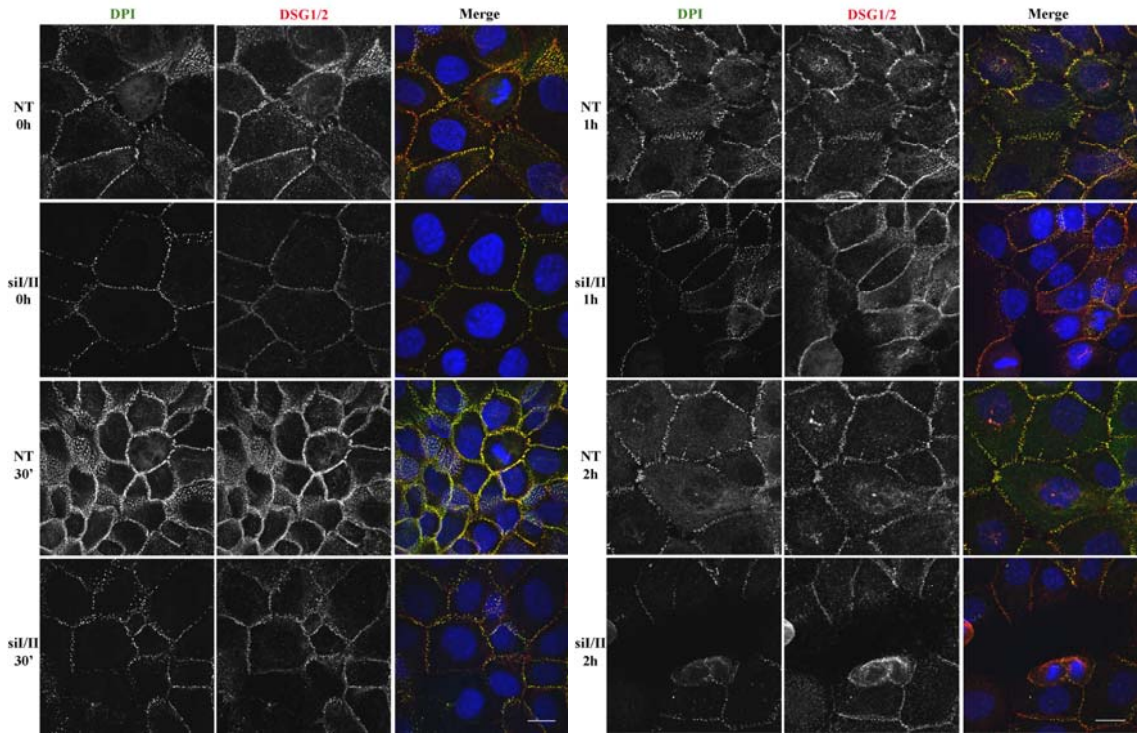

Figure D4. Mechanical stress causes reduced cell-cell adhesion but no changes in DSG2/3 localisation in siI/II HaCaT cells. HaCaT cells transfected with a pool of four non-targeting siRNAs (NT control cells) and a siRNA which targets both *DSPI* and *DSPII* (siI/II) were subject to cyclic mechanical stress of frequency 2 Hz and amplitude 11-14% using the FX-4000T™ Cell Stretcher for zero hours (unstretched), 30 min, 1h and 2h. Double immunocytochemistry of NT and siI/II cells with antibodies against DPI (green) and DSG1/2 (red) before and after stretch. siI/II transfected cells show decrease of cell-cell adhesion with widening of intercellular spaces between keratinocytes following 1h and 2h of mechanical stress. DSG1/2 staining is comparable between NT and siI/II cells before and after mechanical stretch. Scale bar = 5μm.

Appendix E: Materials

E1. Tissue culture materials

100x RM$^+$
40µg/ml Hydrocortisone
500µg/ml Insulin
1µg/ml EGF
10^{-8} (0.84 µg/ml) Cholera toxin
500µg/ml Transferrin
1.3µg/ml Lyothyronine (L4)

E2. Molecular biology materials

10x TBE
9M Tris base
9M Boric acid
0.2M EDTA, pH 8.0

DNA loading buffer
50% (v/v) Glycerol
0.2% (w/v) Orange G

STE buffer
10mM Tris base pH 8.0
50mM NaCl
1mM EDTA

Ponceau stain
20mg/ml Ponceau S
0.3g trichloroacetic acid

2x Laemmli buffer
0.1M Tris-HCl pH 6.8
0.2M DTT
4% (w/v) SDS
0.2% (w/v) bromophenol blue
20% (v/v) glycerol

SDS sample buffer
0.125M Tris-HCl (pH6.8)
4% (w/v) SDS
20% (v/v) glycerol
0.001% (w/v) bromophenol blue
1.44M β-mercaptoethano.

10x Running Buffer
0.25M Tris base
1.92M Glycine
1% SDS

10x Transfer Buffer
0.48M Tris base
0.30M Glycine
0.37% (w/v) SDS
Add 20% (v/v) Methanol to 1x Transfer Buffer before use

10x TBS
0.5M Tris-HCl pH 7.5
1.5M NaCl

1x TTBS (Tween 20-TBS)
0.05M Tris-HCl pH 7.5
0.15M NaCl
0.1% (v/v) Tween-20

10% separating gel (in 5 ml)
1.7 ml of Acrylamide mix [Protogel 30% (w/v) acrylamide:0.8% (w/v) Bis-acrylamide stock solution (37.5:1)], National diagnostics
1.9 ml of ddH_2O
1.3 ml of 1.5 M Tris, pH 8.8
0.05 ml of 10% SDS
0.05 ml of APS
0.002 ml of TEMED

5% stacking gel (in 1 ml)
0.17 ml of Acrylamide mix [Protogel 30% (w/v) acrylamide:0.8% (w/v) Bis-acrylamide stock solution (37.5:1)], National diagnostics
0.68 ml of ddH_2O
0.13 ml of 1.0 M Tris, pH 6.8
0.01 ml of 10% SDS
0.01 ml of APS
0.001 ml of TEMED

<u>Appendix F</u>: Homozygous mutations in the 5' region of the JUP gene result in cutaneous disease but normal heart development in children (Cabral *et al.* 2010)